A systematic study of how molecular structure influences combustion and pyrolysis of novel renewable fuels in a diesel engine and high temperature reactor

James Frost

Submitted in partial fulfilment of the requirement for the degree of Doctor of Philosophy at University College London, University of London

January 2022

I, James Frost, confirm that the work presented in this thesis is my own. Where information has been derived from other sources, I confirm that this has been indicated in the thesis.

Dated: 07/01/2022

Abstract

Internal combustion technology has been employed as the primary mode of propulsion for transportation since the early 1900s, with continual improvements in efficiency ever since. Despite this, issues associated with the fuels combusted have caused a shift towards electrification, but this is not suitable for all applications and geographies. It is therefore necessary to seek sustainable fuels, in conventional engines, for the short to medium-term alleviation of CO_2 emissions, fossil fuel usage and toxic pollution detrimental to air quality.

The work presented uses a compression ignition (CI) engine to test a range of novel fuels, with proven sustainable sources, to detect their impact on exhaust emissions and combustion. Initially, a range of 2nd generation furanic biofuels were tested, in order to understand the effect of molecular structure on combustion. Saturated cyclic molecules with carbonyl side chains possessed strong ignitability, while alleviating particulate mass (PM); these molecular attributes are indicative of lactones. Lactones were therefore tested within the CI engine, with a subsequent investigation utilising a pyrolytic reactor to help understand soot formation from these fuels, since soot is initially formed from gaseous precursors. Gas Chromatography-Flame Ionisation Detection (GC-FID) analysis was used to detect soot-precursor concentrations in the breakdown of a lactone compared to other C10 fuels. It was determined that, despite minor differences in species present and differing precursor abundance, the pattern of pyrolysis products was similar for all fuels; ethylene was most prevalent, with lower levels of C3s (propene) and C4 (1,3-butadiene) gases. Preliminary investigations were undertaken to detect molecular breakdown of fuels in the engine itself, employing in-cylinder sampling to collect cylinder contents. Minor differences were noted between engine and reactor, likely due to air-derived oxygen in the engine.

Finally, an investigation was conducted to gauge the impact of a hydrogen fuel carrier (ammonium hydroxide) on diesel combustion. This is less hazardous than ammonia itself, but the presence of water was shown to be detrimental to combustion efficiency at lower engine

loads, while the fuel- bound nitrogen appeared to contribute to greater NO_x emissions at comparable engine loads.

Impact Statement

The originality of this research centres on the novel use of bioderived fuel molecules. To date, some studies have been performed utilising a small number of 2nd generation-derived furan molecules. However, no work appears to have studied the effect of varying molecular attributes of these structures on the combustion characteristics and emissions from a compression ignition engine. It is hoped that this study will help increase the range of molecules suggested to be compatible as diesel fuel blends.

The outcome of the first systematic study enabled a smaller range of biofuels to be identified based on potential benefits of their bioderived nature, production potential and exhaust emissions. These lactone fuels could be used as pure fuels given a sufficiently high carbon number, and it is the first known example of a diesel engine fuelled with 100% lactone fuel. The versality of nature means that there is likely a scope to obtain lactone fuels from a range of sustainable feedstocks. An upcoming study involving the University of Brighton will look into the use of these fuels in a high efficiency research engine.

Since little is known about these types of molecules in an engine, research was conducted surrounding the breakdown of these fuels and their formation of gaseous hydrocarbon species that are precursors to soot formation. A study into the pyrolysis of higher hydrocarbons in a tubular reactor is original, while the results suggested the effectiveness of esters to reduce hydrocarbon precursor abundance, though the pathway of breakdown between a straight chain and cyclic ester appeared to differ.

Subsequently, a zero-carbon fuel, ammonium hydroxide, was employed in the engine. Previous studies have looked into ammonia assisted combustion, as it is an effective hydrogen fuel carrier, but the advantage of the system employed here is the dilution in toxicity of the ammonia by utilising an aqueous source. One of the main drawbacks of hydrogen fuelled co-

combustion is the safety concern with on-board hydrogen, therefore it is hoped this method (without the need for any major engine modifications) will be discussed as a potential utilisation technique for hydrogen-derived fuel.

The work undertaken has so far resulted in the following publications in peer reviewed journals:

- J. Frost, A. Tall, A.M Sheriff, A.Schonborn and P. Hellier. An experimental and modelling study of dual fuel aqueous ammonia and diesel combustion in a single cylinder compression ignition engine, International Journal of Hydrogen Energy, Volume 46, Issue 71, October 2021, p35495-35510. This work was a collaboration between University College London and the World Maritime University and has potential applications in the marine sector, where hydrogen-based fuels are seen as a likely solution to the decarbonisation of this industry.

- J.Frost, P.Hellier and N.Ladommatos. A systematic study into the effect of lignocellulose-derived biofuels on the combustion and emissions of fossil diesel blends in a compression ignition engine. Fuel, In Press.

Acknowledgements

Table of Contents

List of Figures

List of Tables

Nomenclature

AF	Acetylfuran
ATDC	After top-dead centre
BDE	Bond dissociation enthalpy
BDe	Base diesel end
BDs	Base diesel start
BSFC	Brake-specific fuel consumption
BTDC	Before top-dead centre
CAD	Crank angle degree
CI	Compression ignition
CIgn	Constant ignition
CInj	Constant injection
CN	Cetane number
CO$_2$	Carbon dioxide
CO	Carbon monoxide
COV	Coefficient of variation
CR	Compression ratio
δDDL	Delta-dodecalactone
δDL	Delta-decalactone
DEE	Diethyl ether
DFT	Density functional theory
2,3-DHF	2,3-Dihydrofuran
2,5-DHF	2,5-Dihydrofuran
δHL	Delta-hexanolactone
DME	Dimethylether

DMF	Dimethylfuran
EC	Elemental carbon
εCL	Epsilon-caprolactone
EF	Ethylfuran
EMF	Ethoxymethylfurfural
ES	External standard
FA	Furfuryl alcohol
FAEE	Fatty acid ethyl ester
FAME	Fatty acid methyl ester
FF	Furfural
γCL	Gamma-caprolactone
γDDL	Gamma-dodecalactone
γDL	Gamma-decalactone
FID	Flame-ionisation detector
GC-MS	Gas chromatography- mass spectrometry
GHGs	Greenhouse gases
GVL	Gamma-valerolactone
HAA	Hydroxyalkylation-alkylation
HACA	Hydrogen abstraction acetylene addition
HAVA	Hydrogen abstraction vinyl addition
HCs	Hydrocarbons
HCCI	Homogeneous charge compression ignition
HMF	Hydroxymethylfurfural
HRR	Heat release rate
H_2	Hydrogen
H_2O	Water

ICE	Internal combustion engine
ICT	In-cylinder temperature
ID	Ignition delay
IMEP	Indicated mean effective pressure
IR	Infrared radiation
IS	Internal standard
LA	Levulinic acid
MF	Methylfuran
MMF	Methoxymethylfurfural
MRR	Methyl radical recombination
MTHF	Methyltetrahydrofuran
MTHF-3-one	2,Methyltetrahydrofuran-3-one
NH$_3$	Ammonia
NH$_4$OH	Ammonium hydroxide
n-HP	n-Heptyl propionate
NO$_x$	Nitrous oxide
N$_2$	Nitrogen
O$_2$	Oxygen
OC	Organic compounds
OFR	Ordinary flame radical
PAH	Polycyclic aromatic hydrocarbons
pHRR	Peak heat release rate
PM	Particle mass
PN	Particle number
ppm	Parts per million
rpm	Revolutions per minute

RSR	Resonantly stabilised radical
SFG	Surface functional group
SI	Spark ignition
SOC	Start of combustion
SOF	Soluble organic fraction
SOI	Start of injection
ST	Standard temperature
TDC	Top dead centre
THF	Tetrahydrofuran
UHCs	Unburnt hydrocarbons
µs	Microseconds
VOC	Volatile organic compounds

1. Introduction

The transport sector's contribution to global emissions is well documented; in 2002, transportation attributed 82% of CO emissions, 56% of NO_2 emissions and 45% volatile organic compounds (VOCs) as well as 27% of the total greenhouse gas (GHG) emissions produced in the US[1]. By 2008, the energy consumption of the transport sector made up 27.3% of the global energy consumption, rising from 23.1% since 1973, and a 2012 review ascribed 13.5% of global warming caused as a result of transportation.[2] The use of internal combustion engines (ICEs) (both on-road and non-road) produces almost half (41%) total anthropogenic NO_x emissions worldwide.[3] Approximately 30% of global GHGs are produced from transportation,[4] and about 80% of the CO_2 emissions from this sector can be attributed to road transport.[5] Ultimately, the trend is upwards and therefore the reduction of emissions of greenhouse gases and harmful pollutants, such as soot, is a major priority in the transport industry, particularly with increased understanding of the harm that inhalation of exhaust-born substances can cause.[4] As a result, there is considerable literature regarding ways in which pollutant emissions from both spark ignition and compression ignition engines may be reduced.

Changes in the engine design and operation are possible solutions. In direct injection systems, for example, specifically designed inlet ports enable sufficiently high fuel-air mixing in the smaller sized engines used in automobiles. This both enhances efficiency while reducing incomplete combustion products such as soot.[6] The design of the fuel injector, such as the number and size of nozzle holes present, will dictate the spray characteristics of the fuel and has a major impact on the level of fuel penetration and mixing with air, while changes in the chamber wall design will affect the impingement of the fuel spray on the walls, which has been shown to affect the ignition delay and, subsequently, the overall combustion process.[6] Alternatively, the fuel used for combustion could be altered or replaced entirely. For example, changes to the cetane or octane number of diesel and gasoline fuels respectively (a measure

of the ability of the fuel to autoignite), as well as the viscosity, can have a major impact on the emissions produced. Among other parameters, the viscosity and cetane number of diesel fuel are used to assess the fuel's viability in the real world; a new fuel will need to meet the requirements set in the current standards, such as the UK specification BS EN 590: 1997.[7] The density at 15°C, the flashpoint, water content and sulphur content are also specified so as to ensure the fuel does not plug the fuel system or adversely damage the components. Replacement of the fuel could potentially have benefits both upstream and downstream of fuel utilization; lower harmful or GHG emissions is beneficial in itself, but coupling this with the utilisation of bioderived fuels (making them a 'renewable' resource) is an exciting prospect. Chapter 2 reviews the literature surrounding both the production and use of a range of novel renewable fuels, before looking specifically at emissions of particulates and how a change in fuel might alleviate the production of this pollutant.

The aim of the following research is to investigate potential new bioderived molecules for use in a compression ignition (CI) engine, that can be obtained without extensive processing that would render them economically non-viable. Ideally, these fuels will possess potential production routes from 2nd generation (non-edible) biomass sources; fuel molecules of this description were tested in a CI engine, with the results outlined in Chapter 4. Meanwhile, downstream, determining molecular characteristics that reduce levels of hazardous pollutants is highly worthwhile, as this could help to streamline the production of novel biofuels to afford a fuel blending component that achieves lower levels of these harmful emissions. Chapter 5 experiments utilise the results of Chapter 4 to investigate a relatively unknown group of potential biofuels- lactones- that were predicted to see reduced emissions whilst maintaining combustion efficiency.

Particulate matter (PM) emissions represent arguably the most toxic pollutant from combustion engines. The core soot particulate consists of elemental carbon (EC). This is harmful in itself, and the more stringent emissions regulations, which increasingly includes particulate sizes into the order of nanometres,[8,9] have been shown to actually increase the

cytotoxicity of particulates, despite an overall reduction in particle mass emitted per km. This is due to the increase in functionalisation of the carbon shells as the particle size decreases.[10] Moreover, the ability of other material, ranging from organic compounds (OC) to sulphates and even trace metals, to become absorbed onto these particles and enter the human body (when the sizes are small enough to evade the body's defences) is also a major concern.[11] The organic fraction in particular, is well-documented to possess mutagenic and carcinogenic properties.[11–13] The mechanisms via which these particles form is still under research, but a general consensus is that light hydrocarbon species, formed from fragments of fuel, react to form aromatics such as benzene. These aromatics are able to combine further, either with light species such as acetylene or with other aromatics, to form polyaromatic hydrocarbons (PAHs) and, eventually, a soot particle.[14–16] Practical and computation studies have been performed surrounding the varying effects of oxygenated biofuels in engines on both particulate emissions and indeed on their backbone, the individual PAHs.[11,17–22] However, to the best of this author's knowledge, the formation of individual gaseous species from the initial fuel molecule has not been previously reported for complex molecules that future novel fuels may comprise. This information is not only essential in understanding a biofuel's tendency to produce particulate matter, but also in their mechanism of breakdown. Observing this initial molecular breakdown is imperative to understand how a certain class of molecules can be expected to increase or reduce the formation of particles during combustion- in which local pyrolysis zones exist- before it is tested in an engine. Chapter 6 investigates fuel decomposition in the context of a reactor, where pyrolysis conditions are highly controllable, and in a preliminary study whereby samples were extracted from within an engine.

While fuels derived from biomass represent a promising solution to the world's problem of CO_2 emissions and emissions of toxic pollutants, the rise of electrified transport may be expected to mark the end of the combustion engine. However, there exists multiple industries and geographies in which this solution is not feasible in the short term.[5] For maritime transport, for example, the optimum solution may not be to electrify the sector, considering the range of

autonomous operation, costs and the life-cycle impact of materials. Hydrogen fuel cell technology may represent a solution to the inherent problem of battery range, but even here there are issues, predominantly with storage, and the use of hydrogen as a co-combustion reactant does not necessarily alleviate these issues. Efforts have been employed in the use of on-board hydrogen formation,[23] but these are still in their relative infancy and both necessitate vehicular modifications and do not lessen the inherent safety concerns with hydrogen. As a result, Chapter 7 of this work looks into the use of a potential hydrogen carrier, aqueous ammonia, that does not possess the general safety or potential infrastructural drawbacks of hydrogen fuel.

The investigations of novel fuels in an inherently unmodified, light duty diesel engine, and subsequent specialised analysis within controlled reactor conditions, are hoped to expand the biofuels discussion away from conventional, 1st generation, biodiesel, which possesses its own drawbacks. These include high production costs (due to the high-value feedstocks[24] or the catalysts employed in the synthesis[25]), competition with food sources,[26] reduction in brake thermal efficiency (BTE)[27]- potentially due to low calorific value and/or poor spray characteristics- and general increase in NO_x emissions. These issues have hindered the market penetration of biodiesel for over 20 years,[26] and thus necessitate studies into viable alternatives. The following work is intended to offer a greater understanding of novel fossil fuel alternatives, reducing carbon emissions from source and harmful emissions during combustion itself.

2. Literature review

The following literature review will look at the current and potential prospects of producing biofuels as a fuel-blending component and/or as a drop-in fuel (an alternative fuel that can be used interchangeably in an engine without modification). Focus will be given to future diesel fuels, although alternatives to gasoline will also be discussed when relevant. Subsequently, a review of the current understanding of the effect of using various biofuels on emissions will be presented. This will include both emissions of nitrous oxides (NO_X), particulate matter (PM), carbon monoxide (CO) and unburnt hydrocarbons (UHCs). A review will also be included of the effects of novel fuels on the formation of soot precursors, including polycyclic aromatic hydrocarbons (PAHs), and gaseous hydrocarbons, such as acetylene, and the ways in which these effects can be measured.

2.1. Future renewable fuels

The use of biofuels in internal combustion engines is not a new proposition. The first compression ignition engine patented by Rudolf Diesel in 1892 was designed to work on peanut oil due to crude oil shortages at the time.[6] However, political and economic factors in the post-war era meant that fossil fuels such as gasoline and diesel were favoured and, since then, the world's approach has not changed significantly. Now that the harmful effects that burning fossil fuels have on human and environmental health is better understood, new efforts have been made to use bio-derived sources for fuels. These possess the advantages of being carbon neutral (carbon emissions produced by burning the fuel are those that have been absorbed throughout the plant's lifetime) and renewable, as biomass may be regrown each year to yield a steady supply of fuel. The largest market for biofuels is bio-ethanol,[28] which was first envisioned as an alternative to fossil fuels during the oil crisis of the 1970s[29] and can be

sourced from a wide range of crops varieties, such as sugar cane, corn maze and sugar beet.[30] Bioethanol can be blended at up to 80vol% in gasoline and 15% in diesel to produce a biofuel that can be used in vehicles without engine modifications.[31,32] Furthermore, biodiesel is commonly utilised in heavy-duty and marine diesel engines, often blended at a 20:80 ratio of biodiesel:diesel (B20),[33] and can be sourced from vegetable oils such as peanut and cottonseed oil; these oils are reacted with alcohols via the transesterification process to form biodiesel.[4]

However, the major disadvantage of bio-ethanol, and other so-called '1st generation biofuels', is that they are derived from crops that can otherwise be used for food. This food vs fuel argument is particularly pertinent in countries that already struggle to produce enough food for their ever-growing populations, and thus the need to grow additional crops for fuel is not an option given the limited land availability. The use of lignocellulosic biomass as a fuel source is referred to as 2nd generation, and has the distinct advantage of being the most abundant non-edible biomass type; this element often goes to waste as a result of other industrial production methods, such as paper production, and is simply burnt for use in other operations.[28] Ultimately, to cope with a rising population and the associated increase in food and energy demands that follow, land use needs to be as efficient as possible, and 2nd generation biofuels do not necessarily impact land for food production.[34]

2.1.1.   Production of 'platform chemicals'

2.1.1.1.   Overview

Naturally, biomass cannot directly be used as a fuel source for the operation of internal combustion engines, which require a liquid or gaseous fuel with the necessary properties for efficient combustion. Biomass must therefore undergo various transformation and 'upgrading' processes to form the aforementioned fuel. This upgrading can be a multi-step process depending on the final product desired; in most cases, lignocellulosic material will be converted

into one of a variety of so-called platform chemicals, which will then undergo further processing to meet the requirements of the relevant industry. In addition to the fuel industry, platform chemicals can also be upgraded into chemicals used for the production of a number of polymers, pesticides and perfumes.[35]

Lignocellulose consists of a complex mixture of materials, the proportions of which vary depending on the biomass source; for example, rye straw lignocellulose will have an inherently different composition to the lignocellulose of oak,[31] but in general, lignocellulose consists of cellulose (40-50%), hemicellulose (25-35%) and lignin (15-20%).[36] The cellulose fraction tends to be liberated from the other fractions to then be hydrolysed into glucose monomers, which will then undergo further processing. Hemicellulose consists primarily of xylose, a C_5 sugar that can be hydrolysed into xylose monomers, which are further treated to produce platform molecules of interest. The purpose of lignin within plants is to protect the other two units, thus it surrounds both cellulose and hemicellulose, and given its structure of propyl-phenol polymers it needs to be removed from the rest of the material in order to successfully liberate the carbohydrates. It should be noted that the aromatic nature of lignin means upgrading processes may be employed to yield potential fuel molecules from this component, which will be discussed in further detail in Section 2.1.1.5.

As stated by Serrano-Ruiz *et al*,[28] the splitting of the fractions of lignocellulose before hydrolysis into sugars necessitates costly pre-treatment. This can be avoided with the use of other conversion methods, such as gasification and pyrolysis, but the products of these, such as pyrolysis oil, are limited in their applications. These pre-treatment methods include both thermal and physical methods, while chemical processes may also be employed. According to Menon,[34] the treatment selected depends on the feedstock, but all options possess certain drawbacks such that no single treatment is greatly prioritised over another. For example, an initial stage of mechanical treatment is universally employed, as the biomass requires a degree of size reduction in order to enhance subsequent treatment methods; rates of enzymatic hydrolysis can be improved due to the increase in mass transfer and reduction in crystallinity.

Chemical processes are used in order to decrease the amount of polymerisation and improve the overall degradability of the biomass so that it is more susceptible to hydrolysis and upgrading reactions. Alkalis and acids can be used for this; the former degrades the ester and glycosidic chains within lignin, while acids hydrolyse hemicellulose into monomers, hence the combination of the two can lead to relatively pure cellulose. The use of greener alternatives, such as deep eutectic solvents or ionic liquids, has also been investigated[34,37,38]. Specifically, imidazolium cations have been widely reported to demonstrate high solubility for lignocellulose. Furthermore, work by Binder and Raines[39] investigated the ability of a chloride ionic liquid to yield sugar monomers from a corn stover starting material, with 90% yields achieved. Ionic liquids are notoriously costly and difficult to handle however. Another pre-treatment route involves the use of biological materials. As alluded to earlier, enzymes are effective in digesting raw material into more materials amenable to further processing, but microorganisms such as bacteria and fungi have also been shown to break down biomass. Sun and Cheng[40] outline the ability of different types of rot fungi to degrade different fractions of lignin; white rot attacks both cellulose and lignin while brown rots mainly act on cellulose alone. Knezevic *et al*[41] conducted a comparative study on the use of white rot fungi as a biological pretreatment for the production of sugars from wheat straw, observing that Ganoderma resinaceum was the most suitable species given the high hydrolysis yield owing to its high rate of lignin degradation. Bacterial strains offer greater thermal stability than fungal species, however their use has as yet not been explored to the same extent, therefore screening of a range of different strains is needed to ascertain the effect on hydrolysis.[42] Biological treatment routes possess the advantages of being environmentally benign and they require little energy input, but the drawbacks of such routes include the slow rates, large spaces required and partial solubilization of useful material; as a result it has attracted relatively little attention. Furthermore, product inhibition is an issue that has meant the likes of Zanellati *et al*[43] have investigated 40 fungal strains for their response to such inhibitors as furfural and vanillin etc;

they concluded that only one fungi, Byssochlamys nivea was able to grow in all inhibitors tested.

Obtaining C_5 sugars from hemicellulose and C_6 sugars (predominantly from cellulose), is
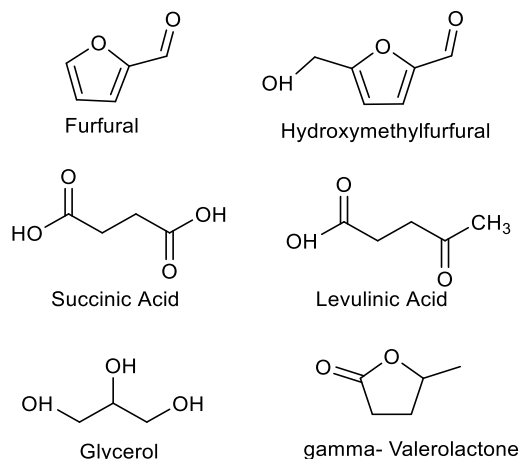
Figure 2.1: : Example 'platform chemicals' derived from biomass

the first major challenge in the production of biofuels for use in internal combustion engines. The next processing step is the production of platform molecules from these monomers. The most commonly employed method for this is a dehydration step whereby the sugar monomers are broken down into a class of monomers known as furans.[44] For C_5 sugars, the major product is furfural, and for C_6 sugars it is hydroxymethylfurfural (HMF). While other platform molecules can be derived from

these monomers, such as succinic and levulinic acid, the initial two mentioned are the first major products formed. The products of this direct synthesis therefore represent the most appealing options to base fuels upon. Figure 2.1 shows the molecular structure of some platform molecules obtained from C_5 and C_6 sugars.

2.1.1.2. Furfural

As illustrated in Figure 2.1, the furfural molecule consists of a furan base with an aldehyde (C=O) group on the carbon adjacent to the oxygen in the furan ring. The potential of this molecule in the production of fuels has long been recognised; it was identified by the US Department of Energy as a top 30 biomass-derived platform chemical in terms of value,[45] and can be produced from petrochemicals through the catalytic oxygenation of 1,3-butadiene.[46] Major energy companies, including Shell, have considered production routes to biofuels from furfural since at least 2003.[44] It is important to note the current status of furfural production, since this dictates, to an extent, the viability of potential fuels that can be derived from this

molecule. Furfural production worldwide was approximately 400kt/year (as of 2012) and, somewhat surprisingly given the potential uses of furfural more recently discovered, most of this production still employs the first commercial process developed in 1921 by Quaker Oats[44]. The yield of this process, which uses sulfuric acid as a catalyst for the hydrolysis and dehydration processes, is fairly poor (50-60%) and relies on feedstocks that are rich in the hemicellulose fraction of biomass which contains the C_5 sugars (xylose). Xylose is found in various forms and fractions depending on the type of biomass; in hardwoods it generally exists as glucuronoxylan and as glucuronoarabinoxylan in grasses, while it can make up to 10 wt% in softwoods and 28 wt% in grasses.[44] The drawbacks of the current process are immediately apparent, the most likely reasoning for the lack of any change in almost a century is that the demand of furfural has not risen significantly in that time and thus the inevitable cost of developing and building new systems and plants to utilise an entirely new system has deterred advances. Recent developments on pilot scales have been made in this area however, especially in the area of biphasic reaction systems.[28] Mittal *et al*[45] utilised a methyl isobutyl ketone - water and toluene - water system to obtain an 80% and 77% furfural yield respectively, where the organic solvent selected and the ratio of organic and aqueous had been optimised. 87% yields of furfural have been achieved from hemicellulose feedstocks at relatively low temperatures using extraction through an organic phase; tetrahydrofuran (THF).[47] The main drawback of biphasic systems, however, is that the recovery of the extractant used can be difficult and the loss of this material makes the process more economically challenging. Acid catalysis is generally employed in the production of furfural; the reaction rate is otherwise low in neutral conditions, and sulphuric acid is commonly chosen. However, there are naturally issues with the use of acids on a large scale, most notably corrosion and associated costs with the replacement of equipment that the acid encounters.[48] Efforts to alleviate this issue are therefore an area of research, with Li *et al*[49] utilising gamma-valerolactone (GVL) and a *dilute* sulphuric acid catalyst, obtaining a maximum yield of 99.5%. GVL acts as a 'polar aprotic solvent' which reduces the activation energy required for biomass hydro-conversion. Ionic

liquids can also be used to increase the 'promotion effect', as they are able to disrupt the hydrogen network within the lignocellulose and increase biomass solubility.[46] Binder *et al*[50] looked into the use of ionic liquid and a chromium halide catalyst to synthesize furfural from xylose, raising the yield to 37% from 8% when using a HCl catalyst.

A potential way around the use of mineral acids altogether is the use of heterogenous catalysts, a newer technique that circumvents many of the issues of liquid acids e.g. the difficulty in separating the catalyst from the products in the same phase. The use of solid acid catalysts in the dehydration of xylose is therefore a significant area of research; the lack of corrosion as well as easier product separation are major benefits. [44-48] Li, Ren *et al*[51] were able to obtain a 76.79% furfural yield through the use of an Sn-MMT solid catalyst, containing both Lewis acid and Bronsted acid sites, with xylose as the starting material.[51] However, deactivation of the heterogenous catalysts, due to fouling of the humins produced as furfural reacts with itself, raises economic concerns since these catalysts tend to be expensive zeolites. Another technique that has been investigated in this area includes the use of solid bases in conjunction with acids to improve the reaction yield. Takagaki[52] utilised both acidic Amberlyst-15 and a solid base, hydrotalcite, to enhance the yield of furfural from a mixture of glucose and xylose. Their findings demonstrated an increase of furfural selectivity from 1% to 34% and an increase in xylose conversion, 72% from 51%, with the addition of the base catalyst, though the extent of this increase was dependent upon the reaction temperature.

The subsequent processing of furfural into more fuel relevant molecules will be discussed in Section 2.1.2, although it should be noted that furfural is in itself a potential fuel if considering only the molecular structure. The carbon-oxygen ratio of furfural is relatively low (5:2), which will be detrimental to the energy density compared to conventional hydrocarbons, therefore its use as a pure fuel cannot be considered. As a blend, however, the possibility is greater as the drawbacks such as its relatively low stability and physical properties (viscosity) will have less impact. Furfural as a biofuel blend would be advantageous on a large scale

based on its production alone; it requires only two major processing steps (biomass-sugar and sugar-furfural); other lignocellulose-derived fuel blenders require further processing.

2.1.1.3. *Hydroxymethylfurfural (HMF)*

While the production of furfural has been commercialised for almost a century, HMF production is a more recent endeavour; only in 2013 was it the main product of a commercial plant[53] due to its potential in the production of polymers, fuels and additives. Previously it was obtained as an intermediate in the synthesis of another platform molecule, levulinic acid.[54] Its role in the production of 2,5-furandialdehyde, 2,5-furandicarboyxilic acid and high value chemicals and fuels, as a result of its high reactivity, give this molecule a high market value.[55] The chemical structure of HMF is similar to that of furfural; it possesses a simple aldehyde group on the carbon adjacent to the oxygen of the furan base (the '2' position), but HMF also possesses a C-OH group on the opposite carbon (position '5'), as shown in Figure 2.1.

HMF can be obtained from biomass in the same process as that of furfural production, although in this instance the raw material consists primarily of C_6 sugars from cellulose rather than hemicellulose. This may put it at a slight disadvantage as a platform molecule compared to furfural given that the structure of C_6 sugars involves branching of the main molecule, as shown in the green outlines in Figure 2.2. This encourages cross-linking between molecules and, therefore, potentially requires harsher conditions in order to break these cross-linkages and process. Furthermore, depending on the starting sugar, yields of HMF vary significantly; glucose reactivity is lower than fructose, and so if glucose is used as the C6 sugar starting material, yield and selectivity of HMF is reduced relative to using fructose.[46] However, glucose is the more desirable reactant on a commercial scale due to its higher abundance and lower cost.[56]
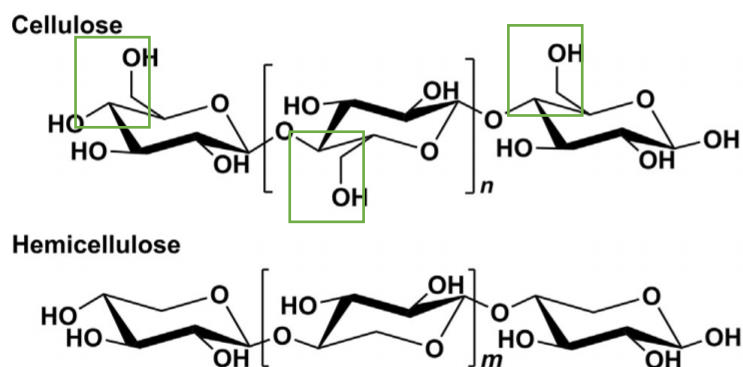
Figure 2.2: Polymer structure of cellulose and hemicellulose[57]

However, the fact that a large portion of plant biomass consists of cellulose means that the scope for large scale production is greater. HMF can be obtained from the dehydration of fructose and glucose via dehydration using an acid catalyst and efforts have been made to dehydrate both these C_6 sugars simultaneously with xylose to produce both HMF and furfural. Zhang and co-workers[48] were able to achieve yields of 30.9 mol% for HMF and 54.3 mol% for furfural using a diphasic solid acid catalyst system and an equal amount of glucose and xylose as a starting material. However, in this study and other similar investigations into the use of solid acidic catalysts, high temperatures, long reaction times and relatively low yields indicate that the process is not yet viable.[48,58–60] Motagamwala *et al*[56] more recently utilised an acetone-water solvent system to recover 96% HMF from a glucose/fructose starting material. The disadvantage of this system though is that the glucose remains unreacted and does not contribute to HMF formation. As with the dehydration of C_5 sugar into furfural, the common use of liquid acid catalysts such as HCl and H_2SO_4 represents a major drawback given that they are not easily recovered from the reaction media and their corrosive nature necessitates frequent equipment replacement. Solid acid catalysts such as zeolites, ion-exchange resins and phosphates have been used in small scale HMF production. A high yield under moderate reaction conditions is necessary for HMF to be viable as a platform chemical for future biofuels, however the yield from the most abundant feedstock available, glucose, is relatively low.

Therefore, in a mixture of biomass-derived sugars, a considerable portion of this biomass would be wasted if the glucose was not utilised.[61] One solution is to first isomerise glucose into fructose; when fructose is used as a feedstock the yield of HMF is much higher, but the extra processing stage will naturally increase costs.[28] Biphasic systems to assist with product separation and reduce unwanted side reactions that negatively impact the final yield have been researched in the production of HMF.[28] As with furfural synthesis, organic-aqueous phases are employed, with ionic liquids being one option to use as the organic phase, though their cost renders them currently impractical to use on a large scale for this application.[62] Work by Dumesic and co-workers[63–65] was able to realise the possibility of using a range of polysaccharides, including glucose, fructose and xylose, to achieve good yields and selectivity of HMF and furfural. However, their use of DMSO in the aqueous phase, DCM as an extracting solvent and mineral acid or noble metal catalysts are major drawbacks.

HMF and furfural vary in their structure only by the addition of carbon and alcohol group in HMF relative to furfural (in adjacent position to the carbonyl group). As a result, both can be used to produce furan derivatives that may be viable fuel options (see Sections 2.1.2 to 2.1.5). The simultaneous synthesis of a fuel from *both* HMF and furfural (and therefore a range of different sugars) is therefore possible; this would increase the amount of fuel produced and negate any requirement for a preceding separation of xylose and glucose (C_5 and C_6 sugars). Zhang's aforementioned work[48] took the process of converting sugars to fuels a stage further, looking at the production of potential fuel molecules dimethylfuran (DMF) and methylfuran (MF) from the hydrogenation of HMF and furfural respectively. While relatively high yields of 60.3mol% DMF and 61.9mol% MF were obtained, Ru/C supported catalysts were required and neither DMF or MF could be detected when using the direct product of the preceding dehydration reaction as the feed for hydrogenation.

Unlike furfural, HMF is a solid at room temperature, therefore its use as a direct fuel is unfeasible; no previous studies into this have been undertaken. HMF possesses a melting point of approximately 30°C, therefore potential solidification of a fuel within a fuel tank in cold

conditions is possible. As a result, there is little possibility for its use as a drop-in fuel or fuel extender.

2.1.1.4. Levulinic acid and others

Both furfural and HMF can be treated further to form other platform molecules that may be used as precursors to fuels, or as fuels directly. Perhaps the most versatile is levulinic acid (LA) which, after undergoing esterification, forms levulinic esters which are used in the food industry.[36] More recently these esters have been considered as potential fuels,[66,67] given their appealing cold flow properties, as well as low toxicity; ethyl levulinate, for example, can be blended at up to 20% with fossil diesel.[68] This has been shown to decrease sulphur emissions in diesel engines, due to the dilution of sulphur bearing diesel, and does not require any engine modifications. Upstream, LA has the advantage of being sourced from biomass and can be sourced from both cellulose (HMF pathway) and hemicellulose (furfural pathway) fractions of biomass. After dehydration of C_6 sugars to HMF, LA can be produced by hydration of HMF in an acidic media, while furfural derived from C_5 sugars can be hydrogenated to furfuryl alcohol (FA), and then converted into levulinic acid via hydrolysis. The continuous and large scale production of LA has been proven in the Biofine process with yields of 70-80% achieved.[36] However, the esterification stage to turn the platform chemical into an ester is an energy intensive process and therefore alternatives away from esterification to produce fuels are necessary.
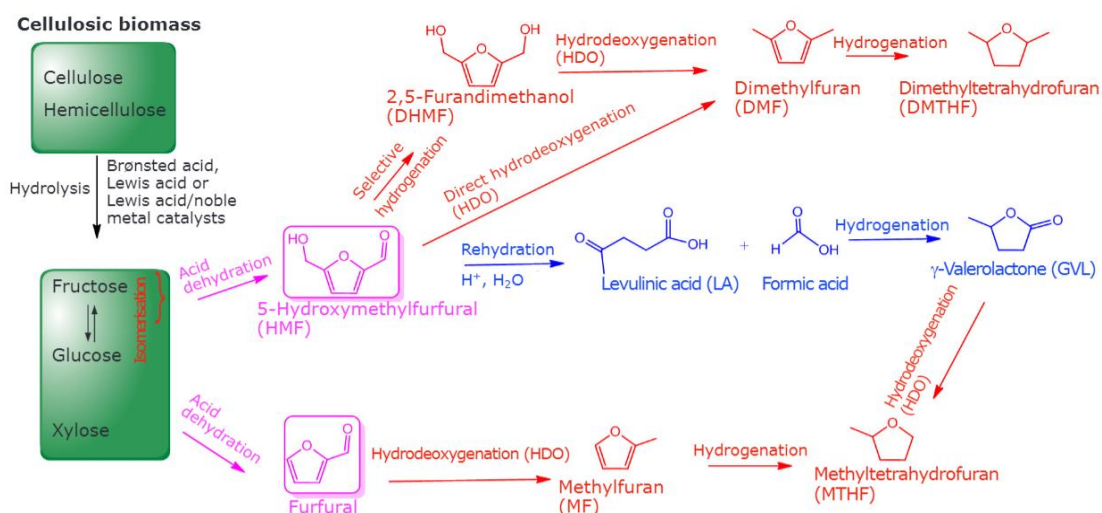
Figure 2.3: Overview of biomass to furan molecule processes[35]

HMF, furfural and levulinic acid are so-called 'platform chemicals' because of the number of possible derivatives each can be transformed into after further processing, some examples of which are given in Figure 2.3. These molecules, in particular, are important to mention because the bio-derived molecules described hereon-in will have been synthesised through at least one of these molecules. One of the major products of LA is Gamma-Valerolactone (GVL), a cyclic ester, which can itself be used as a reactant for the production of molecules such as methyl tetrahydrofuran and 1,4 pentanediol, which are potential fuel molecules. GVL itself has been shown to work as a fuel blending component in gasoline engines,[69–71] or can be used as solvent, but does require precious metals during conversion from the bioderived levulinic acid, therefore its production on a larger scale is problematic.[69]

Lignocellulose is composed of more than furan-based molecules- acids are another component that can be upgraded into value-added products. The production of lactic acid relies extensively on its formation from biomass (the rest from petroleum derived sources) with bacterial fermentation techniques.[28] The annual worldwide production of lactic acid is in the region of 400,000 tons/year, and can be used in the food industry, or in the formation of other

chemicals such as propanoic and acrylic acid (via dehydration) or polylactic acid.[61] Further, its role in the formation of possible liquid fuels has also been explored, as it can be used in the formation of butanol and pentanol. The alcohol and acid groups on either side of this molecule mean that a variety of transformations can take place. However, while this is another exciting prospect of using biomass to produce liquids that can be blended with current market fuels, extensive processing involving C-C cleavage, C-C coupling and hydrogenation is required. Serrano-Ruiz and Dumesic evaluated the catalytic processing of lactic acid into a variety of useful chemicals, including alcohols and ketones, but a platinum catalyst was required for the initial processing and, in order to obtain higher yields of alcohols, an Ru/C catalyst was required for the conversion of ketones into alcohols.[72] It is important that the cost of producing the fuels does not outweigh the benefit of using them in fuel blends, and for this reason the requirement of precious metal catalysts in these processes is concerning. Moreover, an undoubted environmental penalty comes with a greater use of precious metals; the extraction and processing of these materials will bear their own energy costs. Succinic acid can be obtained from biomass via fermentation broths, although unlike lactic acid, its current production relies mainly on petroleum sources. It too can undergo a variety of subsequent processing steps, possessing two carboxylic acid groups that can be used in upgrading strategies. Hydrogenation in particular allows the formation of some potential biofuels (particularly in gasoline given their small molecular structures), such as THF and gamma-butyrolatone (GBL). Again though, the high hydrogen pressures required (60 bar for 4 hours) and precious metal catalysts are conditions that should be avoided on larger scales.[28] Consideration should also be given to glycerol, one of the simplest sugar alcohols, which has a range of uses, including polymer production and pharmaceuticals.[35] Glycerol is obtained as a waste product of the transesterification of oils and fats with methanol for biodiesel production. The fact that the market for glycerol is therefore dependent on the production of biodiesel means that its price fluctuates considerably. As a result, the sourcing of glycerol from a more stable source is preferable; however, there is currently greater production of glycerol than demand for its

market uses.[73] Glycerol's high functionality (3 alcohol groups), makes it a very versatile commodity; dehydration, oxidation and hydrogenolysis can be employed to turn it into a number of high value products. Propylene glycol for example, produced from dehydration and subsequent hydrogenation of glycerol, is used in the pharmaceutical industry, as well as in paints and antifreeze. Converting glycerol into molecules relevant for fuel applications relies generally on reforming reactions. Henao *et al*[74] present a glycerol reforming + Fischer-Tropsch (FT) process that uses a Rhenium catalyst to convert glycerol into liquid hydrocarbons. Literature on the conversion of glycerol into oxygenated fuel molecules that may be used as fuel extenders is sparse; full conversion to hydrocarbons or dehydration into succinic acid or acrylic acid are more common routes to gain value added products, but etherification, esterification and selective oxidation are all potential methods for upgrading this molecule.[36]

The high complexity of lignocellulose is both its main drawback but also its greatest strength, as its possible uses in industry are numerous. The main consideration is the processing power required to reach the desired products from biomass, including the energy requirement as well as the cost of various catalysts and reagents. Most of the processing routes will go through certain platform chemicals, and based on their prevalence in lignocellulose, furans and organic acids are the major examples. However, some attention should be given to lignin, the third fraction of lignocellulosic material that has not been discussed.
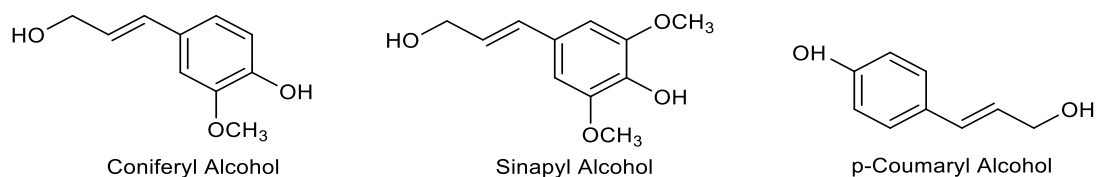
Figure 2.4: Major components of lignin

Lignin is the second largest fraction of lignocellulosic biomass after cellulose. It is a 3D amorphous structure consisting of substituted phenol polymers; three monolignols (coniferyl alcohol, sinapyl alcohol and p-coumaryl alcohol) are able to cross-link with each other to form a complex structure which acts as a protecting barrier to the cellulose and hemicellulose structures in plants.[75] For replacement of petroleum derived products (fuels, polymers, resins etc) by production from biomass, it will be necessary to also obtain aromatic molecules from this source; lignin is the only direct source of aromatics in nature,[76] but is generally burnt as a basic fuel source in the pulp and paper industries. It is therefore underutilized,[77] attributable to its complex structure and resistance to disassembly, as well as the variations in compositions of different plant types; the ratios of the three monomers mentioned can be quite different.[34] Zhou *et al*[77] studied the lignin composition of a hardwood, softwood and herbaceous biomass using thermogravimetric and elemental analysis and subsequently pyrolyzed the different materials to determine the change in phenolic yields. Ultimately, they found that the herbaceous biomass bore the greatest potential due to the higher yields of aromatics obtained after catalytic pyrolysis.

Pyrolysis is one of the main techniques for acquiring the lignin fraction of lignocellulose.[78] Its low capital cost and simplicity are significant advantages over the alternatives, such as the organosolv process.[77] The pyrolysis method involves heating of the lignocellulose in the absence of oxygen; lignin decomposes into phenolic compounds which, along with furans, sugars and acids, can be recovered as 'bio-oil'.[77] However, since the pyrolysis of lignin

happens at higher temperatures than cellulose, yields of the monomers are relatively low, and more char is produced from the pyrolysis of lignin than cellulose. Alternative processes tend to employ the use of chemicals to extract lignin. A review by Lange *et al*[79] gives an overview of some of the current ways in which this can be achieved, including milled wood lignin, acidolysis and enzyme treated lignin. Kraft lignin is highly promising, given its availability from the residues of chemical pulping processes; in this case, the lignin is precipitated by controlling the pH. The organosolv process is also encouraging; this uses organic solvents to solubilise lignin and subsequent extraction is achieved through precipitation with water and distillation. The advantage of the organosolv process over the Kraft process is its use of more environmentally benign reagents- the Kraft process utilised sodium hydroxide and sodium sulphide, whereas the organosolv process can be employed using an ethanol-water mixture. Ammonia can also be used for lignin extraction in the ammonia fiber explosion (AFEX) method, but the ammonia necessitates recycling due to its toxicity and in order to reduce costs, while the lack of selectivity is a further problem.[34,80] As already discussed, there is not one pre-treatment method that can extract lignin in the desired purity and at reasonable cost. Physical treatments are generally used to reduce the size of the biomass components (generally through milling) but, depending on the size reduction required, are extremely expensive given the energy content of the treated biomass. The chemicals involved in chemical or physico-chemical methods, such as ammonia or sulphuric acid, are both toxic to the environment and difficult to handle- research into ionic liquids for pre-treatment has gained significant interest, but these solvents are highly expensive.[34] Nonetheless, the use of lignin as a source of aromatics could be vitally important for the continued supply of day-to-day chemicals. Aromatics are common reagents in the chemicals industry, although as a pure fuel they tend to be avoided in diesel engines due to their low cetane number; however, this makes them more suitable for spark ignition engines. Branched aromatics are more appealing for diesel fuels in this respect since long aliphatic chains increase the cetane number; for the use as a fuel blending component, molecules such as cylohexanol, ansiole, and phenylalcohol could be

employed, which can be derived from lignin via catalytic routes.[76,81] A review by Bu *et al*[75] into hydrodeoxygenation reactions of lignin outlines cyclohexane and toluene as primary products of hydrodeoxygenation of model lignin compounds (in this case, substituted phenols) while also noting that the reactivity of the phenols varies depending on the location of the substituted groups, with 'ortho' molecules demonstrating the lowest reactivity due to steric effects.[75] Due to the complexity of lignin, "model compounds" are often employed in studies to simulate lignin derived molecules; cresols, phenols and guaiacol are common examples of these, but in reality the feeds of the reaction will be a complex mixture of many molecules. Unknown feed compositions, as well as the cost of hydrodeoxygenation processes based on the use of precious metal catalysts, means that lignin-derived fuels may not be economically viable at present. In the future, however, as the understanding and economics of extracting lignin improves, its use in the production of aromatics may increase.

2.1.2.   Furan derivatives

Platform molecules are so-named because, in general, they are not useful as materials in themselves. Upgrading of these molecules is required; Figure 2.5 illustrates many of the possible derivatives of HMF and furfural that form as a result of these upgrading routes.
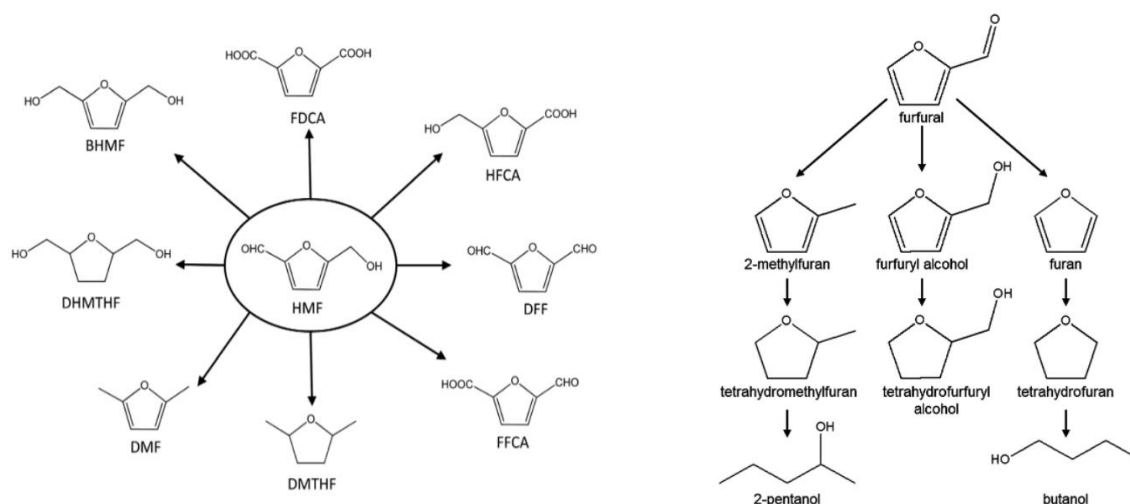
Figure 2.5: HMF and furfural derivatives[69]

These upgrading strategies tend to be energy and resource intensive, generally requiring expensive catalysts and hydrogen as a raw material.[44] Given that the production of hydrogen is still currently based on the use of fossil fuels via steam reforming of methane, its use in the production of a 'biofuel' undermines the goal of reducing the world's reliance on fossil fuels. The aim of some research[36,47,82] is to produce fuel molecules that match those of current gasoline, diesel or jet fuels; but in order to reach this stage, multiple processing steps are needed. As a result, the use of molecules that require fewer processing stages would be advantageous. Rather than undergoing hydrodeoxygenation reactions to linear alkanes, the intermediate furan derivatives can themselves be considered as potential fuels. Furfuryl alcohol (FA) can be produced via simple hydrogenation of furfural for example; alcohols have been extensively researched as fuel blenders/extenders, with notable reductions on pollutant emissions (especially particulates[83]). FA can be used to produce levulinic acid, another platform molecule, 2-methylfuran (a potential fuel), and has a range of uses itself, [69] including as a monomer for poly(furfuryl alcohol),

Figure 2.6: Major derivatives of furfural and HMF

Furfuryl Alcohol

2-Methylfuran

2,5-Dimethylfuran

Ethylfuran

which can be used in adhesives and binders.[84] Alonso *et al*[69] highlight that copper-based catalysts are used commercially to produce furfuryl alcohol through furfural hydrogenation, but the use of bimetallic catalysts for this purpose has also been published. For example, Vetere *et al*[85] were able to obtain high selectivity of furfuryl alcohol from the hydrogenation of furfural using bimetallic catalysts; tin and Pt/Rh/Ni catalysts. The tin distinctly increased catalytic activity, with conversion rates increasing from as low as 15% to 76% conversion. Gong *et al*[86] utilised a sulfonate group grafted active carbon copper catalyst to achieve almost 100% conversion of furfural to FA at 378K. They noted that this catalyst could also be reused without a loss of activity (a major issue with the use of a copper chromite catalyst) over 'several' cycles, although only three were reported.

2,5-Dimethylfuran (DMF) and 2-Methylfuran (MF) are attractive fuel prospects based on the relatively limited processing required for production; these can be produced from HMF and furfural respectively via hydrogenation of the carbonyl (and alcohol) groups on these molecules.[44] Extensive studies of these molecules in particular have been performed, including both diesel and gasoline blending tests in engines, which will be discussed later in Section 2.2.2. The main reason for this interest is the high energy density of both molecules, higher than ethanol and approximately equal to gasoline[35], while the high octane number (119 for DMF and 103 for MF) makes them particularly appealing in spark ignition based applications. A review by Johnson Matthey predicts that the main reason for the limited application of DMF in reality is due to the lack of a cost effective production pathway. The same review outlines a number of examples of research into this area, including notable work by Wang into the use of PtCo nanoparticles to obtain a 98% yield.[87] However, it is clear that in order to achieve such yields, highly complex and expensive supported catalysts are required, and with one active metal alone, the yields drop considerably. The long reaction times also help to explain the lack of any industrial-scale plants. A Palladium (Pd) based catalyst system has achieved 100% conversion to MF via the hydrodeoxygenation of furfural at 180°C and low hydrogen pressures, making MF an exciting prospect for use as a fuel extender.[35] Selective hydrogenation of these molecules (MF particularly) can yield furan itself. The low carbon-oxygen ratio makes this an unlikely fuel blender, but it is worth consideration, particularly when comparing to MF and DMF, so that the impact of the additional methyl group(s) branching from the furan ring can be elucidated. Tetrahydrofuran (THF) can be obtained with full hydrogenation of MF or DMF[36], which possesses a higher energy density than furan. The major use of THF is as a solvent, but its use as a fuel extender is of interest; a discussion of the saturated analogues of furans can be found in Section 2.1.5. Longer chained furan derivates, such as Ethylfuran (EF) and Butylfuran (BF) are also possible to synthesise, albeit only on small scales at this stage.[88]

2.1.3. Synthesis of furanic ethers

Both DMF and MF discussed in Section 2.1.2 have been shown to work as blends with fossil diesel in compression ignition engines,[89–94] while ethylfuran and butylfuran have been evaluated to determine their ignition delay and therefore their applicability in diesel engines.[88] Yet, it is more likely that any future diesel fuel will resemble molecules found in current diesel fuels. This will mean longer chained branches off the furan base, but simply adding more carbon atoms to the alkyl branches is difficult due to the lack of a reactive species. However, another possible route, which has been extensively researched and sees many associated patents, is the formation of ethers. [95–100] The alcohol group on HMF and furfuryl alcohol (FA)- derived from furfural- can be utilised to produce longer chained ether components that possess higher carbon-oxygen ratios than the reactant and more suitable properties for applications as fuels in internal combustion engines. The fact that both HMF and furfural can be used as reactants means that the scope for the synthesis of these ethers is considerable. The etherification is generally achieved via the use of solid Bronsted Acid catalysts (such as Amberlyst-15[101] or active zeolites[102]), and therefore separation and reuse of the catalyst is not generally a problem. More problematic is the yield losses observed as a result of unwanted side reactions and the production of humins as the products react with themselves and polymerise due to the reactivity at the hydroxyl and formyl positions.[103] As a result, there is research on-going into the etherification of HMF and FA.[36,95,104–106]

HMF can be obtained easily after one chemical processing step via the dehydration of C_6 sugars. After etherification of the alcohol group, a carbonyl group will exist in the 2/5 position that will lower the carbon-oxygen ratio and therefore the energy density of the fuel. Acquiring an ether from FA instead may yield a fuel molecule with more appealing combustion characteristics (due to the absence of an aldehyde group). Regardless of the raw material, the overall process is the same; an alcohol reacts with the furanic molecule in the presence of a catalyst, and forms an ether with the removal of a water molecule. Work by Bell at the University of California looked in detail into the production of ethoxymethylfurfural (EMF) based

on its high energy density and favourable blending properties of up to 17wt%.[101] For longer chained molecules, diethers can also be synthesised, or a longer chained alcohol can be used as the reactant as opposed to ethanol. Butanol is one alternative, and is an appealing option based on its bioderived nature.[29] Bell's group also looked into the use of butanol,[98] and were able to tune the yield of resulting products by altering the reaction conditions; lower temperatures favoured the formation of the alkoxymethylfurfurals. Meanwhile, an investigation by Yang *et al*[97] used isobutene to form butoxymethylfurfural using a range of acid catalysts, including zeolites and liquid acids. Their justification for using iso-butene, rather than tert-butanol, was the higher yields and easier separation of the unreacted reagent. Work by Gruter[107] utilised tert-butanol, with conversions of only 49-59%.[108] Etherification of higher alcohols is preferable for synthesising diesel fuels since diesel range hydrocarbons can contain anywhere between 10 and 28 carbon atoms. Furthermore, the longer chained alkyl groups will reduce the polarity of the furan-based molecule and thus will exhibit an increase in blending quality. Work by Avantium on the process (a spin-off from Shell Labs which hold patents in this area), does state that the yields decrease as higher alcohols (up to octanol) are used in the etherification.[109] Overall, they conclude that the blending properties of methoxymethylfurfual (MMF) and EMF are too poor to be considered as realistic fuel blenders, and suggest that the corresponding diethers are employed. The use of diether-based furans as fuel blenders could be preferable, although this does require an extra processing step to reduce MMF/EMF (converting the carbonyl group of HMF or furfural to an alcohol) and subsequently performing etherification in the same way.[109] That said, work by Bell has shown that the dehydration of fructose and reduction/etherification stages can be completed as a one-pot synthesis, which would significantly reduce equipment costs on a larger scale.[98]

2.1.4. Other upgrading strategies

Etherification is not the only method of synthesising longer chained furan derivatives. A review by Biu *et al*[110] highlighted six major ways in which furanics can be upgraded into more stable and practical components; aldol condensation, hydroalkylation, diels-alder cycloaddition, piancatelli ring rearrangement, partial oxidation and dimerization.[110]

Aldol condensation is a common organic reaction, whereby two carbonyl groups react and couple in the formation of a new C-C bond. The reaction cited in this review sees two moles of furfural react with one mole of acetone to form a coupling product with 13 carbon atoms. This reaction can be both acid or base catalysed, and heterogenous catalyst using relatively inexpensive oxides- Mg-Zr or Mg-Al- has been proven to help carry out the reaction.[111,112] The product is water insoluble, which is a desirable fuel characteristic that makes it safer and easier to transport. With many upgrading routes, however, the C_{13} molecule is envisioned only as an intermediate to producing linear alkanes. The subsequent hydrogenation stages to a water soluble saturated analogue and then to the linear alkanes in the presence of precious metal/acid catalysts require 12 moles of hydrogen in total, making it a much less appealing option to produce liquid fuels.

Hydroxyalkylation-Alkylation (HAA) reactions are another way of upgrading furans; this method essentially pre-stabilises the reactive starting material, such as furfural, into intermediates that can then be utilized in reactions to produce desirable components. Such intermediates include furan and methylfuran, which can be used as feeds with any carbonyl containing molecule to produce coupling products with high numbers of carbon atoms. A study by Brown and Sawatzky determined that yields of these products reached up to 58% and 73% for furan and methylfuran feeds with acetaldehyde and butyraldehyde respectively.[113] The study also recognised that the methyl group in methylfuran enhances the molecules activity to react with the aldehydes used. As with the alcohols used in etherification, the aldehydes employed in this process could be high order molecules, thereby increasing the chain length further and hence making the product a more viable candidate as a direct fuel. Utilization of

different aliphatic aldehydes was shown not to drastically affect the yields, though the use of aromatic aldehydes did decrease the yield considerably.[114] The hydroxyalkylation process using methylfuran has been a major area of research by Corma *et al*[115,116] with the aim of producing long chained linear alkanes to be used as diesel fuels. However, the intermediates of this process, on initial observation, could be viable fuel blending molecules, which would then eliminate the need for costly hydrodeoxygenation stages. The 'Sylvan Process' (Figure 2.7) uses two moles of methylfuran with an aldehyde or ketone to produce an intermediate that, after hydrodeoxygenation, produces a linear alkane (11 carbons) with various R groups on the sixth carbon. The first MF molecule is hydroxyalkylated with the aldehyde/ketone, the resulting product is then alkylated with the next MF molecule to produce a molecule with two methylfuran molecules joined by a range of carbon atoms depending on the carbonyl compound involved in the reaction. Corma's group looked extensively at the effect of varying the aldehyde/ketone used, the catalyst and the reaction conditions. Butanal was suggested as the most suitable coupling agent as it can be bio-derived from butanol and produces a molecule that possesses 14 carbon atoms, making it ideal for diesel applications.[115,117]
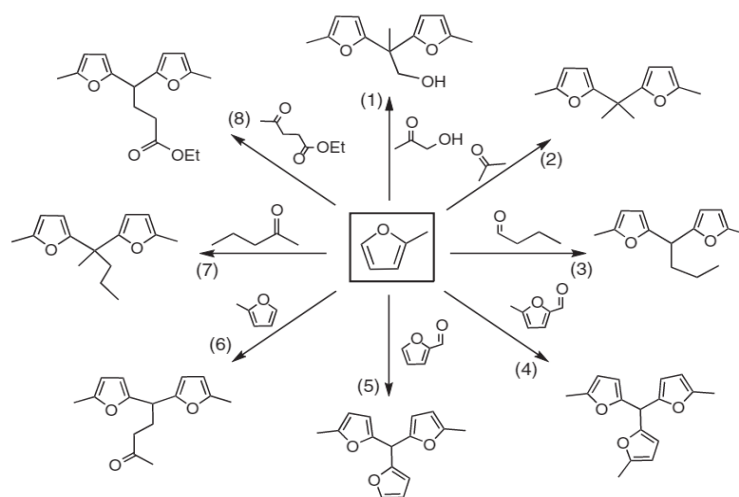
Figure 2.7: Sylvan coupling reactants and their products[110]

Ethanal, propanal and pentanal have also been tested, with high conversions and selectivity (>90%) achieved, indicating that the process is flexible, while the lack of any solvent

requirement is an economic benefit. Acid catalysts are required for the process; HCl is one possibility, but Corma's group utilised para-toluenesulfonic acid for the majority of their experiments, with 88% yields achieved when the MF to aldehyde ratio was increased. Zeolites were also suggested as possible catalysts in order to enhance results based on their high surface area and pore volume, the latter increasing accessibility for successful reactions. More recent work has looked further into the use of alternative catalysts that could act in the HAA and hydrodeoxygenation reactions to produce linear alkanes. Wen *et al*[118] used a combined acid catalyst with Pt nanoparticles to combine the hydroalkylation and hydrodeoxygenation stages so that methylfuran and butanal directly produced long chained hydrocarbons.[118] However, the product of the initial hydroalkylation reaction could be considered a potential fuel in itself, and this could negate the need for precious metals, since hydroalkylation only proceeds on the acid sites.

Other reaction mechanisms (diels-alder cycloaddition, ketonization, piancatelli ring rearrangement, partial oxidation and dimerization) are less relevant in the production of longer chained furan derivatives, and the removal of oxygen from the molecule completely may not be essential to acquire a promising biofuel. However, the importance of stabilizing furan bases such as furfural and HMF before their use in the production of upgraded molecules is clear. Furanics make up a considerable portion of the treated biomass, therefore even after fractionating this, furans appear in several other fractions. Their tendency to polymerize with themselves to form insoluble 'humins' means that forming more stable components is a major obstacle that needs to be overcome before they can be considered viable sources of biofuels.[110]

2.1.5. Saturated analogues

The selective hydrogenation of platform chemicals HMF and furfural can yield 2,5-Bis(hydroxymethyl)furan and furfuryl alcohol respectively under relatively mild conditions (120°C and 1atm[28]) and subsequent deoxygenation of these molecules will form DMF and MF. Alternatively, harsher hydrogenation conditions can be employed to produce fully saturated analogies of these molecules; Dimethyltetrahydrofuran (DMTHF) and Methyltetrahydrofuran (MTHF). More recently, a one-pot synthesis method of 2-butyltetrahydrofuran has been developed, utilising the aldol adduct formed from furfural and acetone aldol condensation, employing an Ru/C catalyst and achieving an 87% yield.[119] This aldol adduct has also been utilised in the formation of a number of fully saturated molecules, some of which are highly applicable for diesel blending, as shown in Figure 2.8.
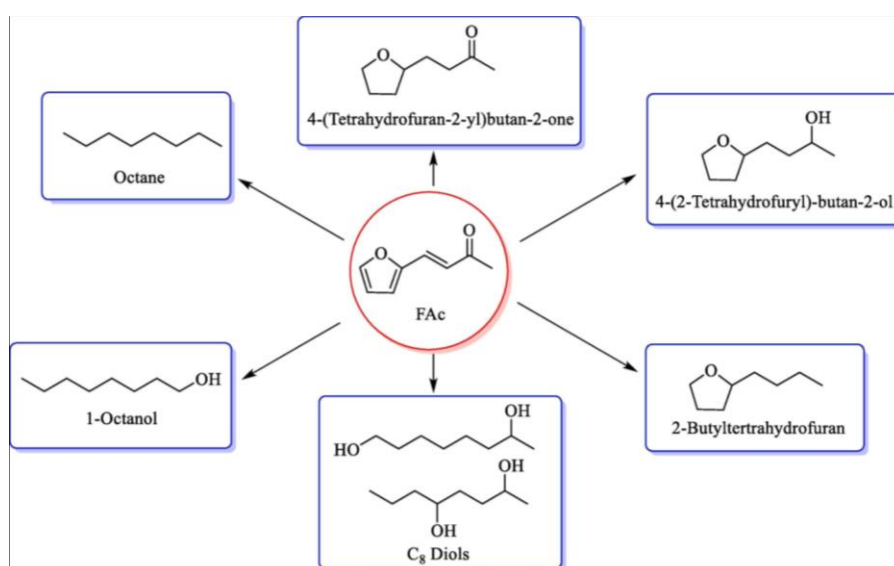
Figure 2.8: Potential products, including saturated furan analogues (tetrahydrofurans), from aldol condensation product of furfural and acetone[112]

Naturally, the harsher conditions employed here make the use of saturated analogues disadvantageous compared to the unsaturated versions from a production perspective; 20 bar

pressures and precious metal catalysts are routinely employed for this process.[28] In order to obtain THF itself, furfural can undergo decarbonylation to afford furan, which is then fully hydrogenated, and therefore necessitates the use of catalysts and harsh processing conditions. Nonetheless, THF and MTHF especially are already widely used, generally as solvents, but have also been shown to work well in fuel blends with gasoline (MTHF can be blended up to 60vol% in gasoline),[28] and therefore the production of these through biomass-derived pathways is an opportunity for a variety of sectors. The high blend ratios that could be employed using a saturated furan is an exciting prospect for strong market penetration, but it is important to compare the properties of these molecules to ensure that the advantages of their end-use outweigh the disadvantages of the extra processing required. Relating MF to MTHF, both possess similar boiling points, with that of MTHF slightly higher (80°C compared to 63°C).[120] The density of MTHF is slightly lower- closer to gasoline- which is beneficial for both blending and potentially during combustion, as the enhanced spray characteristics of a lower density liquid could result in a more homogenous pre-mixed phase, and therefore favourable emissions. The lower heating value of MTHF, at 32.8 MJ/kg, is slightly greater than MF at 31.2 MJ/kg due to the greater number of C-H bonds in the saturated molecule. Other than suitable physical properties, the research octane number (RON) of a molecule is a good indicator of its potential as a spark ignition fuel. A high RON is required in spark ignition engines in order to prevent engine 'knock' (autoignition of the fuel before the combustion flame has reached that point of ignition), as a higher RON means a greater ability of the molecule to resist auto-ignition. The RON of MTHF is relatively low at 86, whereas MF's RON is 103, more comparable with that of ethanol (119), which is currently used as a gasoline fuel blender.[120] This suggests that a saturated furan is more applicable to diesel applications due to their lower resistance to ignition (in diesel engines, a low RON and high cetane number (CN) is desirable). The CN of a fuel is a measure of its tendency to auto-ignite under high pressure and temperature, with a higher cetane number denoting a good candidate for a compression

ignition fuel. This scale is based on the ignition delay of two reference point fuels; cetane itself equals 100, while 1-methylnapthalene (which has poor ignition quality) is assigned a CN of 0.

Direct comparisons between saturated and unsaturated furans as fuels will be discussed in Section 2.2.2.4.

2.1.6. Lactones

Lactones are cyclic esters, and can vary considerably in their carbon number and ring size. ε-caprolactone, for example, is a medium size lactones in terms of its ring-size (7 membered ring), and is particularly pertinent due to its current array of uses, as well as its potential to be sourced from lignocellulose. Currently, the major production route utilised for this lactone is through fossil fuels; cyclohexanone is oxidised in the presence of peracetic acid, the latter of which is produced with the use of hydrogen peroxide, acetic acid and a strong acid catalyst.[121] These factors render this a particularly harmful and unsafe production method, and therefore more environmentally benign chemicals are being explored. However, the biotransformation route to synthesise this lactone is not easily scaled-up, and the demand for ε-caprolactone is extremely high, particularly in the polymer industry, including the synthesis of nylon, which has a demand of more than 25,000 tonnes. More recently, ε-caprolactone (εCL) production has been developed for 3D printing and for cell culture scaffold purposes.[121] There are numerous biopathways for the production of εCL; cellulose may be dehydrated to produce HMF, which in turn (as investigated by the study of Buntara[122]) can form 1,6-hexanediol through catalytic hydrogenation and hydrodeoxygenation, and subsequently the final lactone product. Alternatively, using cyclohexanone monooxygenase from Acinetobacter calcoaceticus and E-coli was found to produce εCL with a fed-batch system and cyclohexanol as the reactant.[121] This bioconversion generally suffers from low productivity and inhibition from both the substrate and product, while the enzyme itself suffers from poor stability. Schmidt *et al*[123] were able to overcome the product inhibition problem using a lipase from Candida antarctica that

results in a ring-opening oligomerisation of εCL, which produces a oligo-ECL that does not interact with the enzyme and can be extracted relatively easily through precipitation.[123]

δ-hexanolactone (δHL), as with other lactones, can be used as a relatively safe and natural food flavouring, but numerous patents have evaluated its use in the formation of esters and even in the formation of diesel-like fuel molecules for potential use in CI engines.[124–127] Microbes have been utilised to produce this lactone from acids[127] or from triacetic acid lactone (TAL) which may be derived from glucose and is subsequently hydrogenated to form δHL and, subsequently, γ-caprolactone (γCL).[128,129] γCL possesses a 5 membered ring and an ethyl chain from the 4th carbon. As with δHL, the interest surrounding this production of this molecule at industrial scale is significantly less than that for εCL. However, Gupta et al[129] show that it is possible to obtain these from second generation biomass (Figure 2.9). Both lactones have also been shown to naturally occur from fungus and even as pheromones in fruit flies and beetles.[130,131] Under anaerobic conditions, a fungus (Mucor genus) was able to produce both δDL and γCL with the corresponding carboxylic acids- this mechanism was patented in 1989.[132]
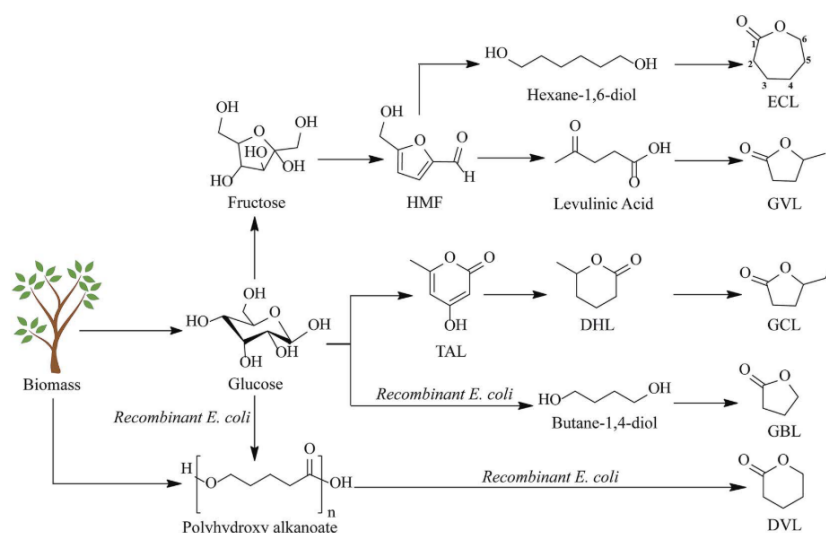
Figure 2.9: Production routes from 2nd generation biomass to the formation of the C6 lactones tested[129]

Lactones with higher carbon numbers can also be sourced from natural sources and are potentially applicable for diesel blends. γ-decalactone (γDL) has been used as a peach flavouring agent for the food industry in very low levels- possessing a detection threshold of just 0.088ppm- and was initially produced directly from fruits or via chemical synthesis.[133] Since γ-decalactone is classed a natural food flavouring agent, its bioderived nature is already proven. Recently, microbes have been used in the production of this molecule and, while the high cost of this production method is a drawback, Schrader notes that the optimization of the bioconversion of decalactone has contributed to a price drop from $10000/kg to $300/kg.[134] For the most part, production of this molecule utilises bioconversion of ricinoleic acid, which may be obtained from castor oil. The first occasion in which this lactone was observed in microbe growth was during the study by Tahara[135] in which a cell culture of Sporobolomyces odorus was analysed using GC-MS to detect the volatile compounds responsible for the fruity odour of the medium. Later, Lin conducted a range of studies investigating the use of Sporobolomyces odorus in the production of γ-decalactone, looking at how parameters including temperature and pH effected yield, also investigating the effect of the acid type used and time of addition.[136] In 1997, a study by Pagot *et al*[137] investigated the optimisation of bioconversion to γ-decalactone using genetically engineered Yarrowia lipolytica. This strain was designed to reduce the growth phase of the yeast as any elongation of this period tends to result in lower yields of product as a result of diverting energy and nutrients to growth. Neto utilised *Geotrichum fragrans* in investigations with enzymatically hydrolysed castor oil, and noted that γ-decalactone production was enhanced with the addition of the ricinoleic acid.[133] Ideally however, a single stage process could be employed, utilising the raw material alone and obtaining γ-decalactone in high concentrations. Moradi notes that castor oil is preferred, not only due to the reduced number of separation stages required, but because the lag phase for the yeast is shorter compared to other oil feedstocks.[138] This study employed both batch and fed-batch systems for the production of γ-decalactone from Yarrowia lipolytica, using castor oil itself as the substrate and obtaining promising results in the fed-batch system as this

minimised the inhibitory effect of the substrate. However, high agitation levels were required to maintain the necessary level of oxygen for the yeast cells, which was detrimental to the cell growth and product formation. Indeed, Aguedo *et al*[139] looked specifically at increasing the pressure of the Yarrowia lipolytica culture in order to increase O_2 solubility and enhance lactone production, noting that an increase in pressure is a more efficient method for boosting oxygen transfer rates compared to the high energy costs and shear stress associated with mechanical agitation.[139] Given that this molecule is already used in foods and flavourings, the large scale production of this molecule is better understood compared to other lactones.

Gamma lactones in particular are versatile in their use as flavouring agents in foods and cosmetics.[140] From its presence in a wide range of fruits, including apricot, peach, strawberry and mango, research has looked into the use of γ-dodecalactone (γDDL) in the aforementioned industries, possessing a butter flavour.[141] Hydroxy fatty acids (HFAs) can be used as precursors to the formation of this lactone, though only ricinoleic acid is found in nature in the quantities necessary for large scale application of the lactone.[142] For others, hydrolysis of vegetable oils, with subsequent hydration, tends to be required- although more recently it has been shown that microbes can once again provide a solution. Using bacteria producing oleate hydratases, these enzymes are able to hydrate acids such as oleic and linoleic acids- more easily obtainable from natural sources in the desired quantities- into the HFAs that yeast strains may use as a substrate for lactone production. Yeast strains are commonly employed for the production of gamma lactones due to the β-oxidation of these microbes that are able to convert 10-hydroxystearic acid (a HFA) to 4-hydroxydodecanoic acid, which then undergoes lactonization to form γ-dodecalactone.[140] An *et al*[140] proposed this synthesis route using Waltomyces lipofer yeast, and looked specifically at increasing the normally low conversion yield that occurs as a result of the low permeability of the cell wall and membrane. Using permeabilised yeast cells, reaction conditions were optimised to produce 75wt% conversion yield, an increase of 3.7-3.8 fold over non-permeabilised cells as the same conditions. A disadvantage of using yeast is the low conversion rates when using free fatty acids, as

opposed to hydroxy fatty acids such as the ricinioleic acid present in castor oil used to make γ-decalactone. In order to boost interest in utilising yeast to synthesise potential fuel molecules, increasing the range of sources that can be used is of high importance. Subsequent testing of various yeast strains by Jo *et al*[141] determined that Candida boidinii yielded the highest production of γ-dodecalactone out of the 11 strains tested, using a lipase-treated safflower oil hydrolysate- containing linoleic acid- as the substrate for the microbes.[141] The synthesis of γ-dodecalactone from microbes such as yeast has not been performed on large scale, thus further research is required for feasible techniques to use this as a potential biofuel. Despite this, it is promising that a variety of oils may be employed for its production, provided the necessary conditions and yeast strains are present and optimised.

An isomer of γ-decalactone, δ-decalactone (δDL) differs in that its ring possesses one more carbon atom at the expense of a carbon atom in the side chain. As with the vast majority of long chained lactones, the primary use of this lactone is in fragrances. δ-decalactone itself possesses a cream-coconut and peach aroma.[143] Corma *et al*[143] note that a large number of patents have been submitted relating to the production of this molecule, signalling that, irrespective of its potential use as a biofuel, research is already underway into larger scale synthesis. One of the main problems is the use of peracids which involve potentially explosive materials to synthesise and Corma's studies look into the use of more benign (heterogenous) catalysts that remove the need for an organic solvent.[143] However, biological pathways are generally of lower yield than that of the chemical routes- which utilise aldol condensation of cyclopentanone followed by hydrogenation and Baeyer-Villiger oxidation- and therefore the biological pathways have not been scaled up to the same degree.[144] On the whole, the production of δ-lactones, including decalactone, appears to herald less interest than corresponding γ-lactones, potentially due to the relative abundance of the γ-lactones. Brown *et al*[145] note that, on the whole, 6-membered rings tend to be more stable molecular structures, except in the case where exocyclic double bonds are present (as they are in the case of lactones). As a result, γ-lactones are likely more easily attainable from natural sources.

However, both 5 member (γ) and 6 member (δ) lactones are of interest due to their stability relative to larger and smaller ringed lactones, caused by the minimised bond angle strains for these structures.[146] δ-decalactone has promising production routes; in fact, provided the right species of microbe are present, it may also be formed from ricinoleic acid upon degradation of the acid by yeasts such as Candida tropicalis and Yarrowia lipolytica.[147] Alam *et al*[144] report a green synthesis of δDL using the product of fermentation of waste lignocellulosic material, such as sugar cane bagasse, and a one-step hydrogenation reaction in the presence of a heterogeneous catalyst to produce δDL via massoia lactone. Another appealing feature of this synthesis is that the hydrogen required, normally produced from fossil fuels, can be supplied in the form of formic acid, derivable from lignocellulose.[144]

The delta C12 lactone, δ-dodecalactone (δDDL), also possesses strong aromatic properties that render it of value to the flavour industry.[148] Furthermore, it has also been noted to be extractable from Kimchi and act as an effective anti-fungal agent; a use that could see considerable research attention from major pharmaceutical companies.[149] As with the other lactone species, microbes are put forward as the solution to synthesising this lactone through bioconversion. Van der Schaft *et al*[148] utilised baker's yeast (Saccharomyces cerevisiae) and Basidiomycetes fungi to hydrogenate the ring double bond found in the lactone present in Massoia bark oil, highlighting the low cost of such a system given the ease of obtaining these microbes.[148] Patents and studies related to the production and use of this lactone, as well as δ-decalactone, suggest efforts are already being made to understand the production of this particular molecule.[150–152] Bretler utilises the aforementioned β-oxidation and the bacteria Saccharaomyces cerevisiae to convert the hydroxy fatty acid (5-Hydroxy-2-decenoic acid) or 2-(do)decen-5-olide- derived from the Massoia bark oil referenced in van der Schaft's study- to the corresponding lactone.[152] Gupta references the fungi Tyromyces sambuceus and Cladosporium suaveolens in converting to δ-decalactone and δ-dodecalactone using ricinoleic acid and linoleic acid respectively.[147]

Common amongst all references is the use of microbes to allow the transformation of hydroxy fatty acids to the lactone, but a lack of a clear consensus as to which microorganism is most effective, nor where the most likely source of the HFA would be derived, suggests that scale up remains a long-term goal.

2.1.7. Hydrogen fuels

It is important to consider transportation methods using technology other than internal combustion engines. Electrification of the transport sector is rapidly progressing as emission regulations become more stringent and the industry converges on low carbon fuelled vehicles, however, there remains limitations; heavy duty machinery- such as HGVs and shipping vessels- continues to require diesel fuelled power units, in particular for the torque potential from these engines that operate at high compression ratios. Moreover, less developed countries will be slower to electrify as the necessary infrastructure is difficult to expand, and thus will likely continue to require more conventional ICEs as a primary means of transport. Hydrogen has been touted as a potential solution[153] as an energy vector of electrical energy. Hydrogen synthesis through renewable energy is possible- producing so-called 'green hydrogen'- but, today, most hydrogen produced using fossil fuels; 'grey' or 'blue' forms are formed through natural gas, with blue hydrogen formed where the carbon emissions are captured pre-emission, while 'brown' hydrogen is produced from coal. Hydrogen-fuel cells are potentially a solution for one of the major practical problems with electric transport- the time required to charge. If hydrogen can replace diesel and gasoline, refuelling methods would be largely unaffected for the consumer. However, while companies such as Toyota, Honda and Hyundai have produced cars that utilise fuel-cell technology, low efficiency as well as the continued safety concerns mean that uptake remains low. As a result, alternative means of utilising hydrogen indirectly, other than fuel cells (given the need for an entire hydrogen network), are needed. Ammonia has been touted as a possible solution. Ammonia-fuelled combustion is not a new concept, having been used to fuel buses in Belgium in the 1940s due

to a shortage of fossil fuels during the Second World War,[154] and even in army vehicles by the US military in the 1960s.[155] While this use of ammonia was employed in situations that necessitated the use of an alternative fuel due to unavailability of fossil fuel, it was a proof of concept that it was possible to run certain engines with an ammonia based fuel and this concept has received renewed interest in recent years given the need for low carbon renewable fuels. Hydrogen and hydrogen-derived fuel combustion will be further discussed further in Section 2.2.2.6

Before this however, Section 2.2.1 provides a brief overview of some combustion fundamentals to assist in the explanation of subsequent discussion of previous experimental studies.

2.2.   Compression ignition combustion and emissions

Combustion within a diesel engine is initiated by fuel injection into air that is heated by compression alone, as opposed to spark ignition (SI) engines, whereby ignition is dictated by the timing of a spark. The fuels used in CI engines are required to auto-ignite, and since there is no necessity to avoid auto-ignition and engine knock, diesel engines benefit from higher compression ratios, making them more efficient than the gasoline alternatives. Furthermore, the engine can operate unthrottled as the air flow is uncharged (torque is dictated by the amount of fuel injected), meaning that pumping work is lower and volumetric efficiency is not reduced; in throttled SI engines, the piston is effectively pulling a vacuum.[6] The higher compression ratio and longer piston stroke mean that diesel engines possess high amounts of torque, and are therefore used in heavy duty vehicles. While electric vehicles may be able to replicate the power of internal combustion engines, it is likely heavy duty machinery will be powered by CI engines for the foreseeable future due to the relatively limited capacity of vehicle batteries to date. A bio-derived diesel replacement is therefore a worthwhile endeavour. Before

potential bio-derived fuels are discussed however, it is important to look first at the fundamentals of diesel combustion.

2.2.1. Fundamentals

2.2.1.1. The compression ignition combustion process

The theoretical diesel cycle envisions a 4 stage process; isentropic air compression,

reversible isobaric heating, isentropic expansion and reversible isochoric cooling. In reality these idealized thermodynamic processes are not exact descriptions of the combustion process; instead, diesel combustion is a 'complex, turbulent, three-dimensional, multiphase process'.[156] As opposed to their thermodynamic cycles, it is instead more accurate to differentiate SI and CI combustion by the type of combustion

Figure 2.10: Typical in-cylinder pressure curve observed in diesel combustion engines[7]

occurring.[7] In SI engines, combustion is usually premixed as the fuel and air mixes during the compression stroke to form a near-homogenous air-fuel mixture that ignites when sparked.[7] CI combustion, however, is more complex as it occurs in both premixed and diffusion rate controlled phases following the ignition delay period which commences as the fuel is injected into the cylinder. Combustion is characterised by high turbulence and air-fuel diffusion as the oxidant diffuses into the fuel side of the flame and combustion products diffuse out of it. Both diffusion and pre-mixed combustion can be enhanced by turbulence, which increases the burning velocity and removal of burnt products from combustion zones, which would otherwise hinder combustion. Turbulence can be achieved through the use of pre-combustion chambers, though these have long been replaced by changes in combustion chamber geometry that

promote turbulence and greater fuel-air mixing with higher engine efficiency. It is important to note that gasoline engines involve some mixing-controlled combustion and diesel combustion involves a degree of premixing- Heywood suggests that, at higher engine loads, approximately 75% of diesel combustion takes place in the mixing controlled phase, with the rest pre-mixed. This can be observed in pressure curves, an example of which is shown in Figure 2.10; the end of pre-mixed combustion is seen at the local minimum (c) in the heat release rate curve after the initial spike, while diffusion-led combustion can occur as injection takes place and after as the remaining injected fuel is consumed.[157] The premixed combustion in diesel engines was an area of scientific contention during the 1980-90s and it took until 1997 in Dec's paper on using laser-sheet imaging to model the combustion flame for an accepted model to be agreed. Dec's model is shown on the right of Figure 2.11, with the 'old' model displayed on the left. Before this, the initial premixed phase was not even considered a source of soot formation, and most discussions were based on whether combustion occurred in a sheath that enveloped the fuel-air mixture or in a number of smaller droplet points.[156] Dec presented an alternative picture that contradicted many preceding views; premixed combustion was shown to lead to the initial soot formation and the majority of combustion in this phase proceeds under fuel-rich conditions (though initial ignition and flame propagation occurs close-to-stoichiometric) prior to reaching the diffusion flame (as opposed to the stoichiometric conditions that were widely accepted before). Diesel combustion simulations have utilised Dec's model for validation of various models; Tao *et al*[158] found that the use of an empirical two-step model, while easy to implement, does not agree with Dec's prediction that soot formation occurs initially in the pre-mixed reaction zone. Instead, this model predicted that soot formation begun close to the injector nozzle tip, whereas more complex phenomenological soot models agreed with Dec's findings.
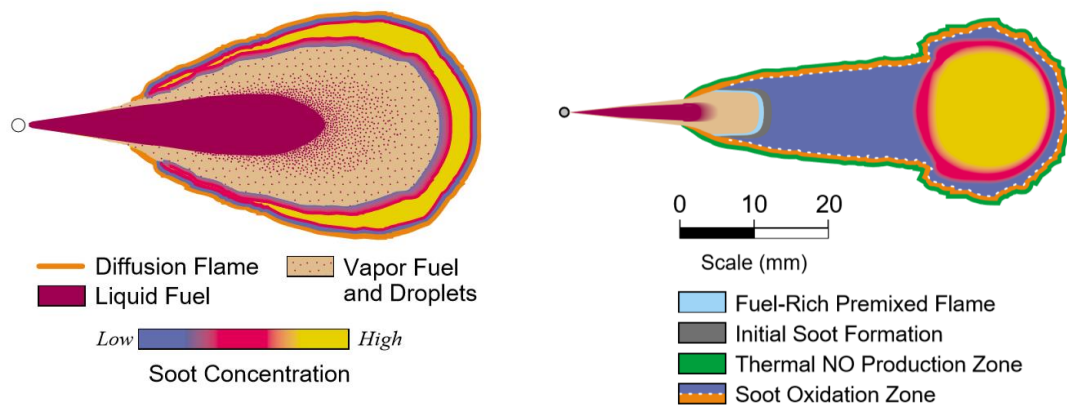
Figure 2.11: 'Old' (left) and Dec's (right) 1997 model of DI diesel combustion during the initial part of mixing controlled combustion[156]

For the diffusion flame itself, Dec's study indicated that the fuel in the combustion zone is all in the vapour phase and that soot formation may occur at any point within the fuel jet rather than only at the edges. The mixing phase of combustion is naturally slower than the premixed phase, as it is limited to the rate that fuel-air mixtures at the necessary ratios are able to form, and this is dependent on atomization, vaporisation, mixing and preflame chemical reactions.[6] As noted, the multiple fuel and engine dependent variables make diesel combustion extremely difficult to model. Work by Arregle and co-workers[157,159] validated theoretical studies using various heavy duty and high speed diesel engines to model the diffusion phase of combustion, predicting rates of heat release and altering parameters such as injection rate, nozzle diameter and oxygen concentration. However, modelling of other parameters such as emissions was not covered, levels of which produced are not only key in themselves, but give an indication as to the combustion process holistically. Heywood explains how high carbon monoxide (CO) concentrations in the spray region indicate that combustion occurring here is fuel rich; initially this forms only in the core of the spray but eventually expands to the cylinder walls where conditions are lean and oxidation is temperature limited.

The extent of the pre-mixed phase of combustion is dictated by the ignition delay period, which is a key parameter in dictating how combustion proceeds.

2.2.1.2. Ignition delay

The timing of fuel injection is controlled, but ignition does not begin immediately; the difference between the start of injection (SOI) and start of combustion (SOC) is termed the ignition delay (ID) period, and is dictated by both physical and chemical properties associated with the fuel.[6] The physical properties include the viscosity, density and flash point of the fuel, and are generally associated with the fuel's ability to atomise and vaporise and form a flammable mixture with the air that has been entrained. For example, a highly viscous fuel will be less able to break apart into small droplets and vaporize as breaking up the liquid fuel spray requires greater shear forces. These physical fuel properties provide an initial indication as to the viability of a given fuel, but the chemical properties will dictate whether the fuel will combust effectively once the necessary conditions have been met. Furthermore, the physical properties of a fuel have only a minor effect on ignition quality in warm engines. Before understanding how a molecule may have a higher tendency to ignite compared to another, it is important to discuss the initiation reactions that begin combustion. There are numerous reports and investigations into the initial stages of combustion; Westbrook,[160] for example, highlights the sequence of reactions starting with initiation, followed by propagation, branching and termination. The initiation reactions amount to a production of radicals species from stable ones, though Zador[161] notes that these reactions are very slow e.g. the abstraction of hydrogen with molecule oxygen:

$$RH + O_2 \rightarrow R^. + HO_2 \qquad \text{(Eq 2.1)}$$

Zador states that it is the propagation reactions that dictate the availability of radicals required for auto-ignition, with these radicals forming a further range of species, including alkylperoxy radicals, alkenes and cyclic ethers, upon reacting with oxygen. The actual radicals

formed have been shown to be dependent on temperature and pressure; the alkylperoxy radicals become unstable at high temperatures and are hence found only at lower temperatures. Since the initial reaction pathways dictate the composition of radical species subsequently present, these initial propagation steps determine the remaining course of combustion. Westbrook notes that propagation does not increase the radical pool, but converts radicals into different forms that may be more reactive and allow the reaction sequence to progress. The alkene production route, for instance, produces a stable HO_2 species that essentially terminates the reaction. However, alkylperoxy radicals can undergo 'internal H-atom abstraction'[161] to produce a hydroperoxyalkyl radical, an isomerization reaction. This process may continue, but chain branching reactions can also ensue as a result of the attack of oxygen molecules onto the isomerization product. In branching reactions, the radical pool increases, the simplest of which is the consumption of one hydrogen radical and an oxygen molecule to produce an O and OH radical. Ultimately, there is a balance between propagation, isomerization, branching and termination reactions, and the conditions dictate the composition of radicals in the pool which will have a bearing on further fuel breakdown. Considerable modelling efforts have been made in attempts to predict how combustion proceeds with different fuel and reaction conditions. While the specifics of these are out of the scope of this review, it is important to mention the importance of these simulations in increasing understanding in this field. Much focus has been based upon the hydrogen abstraction mechanism that is so important in the combustion process. Huynh *et al*[162] studied this using transition state theory in order to obtain rate constants for the abstraction reactions, while Hu and co-workers[163] used a similar method on hydrogen abstraction from propane by hydroxyl radicals. Hu highlighted six different reactions with fourteen potential products of these. This highlights the need for simulation techniques to determine the rate constants of possible reactions and help elucidate the 'dynamical properties' of combustion.

2.2.1.3. Heat release rate and in-cylinder pressure

After the delay period, the net heat release rate (HRR) will become positive, denoting the start of combustion. The HRR is defined as 'the rate at which the chemical energy of the fuel is released by the combustion process' and can be measured using the cylinder pressure and instantaneous in-cylinder volume at a given crank angle degree.[6]

Whitehouse and Way[164] state that the chemical kinetics at the start of the subsequent combustion phase are important as the burning rate is low, and in fact apparent negative heat release will initially be observed as heat is transferred to the walls and is also used in vaporizing and heating the fuel. This paper also refers to the use of single-zone models to attempt to correlate predicted and experimental heat release. However, in diesels there exists a stark contrast in composition and temperature between the combustion zone and unused air, necessitating more complex models. More recently, a multi-zone model for diesel engine combustion has been favoured, as single zone models cannot predict emissions. Single-zone models over-predict engine peak pressure, while multi-dimensional models require CFD that is complex and expensive.[165] The model used, which divided the cylinder into 3 zones before injection (inner, boundary layer and crevice zones), contained 76 species and 327 reactions and allowed for mass and heat transfer zone to zone and zone to wall. It ultimately produced results in good agreement with the experimental data for in-cylinder pressure, SOC and NO_x and soot emissions.
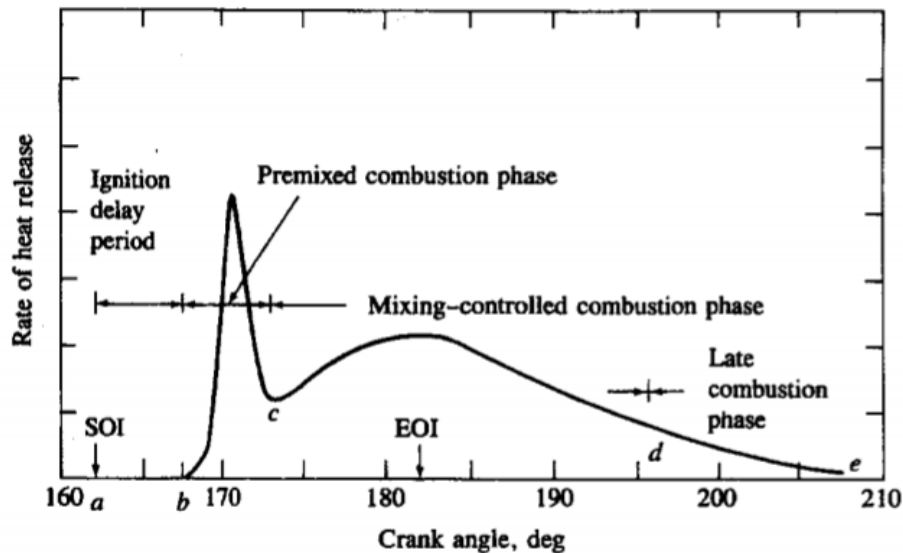
Figure 2.12: Typical heat release rate curve in a diesel combustion engine[6]

Rapid combustion ensues as the fuel in the premixed phase rapidly reacts and expands. Eventually, a thin diffusion flame will encompass the premixed zone (not dissimilar to a Bunsen burner flame with the air inlet collar open) until the time that the premixed phase has been exhausted and the diffusion flame then envelops the fuel spray. At this stage, combustion is controlled by diffusion and is therefore dependent on the rate at which the fuel and air can both diffuse and combine to form a combustible mixture. This phase, as shown in Figure 2.12, is longer and emits lower heat release rates than the initial pre-mixed phase. Changes in engine conditions naturally have a large bearing on combustion phasing relative to position of the piston. The first stage of combustion (the initial phase which lasts only a few CAD is characterised by a sharp rise in heat release) depends predominantly on the magnitude of the ignition delay, which is shorter at higher loads due to higher in-cylinder temperatures accelerating reaction rates.[6] Meanwhile the overall burning rate increases proportionally with engine speed. While ignition delay period is governed primarily by the fuel properties, the heat release rate and in-cylinder pressure are generally controlled through changes in the engine's operating conditions. For example, the peak cylinder pressure can be reduced by retarding the injection timing or by reducing the rate of initial fuel injection. Generally, the peak heat release

is designed to occur at around TDC, and depending on the load, a single (light load) or double hump (high load) plot is observed; the second lower peak being a result of mixing controlled combustion (this can be greater in magnitude than the first peak at high load conditions).[166] As emissions are a major consideration in engine design and operation, delaying the timing of peak HRR, after TDC, is employed to lower combustion temperatures and hence reduce emissions of NO_x.

2.2.1.4.   Efficiency and fuel consumption

A low fuel consumption without compromising the engine's performance is of high priority in the design of a new engine or fuel. The specific fuel consumption evaluates the fuel flow rate for a given power output, an effective parameter to determine the engine's efficiency in turning chemical energy into mechanical energy. For CI engines, this value can be below 198 g/kWh, while for SI engines the consumption is higher with a typical value of about 270 g/kWh.[6] The fuel conversion efficiency is another value, in this case dimensionless, that can relate the amount of energy supplied by the fuel per cycle to the amount of work produced.

The fuel conversion efficiency is not the only efficiency to consider in internal combustion engines because the combustion of the fuel is not the only stage where the system will experience losses. For example, volumetric efficiency demonstrates the engine's ability to induct air, and therefore the extent to which the intake system restricts the amount of air that can be inducted. Meanwhile, the mechanical efficiency is defined as the ratio between the brake power and indicated power, the difference of which is attributed to frictional losses i.e. energy required to overcome the friction of mechanical components.[6] These parameters may not be used specifically in the subsequent investigations, but it is important to note the numerous areas that can explain why the work produced is lower than the theoretical energy input.

2.2.1.5.   Emissions

The emissions of an ICE are an array of different molecules that are formed during the combustion process. Carbon monoxide (CO) and unburnt hydrocarbons (UHCs) for example, are products of incomplete combustion, and demonstrate a lack of effective fuel-air mixing as these products form from zones that are fuel rich (oxygen deficient). Emissions can be controlled to an extent by changing the ignition timing, load and stoichiometry of the engine; it is important to note the relative importance of these variables on specific emissions.

Nitrous Oxides (NO$_x$): Emissions of NO$_x$ are a common problem with diesel engines due to their lean operation and high peak temperatures when pre-mixed combustion is not adequately controlled. However, since the highest temperatures occur close to fuel rich zones where there is little oxygen, a trade-off between parameters is necessary. Stone[7] explains that the maximum NO$_x$ will occur just lean of stoichiometric, where there is both the necessary oxygen and temperature present. The overall reaction is known as the Zeldovich, or thermal mechanism, since it is highly dependent on temperature.

$$O_2 \leftrightarrow 2O \qquad \text{(Eq 2.2)}$$

$$O + N_2 \leftrightarrow NO + N \qquad \text{(Eq 2.3)}$$

$$N + O_2 \leftrightarrow NO + O \qquad \text{(Eq 2.4)}$$

An additional reaction was identified by Lavoie *et al*:[167]

$$N + OH \leftrightarrow NO + H \qquad \text{(Eq 2.5)}$$

Together, the Zeldovich and Lavoie reactions are termed the Extended Zeldovich mechanism and is prevalent when temperatures greater than 1800K are maintained for a sufficient time i.e in the hot products of combustion. A 'prompt' mechanism and nitrous oxide mechanism were also derived, but these are only significant when there is fuel bound nitrogen

(many cetane booster fuel additives contain nitrogen) or at very low temperatures and lean conditions that are unlikely to be met in CI combustion. The effect of fuel bound nitrogen on NO_x emissions is complex; Bar[168] looked into the effect of hydrazides on the formation of NO_x, since these groups could in fact act as reducing agents of NO, but determined that there was little influence since the reducing agent needed to be released in a narrow window to operate effectively.[168] Dilmore and Rohrer, however, concluded that fuel-bound nitrogen (in the form of pyradine) present within a fuel had a large effect on the overall NO formed, but that the impact decreased as the percentage of nitrogen was increased. It should be noted that their study used a gas turbine combustor instead of an internal combustion engine.

$$(Prompt): \qquad CH + N_2 \rightarrow HCN + N \qquad \text{(Eq 2.6)}$$

$$(Nitrous\ Oxide): \qquad N_2 + O + M \rightarrow N_2O + M \qquad \text{(Eq 2.7)}$$
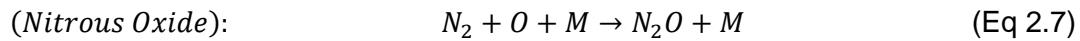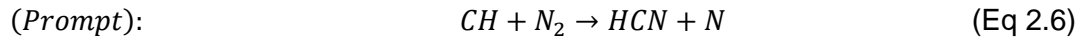
NO_x emissions are inescapable during combustion involving air as the charge gas, but they can be abated by controlling certain engine parameters. The ignition delay period is one of the most important for determining NO_x emissions, even though little/no NO_x is formed during this time. This period of fuel/air mixing will dictate the amount of pre-mixed fuel/air mixture available at ignition for rapid combustion, and therefore the high in-cylinder temperatures which encourage NO_x formation. A longer ID (therefore greater premixing time) can see a sharp rise in peak cylinder temperature and pressure when combustion does occur and, at low loads especially, this will increase the likelihood of meeting the necessary temperatures and providing sufficient levels of oxygen to form NO_x.

Carbon Monoxide (CO): CO impairs the ability of blood to transport oxygen around the human body, causing various symptoms (slow reflexes and confusion) depending on the CO concentration inhaled.[169] According to Heywood,[6] the formation of CO is due to the overall fuel/air equivalence ratio and therefore, since diesel engines operate at lean conditions, are not of major concern in compression ignition engines. However, it should be noted that while

CO emissions are more prevalent in SI engines due to their close-to-stoichiometric operating conditions, diesel exhaust emissions still consist of CO in an order of a few hundred ppm level (similar to NO_x). It has been shown that CO emissions are emitted from lean combustion if the fuel spray droplets are too large and atomization poor, as in the case of highly viscous fuels. In all, CO emissions are predominately seen as an effect of incomplete combustion caused by a local deficiency in oxygen (even if the overall mixture is lean). The globally lean combustion of diesel fuels means that there is lesser scope for CO production, but relative increases or decreases in CO levels can provide an indication as to how the combustion proceeds as a whole. Greater rich zones will see an increase in CO formation; therefore, higher CO emissions could be caused by a fuel with shorter ignition delay, or one that is more viscous, resulting in poor atomization.

Hydrocarbons (HCs): As with CO emissions, HC emissions are formed due to incomplete combustion of a fuel molecule, and therefore the types of hydrocarbons produced are heavily dependent on the fuel used and the engine operating conditions; HC emissions tend to be greater in diesels at light loads. HC formation is prevalent in the zone around the flame perimeter, which is overmixed and too lean to burn. Fuel remaining in the fuel injector nozzle sac following the end of injection enters late into the combustion chamber when conditions are not conducive to complete combustion and not all of this fuel will have time to burn completely.[7] The unburnt hydrocarbons (UHCs) around the reaction zone will contribute more to the final UHC exhaust emissions as the ignition delay period increases. This is due to an increase in the amount of fuel at the edge of the reaction zone, therefore a fuel with higher cetane number should see lower HC emissions. Fuel in the reaction zone tends to overmix with air when the delay period is long and can be close to the relatively cold cylinder wall, experiencing lower temperatures and flame speeds, quenching reactions and reducing rates of complete combustion.[169] HC emissions are low in diesel engines relative to SI engines, but are arguably one of the most important emissions to monitor due to the potential toxicity of the emitted material. Heywood highlights that all hydrocarbons exiting the exhaust, other than methane,

can be assumed to react (potentially forming photochemical smog). Since HC emissions can consist of a complex mixture of olefins, paraffins, aromatics and acetylene, it is vital that these emissions are monitored and alleviated by post-treatment technologies. It is important to note that the level of hydrocarbons exiting the engine cylinder will likely be higher than the levels reaching the atmosphere due to subsequent oxidation in the exhaust system. Many hydrocarbons are proven carcinogens while others produce smog upon exposure to sunlight, and oxygenates can often cause irritation of respiratory tracts. As a result, it is important to select fuels based on their potential for producing UHC emissions. For example, high proportions of aromatics in fuels produce more reactive hydrocarbons in the exhaust gases and are thus undesirable from the perspective of limiting health impacts from emissions.[6] Fortunately, in gaseous form, hydrocarbons are sufficiently dilute in exhaust gases and they do not cause major harm, but these molecules can condense onto particulates which can be inhaled. If sufficiently small, solid particles with adsorbed hydrocarbons can enter the lungs where the harm of the adsorbed hydrocarbons will be amplified.

Particulate matter (PM): Stone[7] defines particulate emissions as any substance that can be obtained by 'filtering diluted exhaust at a temperature of 325K (apart from water). As a result, this class encompasses a range of materials. Emissions of PM and HC are produced under similar combustion conditions, therefore the reduction of one should see a reduction in the other. However, the formation of particulates is complex and initiates with the reaction of hydrocarbon species into aromatic rings, which polymerize and eventually form the basis of a soot particle. A more detailed outline of these mechanisms will be given in Section 2.3. As with other products of incomplete combustion, particulates form in diesel engines as a result of a number of factors; such as fuel rich zones due to poor mixing, which causes fuel pyrolysis; and fuel dilution to the point where the fuel/air mixture is too lean and temperatures too low for complete combustion to occur. The initial formation of soot is a highly debated area of combustion research, with a full understanding yet to be acquired due to the chemical complexity of fuel combustion. More predictable physical processes dictate the growth of the

soot nuclei formed in the high temperature reaction zones. Coalescence is one of these processes, which involves particles merging together to produce one larger spherical particle. Agglomeration is the other particle growth mechanism; in this case particles stick together in chains or clumps. The relationship between particle mass and particle number is highly complex, though oxidation (post formation) can reduce levels of both. As a result, a fuel that has a higher tendency to form soot during the combustion process may not produce the most soot overall; for example, fuel-bound oxygen may be able to contribute to this oxidation phase (this will be discussed in Section 2.3.4). Particulate oxidation is also an area that has been exploited to good effect in the automotive industry using after-treatment technologies. These methods have been used to reduce the amount of PM in the exhaust stream, where emissions post-combustion exceed legislated levels.

2.2.1.6.   After-treatment technologies

Post treatment of combustion gases is an effective way of reducing overall emissions when changes to the fuel (use of additives) or engine design (changes in air motion) cannot achieve the necessary results. Generally, exhaust gas recirculation (EGR), an in-cylinder treatment technique, is the first remedy when emissions of NO_x are excessive. A fraction of exhaust gases are allowed to enter the inlet of the combustion chamber. This has multiple effects; lowering the flame temperature, diluting the level of oxygen from the intake air and altering the combustion process by introducing water vapour and CO_2 into the chamber, which increases the specific heat capacity of the in-cylinder charge. The main advantage of these effects is that NO_x formation is inhibited, primarily through reduced temperatures. This technique is attractive in diesels (with no turbo charger) because the higher pressure of the tailpipe compared to the intake pressure means connection of the two leads to recirculation without additional pumping.[170] However, this comes at a cost of increased particulate emissions as the amount of oxygen available for combustion and soot oxidation is reduced, particularly at high loads. Catalysts have been proven highly effective, if expensive, solutions to emissions that do not

meet European (Euro 6 as of 2014) or US (Tier 3/California LEV III) emission standards. While incomplete combustion products such as CO and HC can be thermally oxidised at high enough temperatures in the presence of a catalyst, utilising temperatures of over 700°C necessary for this oxidation is not practical in an engine exhaust; retarding the ignition timing can be employed to attain these temperatures, but this comes at a loss in efficiency. Oxidation catalysts (diesel oxidation catalysts (DOCs) in this case) are employed to reduce UHC and CO pollutants exiting the engine. The use of catalysts (which lower the activation energy required for a chemical reaction) means that this oxidation can be performed at temperatures of only 250°C;[6] this temperature can easily be reached after an initial heating period in a standard exhaust system. Rhodium can be added as a 'promoter' to Platinum in oxidation catalysts to lower the so-called 'light-off' temperature (defined as 'the temperature at which the catalyst becomes more than 50% effective'). Precious metals are a common choice in catalytic converters due to their resistance to corrosion from sulphur present in the fuel and high specific activity. Due to the cost of these metals, very high active surface areas are achieved using honeycomb-structured supports onto which the active species can be sprayed in the form of a washcoat. This results in an ultra-thin, porous catalyst layer (30–150 μm in DPFs). [171] This ultimately enhances the surface area available for the desired oxidation reactions. DOCs also reduce the total particulate mass formed in the engine as the catalyst is potentially able to oxidise the soluble organic fraction (SOF) is oxidised quickly. This fraction is absorbed onto particulates and makes up approximately 30% of the total PM mass.[172]

NO$_x$ and PM are the main pollutants of concern in diesel engine use, and new treatments have been developed to meet the most recent Euro 6 requirements. To reduce NO$_x$, two-bed systems, three-way catalysts and selective catalytic reduction techniques can and have been employed. The first method requires rich conditions so that there are sufficient reducing species to reduce NO to N$_2$. This comes at a penalty in fuel consumption, and therefore three-way catalysts are preferable because the engine can operate at close to stoichiometric conditions; CO and HC are oxidised simultaneously to NO reduction. However, since diesel

engines operate under lean conditions overall, three-way catalysts cannot be employed for the alleviation of emissions in these types of engines. Selective catalytic reduction (SCR) technology is a relatively new technique of reducing NO_x emissions which is now necessary for diesel engines in order to meet regulations. A paper published in 2000[173] noted that SCR technology had been investigated for 'about 10 years' prior to that work, but only now is it required in new light-duty diesel engines. This requires an external reducing agent to convert NO into water and N_2:

$$4NH_3 + 4NO + O_2 \rightarrow 4N_2 + 6H_2O \qquad \text{(Eq 2.8)}$$

$$2NO + 2NO_2 + 4NH_3 \rightarrow 4N_2 + 6H_2O \qquad \text{(Eq 2.9)}$$

$$8NH_3 + 6NO_2 \rightarrow 7N_2 + 12H_2O \qquad \text{(Eq 2.10)}$$
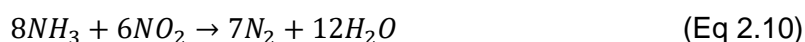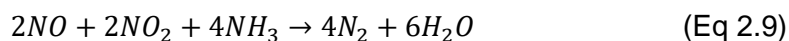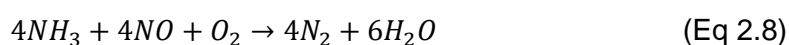
The reducing agent can be anhydrous ammonia, aqueous ammonia or urea, but for safety reasons urea is used today in commercial vehicles; the solution is atomized in the exhaust stream, forming solid urea which can decompose into

Figure 2.13: NO_x reduction from SCR treatment

ammonia and isocyanic acid gas. The latter readily hydrolyses forming ammonia and CO_2. Ammonia is the active ingredient in the reduction of the NO emissions, however it is important to avoid ammonia 'slip', which can lead to poisoning of downstream catalysts, by optimising the doping strategy and adding an additional oxidation catalyst downstream of the SCR catalyst.[173] SCR has distinct advantages over other NO_x treatment methods. For instance, the NO_x reductions are higher than in non-catalytic reduction methods, which is illustrated in Figure 2.13.[174] Furthermore, streams with low NO_x concentrations can be treated, the reactions occur within large temperature ranges

and no modifications to the engine itself are required.[171] The complexity, associated cost, freezing problems and storage space though are considerable drawbacks to urea-SCR technology. To overcome these shortfalls, hydrocarbon-SCR (HC-SCR) offers the potential of reducing NO_x emissions under lean conditions without the need of an external doping agent.[175] This technology has the potential to use exhaust gases or the diesel fuel as the source of the reducing agent after coupling with a catalyst system, rendering it an extremely exciting prospect given that a urea tank is not required and the lack of need of PGMs which are extremely costly. A penalty in conversion efficiency is experienced in these systems, though up to 70% conversion efficiency has been achieved using silver-based catalysts and optimisation in the delivery of the reducing agent into the exhaust.[176]

Particulates are arguably the most important pollutant to reduce, due to the health issues associated with the inhalation of these materials; the harmful chemicals that can be adsorbed onto them as well as the particulates themselves entering the lungs, causing respiratory issues, means they are heavily regulated; 2014 Euro 6 regulations limit emissions to 5 mg/km and the US tier 3 limit will be 1.9 mg/km in 2022.[177] The most common approach for particulate reduction is to trap them on a diesel particulate filter (DPF), where they can be oxidised once the mass accumulated has reached a certain level. Regeneration occurs by raising the temperature and introducing larger amounts of O_2 in the exhaust gases by running the engine in a lean of stoichiometric mode. The temperature is raised to the necessary level either by running at high load or catalysts in the DPF are employed to lower the temperature required for the particulates to oxidize. Particulate filters can be made of a number of materials and constructed into different forms i.e. ceramic filters can be monoliths, foams or fiber mats, while alumina coated wires and silica are also options. Essentially, the type of filter used depends on the application, each will have certain pressure drop and surface area characteristics that make them preferable to applications in small mobile engines or larger stationary plants.

After-treatment technology is a powerful way of reducing emissions exiting a combustion engine, however it should be considered a last resort given the additional cost of installing a

catalyst post-combustion and the potential detriment to efficiency. Ideally, the problems can be dealt with upstream, and while the engine design can be optimised, the fuel involved in combustion will also have a significant effect on the emissions.

2.2.2.   The use of renewable fuels in diesel engines

The use of renewable fuels in engines is advantageous as it reduces the world's dependency on fossil fuels, a finite resource that will eventually be exhausted; considering the growing population, alternative fuels are needed. However, this advantage is difficult to communicate to people until fuel shortages are reached and the price of petrol and diesel rises considerably; therefore there is still a reluctance to make major changes in the near future. However, another opportunity that these fuels offer, which is more immediately beneficial, is the potential reduction in toxic emissions from engine exhausts that their use may provide.

2.2.2.1.   Biodiesel

Biodiesel consists of fatty acid ester molecules, often blended in fossil diesel itself. In fact, 'biodiesel' was first used in 1893 by Rudolph Diesel, where vegetable oil was converted into fatty acid methyl ester (FAME) through the transesterification process.[178] Only the wider availability of crude oil fuel sources in the following years resulted in the use of fossil diesel fuel as we know today.[179] The sources of biodiesel are numerous; olive oil, peanut oil, coconut oil, soybean oil, rapeseed oil and palm oil are all edible oils that can undergo transesterification, while non-edible oils, such as those derived from algae, can also be used. However, while non-edible oils are preferable because they do not compete with food sources, the standard of the fuel from non-edible biomass may not meet the minimum requirements in legislation, such as EN 14214 (EU) or ASTM 6751 (US and Canada), and thus more extensive processing is required.[180] The composition of the biodiesel will naturally vary depending on the feedstocks used; rapeseed derived oil, for example, often contains high proportions of oleic acids. The

source used also varies depending on the location of its production; rapeseed oil is the main source for the EU, while soybean oil is more common in the Americas.[178] Inevitably, the properties of the biodiesel oil source will have an effect on the resulting fuel and its properties, and therefore its combustion characteristics in a diesel engine. In Mahmudal's review,[178] a table of properties of the crude oil obtained from different feedstocks is shown; cetane number ranged from 37.1 for sunflower oil to 51.5 for coconut oil. The heating value also varied slightly- 39.8 MJ/kg for peanut oil down to 37.8 MJ/kg for coconut oil. As a result, research into the use of biodiesel in ICEs tends to specify what type of biodiesel is being used. For example, research by Can *et al*[180] looked into the use of canola biodiesel blends at different blending ratios in fossil diesel. Canola biodiesel is derived from a type of rapeseed oil, and can be obtained from a single stage esterification process. The combustion of this in an engine saw beneficial effects on smoke, CO and HC emissions, but slightly higher NO_x emissions.

The use of biodiesel blends has long been researched,[179] but oxygenated fuels and additives in general have often been employed specifically to influence soot emissions, following the introduction of more stringent regulations of the mass of particulates permitted in exhaust gases. A study by Omidvarborna *et al*[83] used pure diesel and three different biodiesel types to investigate the impact on soot emissions. The major observation was that, for all three varieties of biodiesel, soot emissions were virtually eliminated, suggesting that the oxygenated species were highly effective in reducing/suppressing soot formation and, secondly, that the average diameter of the soot particles decreased as the proportion of oxygen in the blend was increased. This highlights that the oxygen content within the fuel molecule has a significant impact on the oxidation of agglomerated soot particles. This conclusion was drawn by comparing the soot particles emitted from combusting the same biofuel in different blend ratios and by comparing different biofuels for the same blend ratio. The group also noted, using Fourier-transform infrared spectroscopy (FTIR), that the degree of unsaturation of the biodiesel is related to oxygen content; as the level of unsaturation increases, so too does the oxygen content (a less saturated molecule possesses fewer H atoms, therefore the proportion of the

molecule made from oxygen is increased) and the soyabean methyl ester (SME), with the greatest degree of unsaturation, produces particles with smallest diameter (due to the higher oxygen content). A more systematic study into this effect was demonstrated by Hellier *et al.*[181] This study looked at algal, corn, groundnut, palm, rapeseed, soyabean and sunflower oils that had not been subject to transesterification and compared their relative structures to give an insight into the possible reasons for the different combustion characteristics. These oils contained differing compositions of fatty acids, from palmitic (a fully saturated, 16 Carbon chain) to linolenic (an 18 carbon chain with 3 double bonds), which naturally contributed to differences in emissions and ignition quality. The difference in compositions of these oils not only means that the molecular properties varies between each (the degree of unsaturation and average chain length) but also impacts the physical properties of the resulting fuel, which in turn impacts the combustion. For instance, all the vegetable oils exhibited lower peak heat release rates, potentially caused by the higher viscosity of the oils which inhibits fuel-air mixing. A resulting benefit of this is lower NO_x emissions, which tend to correlate with peak heat release rates. Soot emissions were in fact higher on a mass basis for vegetable oils relative to fossil diesel. This could be attributed to higher viscosities increasing the amount of fuel rich zones in the combustion chamber as a result of poorer mixing, however, considering only the vegetable oil, the correlation appears to match more strongly with the C:H ratio of the fuel molecule; increasing unsaturation (a higher C:H ratio) increases the exhaust particulate mass, a trend that is also observed in the case of pure hydrocarbons.[83]

More recently, biodiesels derived from 3rd generation sources have been employed in combustion tests. 3rd generation biofuels are obtained from the use of micoorganisms as feedstocks, such as cyanobacteria or microalgae. However, sourcing biofuels from algae is hindered by the issue of scale-up of such systems, with high capital and processing costs incurred.[182] The combustion studies to date in this field are in the early stages, and have focussed primarily on overall combustion parameters. Sathish and Singaravelu[183] utilised a blend of 80% diesel and 20% Chlorella vulgaris microalgae biodiesel in an unmodified diesel
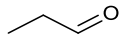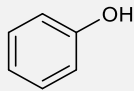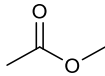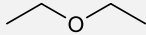
engine, noting a reduction in ignition delay with use of the blend, as well as higher cylinder pressures and a shorter combustion event. Karthikeyan *et al*[184] utilised a variety of blend ratios of S.Marginatum algae biodiesel in diesel, noting that the B20 blend produced the most flammable mixture. This was credited to the high quantity of unsaturated fatty acids and reduction in fuel viscosity. However, higher blends up to B100 noted an increase in ignition delay relative to B20, the potential cause of which is not explained.

While the results in literature often contradict each other due to the complexity of combustion chemistry and its sensitivity to small changes in conditions i.e. the load, speed and design of the engine the fuel is tested in, biodiesel appears to have several benefits, including a cleaner production, safer handling and lower sulphur content compared to fossil diesel. However, there are also drawbacks, such as poor cold weather properties, degradation over time and high viscosity which effects the long-term operation of the engine.[178] Blending with diesel does reduce these disadvantages, but there is a growing realisation that the future of biofuels does not revolve around edible-biomass sources.[182,185,186] If the future is not in biodiesel, then the scope for the makeup of a future fuel molecule is widened; nature is a versatile source, therefore it is important to understand which oxygenated groups are preferable to use as fuels in engines.

2.2.2.2.   Oxygenates

All organisms, plants included, contain carbon, hydrogen and oxygen based molecules. As previously mentioned, some efforts have been made to upgrade molecules derived from biomass to make them resemble molecules that make up conventional fuels.[115,187] However, this involves extensive processing and thus added cost and energy requirements. Therefore, it is likely that biofuels used in gasoline and diesel powered cars in the future will, at least in part, consist of oxygenated molecules.

Table 2.1: Types of oxygenated molecules

Oxygenate	General Formula	Example	Example Structure
Alcohol	ROH	Ethanol	
Aldehyde	RCHO	Propanal	
Ketone	RCOR'	Propanone (Acetone)	
Carboxylic Acid	RCOOH	Ethanoic Acid (Acetic Acid)	
Phenol	ArOH	Phenol	
Ester	RCOOR'	Methyl Ethanoate (Methyl Acetate)	
Ether	ROR'	Diethyl ether	

As shown in Table 2.1, there are a range of oxygen based functional groups that can be found in plants The presence of oxygenated functional group(s) within a biofuel molecule can impact on the resulting combustion and emissions. This could be through changes in physical properties and rates of fuel breakdown reactions that are influenced by the presence of oxygen to carbon bonds. A good starting point for this discussion is the study of Zheng *et al*,[188] who investigated the effect of alcohols, ethers and ketones on diesel combustion, using a 6 carbon structure as a control. 4wt% blends of cyclohexanone, cyclohexanol, 2,5-dimethylfuran, 2-hexanone, n-hexanol and isopropyl ether in diesel were prepared and tested in one cylinder of a 6-cylinder engine. Their deductions were that ignition delay increased for ring structures from ketone to alcohol to ether, and the cyclic molecules exhibited larger differences between oxygenates than the linear molecules. The chain molecules followed a different pattern,

however; alcohols exhibited longer ignition delays than ketones and ethers, which possessed similar delay periods. A potential factor in these patterns was the unsaturated nature of the cyclic ether used (DMF), making it an aromatic species which are known to possess low cetane numbers. The aromatic nature may have counteracted the effect of the oxygen's presence in the fuel on the delay period. The variance observed in ignition delay was found to impact on soot emissions in particular. Using additives to standardise the ignition delay, the authors were able to isolate the effects of the molecular structure and the delay period. Overall, looking at molecular structure alone, the soot emissions of the ethers were the lowest, while the alcohol blends emitted the highest particulate emissions. The relationship between the ignition delay and soot emissions was attributed to the longer ignition delay enabling better premixing of fuel and air, resulting in fewer fuel rich zones that are responsible for the formation of solid carbon particles as a result of the lack of oxygen. Another conclusion of the work was the apparent effect of changing the location of the oxygen group on the same molecule i.e. an alcohol group at the end of a carbon chain was less able to reduce soot emissions than one closer to the centre. Furthermore, emissions of hydrocarbons and carbon monoxide (CO) were also reduced with the addition of oxygenates (at high exhaust gas ratio rates), while there was little effect on NO_x emissions. A kinetic modelling study which preceded this investigation by Zheng was performed by Westbrook *et al*,[189] concluding that the C-O bonds present within oxygenated species reduce the amount of available carbon able to form soot. Moreover, since esters possess a carbon connected to 2 oxygen groups, this carbon is far more likely to form CO_2 than soot, since two carbon-oxygen bonds need to be broken; a study by Buchholz *et al*[190] determined that the carbon oxygen double bond in esters does not break at all during combustion. A recent investigation by Fang *et al*[191] used a burner to analyse the smoke point, and therefore soot inhibition ability, of a variety of potential oxygenated fuel additives. Overall, they observed an increase in the smoke point (denoting an increase in soot inhibition) from dimethylcarbonate and other esters to ethers and finally to butanol and ethanol; the alcohols were observed to decrease the sooting tendency of the fuel to the greatest extent.

Another study by Jenkins, Moore and co[192] also performed a systematic investigation into the effect of different functional groups in fuels. They discuss the overall benefits of an oxygen containing fuel, including the removal of costly processing and more complete combustion and therefore lower harmful emissions; also drawbacks, including the lower energy density, and the likely change in density and viscosity that could have a detrimental effect on combustion. Fuel density is an important factor to consider; too high and fuel atomization will be lower, which reduces combustion efficiency, while viscosity needs to be optimised so that it is low enough for adequate fuel atomization but high enough so that engine seals do not fail. [192] Another important point made is the potential degradation of oxygenated fuels. The lower stability could cause problems with storage, as corrosion in the engine itself, and may result in changes in properties that reduce the performance of the fuel. Jenkins[192] also states that secondary and tertiary alcohols are preferable to primary alcohols in reducing soot emissions, agreeing with the conclusions of Zheng. Furthermore, carboxylic acids as fuels are ruled out based on their poor low temperature properties (they are often solids at room temperature), and their polar nature makes them soluble in water and corrosive. Esters are preferable because they are less polar, but they too can have high melting points and possess a relatively low energy density due to their high oxygen content. Ketones and aldehydes are less polar than alcohols due to their lack of hydrogen bonding, and their solubility in water is lower, which is preferable for transport and in reducing the environmental impact of leaks. However, a detailed understanding of the effect of using aldehydes and ketones in engines is lacking. Ethers are the final group discussed, and often obtained via dehydration of alcohols. They cannot hydrogen bond with each other, therefore have lower boiling and melting points than alcohols of similar carbon number, but can hydrogen bond with water, making them slightly soluble. The cold flow properties of ethers compared to alcohols are an advantage, but the extra processing required for this could make this oxygenated group less appealing.

The cetane number of a molecule is an important characteristic for its use as a diesel fuel. A study into this parameter using an ignition quality tester (IQT)[193] looked at cyclic/acylic,

branched/straight, saturated/unsaturated hydrocarbons, alcohols, esters, ethers, ketones and aldehydes to determine the ignition quality of a range of potential bioderived fuels. This paper looked at validating the results rather than making direct comparisons, but the high cetane number of hexanal compared to butanol could not be explained purely by the chain length difference, suggesting aldehyde-based fuels could be beneficial. A study by Boot *et al*[194] gave an in-depth picture of the effect of different bonds in a fuel molecule on the potential effects of combustion (in gasoline engines in this case). They note that the presence of a carbonyl group will reduce the bond dissociation energy (BDE) of the adjacent C-H bonds but increase the BDE of the remaining bonds. H-abstraction is the first stage of combustion, therefore the addition of an oxygen group will have a fundamental effect on early stage combustion. The type of oxygen functional group will have different effects on the low temperature reactions that start combustion, and the change in BDEs of adjacent bonds explains why the location of the oxygen groups has an impact- for example, they note that 1-butanol has a shorter ignition delay time than its isomers (2-butanol, tert-butanol and iso-butanol). The low stability of aldehydes and ketones has been highlighted as a major barrier in their use as a fuel, and the emissions of aldehyde molecules is a serious concern from an environmental/health perspective. Ketones, being less reactive since the carbonyl group is not on the terminal carbon, are safer alternatives and are suggested as potential biofuels, and can be synthesised through fungal conversion.[194]

Overall, while theoretical experiments looking at different oxygenated groups is important, and will be of use in looking to design an 'ideal' fuel molecule, the practicality of synthesising oxygenated fuels on a large scale from biomass-derived sources needs to be considered too. As a result, the majority of oxygenated species used in engine tests are alcohols. Alcohols are another class of biofuels that can be produced from both edible and, more importantly, non-edible biomass sources. The fact that these molecules can be economically produced from biomass means that they are often the biofuel of choice, particularly in gasoline blends that involve the use of shorter chained alcohols such as methanol and ethanol. In diesel engines

however, higher alcohols are generally required because of their lower resistance to ignition.[194] Some studies into the use of alcohol-diesel are discussed, as well as in tertiary and quaternary blends with biodiesel and vegetable oils.

2.2.2.3. Alcohols

Ethanol is often blended with gasoline as a fuel extender, but it is not a suitable molecule in diesel engines because of its low cetane number and high latent heat of vaporization, making it resistant to autoignition.[29] The low flash point of ethanol also means that its incorporation into commercial diesel fuel would necessitate large changes in infrastructure due to the greater safety precautions required in handling a diesel-ethanol blend. Longer chained alcohols are required as their physical and autoignition properties would render them a more suitable diesel alternative, but the synthesis of these is generally from fossil fuel sources.

More recently however, medium length alcohols (and diols) such as butanol have been highlighted as potential diesel additives; these can be bioderived and possess greater miscibility in diesel, as well as a higher energy density and cetane number, than lower alcohols of methanol or ethanol.[195–197] Microbial production has been identified as a method by which longer chained alcohols can be produced on a large scale; Zeng and Sabra[198] discuss some recent developments in the production of 3 and 4 carbon diols from microbes and genetically modified E.coli strains in particular. 1,3-propanediol (1,3-PDO) for example can be produced using recombinant E.coli strains that first produce glycerol from glucose and subsequently 1,3-PDO from glycerol. Moreover, while no known metabolic pathways in nature produce 1,4-butanediol, work by the company Genomatica has engineered an E.coli strain with a synthetic pathway for butanol production from glucose or sucrose feedstocks.[199] Strains of Clostridium[200] and Escherichia coli, as well as the use of gas stripping or ionic liquids, have also been shown to produce n-butanol from feedstocks such as corn starch.[29] Kumar[29] highlights some key positives in butanol production, notably its ability to use the same feedstocks as ethanol and the ability to retrofit plants that currently produce ethanol to produce butanol instead.

Furthermore, since butanol is a larger molecule, breaking down biomass derived feedstocks to produce it requires less energy than to reach ethanol.[29] This favourable production, coupled with a higher cetane number, hydrophobicity, relatively low volatility and corrosiveness (compared to ethanol), makes butanol an attractive option for blending with diesel. Pentanol too requires only small energy quantities to produce via microbial fermentation from glucose.[201] As with butanol, its high energy density, low corrosivity and high flash point makes it another potential candidate for diesel blending. There are numerous examples of butanol/pentanol-diesel blends being used to test the performance and emissions of diesel engines.[185,201]

A study by Koivisto *et al*[202] analysed the effect of the hydroxyl group present in alcohols, relative to n-alkanes, in a systematic investigation of C8-C16 chain lengths. Overall, longer ignition delays were observed for all alcohols, but the location of the hydroxyl group was of high importance; when closer to the middle of the molecule, the ignition delay was longer. This in turn effects the emissions, with longer ignition delays tending to result in high in-cylinder temperatures and therefore greater emissions of NO_x. The changes in bond strength observed upon hydroxyl group addition is the main cause of this change in ignition quality. H-abstraction is the first stage of combustion, and the presence of alcohol groups hinders H-abstraction; secondary alcohols (alcohol groups bonded to carbon atoms that are bonded to 2 other carbons) impede H-abstraction more than primary alcohols. In all, the addition of alcohols will undoubtedly result in a change in the emissions and engine performance. While longer chained alcohols tend to result in better ignition quality,[202] synthesis of C_{16} alcohols is not currently feasible on a large scale, especially from bio-derived sources. Consequently, the majority of research into diesel-alcohol engine tests has been based on butanol and pentanol.

A review by Babu *et al*[201] gives a thorough analysis of the synthesis of butanol and pentanol, and subsequent emissions tests using these alcohols in blends and as pure fuels. The use of fermentation for producing butanol has long been an effective technique; acetone-butanol-ethanol (ABE) fermentation has been used since World War One, and has since seen ionic liquids, gas stripping and super critical extraction used to boost the butanol yield

specifically. Work by Rakopoulos *et al*[73,203] investigated the effect of using different blending ratios of butanol in diesel on exhaust emissions and engine efficiency; they also suggested that the anaerobic fermentation of glycerol to produce butanol makes its use as a fuel blender highly interesting. In this case a bus engine was used, and the resulting emissions saw a reduction in soot, NO_x and CO emissions, but an increase in HC emissions relative to diesel-only operation. The authors hypothesized that the soot/CO reduction is caused by greater oxidation of soot/CO due to the fuel bound oxygen in butanol, while the NO_x reduction is due to lower combustion temperatures (although the lower cetane number of the higher butanol blends should mean that there is greater pre-mixed combustion and therefore higher peak temperatures). Furthermore, they postulated that HC emissions increase due to poorer mixing due to slower evaporation of the higher butanol blends. In terms of engine performance, the lower calorific value of butanol inescapably leads to higher fuel consumption, though the brake efficiency is higher, suggesting that the combustion itself is more efficient. The authors explain that the increase in premixed combustion as a result of the longer delay period in the blends allows for a greater proportion of 'constant volume' combustion, lower heat losses and leaner combustion overall.

Later work by Yilmaz studied the effect of using 5, 10 and 20 vol% butanol blends, though this time in biodiesel, and compared them to tests of 100% diesel and 100% biodiesel.[204] The results were complex; butanol blends produced lower emissions of CO, higher emissions of NO_x and no change in HC emissions compared to diesel, except for the 20vol% blend, which produced higher HC and CO emissions but lower NO_x. The effect of adding butanol to biodiesel was similar to adding butanol to normal diesel with the exception of CO emissions, which decreased as butanol was added to diesel, but increased as it was added to biodiesel. Overall, the incorporation of butanol into biodiesel and diesel as a tertiary mixture has been identified as a potential way of overcoming some of the disadvantages of using either alcohols or biodiesel alone. Biodiesel can result in incomplete combustion as well as damage to fuel lines as a result of poor atomization due to its high viscosity. Alcohols meanwhile possess low

cetane numbers and poor lubricating properties, but using these two components together with diesel could be a solution.[195]

A further study by Yilmaz *et al*[205] looked into a quaternary blend of diesel, biodiesel, vegetable oil and alcohols, in this case propanol and pentanol. The use of propanol in a blend was advantageous in reducing NO_x emissions, while enhancing 'basic fuel properties' of tertiary blends of diesel, biodiesel and vegetable oil. However, CO and HC emissions increased with the use of alcohol due to the high latent heat of evaporation increasing the relative amount of incomplete combustion. Another study in the same group looked at pentanol blends with diesel and biodiesel specifically.[185] In this, it was noted that the fuel consumption increased while the break thermal efficiency decreased when the engine was fuelled with the tertiary blend, compared to neat diesel. Furthermore, the high latent heat of evaporation contributed to an increase in incomplete combustion products (CO and HCs). It was also suggested that the increase observed in NO_x emissions with the addition of pentanol was due to high temperature zones forming as a result of the fuel bound oxygen. This highlights that the effects of using alcohol blends in diesel are not always beneficial; the benefits tend to lie with their renewable and potentially more sustainable production. However, as already discussed, oxygenated fuel species can possess further benefits, including lower quantities of particulates. Kumar *et al*[206] looked into the effect of using iso-butanol, pentanol, and also dimethyl carbonate, in improving the so-called soot/NOx trade off, which is the concept that when engine characteristics change to reduce soot formation (leaner combustion for example) NO_x emissions will tend to increase and vice versa. Iso-butanol was used in this case, rather than straight chained n-butanol, because it is easier to produce and its lower cetane number would result in increased pre-mixed combustion and better fuel/air mixing. Along with late injection and exhaust gas regulation, it was found that both soot and NO_x could be reduced simultaneously with the addition of the biofuels. Furthermore, the 38vol% butanol blend in diesel showed no drop in efficiency, while pentanol and dimethyl carbonate blends (of 45% and 15% respectively, to match the oxygen content) saw a drop in efficiency. A study by

Fayad[207] took the novel approach of combining fuel injection strategies with the use of butanol blending to increase the effectiveness of the DOC. The study employed a post-injection strategy whereby the fuel was injected late in combustion to increase exhaust gas temperature and therefore DOC operation. This was observed to modify the soot morphology; but the increase in CO and HC emissions meant there was greater competition for sites on the catalyst, reducing its activity. However, this was mitigated when 20% butanol was added to the diesel, as the CO and HC emissions were reduced. Fayad later explored the use of varying EGR rates and a 20% butanol-diesel blend on the particle size distribution and NO_x emissions of combustion. Ultimately, the use of the butanol blend, for a given EGR rate, decreased particle number and size and the NO_x, CO and HC emissions, while increasing the brake specific fuel consumption (BSFC). As the EGR rate increased, the brake thermal efficiency (BTE) decreased, but so too did overall soot and NO_x emissions. Pentanol was recently employed in the studies of Yesilyurt *et al*,[208] comparing binary diesel-safflower oil biodiesel to ternary diesel-biodiesel-pentanol blends. The study noted the reduction in BTE with increasing pentanol usage, up to 20 vol% though NO_x, CO, HC and smoke emissions reduced as a result, highlighting the advantages of using this alcohol as a diesel blending component.

Overall, as outlined in Babu's review, [201] high blend ratios (40vol%) of butanol and pentanol in diesel can be achieved due to their relatively low polarity (compared to methanol and ethanol) which stems from the longer chained structure (which dilutes the impact of the polar hydroxyl group). Common themes of alcohol/diesel blends are longer ignition delays due to the lower cetane number of the oxygenated molecules, thereby increasing pre-mixed combustion and having a variable impact on emissions- generally favourable for soot emissions and for the soot/NO_x trade-off. The lower viscosity of alcohols tends to improve atomization and combustion, resulting in higher brake thermal efficiency, but also higher fuel consumption since the energy density of alcohol-diesel blends is lower than that of neat diesel.[209] Emission studies can contradict one another, and this is likely due to the differences in engine operation used in such studies. For instance, at low loads, the low calorific value and

lower heating value of alcohols mean that combustion temperatures at these loads are low. NO_x emissions are dependent on these phenomena, which helps explain why different relationships between blend ratios and emissions are observed. These contradictory results, which are not resolutely positive in favour of diesel-alcohol blends, explains why diesel is not currently blended with alcohols in the same way as gasoline. While butanol production can be bio-derived, it is more common to use petroleum resources for this, negating the distinct advantage that butanol/pentanol-diesel blends offer.[29] Furthermore, while some emissions can be reduced with these blends, often this comes at a price of an increase in different emissions or a higher fuel consumption. Soot emissions can be reduced on a mass basis, but the number of smaller particles (which are more of a health concern) often increases. Furthermore, NO_x, CO and HC emissions tend to change more as a result in engine operation variations rather than the fuel blend itself. Work by Ibrahim[210] into the use of biodiesel and butanol-diesel blends noted that 'the change in engine load rather than fuel type had a more significant effect on the combustion'. Xiao *et al*[196] utilised iso-butanol/diesel blends in an effort to understand the effect on emissions, observing that, at low engine loads, the butanol blends increased emissions of CO. However, at high loads, the NO_x emissions increased relative to diesel while particulate emissions were reduced across the range of engine loads tested. An unavoidable disadvantage of alcohols is their poor lubricating properties, which increases engine wear, and low energy densities; the resulting increase in fuel consumption is a major hurdle in the use of higher alcohols for diesel blending. Consequently, research into other categories of biofuels are being considered as blending components in diesel fuel.

2.2.2.4.   Furans

Due to their formation from 2nd generation (lignocellulosic) biomass, furans are a novel class of molecules that possess exciting properties that may make them a potentially viable biofuel source. Furans are cyclic ether molecules; the ring itself consisting of 4 carbons and 1 oxygen. These can be fully unsaturated in the case of furan itself, fully saturated, as is the case

in Tetrahydrofuran (THF), or partially saturated e.g. 2,3-Dihydrofuran and 2,5-Dihydrofuran. The basis for the biological production of furans, as discussed, is from HMF or furfural; these molecules are upgraded via various chemical strategies to form more fuel-relevant molecules with lower oxygen content, higher energy density and better blending properties. Due to furan derivatives' relatively recent attention in engine applications,[120] a significant amount of research has been focused on more theoretical aspects, with experimental work investigating fundamentals of their combustion in laminar flames, or determining ignition delay.[120] That said, studies have been performed, on the effect of furan-fossil fuel blends on combustion and the resulting performance and emissions of the engine.[92,93,211,212]

Two of the most well studied furan derivatives are 2-Methylfuran (MF) and 2,5-Dimethylfuran (DMF), most applicable in gasoline engines due to their low carbon number, high octane rating and recent developments in their production.[89,213,214] These also represent highly appealing molecules to use as fuel blenders since the energy density is far higher than that of bioethanol[35,215] (ethanol- 21 MJ/l, MF- 28.5 MJ/l, DMF- 30 MJ/l) and on a par with gasoline itself (31 MJ/l)- therefore, in theory, fuel consumption should not be heavily compromised with their use. The ignition delay exhibited by these furans is highly important in whether they are used as diesel compression fuel extenders and on the impact their presence has on combustion and emissions. A study by Xiao[89] *et al* compared the qualities of MF and DMF along with pure diesel. The use of MF in diesel had not been widely reviewed compared to DMF, despite its potentially preferable properties, such as a lower boiling point that improves fuel-air mixing due to better evaporation, and lower flash point which could improve cold starting properties of the fuel. Ultimately, they observed a longer ignition delay with diesel-MF blends compared to neat diesel with mass fractions of greater than 40% resulting in unstable combustion, while NO_x emissions increased with the blended fuel. An additional study in the same group noted that soot emissions of MF-biodiesel blends decreased across all engine loads, though CO and HC emissions increased at low loads.[216] Liu *et al*[215] utilised MF in an SI engine, comparing its combustion performance to that of ethanol and gasoline. The authors

observed that injection durations required for the same engine load were lower for MF than ethanol, but higher than gasoline. However, the higher viscosity of MF is noted to be a factor behind this, therefore it is suggested that higher injection pressures could be employed to overcome this. DMF-diesel blends have shown promising combustion results, particularly in the ability of this type of blend to reduce soot emissions. Biu et al, [91] for example, note that the higher relativity of the soot particles, combined with an extended ignition delay, is the main cause of this reduction in PM. However, the long ignition delay of DMF limits its blending potential and, in cases, has caused researchers to utilised ignition enhancers (2-ethylhexyl nitrate, EHN) when using this fuel.[92] Furan itself has also been explored in computational studies, though primarily to further understand the combustion of 2-MF and 2,5-DMF (rather than being envisioned as a blending component itself).[217]

DMF and MF are the main furans of interest for combustion studies, due to the relative ease of obtaining them from biological sources, but primarily these are applicable to spark ignition engines.[218] However, for diesel fuels, MF and DMF possess relatively low CNs and so higher carbon numbers (therefore longer chained branches off the main furan ring) are preferable. This has led to some studies looking into the performance of molecules such as ethylfuran[219–221] and butyltetrahydrofuran[222] as fuel blenders. Xu et al looked into the relative reactivity of ethylfuran (EF) compared to DMF, MF and furan itself.[219] Higher reactivity is preferable in diesel engines as it corresponds to faster and more complete combustion; DMF is more reactive than MF which is attributed to the alkyl branches promoting H-abstraction and therefore increasing the radical pool.[223] Furthermore, despite the fact that DMF and EF possess the same number of carbon atoms, EF has been observed to be more reactive, potentially due to the 'higher reactivity to the ethyl radicals and more favourable sites for abstraction'.[219] The methyl radicals formed from DMF can recombine to form ethane, which is stable, while ethyl radicals formed from EF undergo beta-scission, forming ethylene and a hydrogen atom.[224] Xu's paper concluded that the relative reactivity of EF and DMF was actually dependant on temperature, with a point at which EF will be more reactive at high enough

temperatures. Ethylfuran has also been subjected to pyrolysis studies in order to discern the mechanism of molecular breakdown in conditions relevant in an engine. Song *et al*[221] concluded that this molecule was unique, compared to MF and DMF, in that the ethyl chain enabled a C-CH3 pathway to be prevalent in the decomposition; 2-vinylfuran, 2-furylmethyl and vinylketene were noted as key species. The cause of this is due to the lower bond enthalpy of ethylfuran (Figure 2.14), and is a further reason for the greater reactivity of EF compared to DMF. However, these recent studies in pyrolysers and laminar flames heavily implies that research into this molecule as a potential biofuel is in the early stages.[220]
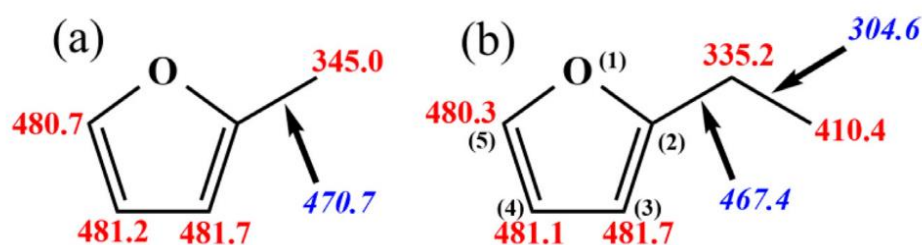
Figure 2.14: Calculated bond dissociation enthalpies (BDEs) of (a) methylfuran (MF) and (b) ethylfuran (EF)[221]

Butyltetrahydrofuran can also be derived from biomass, and its saturation and longer alkyl chain makes it an appealing diesel blender.[119] Cai *et al*[222] observed the laminar burning velocities of this molecule in a combustion vessel and ignition delay in a rapid compression machine, and compared these measurements to numerical investigations. They concluded that their experimental and numerical data were an acceptable match and that the presence of the THF ring had an effect on the relative BDEs of the other carbon sites. In the ring carbons, H-abstraction is easier at high temperatures, while at lower temperatures, ring opening reactions ensue which act as radical sinks and inhibit further fuel reaction. Saturated THF derivatives possess higher energy densities compared to the unsaturated analogues and the actual combustion process may differ. Sudholt *et al*[88] published a high impact paper that systematically studied the ignition quality of alkylated and non-alkylated saturated/partially

saturated/unsaturated furans. The findings suggested that the side chains of unsaturated furans do not greatly impact the ignition of the molecule, whereas saturated THF molecules ignite based on the properties of the side chain, with longer side chains increasing the reactivity of the fuel at low and intermediate temperatures. The reactivity of Dihydrofurans (DHFs) is also noted to be in between that of the more unreactive furans and reactive THFs, as expected, while the addition of an alcohol group onto the side chain of unsaturated furan has a very marginal impact on the ignition behaviour. A shock tube study[225] (where combustion takes place as an adiabatic, constant volume reaction) comparing MF to MTHF appeared to disagree with this relationship in saturation however; the saturated MTHF sees a longer ignition delay than MF, but the authors do note a change in this relationship at lower temperatures and a dependence on stoichiometry. The authors postulate that the ring-opening reactions are faster in unsaturated molecules due to 'low activation radical additions' and that there are differences in the rate of radical attack on the methyl chains, due to the change in electron density that the furan/THF rings causes. A study by Wang *et al*[226] also looked into MTHF as a potential fuel blender, primarily to correlate experimental results with a kinetic model. However, their kinetic models allowed them to conclude that, at high temperature, fuel decomposition reactions are the dominant mechanism for initial combustion, while H-abstraction is more prevalent at lower temperatures. This could be the cause for the different trends observed in experiments with the same fuels. Comparisons with MF were also made in this study, which backed up the work by Jouzdani that MTHF possesses longer ignition delay than MF under the same conditions, but the disparity decreases as temperature increases.

An ignition delay comparison between 2,3-DHF and 2,5-DHF was conducted in shock tube investigations.[227] This comparison is important since the degrees of saturation are the same, but the position of the double bond has changed; therefore observation of the ignition delay in these can give an insight into the mechanisms of how these types of molecules undergo combustion. Coupling these experiments with kinetic models, the authors were able to conclude that 2,3-DHF is converted into cyclopropane, carboxaldehyde and croton aldehyde

by isomerisation. 2,5-DHF meanwhile dehydrogenates to furan. Further to this, ignition delay, which is dependent on bond dissociation energies, was found to decrease in these DHFs compared to furan, with 2,3-DHF possessing shorter delay than 2,5-DHF. The latter's tendency to dehydrogenate to stable furan is the reason for its longer delay and this is suggested to be because the C-H bonds at the 2 and 5 positions are weakest, making them susceptible to H_2 elimination, which then produces furan. Meanwhile, in 2,3-DHF, the C-O bond is relatively weak due to the neighbouring C=C double bond; ring-opening reactions are therefore probable with subsequent isomerization. These fundamental studies are essential in enhancing our understanding of the reactions that dictate ignition. Knowledge of the effects that a change in the location of a double bond or the degree of saturation, will help in essentially designing molecules. For example, work by the company Avantium[109] has looked at designing furan derivatives with ether functionality, partly because this transformation can make use of renewable alcohols and furfural but also because ethers have been shown to possess favourable properties in diesel combustion. Tests of t-butoxymethylfurfural (t-BMF) have exhibited reductions in soot emissions, and can be blended in up to 40vol% ratios.[109] This molecule can be fully etherified however, as there is still a carbonyl group that can be hydrogenated and subsequently etherified. A 2012 study by the same group looked into using etherified furans, ethoxymethyl tetrahydrofuran ether (ETE) and furfuryl ethyl ether (FEE), to determine the emissions produced of various blend ratios in a diesel engine under a certified test cycle.[228] Both biofuels reduced soot emissions at 30vol% blend ratios, although FEE increased the NO_x emissions, suggesting that the hydrogenated ethers were preferable. Meanwhile the absolute fuel consumption increased, although the authors point out that this increase is in-line with the lower energy content of the biofuels; no net adverse effects in fuel consumption are observed by adding these biofuels.

A common theme in the investigation of furanic biofuels in diesel engines is the reduction in soot emissions.[229] While using biofuels to replace a percentage of the fossil fuels used (thus reducing our reliance on finite resources) is appealing, coupling this with a downstream benefit

of lower pollutant emissions (of soot for example) makes their use more impactful. In the case of furans, Sirignano et al[230] conducted experiments in diffusion flames to analyse the sooting tendencies of different ethylene/furan blends, finding that the sooting tendency increased from furan to DMF to MF. A study by Gogoi et al[90] investigated the sooting propensity of DMF in diffusion flames, although in this case in diesel blends of up to 15vol% DMF. They determined that particulates derived from biofuel blends were more easily oxidised, potentially due to the different soot nanostructures that are formed when DMF is present in a fuel blend. It was detected, using a number of characterisation techniques, that higher DMF blends produced soot particles that were more amorphous in nature, while the aliphatic content increased, and the length of PAHs in the soot decreased. The same reduction in soot emissions is observed in diesel engine studies using some of these furan derivatives as blends. Chen[231] observed lower soot emissions relative to butanol blends, likely as a result of the longer ignition delay. An investigation into blends of DMF in diesel found that there was no soot- NO_x trade off at high DMF fractions.[232]

The formation of NO_x is fairly well understood (as discussed in Section 2.2.1.5), but the formation of soot particles is a more complex process involving more variables. An oxygenated fuel is a powerful way to reduce particulate emissions, but understanding how these emissions are formed in the first place is important in determining how fuel formulation can be manipulated to reduce them.

2.2.2.5.   Lactones

Lactones are a class of molecules that overlap in their molecular characteristics with the furans. However, these molecules are cyclic esters, rather than cyclic ethers, with the addition of a carbonyl group on the carbon adjacent to the ether functionalised oxygen atom. Moreover, unlike furans, this class of molecules can vary considerably in both the number of members of the ring, as well as the length (and number) of side chains. This makes them versatile; their uses are numerous- as solvents, food additives or perfumes.[233] One lactone, gamma-

valerolactone (GVL), has also been tested as a biofuel based on its ability to be derived from 2nd generation biomass.[234] Bereczky performed the first detailed study of this molecule's combustion in a direct injection, turbocharged diesel engine, referencing the potential advantages in the reduction of emissions to compensate for the low cetane number.[235] Overall, while engine performance was diminished with the addition of biodiesel and GVL, incomplete combustion products, THC and CO, as well as smoke emissions, were significantly reduced, while NO_x emissions were not greatly affected. Due to the size of the GVL molecule, it has been more common to test the lactone in SI engines with higher concentrations than that used in the study of Bereczky (7%). Horvath noted that, compared to ethanol, GVL possesses a similar octane number, but improves combustion due to lower vapour pressure and also has higher energy density compared to ethanol.[236] Furthermore, from a production perspective, GVL is advantageous based on the fact that it does not form an azeotropic mixture with water, which makes the catalyst used in the production both recoverable and reusable, while its high flash point and low toxicity make it a relatively safe molecule to work with.[35] However, in a study by Gschwend looking at 50 alternative fuels, while GVL possessed the basic requirements for an alternative SI engine fuel, the fact that it is also an addictive drug was deemed to render its widespread use unlikely.[237] For compression ignition engines, the molecule requires greater molecular mass to enhance ignition propensity with a potentially larger radical pool exploited. At this stage, limited investigations have been conducted into the use of bioderived lactones in diesel engines but, given that these molecules may possess a carbon number within the range of conventional diesel fuel (generally between 8-20), blending in diesel- or even using as a pure fuel in itself- could be feasible.

Lactones are named based on two features, the number of atoms in the ring element, and the total number of carbons overall. The Greek symbol at the start is a reference to the former, while the -lactone suffix a reference to the number of overall carbons:

Table 2.2: Naming of lactone molecules

Number of elements within the ring	Greek Symbol	Total Number of Carbons	-lactone
3	α	2	Aceto-
4	β	3	Propio-
5	γ	4	Butyro-
6	δ	5	Valero-
7	ε	6	Capro/hexa-
		7	Hepta-
		8	Octa-

So the aforementioned gamma-valerolactone possesses a 5 membered ring (including oxygen) and 5 carbons overall.

The suffixes are generally determined by the acid used in the synthesis of the corresponding lactone. However, many lactones occur naturally thus their use as a biofuel is particularly attractive. Furthermore, many lactones are already synthesised on large scales due to their use as natural food flavourings, including coconut, molasses and nut flavourings;[233] the scale up of these 'fuels' is therefore envisioned to be less energy intensive than a fuel based on a more novel molecule, with a lower capital cost and where the research is less advanced. The aforementioned GVL molecule is of particular interest given that it can be formed from the versatile levulinic acid (LA), which can be obtained from both cellulose and hemicellulose fraction of biomass components. LA undergoes dehydration to form angelica lactone and is subsequently hydrogenated to form GVL.[238] Larger lactones appear to have received less attention as potential fuels. However, there are promising solutions to the sustainable production of the most commonly utilised of 'mid-size' lactones; ε-caprolactone (εCL). εCL inherits uses as a solvent, in the polymer industry and, majorly, in the production of polycaprolactone and nylon.[239] While its current production is based on fossil fuels, recent studies have indicated it may be sourced from lignocellulose- specifically HMF- through a 4-step process via hexanediol, or even incorporating cell media to biotransform hexanediol directly into εCL.[121] ε-caprolactone is promising as a fuel blending component when compared to furan molecules that generally possess a lower carbon number (making them more

applicable to gasoline blends), while the ester functionality is potentially of benefit in reducing the emission of particulate mass as the number of oxygen atoms available for soot oxidation is increased. ε-caprolactone contains 6 carbon atoms in a cyclic ester structure. Based on the current production potential and higher carbon number of ε-caprolactone, compared to GVL (an extensively researched lactone),[70,71,235] the possibility to utilise larger lactones, such as εCL, in diesel engines is highly intriguing.

2.2.2.6.   Hydrogen derived fuels

As discussed in Section 2.1.7, hydrogen as a transportation fuel has generally been envisioned as an energy source for fuel cells, converting hydrogen and oxygen to water, releasing energy in the process. However, the uptake of this technology is limited. On the other hand, the use of hydrogen directly in a conventional spark or compression ignition engine is possible; some studies have been performed to decipher the ability of hydrogen to add to the energy content of the charge gas. Saravanan[240] states that hydrogen could substitute the diesel by up to 38 vol% with no loss in thermal efficiency through a dual fuel system, in which the hydrogen is injected into the intake air stream and diesel is used as an ignition source. Lee *et al*[241] experimented with dual injection, in which the hydrogen was injected with an in-cylinder solenoid. Hydrogen injection can be advantageous over carburetted setups, with backfire and pre-ignition issues eliminated with precise control over the hydrogen injection timing. In addition to the fact that hydrogen can be derived from water and renewable resources, as well as its own clean combustion, the use of hydrogen in a compression ignition engine has also been shown to reduce amounts of harmful emissions beyond its role in replacing a percentage of carbon-derived fuels. For example, Christodoulou and Megaritis[242] note that CO emissions decreased as hydrogen energy contribution increased, and this was not entirely explained simply by the replacement of fuel carbon. That said, a maximum hydrogen supply rate was required in order to avoid misfire. As is common in diesel engines, while CO and smoke emissions decreased, NO_x emissions were observed to increase, in particular at higher loads

with low speeds. Talibi's study[243] into hydrogen-diesel co-combustion also noted a trend of increased NO_x with increasing hydrogen content, likely as a result of higher peak heat release rates, and therefore cylinder temperatures. However, this study observed that this trend was more evident at lower loads, and at higher loads the NO_x levels remained largely unchanged with increase H_2. Differing engine speeds could be a factor in explaining these opposing observations.

Tartakovsky and Sheintuch[23] provide an extensive review into the use of on-board steam reforming, which can utilise renewable feedstocks such as ethanol[244] or methanol,[245] partial oxidation of liquid petroleum gas,[246] or exhaust gas recirculation,[247] to produce hydrogen. This sees the benefits of hydrogen combustion i.e. no CO_2 is produced from the reaction of hydrogen and oxygen, but means that hydrogen refuelling itself is not required. However, this does not entirely alleviate safety issues of hydrogen, particularly its flammability. Furthermore, the energy density of hydrogen is very low (10 kJ/l) at ambient conditions. These factors have resulted in increased interest in ammonia (NH_3). Ammonia is effectively a hydrogen carrier, with a hydrogen content of 17.8wt%,[248] but is significantly more stable than hydrogen itself, although it possesses a higher toxicity that requires careful handling; between 150-300ppm is considered the maximum exposure.[249] However, only moderate pressures and atmospheric temperatures are required to generate liquid-state ammonia, making transportation and storage much simpler relative to that of hydrogen.

Several studies in the 1960s investigated the fundamental reactions and flame characteristics of ammonia with various co-reactants[250]; various stoichiometries of air, in H_2/O_2 and H_2/H_2O flames, as well as a pure oxygen environment, with Fenimore and Jones observing the reaction between NH_3 and NO as the dominant mechanism of ammonia consumption in H_2/O_2 flames; NO is initially produced from the oxidation of ammonia, potentially through 'attack of O atoms on ammonia'.[251] One subsequent study by Bian and Vandooren determined that hydroxyl radicals primarily consume NH_3 molecules to produce NH_2 radicals, which either react

with H or OH radicals to form NH, and subsequently NO, or interact with NO directly to form diatomic nitrogen.[252]

The aforementioned studies primarily explored the fundamental mechanisms of ammonia combustion, and the resultant products, but others have looked into strategies to use ammonia in ICEs[249,253–256]. Clear from these investigations is the need for a variety of techniques to enable stable ammonia combustion, with Starkman[257] referencing the requirement of partially (25%) disassociated ammonia in the fuel feed- to yield a hydrogen level of at least 4-5wt%- to reach satisfactory performance (equivalent to 70% of the total engine load of hydrocarbon fuelled combustion). The conversion of ammonia to hydrogen requires high temperatures and expensive catalysts, therefore research into using ammonia directly in energy applications without the addition of hydrogen has been considered.[258] For some applications, it has been deemed non-feasible to use pure ammonia; the aforementioned spark ignition engines, tested in the 1960s with ammonia, can be operated with the pure ammonia, but the very high compression ratios required (13:1) and poor ammonia combustion render this an unlikely solution for literal zero-carbon fuels.[250] In addition to raising the compression ratio in order to reduce the levels of unburnt ammonia in the exhaust, other strategies employed are H_2 doping, improved ignition systems and elevated engine load, though NO_x levels increase as a result of the latter.[257,259] Additives are commonly employed in combustion experiments to enhance the ignition quality of a given fuel to bring it more in line with conventional fossil fuels and assist in drawing comparisons.[260] Nitrates and peroxides are commonly used but, in the case of ammonia combustion, hydrogen itself could be an attractive solution since it can be directly obtained from the ammonia utilised as the primary fuel.[258] A catalyst can be used to decompose a proportion of the ammonia into pure hydrogen before entering the combustion chamber itself. Wang *et al*[258] utilised the exhaust gas as an oxygen source for the decomposition of ammonia over a ruthenium catalyst. However, despite the use of a catalyst, temperatures of 500°C were required, necessitating partial oxidation of the fuel to raise the

temperature above that which the exhaust gas temperature of a diesel engine is normally able to reach.

Alternatively, blending of ammonia and gasoline could assist in the combustion quality; the carbon-based fuel essentially acting as a promoter to allow the necessary temperatures and pressures to be reached for the ammonia to combust completely. Grannell *et al*[54,256] determined a blend of 70% ammonia and 30% gasoline to work well on a supercharged SI engine; the NH_3 emissions in the exhaust were proportional to the amount of ammonia in the fuel, while incomplete combustion products, CO and UHCs, increased as the proportion of gasoline was increased. It was also deemed essential that, for the after-treatment three-way catalyst to operate effectively, the fuel-air mixture should be maintained between stoichiometric and 0.2% rich, since lean operation was found to see over-oxidation of NH_3 and therefore a significant increase in NO and N_2O emissions. Furthermore, while NO_x emissions are prevalent, even in the absence of ammonia, levels of these emissions become much more sensitive to combustion stoichiometry where ammonia is present. Westlye *et al*[261] measured NO, NO_2, and N_2O emissions in a spark-ignition engine fuelled with ammonia, and reported that the amount of NO_2 formed was approximately 4% higher than under equivalent conditions with conventional gasoline used as fuel. The authors concluded that the increased amount of NO_2 produced during combustion was partly responsible for the formation of N_2O in the exhaust gases. The emissions of N_2O in the exhaust gas were below 60 ppm at all conditions tested, and were highest under the leanest conditions within a range of fuel-to-air equivalence ratios of 0.5-1.0 tested. A study by Ryu *et al*,[262] however, noted the requirement for 'substantial' gasoline injection, even at idle speed, for ammonia to combust, with increased ammonia injection duration and advanced injection timing contributing to further power output. As the amount of gasoline injected was increased, the contribution to power output from the ammonia decreased. Moreover, while increased ammonia injection lowered peak pressures due to lower flame speed and temperature, NO_x formation increased- suggesting that a portion of this NO_x was formed directly from the fuel- as did the ammonia slip, caused by traces of ammonia

remaining unburnt. Emissions of both NO_x and ammonia were found to decrease at higher engine loads, suggesting preferential use of ammonia as greater power is demanded.

Compression ignition combustion is arguably a more promising solution given the ability to potentially overcome the high resistance to autoignition exhibited by ammonia using higher compression ratios than that of spark ignition engines. However, Reiter[249] notes that ammonia is only combusted successfully if introduced in the air intake system and diesel is injected to provide the ignition energy; controlled autoignition of ammonia only was found not to be possible, even at a 30:1 compression ratio. Several studies[260,263,264] have used homogenous charge compression ignition (HCCI) combustion with a variety of fuels based on the high compression ratios and low combustion temperatures (for low NO_x output) exhibited, such that an almost limitless number of fuels could be tested.

Overall, while the use of a hydrogen-based fuel has been shown to be possible in conventional combustion engines, there appears to be a limit to the maximum level of energy contribution from this source- therefore fossil fuels would still be utilised to ensure engine compatibility. Furthermore, the effect on emissions remains unclear. Greater impetus to shift away from fossil fuels will be gained by proving a fuel's ability to reduce the level of harmful products emitted to the environment. Arguably the most significant type of pollutant, based on both the amount and potential health problems caused by it, are particulates.

2.3. Soot formation

The emission of soot particles is governed by regulations that have become more stringent in recent years as the understanding of the health defects that the chronic exposure of these particulates can cause becomes greater. Currently, the main method of dealing with these emissions in diesel engines is via a diesel particulate filter (DPF), which traps soot particles and oxidises them into CO_2 at sufficiently high temperatures.

Exhaust gas recirculation (EGR) can also be employed to reduce NO_x; this entails recirculating some exhaust to alter properties such as temperature and fuel composition. Generally, this reduces NO_x emissions, since the displacement of air (and oxygen) in the engine intake by exhaust gases reduces the combustion temperature and this leads to a reduction in thermal NO_x formation. However, as stated by Kittelson and Kraft,[265] EGR also has an effect on particle size distribution- some of the particulates that re-enter the engine will be oxidised completely, while others may expand and agglomerate, causing a shift in average particle size to larger mean diameters.

In order to tackle the emissions of soot through the use of alternative fuels, some knowledge of the mechanisms of soot particle formation is needed. The overall mechanism will initially be discussed, with particular focus on the fundamental chemistry in later sections.

2.3.1. Current understanding

Considerable research into the formation and growth mechanisms of soot particles has been made over the years; Palmer and Cullis' 1965 review[266] presented the first ideas that soot formation takes place in a set number of stages. Later, in 1991, a high impact paper by Frenklack and Wang[267] presented a 3 stage process by which soot particles form in a laminar premixed combustion flame; this work has been the basis for future studies in various types of flame systems and engine combustion itself. Their proposal was that initial polycyclic aromatic hydrocarbon (PAH) formation was the first stage, followed by 'planar' PAH growth and finally spherical particle formation and growth. These processes occur at atomic levels, but in order to form an entire soot particle from a fuel requires physical processes. Tree and Svensson's soot formation review[268] outlines six commonly identified mechanisms, starting with pyrolysis to form soot precursors (PAHs), nucleation into soot nuclei, and subsequent growth by coalescence, surface growth, and agglomeration. The final stage is oxidation of the soot, which reduces soot mass, and is an important process to consider.

Pyrolysis of the fuel is agreed upon to be the first stage of soot formation as it forms known soot precursors.[265] This process occurs in fuel rich regions of the combustion flame where there is not enough oxygen to fully oxidise the hydrocarbon into CO_2 and water. Pyrolysis and oxidation are competing processes that increase with temperature; diffusion flames tend to soot more because there are fuel rich zones while premixed flames soot less because the oxygen present is distributed evenly within the mixture. Pyrolysis products include unsaturated hydrocarbons, polyacetylenes, PAHs and acetylene, the latter two of which are particularly important in soot formation. PAH formation is essentially analogous to the formation of the first aromatic ring (benzene); benzene is the building block by which PAH growth and soot formation occurs. Frenklach and Wang highlight a number of possible pathways of forming this first aromatic ring, the most significant of which being the reaction of C_4 species with acetylene to form phenyl and benzene groups, and subsequent aryl reactions with H radicals and acetylene also forming aromatic products. Once the aromatic products are formed, PAH growth transpires as a result of the so-called HACA (Hydrogen Abstraction Acetylene Addition) mechanism, a process that can occur since the Gibbs free energy is negative as a result of the increase in entropy that the H-abstraction causes (despite overall aromatic growth). The HACA mechanism has been employed in kinetic studies on numerous combustion systems and matches closely to experimental results, including flames in diesel engine combustion.[269] The formation of the first and second aromatic rings is a critical step in soot formation and, according to Svensson's review, this stage dictates the overall rate of soot formation and is the main factor that can be altered by the use of different fuel sources; nucleation and subsequent growth occurs relatively quickly, thus making aromatic formation the rate determining step. The aromatics at this stage are in the gas phase, thus transition into solid nuclei is required for further physical growth, a process which is not entirely understood, but most models base their assumptions on Frenklach's study.[265] This model takes particle inception to be determined by collisions between PAH molecules resulting in dimerization. Subsequent growth of these PAH clusters is attained through condensation of PAHs, the HACA mechanisms and coagulation.

Surface reactions involving acetylene are understood to play a key role in particulate growth, and Frenklach discusses the hypothesis that soot particle growth is analogous to PAH growth because the edge of the soot particle will be similar to the edge of a large PAH molecule, thus the growth of soot particles can also be governed by the aforementioned HACA mechanism. However, it is important to realise the non-linear growth rates of particles, which can be explained by phenomena known as surface migration and surface ageing.[270] Surface migration is based on a radical's ability to migrate within a species and consequently distort the overall structure, potentially turning a reactive species into a stable one that no longer supports further growth. Surface ageing, meanwhile, can be attributed to a decrease in the number of H atoms in the gas phase as well as a reduction in the number of active sites on the particulates themselves; the latter effect a consequence of surface migration that reduces the particle activity by introducing more surface defects over time. Subsequently, the coalescence and agglomeration of these 'primary soot particles' sees significant increases in the particle diameter to the order of micrometres from the nanometre scale of primary particles. These physical processes involve the merging of particles into one another (coalescence) or sticking together (agglomeration), often into chain-like structures, [268] which occurs relatively late in combustion. Coalescence enters different regimes depending on whether the system is at high or low pressures; at low pressure coagulation is in the free-molecule regime (whereby particles are so small that collisions are negligible), at high pressures the continuum regime (in which particles move as a continuous fluid) and in between is a transition regime. The first two are well developed regimes that can be reliably modelled, therefore simplified models of soot formation can use one of these to approximate the particulate output. However, the different phases are not distinctly separated, and happen in tandem with each other; the transition between coalescence and fractal growth (agglomeration) is not fully understood while, according to Frenklach, 'agglomeration begins with the onset of nucleation'.

While some questions over the physical processes that govern the growth of soot particles still remain, these processes are generally temperature/pressure dependent and therefore are

amenable to model. The formation of the first aromatic ring and PAH growth from this into larger entities is more of an unknown, and significant efforts have been made in this area, particularly in generating models to accurately enact the processes by which PAHs form and grow. The HACA mechanism proposed by Frenklach remains an important route in the formation of soot, but more recently reactions involving odd carbon species and PAH growth from C_1 and C_2 fuels have been proposed and show promising results, indicating a complex and variable process that cannot be explained with one mechanism alone.[271] Wang *et al*[272] investigated the modelling of soot formation in counterflow diffusion flames using ethylene based binary mixtures- addition of 5% propane or ethane saw similar effects in both model and experimental data on the soot formation (soot volume fraction increased by 32% in the model and 37% in experiments), suggesting that the model used was viable. In this case, 36 nucleation reactions from 8 PAHs were used, with the HACA mechanism simulating the surface growth reactions (though CH_3, C_3H_3 and C_2H radicals were also included in this mechanism, in addition to H radicals). However, as with all models, the matching of results to experimental data does not necessarily mean that the correct mechanisms have been identified and employed. The uncertainty is based upon the reactivity and instability of the PAHs. Before this is discussed further however, some focus should be given to PAHs themselves.

2.3.2.   Polycyclic aromatic hydrocarbons (PAHs)

PAHs are a group of molecules consisting of multiple aromatic rings groups. PAHs can contain elements other than carbon and hydrogen as well as aliphatic chains, but these species are rarely measured and the priority PAHs contain only carbon and hydrogen with no branching groups. The absence of stabilising side chain groups means these molecules are generally toxic, and some have been shown to possess mutagenic and carcinogenic properties.[273] The 'polycyclic' element of the name explains why benzene and naphthalene are not classed as

PAHs, though their formation is naturally required in order for subsequent PAH formation and further growth into heavier molecules to take place. Most PAHs are formed as unwanted products of incomplete combustion, hence their presence is a sign of inefficiency, and are generally characterised by high melting points, low aqueous solubility and high solubility in organics. Moreover, PAHs generally possess low vapour pressures, more so as the size of the molecule increases. This explains why, at any given pressure, higher molecular weight PAHs will tend to adsorb onto soot particles, more so than smaller PAHs, entering essentially a solid phase. While PAHs are formed as pyrolysis products (pyrogenic PAHs) some are of use in the industrial production of pharmaceuticals and agricultural products; pyrene is involved in the manufacturing of pigments and fluorene in the manufacturing of pharmaceuticals, pigments, dyes and pesticides.[273] Furthermore, PAHs can be formed from biological sources, including forest fires and the synthesis of bacteria and algae.[273] However, these sources are minor in comparison to the overall emission of PAH material from human-related activities (heating systems and transportation). This is apparent from the fact that greater concentrations of PAHs are found in urban environments;[273] since these environments are densely populated, the air quality is an even more pertinent public health issue. The known toxicity of these materials makes their presence in city environments more sensitive, therefore understanding how they are formed in major sources, such as vehicle engines, is imperative.
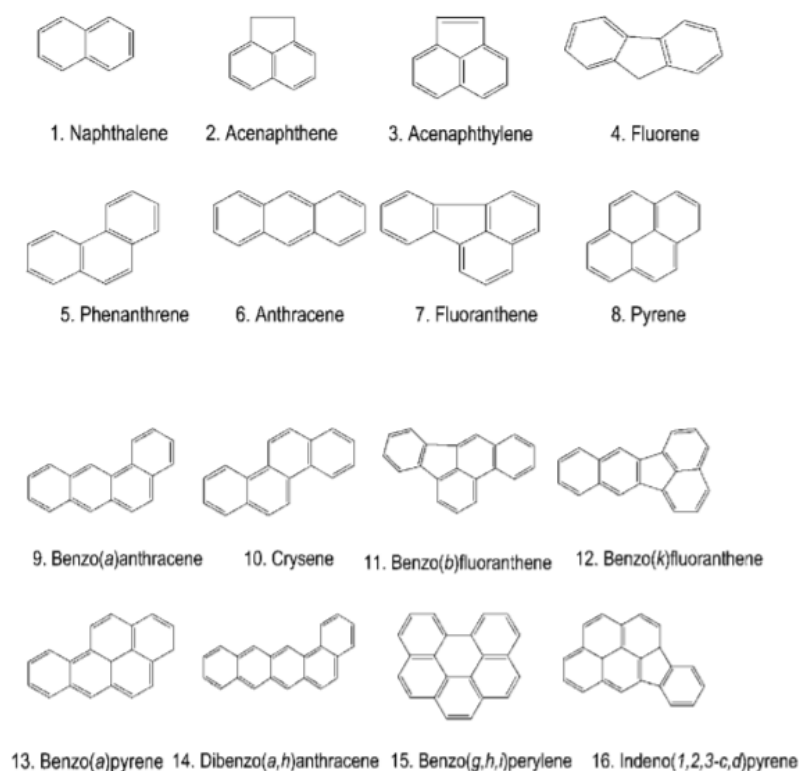
Figure 2.15: 16 priority PAHs[274]

An important attribute of PAHs in engine exhaust gases is the partitioning of solid and gas phase molecules; as discussed, lower vapour pressure PAHs have higher tendency to adsorb onto solid particulates (this is soot that has been formed from PAHs produced earlier in combustion). This is physisorption, and should not be confused with particulate growth where chemical bonding is involved. Heavier PAHs possess lower vapour pressures, therefore these are the molecules that are more likely to be present in the solid phase, while gaseous phase PAHs tend to be the lighter species with lower ring numbers. When adsorbed onto particulates, the PAHs may be ingested through the airways, and if the particulates are small enough, the PAH-containing soot could pass through the protective human cilia and enter the lungs, where they will be adsorbed into the bloodstream and be allowed to exert potentially harmful effects. This is also why the particle size distribution in engine exhausts gases is an important parameter to consider; a greater particulate number, or total particulate mass, may be

preferable if there is a lower proportion of small particulates that can enter human respiratory tracts. It is also important to note that inhalation in city environments is not the only way in which humans may be exposed to these chemicals. PAHs can be deposited into soil and therefore have been shown to occur in food sources. While the number of polycyclic aromatic hydrocarbons that could exist is almost limitless, 16 are defined as 'Priority PAHs' by the EPA,[275] (see Figure 2.15) while, according to Abdel-Shafy and Mansour, 17 PAHs have been identified as potentially harmful to humans and these in turn are split into further groups that dictate the relative toxicity; Group 1, 2A and 2B.[273] Mitigation methods are clearly vital in ensuring the environment and the air of urban environments is safe for humans to breath daily. The fact that the formation of PAHs is not totally understood,[265] together with the fact that they are difficult to remove from engine exhausts since current catalysts cannot completely oxidise all soot particles and the associated PAHs, particularly during warm-up, means that new mitigation methods are being researched. If PAHs cannot be reduced using aftertreatment technology, then looking at their inception may be the most effective way in ensuring a cleaner exhaust. The following sections will look at the formation of PAHs in both premixed flames and internal combustion engines, comparing the effects of various molecule characteristics.

2.3.3. PAH growth in flames

Michael Frenklach and co-workers[267] can be said to be the pioneers of understanding PAH and subsequent soot formation in flames, noting the existence of four main processes involved in soot formation; nucleation, coagulation, surface reactions (growth and oxidation) and physical agglomeration. One of the main areas of contention is understanding how the first aromatic ring is formed which then leads to further growth into PAH molecules and soot. The method of formation is not totally certain; a number of routes could be involved, with a prevalent theory suggesting that odd-carbon number radicals are involved, the stability of these radicals meaning that it is likely to exist for long enough to be able to combine and form the first ring.

This theory has been questioned however, as the stabilities of these radicals, which are a key point of this theory, are based on enthalpies of formation of n- and iso- forms that do not match experimental results. Another possibility put forward is the reaction of propargyl and acetylene radicals to form a 5 membered ring- a cyclopentadienyl radical- which quickly forms benzene. A further factor to consider is that PAH formation may bypass the formation of the first aromatic ring altogether (although Frenklach believes that it is likely to be the dominant mechanism); condensation of polyacetylenes and combinations of larger radicals may also be involved.

The growth of the benzene ring into PAHs is generally accepted to follow the HACA mechanism put forward by Frenklach, involving 'low reaction barriers and high exothermicities'.[276] This mechanism proposes an initial abstraction of hydrogen from a hydrocarbon by a gaseous hydrogen atom, and subsequent addition of an acetylene molecule onto the radical site formed in the initial step.[270] Overall, the high abundance of acetylene and benzene in flames, regardless of the fuel source, supports the HACA theory and explains why this method of PAH growth has been so widely embraced. While these reactions are generally agreed to be occurring, some studies do provide certain variations of the HACA base mechanism; Chernov explains that the HACA theory 'does not provide sufficient pyrene production', and therefore additional pathways are required to acquire a full picture.[277] A Hydrogen abstraction vinyl addition (HAVA) mechanism has also been proposed to explain the formation of all six-member ring PAHs.[278] This study only looked into growth up to PAHs with 5 and 6 rings, since these are deemed the most carcinogenic, but it is important to note that heavier PAHs are more likely to condense onto soot particles and enter respiratory tracts of organisms. Wang *et al*[272] studied PAH growth in counterflow diffusion flames up to coronene (C_{24} -7 rings). Their efforts were to ascertain PAH profiles within the flames while altering concentrations of propane and benzene in the fuel source. In ethylene-propane flames, PAH concentrations first increased then decreased with higher proportions of propane, an effect which was more pronounced for heavier PAHs. A greater understanding of the reaction pathways, particularly for heavier PAHs where reaction channels become less reliable, is

needed to model PAH formation beyond small hydrocarbons. Wang's study demonstrated that odd carbon number fuels are important in the synergistic effect mentioned, particularly for heavier PAHs, which highlights their importance in PAH growth past the first aromatic ring. Chernov[277] used co-flow flames in a study to understand the chemical mechanisms leading to soot formation from C_1 and C_2 fuels in an attempt to incorporate a wider variety of fuel sources into an accurate model that predicts soot-precursors. This was achieved to an extent, while the experimental results also showed that ethylene flames form soot earlier than methane flames. Mixing fuels with air in controlled flames is a common way of understanding reaction mechanisms in real-world combustion environments (including ICEs), though pyrolysis of fuels allows a more fundamental picture of a molecule's tendency to soot. Dandajeh[275] looked into the effects of unsaturation of low order hydrocarbons on the toxicity of the resulting PAHs and soot formed. In C_2 fuels, PAHs tended to exist in the gas phase (bias was given to lighter forms), whereas C_3 fuels encountered the opposite phenomenon. Moreover, a greater degree of saturation in the fuel molecule appeared to result in greater amounts of soot and particle phase PAHs, at least in C_3 fuels, while the carcinogenic potential was highest in double bonded propylene. The tendency of double bonded (and triple bonded) molecules to form radicals that contribute to the formation of aromatics in combustion is consistent with the greater ability of the unsaturated molecules to produce PAHs and soot. The study also conducted a temperature-based study on the fuels, surmising that higher temperatures produce more soot but lower PAH concentrations, potentially as a result of isomerization and other temperature dependent reactions which essentially rapidly lock up PAHs in soot via chemical bonding.

Considering that biofuels are a major element of current fuel research, the impact that oxygenated molecules might have on PAH formation and potential toxicity needs to be critically evaluated. Llamas *et al*[279] used a constant volume bomb calorimeter and fatty acid alkyl esters (FAME and FAEE) to analyse the mechanisms of PAH formation at these conditions. The authors propose that the 1,3-butadiene and ethylene formed from esters can then generate soot precursors such as benzene and naphthalene by Diels-Alder reaction and aromatization,

but that there are little or no differences in the ability of FAME or FAEE from different sources to produce PAHs. The major factor that influenced the amount of PAHs formed was the oxygen pressure employed and the iodine value of the fuel i.e. the degree of saturation.

2.3.4. Effect of oxygenated fuels on PAH formation

Given that an increase in oxygen content reduces the initial formation of soot and increases potential for oxidation of particulates, using oxygenated fuels to reduce soot, and therefore its precursors, is an appealing prospect. The advantages of using biofuels upstream of combustion i.e. in production, have already been highlighted and reinforce the potential of replacing fossil diesel with bio-derived alternatives. A major boost to the research and interest in biofuels would be in showing that their use sees a decrease in toxicity and harm caused by engine emissions. While there are numerous studies on the impact of biofuels on overall soot formation,[280,281] fewer look at PAHs specifically. A study by Dong an co-workers[22] observed, using kinetic modelling, that the PAH formation under oxidative conditions was largely unaffected by oxygen content, and was more heavily linked to the length of the carbon chain. Tran *et al*[282] evaluated the impact that using biofuel candidates dimethylfuran and methylfuran had on the formation of PAHs in laminar premixed flames, compared to a standard octane improver, in this case toluene. In this study, DMF was shown to increase the formation of one particular PAH precursor, cyclopentadiene, by a factor of 20 compared to MF. This is potentially as a result of the radicals formed from H-abstraction of DMF being able to react via ring enlargement to form PAHs in a way that MF radicals cannot. The suggested reaction pathways towards individual PAHs are presented in Figure 2.16 below.
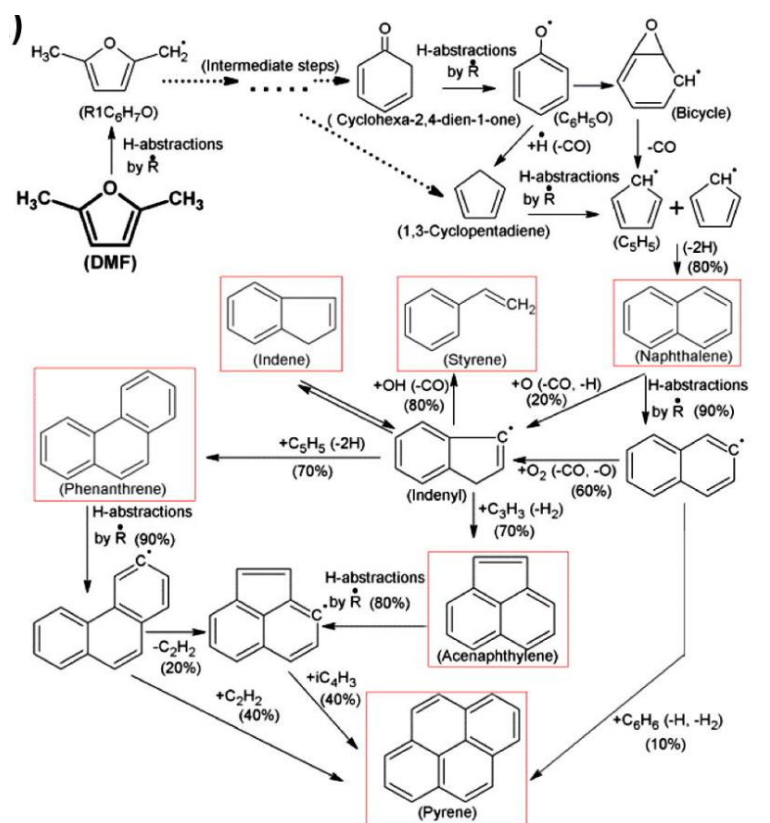
Figure 2.16: Production of PAHs in DMF flames (at 1600K)[282]

However, while PAHs tended to form in higher amounts in DMF compared to a toluene reference, the group referenced work by Chen[231] that indicates a decrease in overall soot formation in a DMF-diesel blend compared to a gasoline-diesel blend. This is due to the effect that DMF has on ignition delay, which highlights how the practical effects of fuels cannot always be captured in these theoretical (laminar flame) conditions. Given the recent interest in these furanic fuels, further studies have advanced the understanding of the molecular breakdown of these fuels. Liu *et al*[283] observed a greater ability of butanol, over DMF, to decrease PAH emissions from a CI engine owing to the increase in formation of the cyclopentadienyl radical (C_5H_5) during DMF blended combustion. A kinetic study, coupled with flow reactor experiments, conducted by Cheng,[284] noted higher emissions of aromatics in MF pyrolysis, compared to DMF. This was postulated to be due to the greater formation of propargyl radicals

(an aromatic precursor) generated as a result of the unimolecular dissociation pathway identified as prevalent in MF pyrolysis.

While furans are an exciting class of oxygenated biofuel, more established fuels have also been investigated for their tendency to form PAHs. Wu *et al*[17] investigated the PAH concentration from the combustion of tripropylene glycol methyl ether and polyoxymethylene dimethyl ether, compared to diesel, and determined that the oxygenated fuels reduced the formation of particulate and gaseous phase PAHs and decreased PAH toxicity by 32%-55%. Zhang and Balasubramanian[285] used a single-cylinder, direct injection diesel engine in their studies into the effects of oxygenated fuels on the size distribution of soot particles and the final phase of PAHs associated with these particles. The authors also investigated the toxicity of engine-out particles by performing cell viability studies, and is reflected in PAH quantification by a parameter known as BaPeq, which is an equivalent compared to the toxicity of Benzo[a]pyrene as the standard. The key points to draw from this study were that oxygenated fuels reduced the particulate mass, but primarily only in larger particles, while blended fuels appear to increase the toxicity of the soot they produce, with a higher organic carbon (OC) fraction. The authors highlight that the soluble organic fraction (SOF) can induce a negative response in human airway cells, and the SOF increases when using 4wt% dimethyl carbonate, diethyl adipate and butanol in diesel blends.

From this review into the current knowledge of PAHs, both in their fundamental formation and presence in internal combustion engines, it is apparent that there are still knowledge gaps. In particular, there are few studies into the effects of biofuels on the amounts and types of PAHs produced in actual combustion engines. In flame studies, there are often contradictions in the effect of introducing oxygenated fuels into the fuel mix, with some observing increases and others a decrease in overall PAHs.[268] In order to better understand how oxygenated molecules combust, and therefore their tendency to form PAHs and subsequently soot, it is also important to consider the initial formation of the PAH molecules themselves, through

reaction mechanisms that include light hydrocarbon species formed as the fuel molecule breaks down in the early stages of combustion.

2.3.5. Formation of PAHs from gaseous precursors

Richter and Howard's extensive review published in 2000 provides an in-depth history of the understanding of how soot is formed, including the formation of the first ring and subsequent polyaromatic hydrocarbons (PAHs).[14] Firstly, and perhaps unsurprisingly, it is noted that aromatic fuels readily form soot precursors, such as acetylene, in high concentrations during fuel breakdown. These precursors not only react with each other- re-forming aromatic rings (benzene and naphthalene) and PAHs, which in turn react and polymerise to grow and ultimately form soot- but can also react with the initial aromatic fuel molecule. The authors highlight that aliphatic molecules, meanwhile, form the first ring from fuel decomposition products which exist in far lower concentrations than in aromatic fuel flames, limiting overall PAH and soot formation. In general, PAH precursors are more easily and abundantly formed when an aromatic structure is present in the initial fuel molecule. It is therefore expected that the trend in sooting tendencies increases from paraffins to monoolefins to benzenes to napthalenes. Also of note is the role of oxygen in radical removal, with sufficient oxygen allowing radicals to be removed and therefore hinder chain polymerisation reactions that form heavier hydrocarbons.

Acetylene has been studied in great depth based on the understanding of how this molecule is involved in soot inception and, subsequently, growth to increase particle mass. Smith notes that this interest has led to ample evidence that acetylene is the 'last stable species to be detected' before soot formation begins.[286] Berthelot[287] was among the first to suggest that benzene forms through polymerisation of acetylene. The HACA mechanism described previously contributes to aromatic ring growth through acetylene reactions with aromatic radicals, but acetylene addition reactions also leads to species such as butadiene,[288]

which are themselves precursors to aromatic ring formation due to their polarity making them readily able to react with species such as ethylene, and grow to higher hydrocarbon products. In addition, these radical hydrocarbon species have been shown by Bittner and Howard[289] to be important in nucleation of soot particles, reacting with phenyl radicals to eventually form naphthalene.

The Diels-Alder addition of 1,3-butadiene and ethylene, as well as alkene trimerization, are also potential pathways.[290–292] Cole *et al*[293] highlight the 1,3-butadienyl radical as a vital intermediate in benzene inception, through attack by acetylene. Frenklack and Warnatz[294,295] investigated low pressure acetylene flames and the reactions that determine the formation of benzene, inferring similar reaction mechanisms to those suggested by Cole, with the exception of cyclisation and hydrogen loss. These latter mechanisms were seemingly sensitive to the fuel composition. The cyclisation of n-C_6H_5 was observed as the dominant method of benzene production at higher temperatures, with this precursor forming through the reaction of acetylene with n-C_4H_3. C_4H_3 can be produced through hydrogen abstraction of vinylacetylene or reaction between C_2H_2 and C_2H. The results were reinforced by Colket[296], who put forward the case that, at different temperatures, cyclic molecules are formed through different mechanisms where, below 1500K, growth via butadienyl radical dominates but, above this temperature, addition to n-C_4H_3 is dominant. Ethylene flames have also been employed in reaction modelling, partly based on the prevalence of this molecule during combustion of molecules like octane.[297] Very recently, laminar co-flow ethylene diffusion flames have been studied by Jin *et al*[298]- utilising this type of flame based on the limited oxygen that premixed flames afford. The authors summarise though that kinetic modelling is limited by the fact that, other than HACA and HAVA mechanisms, PAH formation is not well understood.

While knowledge gaps remain, a better understanding of soot formation has been acquired through more advanced kinetic modelling techniques. Shukla[299] highlights that since the early work by Berthelot and others described above, further pathways to soot have been put forward by various research groups. Skjøth-Rasmussen,[300] for example, outlines the propagyl radical

as the dominant species responsible for benzene formation; propyne (the source of these radicals) was detected in significant quantities during acetone pyrolysis, suggesting the dimersiation of this C3 radical as a major influence on the formation of benzene.[299] Jin and Guo note that, in ethylene decomposition, propagyl radicals recombination is the dominant mechanism to benzene formation.[298] Modelling studies by Miller[301] have indicated the importance of propargyl radicals on benzene formation, while McEnally[302] concludes that these radicals are also of high importance in the formation of naphthalene. D'Anna and Kent[303] meanwhile, indicate the relative effect of various flame types on the reaction pathways that dominate aromatic formation. Under the conditions tested, propargyl radical addition actually contributed to naphthalene formation to a greater extent than the well-studied HACA mechanism, and in fact, acetylene addition to C4 species is a moderate contributor to initial benzene formation compared to propargyl combination. Meanwhile, the role of cyclopentadiene derived radicals in the formation of naphthalene, was determined as 'insignificant' in these doped and undoped diffusion flames; though in premixed flames this reaction is of high importance. Wang and Chung's review[304] on soot formation in laminar counterflow diffusion flames references work by Westmoreland *et al*,[305] whose investigations using acetylene/oxygen/argon flames suggested that propargyl recombination was not a major pathway to benzene. More recently though, with greater understanding of reaction kinetics, the propargyl radical has been investigated based on its relative stability- considering its free radical property- but nonetheless higher reactivity than radical-molecule reactions such as those put forward by Westmoreland.[305] The reaction between acetylene and n-C_4H_3 and n-C_4H_5, highlighted as important in benzene production by Westmoreland, was investigated further by Miller *et al*.[306] The investigation indicated that the aforementioned C4 species and their reaction with acetylene were insufficient to produce the observed benzene concentrations, and the authors instead suggested the recombination of propargyl radicals to form benzene or phenyl and hydrogen radicals. Georgievskii[307] meanwhile outlined alternative primary reactions of propargyl species, recombining to form fulvene or 2-ethylnyl-1,3-

butadiene- which can be converted to benzene through isomerisation. Propargyl radicals are known as resonantly stabilised radicals (RSRs), hence they are able to exist in relative abundance in a highly dynamic environment, such as a combustion flame, and thus expected to represent a significant component in first ring formation. Allyl radicals are also RSRs, and thus the reaction between allyl and propagyl radicals has been proposed as significant, but only in reactions involving certain fuels, such as allene; Wang notes that propagyl reactions meanwhile are 'always important', regardless of the initial fuel, and provides Figure 2.17 below to illustrate the major reaction schemes identified in forming the first ring.
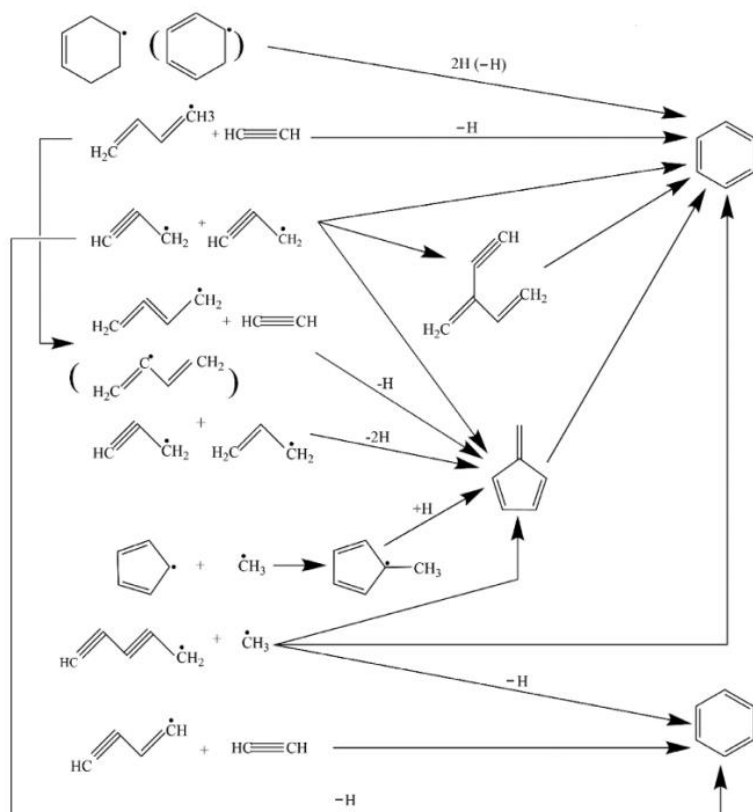
Figure 2.17: Identified formation mechanisms in the formation of the first aromatic ring, benzene[304]

Shukla[299] concluded that, depending on the fuel, the first ring can be formed through propagyl, vinylacetylene and methyl-cylopentadiene routes, or through reaction of vinylacetylene radicals (C_4H_4/ C_4H_3) and vinyl (C_2H_3) radicals. It appears a number of C2-C4 species are involved[14] however, as well as the C5 cyclopentadiene. Kislov *et al*[308] reference that benzene and naphthalene form as a result of propargyl and cyclopentadienyl radicals respectively. Studies have suggested the reaction between methyl and cyclopentadienyl radicals as another pathway towards fulvene- a benzene precursor.[309,310] However it should be noted that, even in a flame containing cyclopentene- readily able to form cyclopentadienyl radicals- propargyl recombination is the dominant reaction pathway.

A study by Blanquart *et al*[311] bears particular relevance in the case of precursor formation as, not only are species such as acetylene, propyne, propene and butadiene investigated based on their role in soot formation, but a range of 'engine relevant' fuels were tested. Combining modelling and previous experimental data for premixed flat and counterflow diffusion flames including iso-octane/air, n-heptane/air and acetylene/air, indicated that the type of flame was actually of lower importance than the type of fuel used in soot formation, as the type of fuel could disable entire reaction routes; appearing to disagree with the results from D'Anna, which suggest a strong effect of the flame condition.[303]

The impact of fuel molecular structure on types and relative quantities of soot precursors is an area that has not been fully explored. In 2006, Westbrook *et al*[189] used simulation techniques- particularly of esters- to support the theory that the amount of oxygen present in the fuel molecular structure is not the only factor influencing sooting tendencies of oxygenated molecules and, in fact, esters are perhaps less efficient in oxidising soot post formation with fuel-borne oxygen, as they are more likely to form CO_2 straight away, as opposed to single oxygen moieties. A study by Mueller *et al*[312] demonstrated that 'over 30%' of oxygen in the ester, di-buytl maleate, is not involved in soot oxidation. However, this study looked primarily at the effect of oxygen *post* soot formation, as opposed to how these oxygenated functional groups might impact initially precursor formation. Eveleigh[313] utilised carbon-13 tagged

molecules in order to elucidate the propensity of a specific atom in a fuel molecule to form soot, noting that the carbon atom connected to two oxygen atoms in an ester- ethyl acetate- has a negligible contribution to soot formation, suggesting this carbon remains bound to oxygen as CO or CO_2. Furthermore, the carbon atoms bonded to oxygen atoms in ketone and alcohol moieties were found to contribute to soot formation to a lesser extent than alkyl carbons.[314] Importantly, in an engine there exists regions of varying temperature and concentration of fuel that introduce a vast range of factors that can be expected to decrease or increase soot concentration. Smith[286] highlights the point that in high temperature premixed zones of an engine, the amount of oxidative species coupled with the expected temperatures, mean that fuel molecular structure likely has little bearing on soot emissions. Instead it is in the diffusions flames, and lower temperature regions where reactions are likely more sensitive, and possess sufficient residence times for the molecular structure of the initial molecule to have an impact on the reaction pathway, where there are also fewer oxidative species to interfere.

A combination of Dec and Argachoy's model is supplied below,[156,315] highlighting regions of the fuel jet reaction profile in which emissions formation occurs.
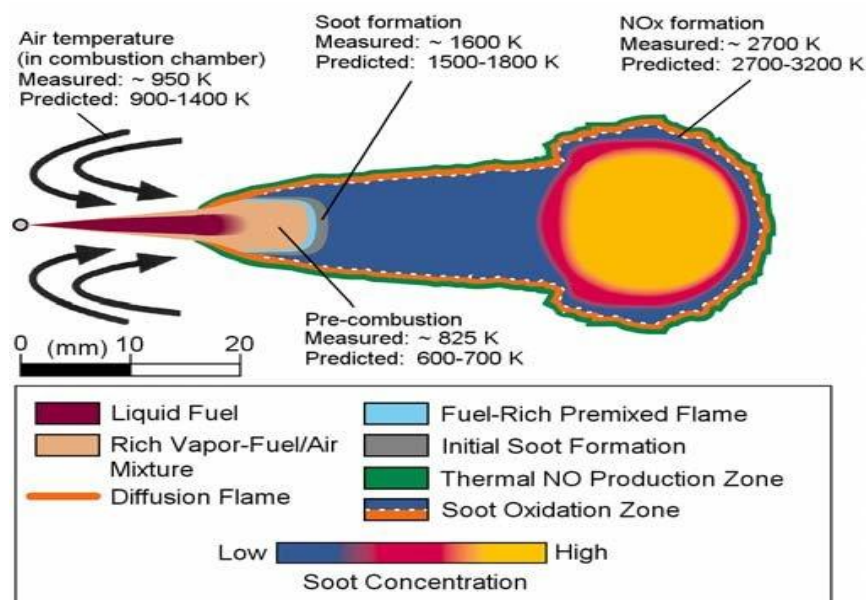
Figure 2.18: Illustration of diesel fuel jet reaction profile, combined with measured[316] and predicted[315] temperatures

Figure 2.18 illustrates the regions of a fuel spray and the varying temperatures measured/modelled therein. It is clear that diesel, with or without the presence of oxygen, may be exposed to temperatures varying from approximately 600K to 3200K- and this does not account for inhomogeneities and hot spots that could see higher temperatures still. Overall though, the primary area of soot formation is found just on the edge of the premixed rich zone, and within the diffusion flame whereby combustion products move outwards and reactants move inwards, encapsulating the jet. Temperatures within the flame are high, sufficient to produce NO_x, but the stoichiometry is too lean for soot production, hence fuel pyrolysis products are mainly found downstream of the diffusion flame, and the pyrolysis initially occurs at temperatures of approximately 1500K. Subsequent soot oxidation requires temperatures exceeding 1800K.[317]

2.3.6.   Experimental studies into the formation of PAH precursors

2.3.6.1.   Flame and reactor studies

Internal combustion engine emissions provide a real-world picture into the various degrees of pollutant formation of the fuels tested. Often, however, the understanding of the fuel in question is not well-developed and the complexity of combustion in an engine, as well as residence times of combustion of approximately 8 ms,[318] can obscure more subtle fuel effects. For instance, the ignition delay time of a fuel is one of the most influential parameters in dictating subsequent combustion characteristics, such as peak heat release rates and emissions of CO, NO_x and particulates. Therefore a shortened ignition delay will likely impact emissions of particulates more so than a change in the fuel molecular structure.[83,319] For this reason, more controlled conditions are employed to enhance the understanding of molecular breakdown. Liu *et al*[320] recently performed a comparison of sooting tendencies of different butanol isomers in laminar diffusion flames, finding that sooting rates decreased from t-butanol> i-butanol> s-butanol> n-butanol, referencing that coflow diffusion flames are often

used in studies of soot growth and oxidation in different fuels.[320] Saffaripoir *et al*[321] utilise these types of flame also in determining soot formation and size distributions of an aviation surrogate fuel, in order to develop models for future jet engine designs and operation techniques. Botero[322] utilised diffusion flames to test liquid hydrocarbons- noting that the *liquid* fuel tests in these flames are more scarce, potentially based on difficulties in vaporisation- observing a general decrease in particulate diameter as carbon number of the tested fuels increased, and a decrease in size from cyclic paraffins, to iso-paraffins to n-paraffins. There is naturally significant research into the development of modelling methods; accurate models negate the need for expensive experimental apparatus and potential associated errors. Blacha *et al*[323] developed soot predictions for laminar flames in their study of fuels from ethylene to toluene- 1D premixed, asymmetrical premixed and non-premixed regimes were employed in order to develop CFD modelling techniques. However, while flames are the primary mechanism to simulate fuel breakdown, often in combination with computational models, Kc[324] references the problem of molecular transport and heat transfer in the validation of these models. They put forward the use of shock tubes as a potentially more controllable experimental device; with a stationary gaseous sample and tuneable temperatures and pressures. Manzello *et al*[325] utilised both a stirred reactor and plug flow reactor in series to investigate the formation of PAHs and particle size distribution, while Sanzhez[326,327] conducted studies into PAH and soot formation of acetylene and ethylene in a tubular flow reactor- one of the first to investigate the pyrolysis of these molecules in such a reactor. A flow reactor was also employed by Esarte *et al*,[328] looking at the pyrolysis of acetylene and ethanol blends utilising different blend ratios and temperatures between 975-1475K. This system indicated that, at higher temperatures, amounts of gaseous soot precursors decreased, while higher ratios of ethanol in the initial blend decreased soot formation- although not linearly- while increasing precursors to PAHs, such as methane, ethylene, ethane and benzene. Flow reactors and shock tubes have been used extensively in the pyrolysis of acetylene- Sanchez[326,327] performed a series of investigations using a plug flow reactor and pure acetylene, while Shukla *et al*[99] utilised the

same type of reactor to investigate benzene and toluene pyrolysis, in addition to acetylene. Bensabeth et al[329] looked specifically at quantifying the aforementioned 16 Priority PAHs during acetylene pyrolysis, also utilising a tubular reactor, at low pressure (8kPa) conditions at 1173K; they observed a general increase of PAHs with residence time, as well as a decrease in PAHs when using pure acetylene, as soot itself was formed from the PAH precursors. To date, there are few studies looking into pyrolysis products of more complex fuels beyond the formation of soot particles. Jiang[330] conducted an investigation into sooting tendency of blends of DMF and iso-octane in inverse diffusion flames, while Wang et al[331] utilised co-flow laminar diffusion flames in an investigation into soot formation of heptane blended with various oxygenated- potentially bioderived- fuels, such as anisole and benzyl alcohol. Liu and Cheng,[332] meanwhile, recently investigated the use of ammonia in reducing soot formation in ethylene diffusion flames. Utilising tubular reactors, investigations involving ethanol were undertaken, given its plentiful supply and proven use in low blend ratios in gasoline fuel today.[333,334] Viteri's study[333] investigated the effect of temperature and residence time on the formation of certain PAHs, while Zhao[334] performed a similar study- though also studied the effects of the addition of methane, water vapour and oxygen- on the formation of soot in the rector effluent. Alexandrino[335] utilised a potential biofuel- dimethyl carbonate- in a flow reactor at temperatures of 1075-1475K, due to its ability to reduce emissions of benzene and 1,3-butadiene in diesel engines. Looking at the soot formation, DMC was noted to produce low amounts of soot due to preferable formation of CO and CO_2. The same author also used DMF under similar conditions, and varying concentrations, to determine the effect of this molecule on the soot formation under pyrolytic conditions, noting an effect on the soot yield, but not the gas yield.[336] γ-valerolactone, already alluded to as a molecule of interest as a fuel extender of gasoline, was also investigated in an experimental and computational pyrolysis investigation,[337] whereby isomerization of the molecule to 4-pentenoic acid and hydrogen abstraction were the main reaction pathways during the breakdown of this molecule.

Overall, however, the lack of any investigation into the formation of initial soot precursors- and molecular breakdown as a whole- of more complex biofuels, particularly those for diesel engines, is a significant knowledge gap.

2.3.6.2. *In-cylinder sampling studies*

The majority of literature surrounding particle emissions centres around the exhaust output. The exhaust emissions are released into the atmosphere where the toxic contents are exposed onto people, resulting in the aforementioned health issues such as asthma and, potentially, cancer from carcinogenic particulates. However, understanding of how soot particles are formed can only be ascertained by gaining the ability to 'see' the soot formation in real time. In the case of an engine, this means being able to determine species formation within an engine cylinder while combustion progresses at different crank angle degrees. Such understanding can help decide whether a certain fuel or development in the engine combustion system can help inhibit pollutant formation.

The first employment of in-cylinder sampling techniques can be traced back as far as the 1970s. Bennethum's preliminary study[338] investigated the sampling valve design itself and determined effects of valve operation on the composition of an actual sample, noting that nitric oxide reactions ceased due to the temperature reduction within the cylinder caused by valve operation. A few years later, Duggal, Priede *et al*[339] utilised a gas sampling valve to detect concentrations of CO, NO and soot on a time basis in an indirect, swirl diesel engine. Prior to this, Miwa *et al*[340] performed their own in-cylinder sampling studies within a two-stroke engine to determine spatial distributions of pollutants within the swirl chamber; at that time, photographic imaging was also being used in studies aiming to gain insight into pollutant formation,[341,342] with sampling techniques in their infancy. In the early 1980s, Aoyagi *et al*[343] used a cylinder sampling technique in order to measure concentrations of soot, in which there was still a great deal of uncertainty. In that study, spatial distributions of pollutants were also investigated in a direct injection diesel engine, while the effects of parameters such as injection

timing and swirl ratio were also analysed. Soon after this study, Kittelson *et al*[344–350] carried out in-cylinder sampling investigations, noting that previous gas sampling experiments saw no spatially integrated time-resolved measurements. Their initial study[344] marked the start of a series of papers, dedicated to bettering our understanding of soot emissions of different engines operating under varying conditions, while also making comparisons to modelling data to simultaneously advance these theoretical techniques. They observed particle distributions at different engine load conditions, which suggested a far greater rate of soot oxidation at low loads, when more oxygen was present. Soon after, sampling was performed as a function of CAD to more accurately elucidate engine conditions during which the sample was taken.[351]

However, one of the first examples of in-cylinder sampling during the use of alternative fuels was carried out by Bertoli and Giacomo[352] who used ethylene-glycol dimethylether, diethylene-glycol- dimethylether, diethylene-glycol-diethylether and butylether, compared to tetradecane and n-octane in a single cylinder DI engine. They noted an increase in heat release rate during diffusion-led combustion, suggesting that the fuel oxygen was responsible for the oxidation of intermediate products. They also concluded that fuel physical properties have a large effect, since fuels with higher volatility and cetane number tend to produce larger amounts of pyrolysis products, though in the case of the oxygenated fuels this pattern was less pronounced. Furthermore, aldehyde formation appeared to be prevalent in the premixed phase of combustion and, again, the emissions of these was significantly reduced with the use of oxygenated fuels. A subsequent study by Pungs *et al*[353] into the particle distribution of in-cylinder samples also noted a change in soot concentrations depending on the aromaticity of the fuel, determining that aromatic content increases soot output until approximately 10-12% aromatic content, after which there is little further effect. No effect in the size distribution was noted with a change in fuel aromaticity. However, oxygen-containing fuels were shown to produce smaller particles and also decreased tailpipe emission of soot (on a mass basis) for a given aromatic content.

The ability to determine in-cylinder concentrations of soot and NO_x has long been established, but the elucidation of PAH formation, which are soot precursors, was slightly delayed. In the later

1980s, Barbella *et al*[354,355] performed in-cylinder analysis on a diesel engine to determine concentrations of light hydrocarbons and inorganic species, as well as soot, using a highly aromatic diesel fuel and two distinct sampling spatial positions, chosen to capture different times at which the swirling air would cross these points. No acetylene or ethylene was detected, while methane was more prevalent at the position that encountered air motion earlier. They noted that the choice of fuel perhaps obscured the likely low concentrations of gaseous hydrocarbon precursors. Likely as a result of these findings, the same group undertook a similar study, though using tetradecane as their primary fuel, and compared this to a blend of 10% methylnaphthalene and 90% tetradecane in order to gauge the effect of aromaticity on the evolution of pyrolysis.[356] On this occasion acetylene was detected, attaining its maximum concentration before maximum soot concentrations, and was found in higher abundance with the use of the aromatic blend. Wang *et al*[357] meanwhile performed a similar investigation while using heptane and toluene blends, highlighting the need for 'systematic data on the evolution of in-cylinder PAHs'. This was one of the first studies looking at the types of PAHs formed, with the authors observing that naphthalene was the most abundant PAH detected, while PAHs with five membered rings were also observed in relatively large concentrations, suggesting their importance in soot growth. Furthermore, the addition of the aromatic toluene molecule into the fuel reduced the relative amount of naphthalene, but increased the amounts of larger PAHs, hypothesised to be due to the simultaneous increase in species such as methane, which would aid ring growth towards species such as fluorene, while toluene rings themselves have been shown to combine to form anthracene and phenanthrene.[358] Additional work by Liu *et al*[359] looked into the groups absorbed onto soot particle surfaces, using the same heptane/toluene fuel. Before Liu's study, this type of investigation had mainly focussed on soot produced from exhaust emissions or from synthesised premixed/diffusion flames.[360,361] Liu detected an extremely non-linear relationship between the variation of surface functional groups (SFGs) and combustion phasing; an initial increase in aliphatic groups was noted in the engine premixed combustion stage, potentially from early-stage soot particles with aliphatic shells, with a decrease then seen as premixed combustion temperatures and pressures increased to promote

dehydrogenation/carbonisation. A further increase was then noted in the diffusion phase where more soot begun to form, followed by a final decrease. The same overall pattern was observed for oxygenated functional groups on the soot surface (C=O and C-OH). Meanwhile the pattern remained largely unaffected by the type of fuel used i.e. heptane or heptane/toluene, though the more aromatic blended fuel produced higher amounts of each SFG overall. Research by Malmborg and Eriksoon[362] also performed in-cylinder analysis on a heavy duty diesel engine, looking more specifically at the soot's nanostructure, which is key in determining particle reactivity (particularly its oxidative tendency) and therefore the ultimate soot emissions. It is referenced[363] that high curvature soot structures have been observed for biodiesels, implying a change in formation and oxidation rates; Liu's study in SFGs also highlighted higher curvature as important in providing more sites for binding of functional groups (C-H (aliphatics), C-OH (alcohol) and C=O (carbonyl) species), thus making the soot particles potentially more reactive by affording very reactive edges.

In-cylinder sampling is a powerful tool in allowing a real-time picture of combustion processes to be observed. In the past, soot particles and their properties have been focussed on, with some research performed on the formation of particulates from PAHs. To date, however, no work has focussed on in-cylinder samples of the gaseous precursors discussed in Section 2.3.5.

2.4. Conclusions and knowledge gaps

From this review, it is clear that sourcing fuels from biomass to yield a cleaner diesel combustion process is not a new concept. A number of conclusions in this area can already be made. On biofuel sources:

1. Lignocellulose, as a "second generation biofuel", has distinct advantages over current ethanol/biodiesel fuels that rely on edible sources of biomass that compete for land space with food sources, such as sugar cane for the production of ethanol.

2. The complexity of lignocellulose is both an advantage and a drawback- it is difficult to attain individual pure fractions, but the available chemicals that may be derived from it are numerous.

3. Furan-based molecules are one of the main types of molecule that can be derived from lignocellulose, therefore derivatives of these are highly interesting as future fuels. The lack of precious metals and energy intensive steps to attain these molecules could make them economically viable fuel candidates.

4. Lactones are a further class of fuels that have been shown to work in engines, however these have received relatively little attention as a diesel blending component, as the most widely used, GVL, possesses a low carbon number.

5. Hydrogen fuel potentially circumvents the entire combustion process and associated emissions drawbacks, but the use of fuel-cell technology has not become widespread, primarily due to issues associated with the handling of hydrogen, as well as the high cost of fuel cell technology.

On diesel combustion and the effect of biofuels:

6. Diesel combustion can be divided into four main phases; ignition delay, premixed combustion, diffusion controlled combustion and late-stage combustion. Diffusion/mixing-limited combustion is dominant in CI engines operating at high load.

7. The use of biofuels have various and sometimes opposing effects on the diesel combustion process through a range of factors. Ignition delay depends on both physical and chemical factors and the use of some biofuels can reduce viscosity to increase atomization, hence improve ignition quality, but the presence of oxygen can hinder low temperature reactions and result in an increase in ignition delay.

8. The lower calorific content of oxygenated fuels means that fuel consumption increases, especially with higher blend ratios, but this can be counteracted to an extent with more efficient combustion.

9. Emissions of PM, NO_x, CO and hydrocarbons are all effected by using biofuels, but the effect changes depending on the engine operating conditions, such as the speed or load.

10. CO and HC emissions are generally formed due to a lack of oxygen present (in a locally rich air-fuel mixture), therefore the presence of fuel bound oxygen could reduce these species.

11. NO_x and PM emissions tend to oppose one another, generally resulting in a 'trade-off'. Leaner combustion can increase emissions of NO_x, however if the mixture is too lean then the prevalent thermal NO_x mechanism is inhibited. A longer ignition delay (from a fuel that possesses a lower cetane number) can result in reduced PM emissions due to better air-fuel mixing, but greater NO_x emissions because of higher in-cylinder temperatures.

12. Hydrogen as a fuel possesses drawbacks that have limited its use in the transportation sector. However, on-board reforming and the use of ammonia could provide a solution to safety issues and have been shown to provide additional energy within conventional combustion engines. This tends to result in higher NO_x emissions, due to higher combustion temperatures associated with hydrogen burning, but lower soot emissions due to the reduced fuel carbon energy contribution.

On particulate emissions:

13. PM emissions are heavily regulated and will likely become even more so in future iterations of emission standards. Their detrimental health effects are known and

reducing overall PM mass and number is a key challenge in engine design; meeting these regulations can also be aided by the use of biofuels.

14. Oxygenated fuels reduce overall soot emissions due to an increase in oxidation of the particles post-formation, however smaller soot particles are more likely to cause human health problems. Furthermore, the type of oxygenated molecule and the location of the oxygen group within a molecule can change its relative ability to reduce soot emissions.

15. PM is formed via a multi-stage process, with one of the main precursors being PAHs, which are also toxic to humans. These can either form part of the soot itself or adsorb onto the surface and hence become available to interact with human tissue. Particulate growth is then governed by a number of physical processes such as coagulation and agglomeration.

16. PAHs are themselves formed via multistage processes involving gaseous precursors, often radical species, including ethyl, propargyl and cyclopentadienyl radicals and acetylene.

A holistic picture of the entire process of converting plants (biomass) to future fuels and using these in a real engine is difficult to find in the literature. For the most part, the production of a potential fuel is specifically discussed, alternatively an oxygenated fuel is taken and the downstream consequences of combustion are investigated. The main areas identified that require further research include:

17. Oxygenated group comparisons (aldehydes/ketones/esters/alcohols etc); these have already been carried out on aliphatic molecules, but not for furan-based molecules. As such, a systematic study of oxygenated fuels, but with furan bases involved, could help in developing a molecule that can be relatively easily synthesised from biomass.

18. The majority of bioderived, oxygenated fuels employed in diesel combustion experiments are relatively conservative, centering on alcohols (butanol and pentanol),

esters produced from transesterification or MF/DMF. Biomass can provide an extensive range of fuels that could possess the carbon number and energy densities needed for use as a substitute to (or blended) diesel fuel.

19. Analysis of the types of PAHs produced in experiments of using biofuels is fairly limited, and increasing the understanding of PAH formation may help in gaining support for the use of biofuels; for example, by potentially confirming their ability to mitigate the toxicity of exhaust gases on humans.

20. While reactor and flame studies provide a controlled environment to accurately detect the formation of soot precursors from novel fuels, sampling from an engine is a powerful tool to detect the real-world impact of combusting these fuels on gaseous hydrocarbons and, therefore, soot.

From these conclusions of the literature survey, the fundamental aims of the current research were determined:

- Investigating a range of novel biofuels, ideally derivable from non-edible sources, to outline the effects of these fuels, and their specific molecular structures, on combustion and emissions when used as a diesel fuel extender in an unmodified CI research engine. Furanic species will be selected for this systematic study.

- To identify, and investigate the combustion characteristics of, a further class of renewable fuels informed by the influence of specific fuel molecular structures observed in the study of furanic species. Employing these fuels in potentially higher blend ratios, or as pure fuels, is hoped to broaden the discussion of 'advanced biofuels'.

- Further understanding the combustion of novel fuels requires the utilisation of bespoke sampling techniques to determine the initial products of fuel breakdown; this has the benefit of enhancing understanding of early stage combustion reactions, as well as the tendency of a molecule to potentially form PAHs and particulates. Utilising novel fuels in both an engine and (for a more fundamental understanding) a tubular reactor,

sampling and specification of fuel decomposition and pyrolytic reformation products will be performed.

- Exploiting the benefits of hydrogen fuel, in a way that is both safe and cost-effective, is a major challenge for this technology; aspiration of an aqueous ammonia solution, to supply energy to the research engine, will be experimentally investigated as a potential way of realising the benefits of hydrogen as an energy vector without major engine modification or safety concerns.

In order to achieve these aims a single-cylinder, light-duty diesel engine will be utilised to combust the wide variety of potential renewable fuels envisioned. A detailed description of this, as well as the other hardware used in the study (such as the in-cylinder sampling valve, tubular reactor and GC-FID), will be outlined in Chapter 3.

3. Experimental setup and methodology

The following section discusses the various experimental procedures used in the tests undertaken. The diesel engine used in this system is discussed, as well as the fuel injection system used for base diesel and test blends, and the instruments used for exhaust analysis. The software utilised for testing will also be discussed, although a more detailed review of the instrumentation and data acquisition can be found in the thesis of Talibi;[364] no major changes to the engine or fuel delivery hardware were made between the work by Talibi and the current study; however, some changes were made to the injection software during this research. The various fuels were blended in the required ratios, whilst ensuring a single-phase mixture had been formed that would produce consistent results upon combustion in a single cylinder diesel engine. A sampling valve was utilised to extract cylinder gases during different stages of combustion, with the subsequent sample injected into a Gas Chromatography-Flame Ionisation Detector (GC-FID). The tubular reactor used for pyrolysis of fuels will also be explained, from which samples were extracted and also analysed by GC-FID.

3.1. Diesel test engine

The research engine, specified in Table 3.1 below, was a direct-injection, custom built, 4-stroke single cylinder compression-ignition engine. The majority of components (cylinder head, intake manifold, fuel injector, piston and connecting rod) were from a 2.0 litre turbocharged diesel engine (Ford Duratorq CD132 130PS). For the engine crank case, a Ricardo Hydra single cylinder crank case was employed; an adaptor plate was required to utilise the head into the single cylinder configuration. A David McClure DC motor dynamometer, capable of motoring the engine up to 5000 rpm, was controlled by a Cussons test-bed console. The

combustion chamber itself, as stated in Table 3.1, consisted of a ω shaped bowl piston and a flat roof with two intake and two exhaust valves, and a centrally located injector.

Control of injector opening time and duration was initially undertaken with an Emtronix EC-GEN-500 electronic control system in conjunction with an associated software program (Emtronix EC Lab), utilising a timing signal from a crankshaft-mounted Hall Effects sensor; results found in Chapters 4 and 5 were obtained using this setup. Subsequently, a custom made Labview code was employed in conjunction with an injector driver, utilising the shaft encoder to reference injection timing, with an output signal on an independent time basis by making use of a separate Data Acquisition (DAQ) counter task. In-cylinder pressure was monitored using a pressure transducer (Kistler 6056A) and charge amplifier (Kistler 5018) at a resolution of 0.2 CAD, as measured by a crankshaft-mounted shaft encoder.

An external pump was used to pump lubricating oil around the crankcase and cylinder head, maintained at a pressure of 4 bar and heated to a temperature of approximately 80°C. An external cooling system was also used, allowing for the engine to be preheated to a steady state temperature prior to the start of running. The control system of this is provided in greater detail in the thesis of Talibi.[364]

For all tests included in this report, the engine was run naturally aspirated (although the experimental setup includes a supercharger for running at boosted intake air conditions). Naturally aspirated, atmospheric air is inducted through a filter into a Romet Type G65 air-flow meter (volumetric flow rates were converted into mass flow rates at this stage using a pressure transducer (Druck PTX 717-3257) and K-type thermocouple) and, subsequently, a damping chamber (plenum) after which it enters the intake manifold. For the tests outlined in Chapter 4, an external heater (Secomak Model 571) was applied so that the intake air could be heated to 120°C before entering the manifold system so that all test fuels ignited.

Exhaust gases exited through the laboratory extraction system via a silencer. The exhaust pressure and temperature were measured using a pressure transducer (Druck PTX 717-3275) and a type-K thermocouple placed downstream of the exhaust port.

Table 3.1: Diesel engine specifications

Engine Head Model	Ford Duratorq
Engine Crankcase Model	Ricardo Hydra
No. of Cylinders	1
Cylinder Bore (mm)	86
Cylinder Stroke (mm)	86
Swept Volume (cm^3)	499.56
Geometric Compression Ratio	18.3 : 1
Max In-Cylinder Pressure (bar)	150
Piston Bowl Design	Central ω bowl
Fuel Injection Pump	Delphi single-cam radial-piston pump
High-pressure Common Rail	Delphi solenoid controlled (Max 1600 bar)
Diesel Fuel Injector	6-hole solenoid valve injector (Delphi DFI 1.3)
Fuel Injection System	1 µs duration (EMTRONIX EC-GEN 500 & in-house Labview system with injector driver)
Crank Shaft Encoder	1800 ppr (0.2 CAD resolution)
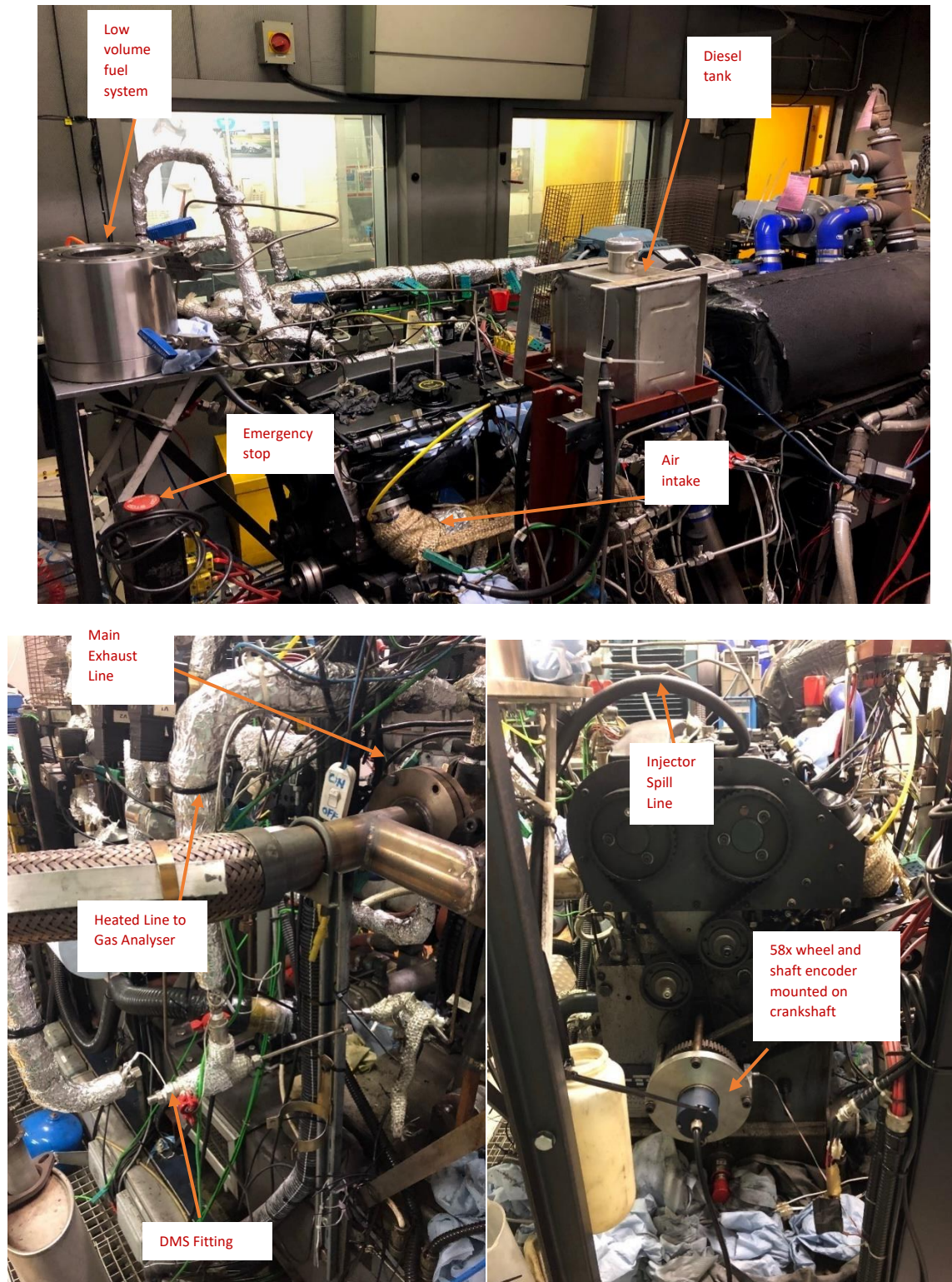
Figure 3.1: Single cylinder diesel engine research facility

3.2. Fuel injection system

For base diesel testing, the engine was supplied with fuel directly using a conventional common rail circuit fed by a header tank via a high pressure fuel pump. These tests were conducted at the start and end of each day to determine any drift in engine performance that may have occurred during testing.

3.2.1. Common rail fuel circuit

The header tank possessed a capacity of 2 litres and was located 350mm above the fuel pump (Delphi 33100-4X400). Before entering the fuel pump, the fuel passed through an inline filter (Delphi HDF924) to remove any particles in the diesel fuel. After leaving the fuel pump, the fuel entered the high pressure common rail (Delphi B47KA). At one end exists a pressure transducer and at the other a pressure relief valve (PRV). For this study, an adaptor was produced such that a Bosch PRV (CR/DRV-PSK/20S) could be installed instead of the Delphi valve; signals from both met the same electrical output specification so that this was a like-for-like replacement. Fuel spill occurred from the pump, common rail and injector, this was cooled (additional information provided in Talibi's study[364]), and was fed back into the fuel supply system before the re-entering the fuel pump.

A commercially available 6-hole (154µm diameter) servo-hydraulic solenoid valve diesel fuel injector was utilised for all experiments.

3.2.2. High pressure low volume fuel system (HPLVFS)
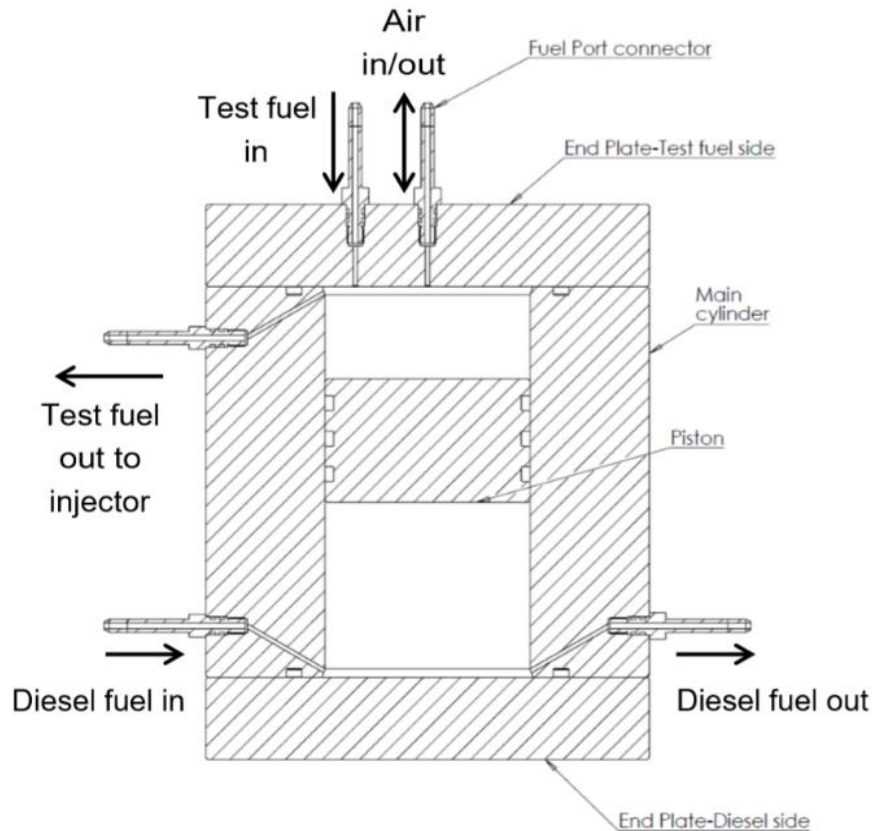
Figure 3.2: Cross sectional view of high pressure fuel system

For the test blends, a novel fuel system was employed for the injection of a blend into the combustion chamber. There existed three fundamental issues with using the standard header tank for these fuels; the cost of some of these molecules was such that testing these in the quantities required for the standard system was not economically feasible; secondly, the inability to purge the header tank from contamination of other fuels meant that residual test fuels would likely render results invalid if ignition properties had varied significantly between sequential fuels. The final problem was that the properties of some of the test fuels, such as viscosity and density were not suitable to use in the standard common rail system.

As a result, a fuel system that had been previously designed and was able to utilise low amounts of fuel (less than 1 L), be easy to clean and reuse for different fuels in relatively quick

succession, and bypass the most sensitive components on the standard injection system (such as the fuel pump) that would be most susceptible to corrosion or failure due to a lack of lubricity, was used for all tests described in this report. The design of this fuel system is shown in Figure 3.2.[364] The stainless steel vessel is capped at both ends, with one end readily available to remove the vessel's lid. A free moving piston travels inside which divides the vessel into two chambers; the one below the piston is connected to the standard common rail injection system and therefore can be pressurised using the common rail fuel system. The chamber above this is for the test fuel; for each engine experiment, approximately 180 ml of test fuel was added to this and the vessel sealed. Mixing of the diesel and test fuel, as well as leaking of the diesel or test fuel from either chamber, was prevented using O-rings on the lids, the top and bottom of the vessel and the piston itself.

A two-part high-pressure housing, containing sintered steel filter elements of a pore size of 1μm, was placed between the fuel system and injector to prevent any particles damaging the fuel injector; this can also operate at pressures up to 2000 bar.
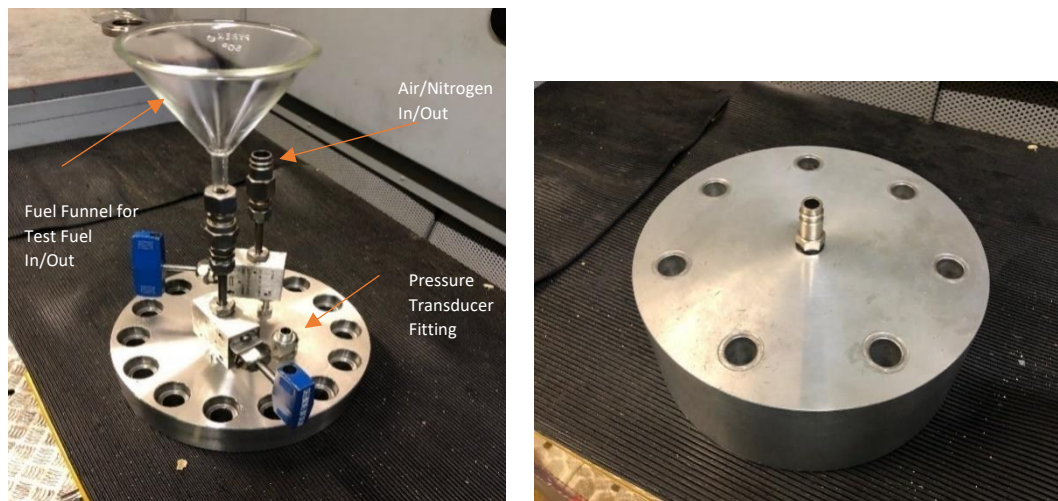
Figure 3.3: HPLVFS lids; during testing (left) and to remove piston/piston O-ring (right)
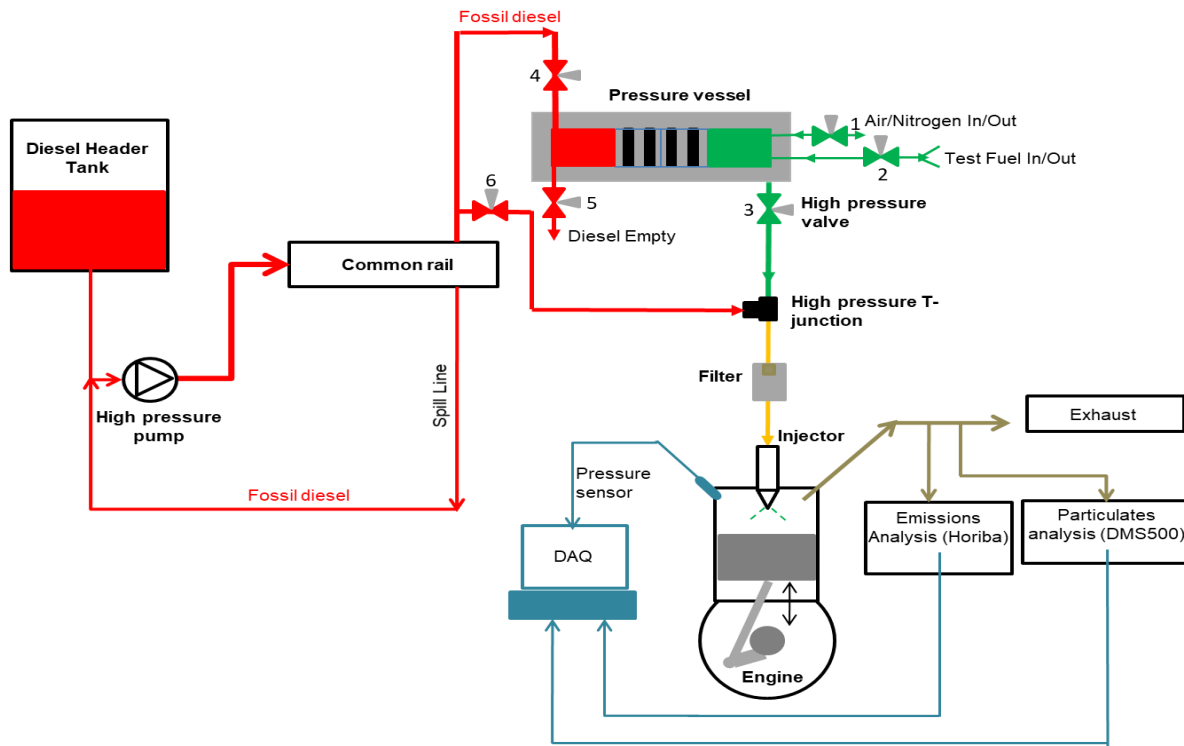
Figure 3.4: Schematic of experimental setup, including injection directly from the common rail (through valve 6) and via the low volume fuel system

The following procedure was used for the filling and subsequent cleaning of the fuel system following each test.

With all valves kept closed unless specified otherwise:

1. (Valve 4 open and Valve 2 open until fuel rises into the funnel) Upon adding the test fuel, the system was first pressurised with diesel fuel (motoring the engine subjected the necessary pressure to move the piston) using the Emtronix control system so that the air in the system could be bled and the test fuel was at the top, and therefore immediately available for injection. The piston was free moving therefore the pressure applied to the diesel below the piston was directly subjected onto the test fuel above the piston

2. (Valves 3 and 4 open) During testing, the engine may be operated using the DAQ software (see Section 3.4) in the same way as with the normal common rail injection system.

3. (Valve 6 open) Once the test has been completed, fossil diesel was run through the fuel line (orange line in Figure 3.4) to purge any residual test fuel within.

4. (Valves 1 and 5 open) Diesel fuel was extruded from the bottom of the vessel using nitrogen subjected to the top of the vessel. If the next test utilised the same fuel, the system could be refilled at this stage.

5. (Valve 5 open) To change fuels, the top O-ring on the piston was replaced to avoid contamination. This was performed using nitrogen supplied from the bottom of the fuel system and an alternative lid (no valves 1 or 2) that allows movement of the piston slightly above the top of the chamber for the O-ring to be exposed (lid comparison shown in Figure 3.3).

6. (Valve 5 open) The piston was pushed back down using nitrogen, the lid removed, the test chamber thoroughly cleaned and the next test fuel added before the procedure was repeated.

3.3. Emissions analysers

Gaseous emissions (CO, CO_2, NO_x, O_2 and EGR-CO_2) were all measured using a Horiba MEXA 9100H EGR automotive gas analyser pictured in Figure 3.5. (O_2 was measured but is not herein reported, while EGR-CO_2 was not measured since exhaust gas recirculation was not performed in these tests). Particulate emissions (size distribution, mass and number) were measured using a particulate spectrometer (Cambustion DMS500).

3.3.1. Gas analyser

The heated line connecting the engine exhaust to the gas analyser was maintained at 190°C to prevent condensation of gaseous species in the exhaust. The heated line connected

to the gas analyser transports exhaust gas first to a filter and then a condensation unit where water and gaseous hydrocarbons were removed.

CO and CO$_2$: A non-dispersive infrared (IR) adsorption analyser was used to determine the concentration of CO and CO$_2$ in the exhaust sample. Infrared analysis utilises the individual wavelengths at which specific bonds absorb energy, and this depends on the type and number of vibrational modes of a molecule. CO$_2$, for example, has four vibrational modes, which all result in different wavelengths of absorption (not all of which are infrared active).[365] This produces a specific IR signature; radiation at 2349 cm^{-1} and 667cm^{-1} excites particular vibrations in CO$_2$ that can be detected using IR. CO meanwhile possesses only one vibrational mode since it is diatomic. The degree of absorption at this wavelength can then be used to calculate the concentration of these species based on the temperature and pressure of the sample.

The frequency of the infrared beam was modulated and the intensity of this beam that reaches the detection cell is determined by measuring the deflection of a metallic membrane within this detector; this deflection is measured by a capacitive sensor.[366]

Two detectors in series are used in this instance; the first measures both low concentrations of CO and CO$_2$ (although the latter contributes only minor amounts to the overall output signal), while the second monitors the concentration of high levels of CO and CO$_2$. The absorption energies of these molecules do not overlap,[366] therefore can be measured at the same time by the second stacked detector if both exist in similar concentrations (CO-high and CO$_2$ detection measure similar levels).

Figure 3.5: Horiba gas analyser

NO$_x$: Nitrous oxide emissions were measured using a chemiluminescent analyser (Horiba CLA-150), which operates by mixing the gas sample with ozone (O$_3$) and measuring the photons emitted by the electrically exited NO$_2$ that is formed from the subsequent reaction (equation 3.1). The analyser can be used to measure NO emissions or NO$_x$ emissions; for the latter, the sample needs to pass through a NO$_2$ to NO converter before entering the reaction chamber with O$_3$. In the reaction chamber itself, the following reaction ensues:

$$NO + O_3 \rightarrow NO_2{}^* + O_2 \qquad \text{(Eq. 3.1)}$$

The excited NO$_2$ emits photons as it returns to its ground state, and the luminescence produced can be measured using a photosensitive diode, which produces an output signal that is proportional to the concentration of NO (+ NO$_2$ if the aforementioned converter has been used). In these tests, only the overall NO$_x$ was measured.[366]

O$_2$: The emissions of oxygen were recorded in these studies, although they were not relevant to the current work and are therefore are not provided in this report. However, a brief description of the method in which they are recorded is explained.

A magneto-pneumatic cell (Horiba FMA-125) was used which attracts oxygen molecules towards a charged pole. Since O$_2$ possesses a significantly higher paramagnetic value than any other of the exhaust gases, other gases are unaffected. This migration of O$_2$ disrupts the flow of nitrogen within the sample, and this disruption can be measured as a pressure differential between two of these poles. The pressure difference is converted to an electrical output that is relative to the oxygen concentration.[366]

Unburnt Hydrocarbons: In general, hydrocarbons are detected using a flame ionisation detector (FID) that utilises a hydrogen and air flame to break hydrocarbon bonds into ions and electrons. These can subsequently be detected using two electrodes at either end of the flame, which generates a current that is proportional to the number of carbon atoms. However, due to an equipment fault, hydrocarbon emissions were not recorded in these experiments.

3.3.2. Particulate spectrometer

A Cambustion DMS500 was used to detect the mass and number of particles, as well as the size distribution between diameters of 5nm and 1000nm. The exhaust gas passes from the engine exhaust to a heated (80°C) cyclone, where the gas is diluted (1st dilution factor set to 5) and larger particles (greater than 1µm) are removed. The sample is then again diluted (this was set to 50 for these experiments for accurate sampling) and flow through a corona discharge charger which ionises the particles. The particulate emissions are determined based on their specific ratio of electric charge to aerodynamic drag, therefore adding charge to these particles is necessary before they enter a classifier column which deflects particles towards grounded rings. The deflection of these particles depends on the particle size and the charge, which can both be used to determine particle size and number of particles, while the mass is determined through assumptions of particle shape and density.[367]

3.4. Data acquisition and control software

With the exception of the particulate emissions, the experimental data was recorded using data acquisition hardware from National Instruments (NI) and the associated software, NI LabVIEW 2017. Pressure data from the various transducers (in-cylinder, inlet manifold, exhaust and fuel line) was attained through a high speed data acquisition card (NI PCI-6254), containing 16 multiplexed differential analogue inputs with a sampling rate of 1.25 mega-samples per second and using a single analogue to digital converter and multiplexer. This data was recorded in conjunction with the crank angle degrees at 0.2 CAD intervals, which required a crankshaft encoder and camshaft sensor to time the data with respect to combustion TDC once per cycle. A second DAQ card (250 kilo-samples per second) was used to record the thermocouple readings and air flow measurements; this averaged and output temperature

readings every 100 samples (therefore 1 sample produced per second).[364] The LabVIEW software was able to use the measured parameters, along with preloaded geometry parameters, to calculate indicated mean effective pressure, heat release rates, start of combustion and peak heat release rate timing, P-V diagrams, in-cylinder temperature (global average) and entropy. In order for comparisons to be made between blends, the IMEP was maintained as close to 4 bar as possible during tests; this was tuned by varying the injection duration.

Engine speed was initially measured on the Emtronix interface through signals from a Hall Effect sensor on the flywheel and camshaft sensor; this also enabled injection timing to be controlled based on the TDC position (accurate to +/-0.1 CAD for the Emtronix). In these tests, engine speed was maintained at 1200 rpm throughout the runs. Injection pressure was regulated by the Emtronix system or labview card using a pulse-width-modulated current to the PRV on the common rail, which would vary the time at which this valve closed or opened depending on the feedback signal from the pressure transducer mounted on the other side of the common rail;[364] the rail pressure was accurate to +/- 1 bar and was maintained at 550 bar for these tests. The injection duration could be set to the nearest 1µs; this was not constant as varying injection durations were required, depending on the fuel, to maintain constant IMEP. Upon failure of the Emtronix system, the slow speed DAQ card was used, in combination with an in-house designed code, to control injection parameters using the shaft encoder signals (accurate to +/- 0.2 CAD). In-house developed hardware was utilised to supply a high voltage signal to the injector upon receiving the Labview-supplied TTL (also accurate to 1µs). The common rail pressure was subsequently regulated using a standalone PID controller; receiving a signal from the pressure transducer on one side of the common rail (for pressure measurement) and sending a signal to the pressure relief valve (for pressure control).

The volumetric flow rate of the inlet air was also measured and displayed and the pressure and temperature readings at this point were used to determine the corresponding mass flow rate. In order to improve the ignition quality of the ignition-resistant blends, such as diesel:furan

and diesel:MF blends outlined in Chapter 4, and therefore make emissions comparisons more valid, the inlet air temperature was maintained at approximately 120°C through an external heater applied after the plenum and before the manifold. Due to heat loss between the heater and the manifold, the set-temperature of the heater itself was raised to approximately 180°C to account for this.

Emissions data recorded by the Horiba MEXA 9100H EGR analyser was read using a GPIB to USB module (NI GPUB-USB-HS), the program used was developed by Talibi[364] to log real-time emissions. The particulate data meanwhile was recorded using Cambustion software (DMS User Interface V4.10) and the Cambustion DMS500 spectrometer itself. The program displayed real-time particulate size distribution while recording, and allowed the user to turn the instrument ON and OFF, to calibrate the instrument (AUTOZERO) or record data (SAMPLE), to set the gain for the data (HIGH or LOW) and to alter the temperature and dilution ratio to tune to instrument to record accurate data based on the exhaust flow rate. For these experiments, the first dilution factor was maintained at 5 (the automatic value), while the second was increased to 50 (overall dilution factor of 5 x 50 = 250).

3.5. In-cylinder sampling valve

As referred to in Section 2.3.6.2, in-cylinder sampling can allow a more detailed picture to be drawn in the formation of combustion products as the cycle ensues. Exhaust emissions are of high importance due to the species present and being released into the atmosphere, exposure of humans to these pollutants where they can cause toxicological effects, but in of themselves the exhaust emissions do not necessarily help us to understand how the fuel breaks down.[368] A more specific study into molecular breakdown at very early stages of combustion is required to understand the initial formation of exhaust emissions, especially soot emissions. These are formed as a result of complex processes (see Section 2.3) that are

initially instigated in the very early stages of combustion with carbon radical species, such as methyl and ethyl radicals, formed during the early phase of fuel decomposition.

The sampling valve employed here was commissioned by Talibi, the thesis of whom gives an in-depth description of the initial development.[364] However, the initial work using the valve looked to sample only a limited number of species (principally NO_x, CO, particulates) and was aimed at establishing the effects diesel fuel co-combustion with aspirated hydrogen and methane. Samples were directed through a dilution tunnel before analysis using the gaseous analysers outlined in Section 3.3. A more concise overview will be given here to indicate the slightly different utilisation of the valve here in which a direct sample was taken from the cylinder, diluted within the sample syringe with an internal standard, and injected directly into a GC-FID.

3.5.1. Valve operation
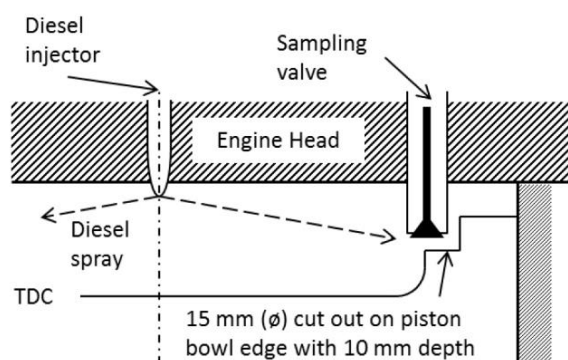
Figure 3.6: Cross-sectional view of sampling valve installation into engine head[369]

An electromagnetically actuated sampling valve was installed within the head of the engine in order to extract samples from the cylinder within a window on order of 1 or 2 ms (approximately 7 CAD). The sampling system was controlled using an in-house developed Labview program, the output of which is shown in figure 3.7 below, which controlled both the timing and duration of a fast acting relay using a 0-5V signal from the National Instrument

PCIe-6323 data acquisition card. The relay supplied current at higher voltage to the sampling valve electromagnet.
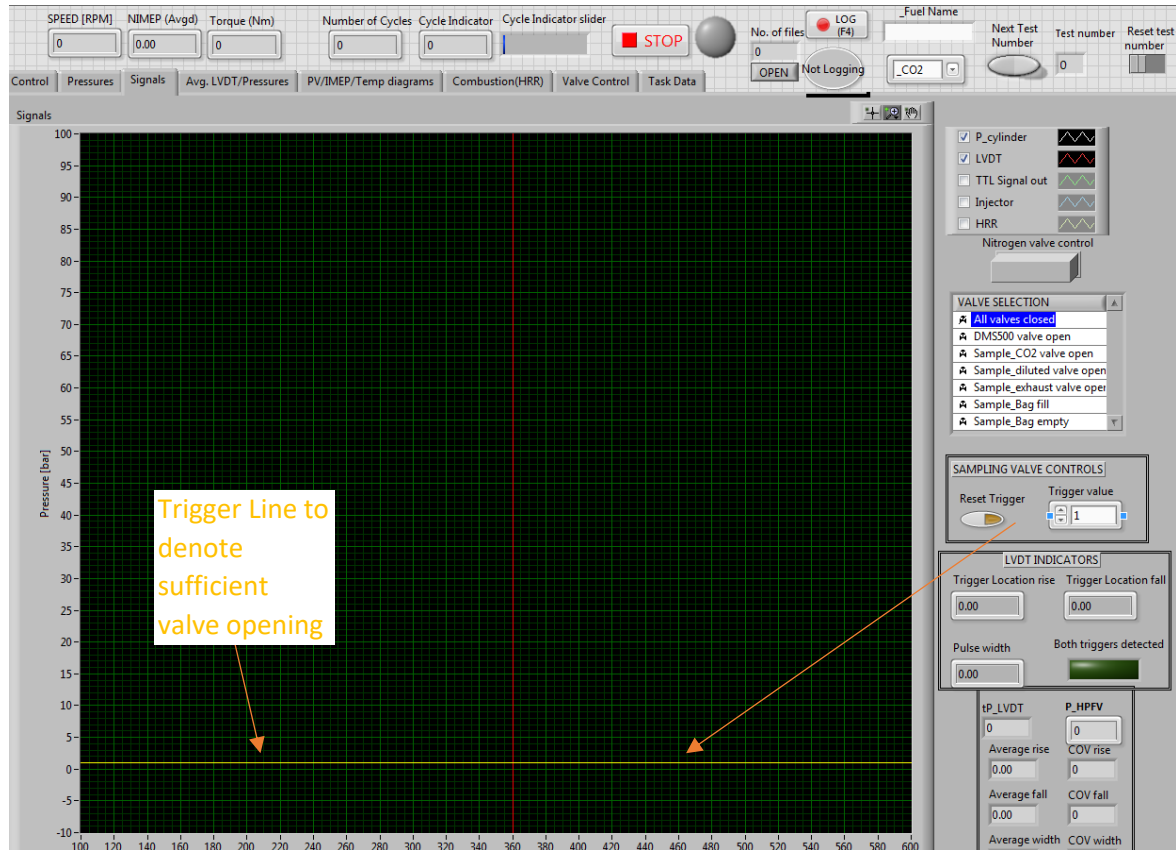
Figure 3.7: Illustration of sampling valve control on front panel of Labview data acquisition and engine control software

The Labview-controlled sampling valve operation utilised the shaft encoder input to control the timing of the valve actuation signal, with 3600 pulses obtained from the engine crank encoder to the input of the DAQ card per engine cycle (providing a resolution of 0.2 CAD). The output pulse to the relay was then sent on a time basis (in microseconds). Opening the relay (at the set timing entered in Labview) allowed an adjustable 0-120V DC power supply to the electromagnet actuating the sampling valve. Talibi[364] outlines the design features of the opening mechanism; utilising a percussion system whereby the armature operated within the magnet is not directly connected to the rest of the valve stem, helping to overcome the issue

of slow responses in electromagnets as a result of the necessity for magnetic flux build-up before the armature moves. This set-up also meant that the magnet could be switched on so as to allow flux build-up before the desired opening time, thus minimising valve opening delays. The valve opening durations were sufficiently small such that electromagnet 'on' periods were no greater than 10% of the total cycle, which meant that supply voltages far greater than the theoretical coil rating were possible. The maximum supplied voltage was 120V, but this was tuned (between 80-120V) in order to attain the desired opening timing and as short duration as possible so as maximising timing (crank-degree) resolution of the sampling extraction. Higher voltages increased the armature acceleration, resulting in a greater striking force that meant that the sampling valve poppet could open to a greater extent - and therefore a greater time overall for a given opposing force. More rapid responses were also observed as the voltage increased.

Tuning of the electromagnet armature weight was key to valve short opening duration, with greater weight tending to increase momentum but reducing acceleration.[364,370] Ensuring the valve and anvil returned to their original positions was vital so as to attain consistent operation and sampling , therefore a second spring was used for the armature. However, this spring was required to withdraw rapidly enough to prevent collision between the anvil and the striker as the poppet closed and returned upwards; if spring movement was too slow, the valve stem would collide with the anvil and cause a delay in closing time. However, Talibi's investigations noted that even though some collisions did occur, the returning force of the valve stem from the high in-cylinder pressures was sufficient to push the anvil away without sufficient obstruction causing notable delays in closing time.[364]

A labview code was developed (see appendix Figure D7) to enable the valve to be opened every set number of cycles, an important feature as opening of the valve every cycle was found to yield extremely variable opening times and would also have caused damage to the valve over relatively short periods of consistent use as a result of overheating. Previously, valve opening durations and timings were only possible to control in terms of crank angle degrees,

restricting sampling times. Opening every cycle at an engine speed of 1200 rpm would have meant the valve opened 10 times every second, not allowing sufficient time for the heat transferred from the cylinder gases to the valve components to dissipate. Furthermore, Talibi noted that opening every 3 cycles reduced the standard deviation in opening time by 60%, compared to opening every cycle, and suggested that this was due to the fact that the O-rings within the valve did not have enough time to decompress fully during valve operation at higher frequency.

Using both the shaft encoder input as a source of timing pulses and the top dead centre (TDC) 'Z' index signal to denote the start of another digital output pulse to the valve relay, the input was configured such that the delay between the Z index digital signal and the pulse sent to the sampling valve could be defined in terms of CAD. An additional function was included so that the valve opened every set number of cycles; as discussed, valve operation every cycle meant sporadic opening times and potential valve damage. The code within the while loop was utilised so that the sampling duration could be altered on the fly. A similar LabView code was used for the injection system as the replacement for the Emtronix system outlined in Section 3.4.

3.5.1.1. Valve construction materials

The majority of the sampling valve components - outer body, annulus, striker and valve extension - were manufactured using stainless steel (grade 304) as a result of its resistance to corrosion and strength against the temperatures unto which it was exposed. However, the poppet itself was exposed to even higher temperatures - those of the cylinder gases themselves (approximately 800-2000K) necessitating the use of silver steel to manufacture this part, which also improved the rigidity of the long valve stem. The poppet seating was made from copper, and the high temperatures allowed for thermal softening of this metal to generate a durable surface and good seal by conforming to the geometry of the poppet. The other

primary material utilised was a polymer material used to house the proximity sensor. Talibi[364] informs that this material was used to prevent interference in the LVDT signal utilised to monitor valve operation.

3.5.2. Sampling mechanism

A schematic of the valve tip is illustrated in Figure 3.8 below. The aforementioned electromagnet was responsible for hammering the armature at the end of the valve stem, opening the valve poppet just enough to take a small sample of high pressure/temperature in-cylinder gas sample. The movement of the poppet-type valve was recorded using an LVDT signal recorded from a Kaman 1U1 proximity sensor, placed adjacent to the anvil onto which the hammer struck. The movement of the valve was within 0-0.3mm, indicating the sensitivity of the sensor. This signal was referenced against the crankshaft encoder such that the opening time was known and could be controlled on the fly and samples could be taken at the combustion timings desired. The exact opening time and duration, in CAD, could be determined from Labview by assuming an LVDT increase above a set threshold corresponded to valve opening - in this case 0.05mm, though this could be altered manually in the Labview code. The LVDT rise and fall timings therefore corresponded to the valve's opening duration, with the average of the two values equating to the opening time.
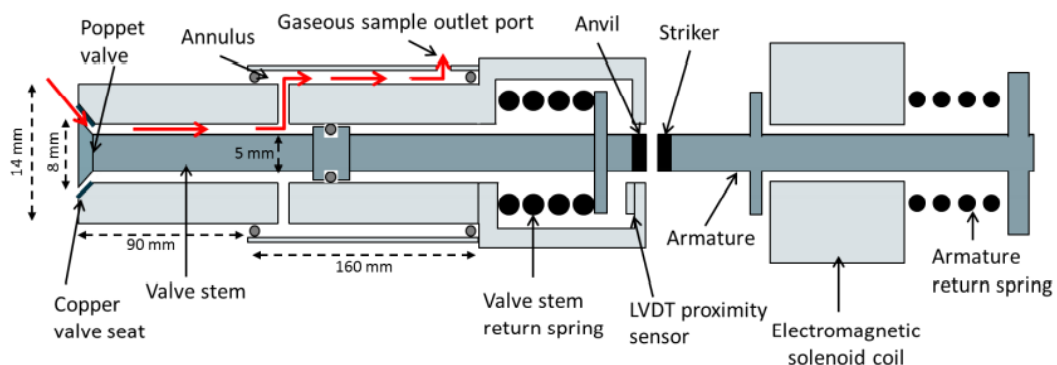
Figure 3.8: Schematic of sampling valve, with red arrows indicating direction of gas flow[369]

The sampling valve was installed into the engine in place of one of the two engine inlet valves. The valve was screwed into the engine head on a thread pressed into the cylinder head that was otherwise be occupied by a dummy valve, so as to seal the hole when the valve was not installed. Talibi conducted an investigation into the position of the sampling valve relative to the orientation of the injector's six fuel sprays, in order to gauge the effect of samples taken when one of the sprays passed over the valve or when two of the sprays straddled the valve. It was concluded that there was little effect on hydrocarbon concentration regardless of the spray orientation, suggesting that, despite the removal of an intake valve, the engine in-cylinder swirl rate was not reduced enough to produce asymmetrical charge motion. For the current study however, it was ensured that sampling was performed between two sprays so as to not saturate the sample with unburnt fuel and thus obscure lighter species – products of pyrolysis – present in much lower abundance. A further factor to consider was the penetration of the valve tip into the combustion chamber. A balance was required between sampling being deep enough to avoid the boundary quench layer on the surfaces of the combustion chamber, but not so deep as to risk the poppet hitting the top of the piston at TDC. To mitigate this risk, the piston was machined to have a small cut-out section at the edge of the bowl, as shown in Figure 3.8. Ultimately, the valve was installed with a penetration of approximately 9mm. A further consideration was the effect of cylinder pressure; greater penetration resulted in reduced cylinder clearance volume (higher engine compression ratio) and therefore higher average cylinder pressures. It was therefore of high importance to maintain consistency in the penetration of the sampling valve across all tests while not adversely effecting cylinder pressures from their nominal values. Typically, peak cylinder pressures without a sampling valve, while motoring, were 41 bar, while a slight reduction to 39 bar was seen with the installation of the sampling valve. The consistency of this reduction though meant that samples tested across different days and with different fuels were considered comparable.

Upon opening of the valve, the high pressure cylinder gases were forced through the opening between the poppet and its seat. Under normal operation, with no voltage supplied to

the electromagnet, the poppet was sealed against the seat, both from the force of the return spring (illustrated in Figure 3.8) and also, when installed in the engine, from the high pressure environment within the cylinder forcing the poppet shut. The sample, still above atmospheric pressure, was forced out of the valve through the valve outlet port and then entered two consecutive heated lines (190°C) of approximately 150cm followed by 500cm length. This combined heated line was ultimately connected to the laboratory exhaust extraction system, but prior to joining the exhaust system it was diverted into the test cell control room where a pressure transducer (PT) and a manually adjustable pressure control valve were used to monitor and adjust the pressure of the sample gas within the heated line (the set-up of which is shown in Figure 3.9 below). Under normal operation, this control valve was kept fully open to avoid any back pressure that would interfere with the sampling valve opening.

Table 3.2: Characterisation of flow rates of cylinder gases extracted using the sampling valve at different CAD[369]

Sampling timing (CAD ATDC)	Duration of sampling window (CAD)[msec]	Cylinder gas pressure (bar)	Bulk cylinder gas temperature (K)	Sample flow rate at atmos. P and T (cm³/sec)	Sample volume/cycle at atmos. P and T (cm³/cycle)	Sample volume/cycle at cylinder P and T (cm³/cycle)
10	6 [0.83]	64	1250	67	6.7	0.44
25	10 [1.4]	33	1200	33	3.3	0.40
40	15 [2.1]	16	1000	17	1.7	0.35

In the current study, sampling times of 370 CAD (10 CAD ATDC) and 420 CAD (60 CAD ATDC) were used. Extrapolating the sample flow rate expected at 60 CAD ATDC, based on the information supplied in Table 3.2,[369] gives a flow rate of 0.29cm³/cycle, or 2.9cm³/s at 1200 rpm. During sampling, it was important to purge the heated line of atmospheric gases and ensure that the samples collected would be indicative of those in the engine cylinder at the time of sampling. Due to the expected flow rates, as well as the speed of the engine and length of the heated line from the exit of the valve to the sampling port (value), a period of 65 seconds elapsed before the control valve was gradually closed.
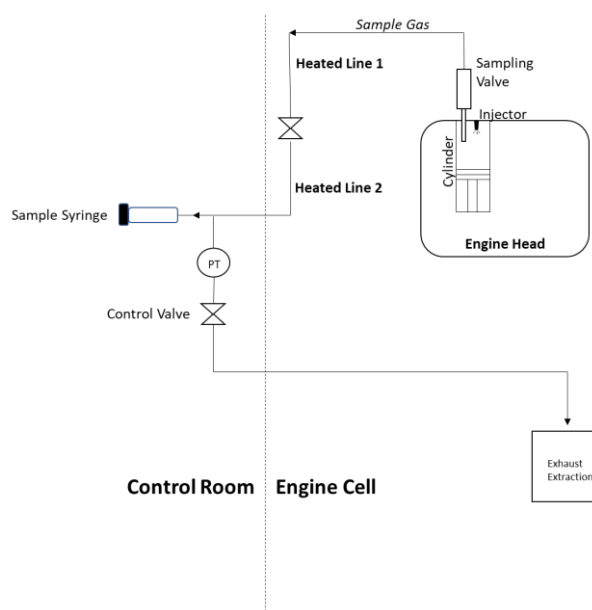
Figure 3.9: Overview of sampling set-up for extraction of in-cylinder gases

Noting the pressure from the transducer located between the sampling port and valve, the sampling syringe was inserted into the septum with the valve closed to the point where between 0-0.5barg pressure was measured or when the plunger on the syringe began to be forced upwards. Approximately 20cm^3 of sample was collected, the luer lock closed on the syringe, and the control valve reopened.

To reduce the amount of condensation and therefore loss of higher boiling point species within the sample, most notably the unburned fuel, samples were either immediately mixed with internal standard (IS) - discussed in Section 3.7 - and injected into the GC-MS, or kept in an oven maintained at 100°C until GC analysis could be performed. Tests were conducted to analyse the effect of injecting the same sample immediately from the engine and then the next day - these are outlined in Section 3.7.4- but an appreciable decrease in species concentration could be observed, therefore samples were tested within the same hour of the extraction.

3.6. Pyrolytic tubular reactor

The use of an internal combustion engine to determine the validity of various fuels or fuel properties is advantageous in providing a real-world set-up for which to test levels of toxic emissions, either within the cylinder in early stages of combustion, or in the actual emissions. However, obtaining a more fundamental understanding of fuel chemistry requires the use of more controlled conditions. As alluded to in Section 2.3.6.1, flames, shock tubes and laminar flow reactors, among others, have been utilised for this purpose.[320,323,326,327] The current study employed a laminar flow reactor facility to determine the breakdown of a variety of fuel molecules, with an effort to understand the difference in molecular decomposition and gaseous PAH-precursor formation and their dependence on the type of molecule used. Norinaga *et al*[371] utilised a plug-flow reactor to conduct a study into the initial pyrolytic products of acetylene within the temperature range of 1073-1373K. The main hydrocarbon products detected were methane, ethylene, vinylacetylene, benzene and naphthalene. These species are known precursors to PAH formation and thus all but naphthalene were investigated in the current study for relative abundance during fuel pyrolysis (naphthalene was not included as the formation of the first ring was the area of interest in the current work).

A primary feature of the reactor used in the current study was the absence of oxygen, which limits the formation of CO and CO_2 and- more importantly- the consumption of the species of interest. This would have limited the formation of potential products formed in an engine. Ultimately, the purpose of this reactor was to emphasise the formation of pyrolysis products formed in regions of a diesel flame where temperatures are high and oxygen concentrations are deficient, in order to amplify any influence of fuel composition or reaction temperature on the formation of certain gaseous pyrolysis species. Previous investigations in this Research Group at UCL have utilised this flow reactor to study a range of molecular properties, including the sooting tendency of C2 fuels[275] and the carbon-13 tagged molecules and the abundance

of tagged carbon in the resulting soot formed.[314,372] The overall experimental set-up is illustrated in Figure 3.10 below.
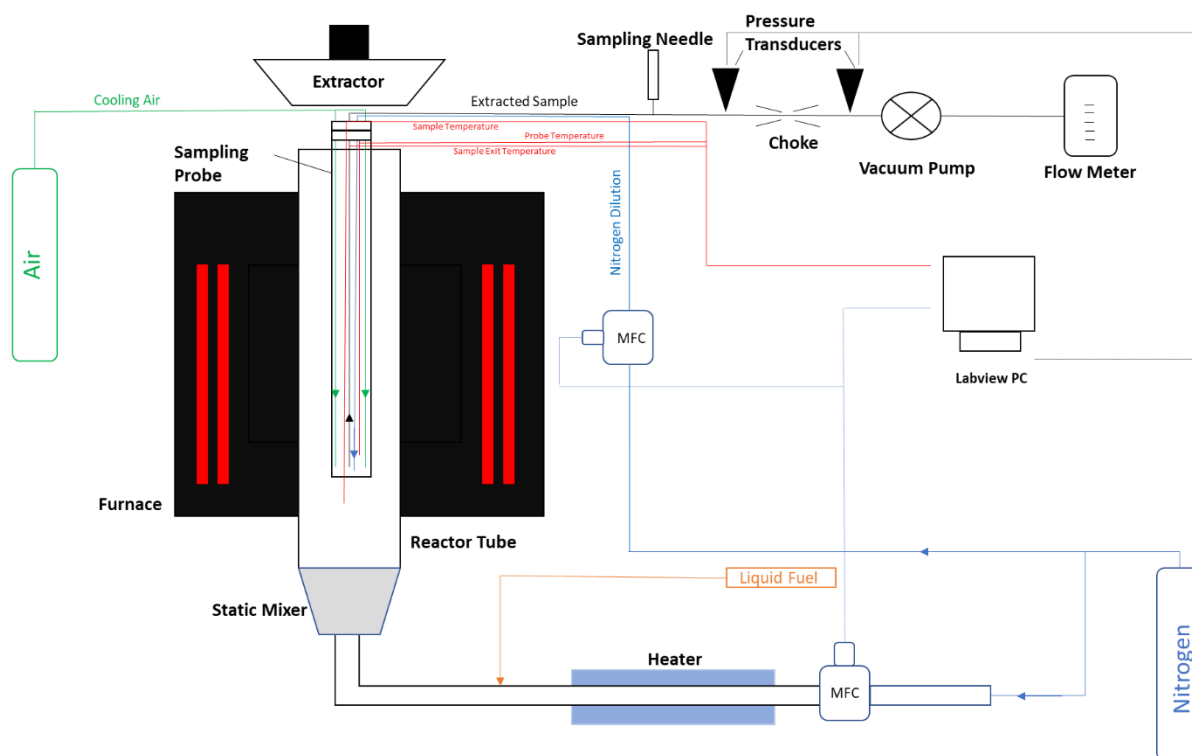
Figure 3.10: Overall experimental setup of the pyrolytic reactor

3.6.1. Fuel supply system

Pure nitrogen (supplied by BOC) was used as the carrier gas for the fuel itself, set at a rate of 20 l/min using a Bronkhorst EL BASE mass flow controller- ensuring laminar flow conditions were met within the tubular reactor (the Reynolds number within the reactor was calculated as 49 when nitrogen flow was set to 20 l/min at a thermocouple temperature of 887°C). The nitrogen was heated to 400°C- controlled using a Tempatron temperature regulator (TL4800) in combination with a type-K thermocouple, operating a PID control system, with the nitrogen lines feeding the reactor wrapped with tape heaters and bound with glass-fibre insulating material. Power to the tape heaters was only supplied when nitrogen flow was detected, in

order to avoid heater damage. A period of warm-up at the start of a test was required to ensure that the nitrogen flow had reached the desired temperature before fuel injection. The fuel itself was supplied to the system using a Chemyx, Fusion 100 Touch syringe pump set at a rate that varied for each fuel to ensure that a consistent 5000ppm C1 concentration of carbon was entering the reactor with varying molar mass, carbon number and fuel density. The syringe pump was attached via a luer lock to a 1mm (OD) x 0.7mm (ID) x 80cm (length) stainless steel capillary obtained from Coopers Needle Works Ltd, fitted with 250W, 240V tape heaters- supplied by Omega- that enables the capillary to be heated to temperatures of up to 482°C. 10mm of the end of the capillary was inserted into the vaporiser- ensuring the fuel was injected into the central flow region of nitrogen and not impinged on wall, which might have distorted the concentration profile. Borosilicate glass beads were packed just downstream of the capillary so as to ensure full vaporisation and homogenisation of the vaporised fuel. Before entering the reactor tube, the nitrogen/fuel mixture was first sent through a static mixer made of stainless steel ball bearings placed at the reactor inlet. The reason for such a system was to ensure a homogenous planar flow of the mixture of fuel and nitrogen entering the reactor tube, while also adapting the stainless steel feed tube (18mm) to the alumina reactor tube (104mm). 8mm steel ball bearings were packed into the mixer, which was suspended from a water-cooled reactor support, this connection sealed using a Polymax Viton O-ring. More details of this mixer can be found in the PhD thesis by Eveleigh.[318] Homogenously mixed, the fuel-nitrogen stream entered the reactor tube.

3.6.2. Laminar flow reactor

Pyrolysis of the test molecules took place within a reactor tube made of C799, recrystallized alumina, which could withstand the high temperatures necessary to observe fuel decomposition. Heating was achieved using a furnace (Nabertherm- RHTV 120-600) which encompasses the reactor tube (120od, 104id x 1440mm length), placed vertically within the

oven. As mentioned, due to inevitable heating losses, the entirety of the tube was not at uniform temperature - between 41cm and 91cm (500mm) was considered the uniform temperature reaction zone. Water cooling flanges- supplied by Nabertherm- were utilised to support the two high temperature ends of the reactor. Pyrolysis products were exhausted from the top of the reactor, with an extraction system placed above to remove the products without entering the surrounding atmosphere.

3.6.3. Sampling probe

In order to take gaseous samples from the laminar flow tube, a sampling probe was used. Further details of this design can be found in the work by Khan[373] but an overview will be described herein and illustrated in Figure 3.11. The probe was made of two 1m long concentric ceramic tubes, the inner tube facilitated sampling and dilution of the sample while the outer tube was used for probe cooling (ceramic tube dimensions are shown in Figure 3.11). Two 3mm internal diameter stainless steel capillaries were set within the inner ceramic tube and two more 3mm capillaries were placed on opposing sides within the annular space between the two concentric ceramic tubes. Two thermocouples were placed one within the central tube and the other in the annular space between the inner and outer tubes. The entire construction was held together using a 20mm long ceramic tube which was glued in the annular space at the bottom end of the 1m ceramic tubes using Aramco ceramabond 569 adhesive. This 20mm tube ensured that the annular space between the two 1m tubes was maintained and it also provided structural strength. In a similar manner, the top of the two 1m tubes was held together using PTFE sealing caps that also prevented the escape of nitrogen dilution gas, or sample, or coolant air.
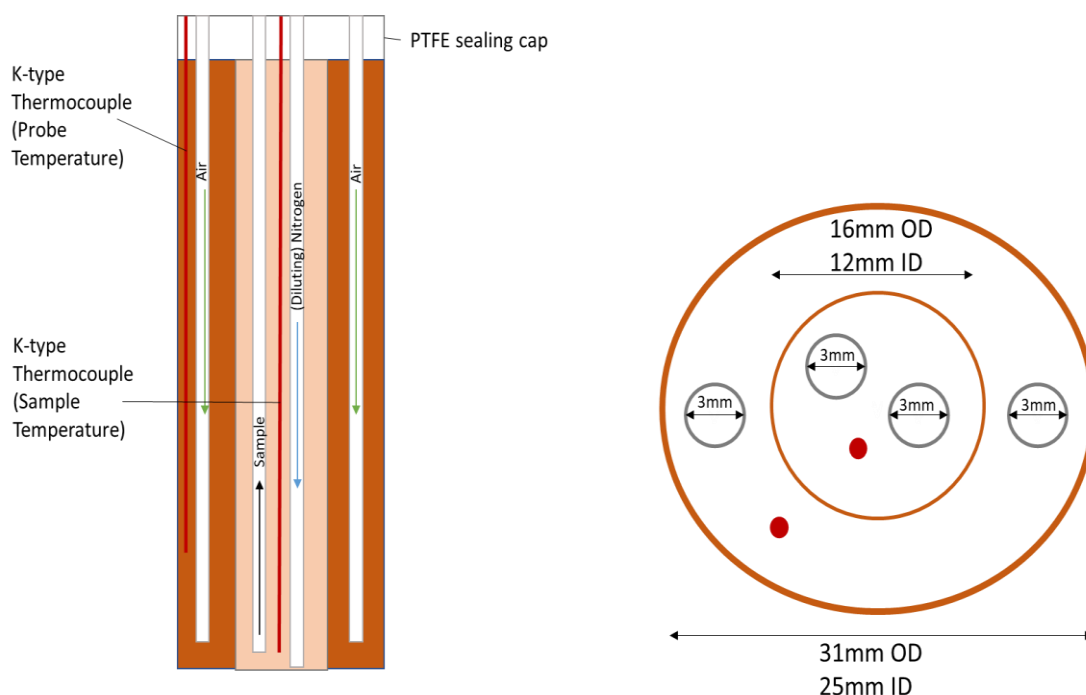
Figure 3.11: Cross-sectional (left) and top (with PTFE cap removed) (right) view of sampling probe assembly

One of the two central stainless steel capillaries was utilised for sampling. A vacuum pump, set at approximately 2 l/min, was used to pull sample from the reactor itself. Placed between the reactor outlet and a choke point upstream of the vacuum pump was a septum through which samples could be collected using 100ml glass syringes (purchased from Sigma Aldrich). The overall schematic is illustrated in Figure 3.10. Pressure transducers were placed before and after the choke point in line with the sample flow so as to ensure that the sample taken consisted entirely of the contents of the furnace and that it was possible to pull easily the sample into a syringe. Once pressures measured indicated an effective choke, approximately 20ml of sample was gradually taken. After the sample was extracted, a small volume of gas was then ejected from the syringe- by pushing in the plunger- in order to ensure an accurate volume at atmospheric conditions was measured. An equal amount of internal standard was then obtained into the same syringe (from atmospheric conditions) and the sample and

standard mixture was injected into the GC-MS instrument outlined in Section 3.9. The second capillary of the inner tube was not used in the current study, but was part of a dilution system in which nitrogen could be injected at a set rate and mix with the reactants, reducing overall levels of fuel concentration and freezing the reaction, allowing for more repeatable results when fuel and/or species concentration was too high. This capillary was slightly more inset by 2-3mm into the probe and away from the point at which samples were drawn from the tube reactor in order to ensure the sampling capillary was extracting a relevant sample of diluted pyrolysis gases and not simply the diluting nitrogen flow.

The two outer capillaries were employed so as to pass cooling air down the probe annular space. The air cooled the probe assisted in freezing further reactions in the sample as it was passing up the sampling capillary. As it was likely that species within the sample would be highly reactive, reducing temperatures and reaction rates within the sampling system was a priority to ensure that the sample output from the FID analysis was representative of the mixture within the tubular reactor. The sample exit temperature was maintained below 50°C in order to reduce these potential reactions.

3.6.4. Residence time

The sample probe was withdrawn and secured above the tubular reactor outlet when not in use, and was possible to elevate and lower it easily when each sample was taken. In order to ensure consistent sampling depths, a depth indication was secured parallel to the probe and set-points - denoting different depths- 81cm, 76cm, 71cm etc - with the depth of 71cm used for these experiments. Calculations for gas residence time are outlined in previous work in the group, but can be taken as simply the ratio between reactor volume and the volumetric flow rate of the gas, hence the units of seconds.

$$Residence\ Time\ (s) = \frac{Volume\ (m^3)}{Flow\ Rate\ (m^3/s)}$$

However, the complexity of this calculation comes when taking into account temperature, which, in addition to the depth, changes the volumetric flow rate; as temperature increases, residence time decreases, since the nitrogen flow becomes less dense at higher temperatures and the volumetric flow rate increases. Using the density of nitrogen at various temperatures, and assuming that a sample depth of 71cm equates to a penetration into the uniform reaction zone (before or after which no reactions are assumed to occur) of 30cm, residence time can be calculated depending on temperature, with calculated values shown in Table 3.3.

Table 3.3: Residence times and respective temperatures, illustrating continuity of 'residence time x temperature'

Temperature (K)	Calculated Residence Time (s)	Residence Time (s) x Temperature (K)
922	1.62	1493.04
973	1.53	1493.07
1024	1.46	1493.10
1075	1.39	1493.14
1126	1.33	1493.17
1168.5	1.28	1493.18
1219.5	1.22	1493.20
Average		1493

Overall, residence time can be calculated as:

$$Residence\ Time\ (s) = \frac{1493}{T\ (K)}$$

3.6.5. Temperature profile

The laminar flow reactor used enabled good control over the temperature that the fuel was exposed to. Figure 3.10 indicates the experimental setup employed, whereby the controllable furnace temperature was set to nominally between 700°C and 1300°C. Central point temperatures of the sampling probe were lower due to inevitable heat losses; these latter temperatures more accurately represented the pyrolysis temperatures, but radiative effects also need to be considered.

The reactor temperature profile itself was explored further by Eveleigh[318] and Khan,[373] investigating the various wall temperatures at different furnace depths. Figure 3.12 below indicates the location of the uniform temperature zone within the tubular reactor which, depending on the set furnace temperature, ranged between approximately 41cm to 91cm of the overall tube length; this range was used in the residence time calculations. Apparent from this figure is that, as temperatures increase, the uniform temperature region stabilises such that a greater length can be assumed consistent. However, the higher set temperatures also see more evident heating losses; a 700°C furnace set temperature is reflected in a 700°C wall temperature, while a 1300°C set temperature sees maximum wall temperatures of approximately 1240°C. The maximum set temperature used in this study was 1000°C, equating to wall temperatures approaching 970°C.
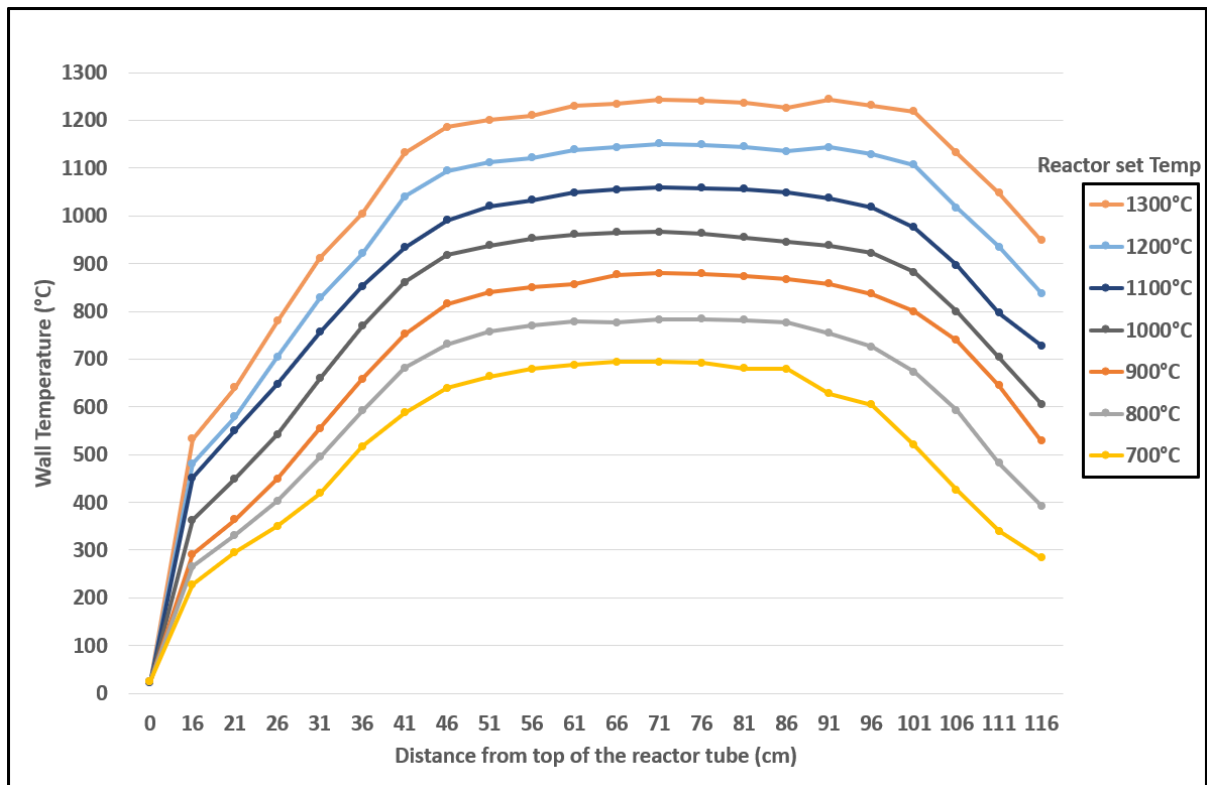
Figure 3.12: Wall temperature variation with respect to distance inserted into the furnace[373]

It was important to consider that the actual gas temperature i.e. the temperature the reactants tested were exposed to, would differ slightly from the measured temperature using the central thermocouple at the tip of the sampling probe. The measured wall temperature profile was utilised to calculate the radiation received by the thermocouple at the sample probe tip and subsequently used to correct the measured temperature, in order to determine the actual temperature at which the sample is taken.

Figure 3.13 below indicates the average thermocouple temperatures relative to the set temperatures of all pyrolysis tests; 1000°C furnace temperature meant an average thermocouple temperature of just 884°C though, as shown by the standard deviation, some tests were conducted at temperatures just above 900°C. With this experimental variation, it was important to gauge whether the true gas temperature varied to a greater or lesser extent. These temperatures were employed so as to detect initial fuel breakdown; temperatures which

were too high would have resulted in low concentrations of gaseous light hydrocarbons and, instead, soot formation would have been far more advanced to the point where larger aromatics and soot would have been the prevalent species.[374]
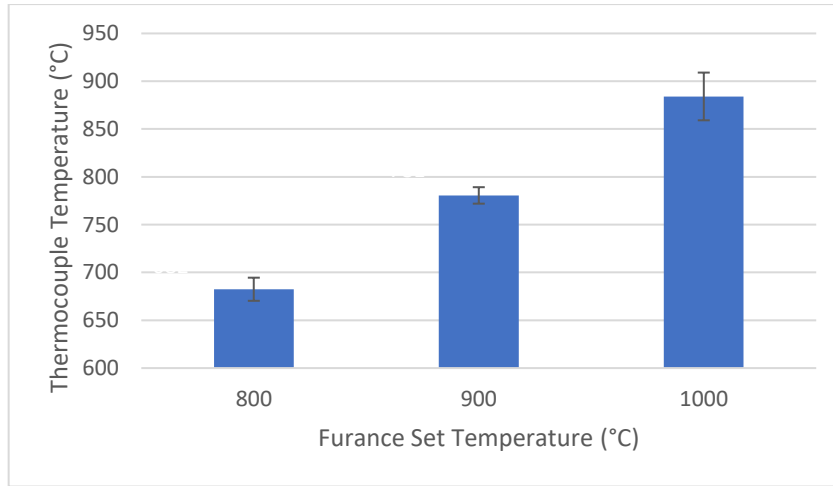
Figure 3.13 Measured central thermocouple temperature with respect to input set furnace temperature, across all tests

Leaney[375] performed temperature profile calculations when undertaking experiments investigating the pyrolysis of butane in a laminar flow reactor, finding a region of 30cm long as approximately isothermal. Variations in the gas temperature itself were also investigated, which differed from the thermocouple temperatures due to radiation from the tube wall that would result in an increase in recorded temperature. The following equation was supplied by Leaney:

$$T_g = T_s - \frac{\varepsilon \sigma_c T_w^4}{h}(1 - (T_s/T_w)^4) \qquad \text{(Eq 3.1)}$$

where T_s is the thermocouple temperature (the value of which was substituted with the average temperatures indicated in Figure 3.13 above), T_w is the wall temperature (both temperatures measured in Kelvin), ε is the emissivity (of Inconel alloy used in the thermocouple = 0.36)[376],

σ_c is Stefan's constant (5.75×10^{-8} W/m^2 K^4) and h is the heat transfer coefficient between the thermocouple tip and process gas (W/m^2 K), calculated using the equation:

$$h = \frac{Nu * K}{dt}$$ (Eq 3.2)

where Nu is the Nusselt number (calculated from Reynolds and Prandtl numbers and measures the ratio of convective to conductive heat transfer), K is the thermal conductivity (W/m*K) of nitrogen at the measured temperature and dt is the thermocouple diameter.

As from the wall, radiation from the thermocouple itself would also be present. However, Leaney notes that the effect of the thermocouple probe on the thermal profile would be 'insignificant' relative to the reactor diameter. Leaney's reactor tube possessed an internal diameter of 5.25cm, even less than the current study (10.4cm) and further negating thermocouple radiation effects.

Table 3.4 below indicates the temperature changes associated with each average thermocouple temperature condition.

Table 3.4: Calculated gas temperature correct for wall radiation with respect to average recorded thermocouple temperature

Average Recorded Thermocouple Temperature (°C)	Corrected Gas Temperature (°C)
884	879
781	775
682	678

Overall, a drop of only 4-6°C was within one standard deviation of all thermocouple temperatures recorded during testing, therefore additional consideration of radiative heat losses was not required in the results obtained from the reactor. In Chapter 6, actual gas temperatures will be quoted as opposed to corresponding nominal 800°C, 900°C and 1000°C furnace set-point temperatures.

3.7. Gas chromatography-flame ionisation detector (GC-FID)

An Agilent Gas Chromatogram (GC) 7980B, coupled to a flame ionisation detector (FID) was utilised for the analysis of gaseous samples detected in the pyrolysis reactor and in-cylinder engine environments. This technique employed the use of an FID to detect individual species and their concentrations. Hydrogen flames are used for this purpose, as the formation of ions in hydrogen flames is limited, therefore ions detected can be assumed to be due to the presence of hydrocarbons within the sample injected. The carrier gas used to move the solutes through the GC column forward was helium; nitrogen is often used as the analyte carrier gas, but results in much longer elution times. Nitrogen is instead used as a 'makeup' gas, serving the purpose of optimising the carrier gas flow through the 'jet', increasing detector sensitivity, while also reducing peak broadening by sweeping the area inside the detector base. High purity air was employed as the oxidant utilised in the FID flame the effluent/hydrogen mixture; oxygen enriched air can be used for this purpose, with Hilscher[377] indicating a 28-100% improvement in FID sensitivity with this method. Details of the gas flow rates utilised are supplied in Table 3.5 below. All gases were supplied by BOC.

Table 3.5: Parameters used for FID Testing

Splitless Liner	Restek Ultra Inert Liner, Single Taper, Wool
Split Ratio	10:1
Split Flow	20 ml/min
Sample Flow	5 ml/min
Inlet Pressure	10.7 psi (0.738 bar) gauge
Inlet Temperature	270°C
FID Heater Temperature	250°C
Synthetic Air Flow Rate	400 ml/min
Hydrogen Flow Rate	40 ml/min
Helium Flow Rate	2 ml/min
Nitrogen Flow Rate	20 ml/min
Oven Ramp Rate	30-40°C (2 minutes) 40- T_{max} (5°C/min) (T_{max} ranged between 190-250°C)
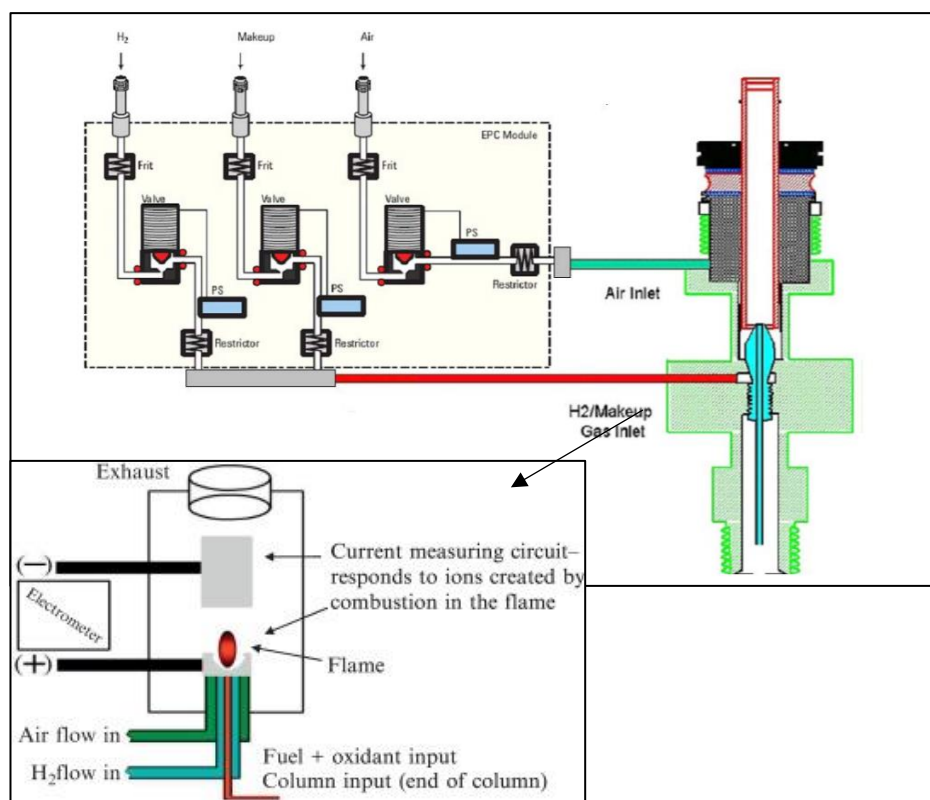
Figure 3.14: Generic illustration of Flame Ionisation Detector (FID) and routes of gases required for operation[378,379]

Hydrocarbon abundance (relative to each other) can be detected, as hydrocarbons form ions when they combust in the hydrogen flame of the FID. The amount of these ions- detected using two electrodes- is ultimately proportional to the number of carbon atoms. Peak area integration therefore gives an approximation as to the relative concentration in the injected sample of each hydrocarbon species. The FID current produced from the ions is a function of the number of ionised carbon atoms contacting the electrode in a given time, therefore mass, more so than concentration in the injected sample, is being measured. The fact that these masses are 'relative' to each other, however, necessitates an internal standard introduced within each injected sample, of a known concentration, that would be added at a set volume into the sample before injection into the gas sampling system of the GC-FID. Corresponding

concentrations of the various hydrocarbon species in the sample could be determined using calibration curves for the individual species of interest, which were plotted using an external standard (a gaseous mixture of hydrocarbon species of known concentration) which was manually diluted with varying levels of nitrogen and a constant volume of internal standard. The internal standard peak integration was used to ensure consistent FID operation. The internal standard was chosen based on its approximate boiling point and molecular weight, such that it would be within the range detectable with the column. However it was important that the internal standard peak would not overlap with another peak of the hydrocarbons in the actual sample. A unique hydrocarbon species was therefore selected as an internal standard, which was not expected to be present in the samples collected from the engine and the furnace. As a result, difluoroethane was utilised as the internal standard; all fuels tested contained carbon, hydrogen and oxygen only. This gas was supplied in 100ppm concentration (nitrogen used as balancing gas) by BOC.

3.7.1. Column selection

A Restek RT-Q-Bond column (0.32mmID, 30m length, 10μm film thickness) was utilised for the separation of individual species. This porous polymer column is non-polar and, because of its hydrophobicity, is insensitive to water- an advantage in the testing of engine gases that will possess water as a combustion product. The non-polar nature is also appealing for the species expected (i.e. hydrocarbon species that are generally non-polar), as with similar polarities the attractions onto the film are stronger, increasing retention and resolution. This column was chosen specifically to differentiate lighter hydrocarbon species. It was noted that, despite the maximum column temperature of 300°C, temperatures exceeding 250°C caused excessive bleed, and therefore species beyond C7 alkanes were difficult to detect in low concentrations. However, the alternative use of a HP-1 column was noted to result in poorer

separation of lighter species, notably between ethylene and acetylene, as shown in Figure 3.15 below.
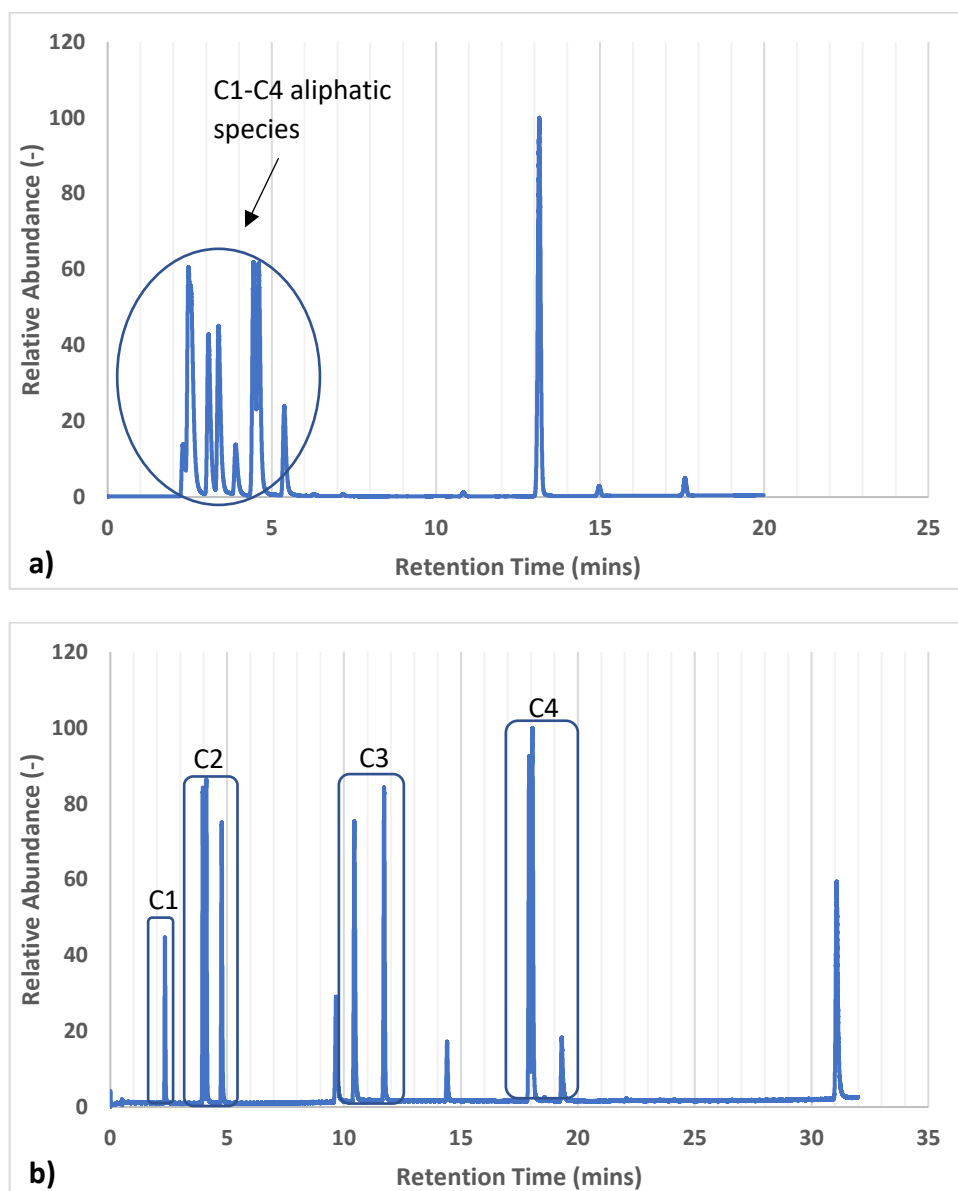
Figure 3.15: Comparison of chromatograms produced by HP-1 (a) and RT-Q-Bond (b) columns with the injection of undiluted external standard

As illustrated in these chromatograms, the elution of all C1-C4 aliphatics occurred between 2 and 6 minutes when using the HP-1 column. Considering that additional species could potentially be detected in the samples themselves (the range of species in the external standard may not be exhaustive) it was likely that extensive column overlap would exist when using the HP-1 column on samples. The RT-Q-Bond column on the other hand, while it was unable to be used for species above benzene (other than the C7 fuels), exhibited more gradual separation across the whole run, making individual peak analysis far more reliable.

Therefore, despite greater stability (lower column bleed) of the HP-1 column, noted as the 'industry standard',[380] the Rt-Q-bond was preferred since the separation between C2 species was of greater importance to the current study than detecting species beyond benzene that were not the original fuel molecule. The RT-Q-Bond column was able to detect benzene in low concentrations, while the fuels, heptane and heptanone, were detectable when setting the maximum oven temperature to 210°C and 250°C respectively. These C7 fuels were necessary to detect due to their use as fuel the engine.

3.7.2. Oven temperature

As alluded to, the column chosen possessed significant bleed at high temperatures. The recommended maximum temperature was 280°C, and to maintain column integrity and repeatability of results, this temperature was not exceeded. The maximum temperature used corresponded to the retention time of heptanone- the fuel that possessed the longest elution time while still being detectable with this column. It was desired to obtain the relative concentration of the fuel molecules used in the furnace and the engine, but the C10 fuels used in the furnace were not detectable without exceeding recommended temperature limits. For fuels other than heptanone, a lower maximum temperature was employed, primarily to extend column stability. It was noted that species above benzene, other than the fuel species, were negligible in number and concentration, therefore exceeding the retention time of benzene (31

minutes corresponded to a temperature of 185°C) when testing C10 fuels was avoided. The maximum temperature was not the only pre-set temperature parameter, the ramp rate also could influence column bleed and peak separation. Ramp rates too high would have resulted in greater column bleed and peaks closer together, which, in the case of acetylene and ethylene, would have meant potential overlap. However, temperature ramps too low would have exposed the column to these higher temperatures for longer, and resulted in excessive run times. The 5°C/min ramp rate used represented a compromise between run times and column preservation.

3.7.3. Species calibration

A common theme with gas chromatography columns and FID detectors is their non-linearity, both in terms of their response and sensitivity, depending on analyte structure and functionality,[381] as well as experimental control parameters such as the geometry of the FID and the flow rate of carrier gas.[382] For this reason, the external standard (ES) was employed to establish the response of the FID over an extended period of testing to note any major changes. The use of external standards in chromatography means that a calibration curve can be plotted over the range of concentrations of species reasonably expected to be present within the sample. Column saturation of high boiling point and high viscosity species, as well as degradation of the stationary phase, were concerns as these would cause column bleed and peak tailing, and thus potentially invalid results. As a result, daily testing of pure ES was able to note minor changes in response before becoming significant enough to necessitate maintenance on the column. The external standard also fulfilled the purpose of allowing relative responses to species of interest and their residence times to be determined at the beginning of each day of testing. The species of interest, to include in the ES, were determined through literature searches referencing the products of hydrocarbon pyrolysis (preliminary testing and analysis would not have helped in selecting species for the external standard). As

stated by Esarte,[328] methane, ethylene, ethane and benzene could be expected to be present here, while the work by Smith and Norinagia[286,371] noted the presence of vinylacetylene, while the presence of propene, propyne and butadiene has also been referenced in various pyrolysis experiments.[299,311,383] These molecules were used, in addition to acetylene, the most widely accepted gaseous PAH precursor at 1000ppm concentrations in nitrogen, supplied by BOC.

Cyclopentadiene was also a species of interest; Sidebotham and Glassman noted that this was the only C5 species detectable in their pyrolysis experiments in inverse diffusion flames.[383] However, it was not possible to use within the external standard due to its instability, creating safety concerns. Using this gas mixture comprising known concentrations of each species, a sensitivity check could be performed. The results indicated in Table 3.7 and Figure 3.16 below show the retention time and calculated concentration (from peak integration) of the same gas mixture, diluted at different levels with nitrogen, on conclusion of the furnace testing outlined in Chapter 6. Various mixtures of ES:IS:N_2 were synthesised to create different concentrations of the ES species (with IS maintained at a constant volume in order to detect the potential experimental variation between samples i.e. changes in FID sensitivity).

Table 3.6: Dilution levels of external standard to create calibration curves shown in Figure 3.16

Mixture	Volume of ES (ml)	Volume of IS (ml)	Volume of N_2 (ml)
25ppm	2	20	78
100ppm	8	20	72
300ppm	24	20	56
500ppm	40	20	40

Table 3.7: External (and Internal) standard species and retention times

Species Selected	Retention Time (mins)**
Methane	2.34
Ethylene	3.96
Acetylene	4.12
Ethane	4.77
Propene	10.46
Propyne	11.73
Acetaldehyde*	14.43
Vinylacetylene	17.93
Butadiene	18.07
Ethanol*	19.35
Benzene	31.08
Internal Standard (Difluoroethane)	**9.68**

*oxygenated species (used to determine molecular breakdown, than rather PAH formation pathway

** Rounded to 2.d.p
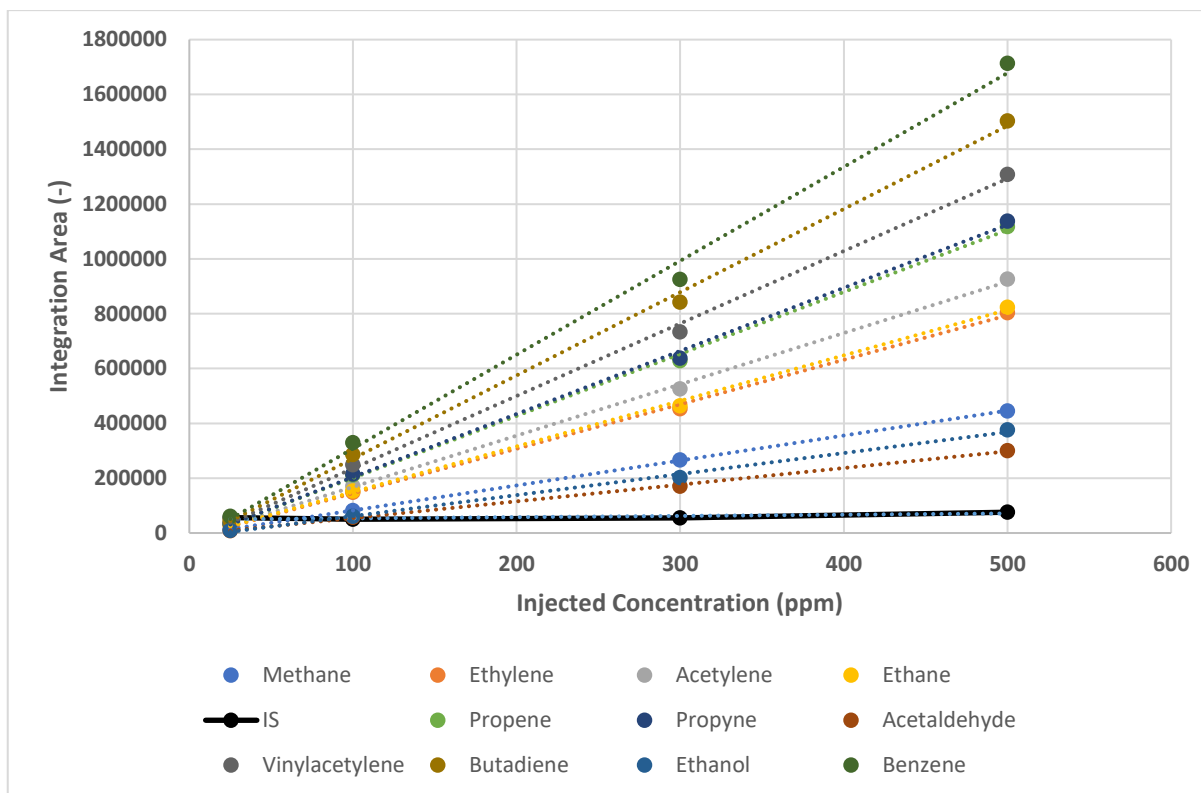
Figure 3.16: Calibration curves of external standard species at 25ppm, 100ppm, 300ppm and 500ppm concentrations, conducted at the end of pyrolysis testing

One of the fuels tested (gamma-decalactone) possessed a higher boiling point than that which the GC oven was set to during the experiments, therefore ensuring this did not absorb onto the column and affect results over time was highly important. During testing, in between each run, a short sample using pure nitrogen was employed to firstly make sure results were not affected from an accumulation of low boiling point species over time- as these were often present in high concentrations- but also to ensure that higher boiling point species were desorbed from the column. Comparison between calibration plots at the start and at the end of the furnace testing indicated, with the exception of benzene, no major changes to the FID sensitivity or column separation over the course of testing (see appendix Figure B2 for initial calibration plot), implying that steps taken to avoid build-up of high boiling point species were effective. The differences could be suggested to be due to the difference in split ratio used for

the tests. These were corrected (the 2.5:1 split ratio used initially was calculated to produce a sample 2.5 times more concentrated than a 10:1 split), but the exact split ratios cannot be relied upon as exact dilution ratios of the sample, as a splitless liner was employed in the set-up. It was noted by the manufacturer that a splitless liner may not achieve exact split ratios- split liners are designed with an open bottom in order to accurately split the sample, while splitless liners (like the one used) are tapered in order to maximise sample throughput for splitless injection. As a result, it was observed that split ratios below 5:1 and above 75:1 did not produce the dilution levels expected, therefore 10:1 splits were subsequently employed.

Figure 3.16 indicated that, despite equal concentrations of the individual ES species, the sensitivity of the FID to different species varied. The FID response will also exhibit a specific degree of linearity at varying concentrations of I.S, therefore the I.S cannot be used to correct all species concentrations in a sample. As a result, the end calibration curve was used to calculate the concentrations of species within the test samples, using the line-of-best-fit equations for each individual species (Table 3.8).

Table 3.8: Calibration curve equations of all species in the external standard

Species	Gradient (m)	y-intercept (c)
Methane	910.21	-8521.1
Ethylene	1623	-17185
Acetylene	1872	-19265
Ethane	1661.2	-16436
Propene	2261.8	-25367
Propyne	2300.8	-26051
Acetaldehyde	608.48	6294.4
Vinylacetylene	2643.7	28839
1,3-Butadiene	3035.6	-32244
Ethanol	766.99	-15145
Benzene	3425.2	-34553

Not included in the calibration gas was heptane, therefore a separate curve was produced for this species, the equation of which was also used to calculate the concentration of heptanone (see appendix Figure B1).

The coefficient of variation of the internal standard across the whole test range was 6%. Therefore, in addition to the test-to-test variation (shown by the standard deviation error bars in Chapter 6 results), minor differences in species concentration are not used in drawing conclusions. This variation of 6% could have either stemmed from variation in the extraction from test to test (the markings on the syringe measured $2cm^3$ ($1.2cm^3$ difference in volume of a $20cm^3$ sample would have been enough to account for this error). Of course, some variation may be due to the FID itself but, because the degree of error was not consistent (and so it is not known whether this 6% was caused by handling error or FID response changes) a correction factor was not applied.

3.7.4. Effect of time on sample concentration

It was found that time delay in injecting a gas sample through the FID after collection from the engine or furnace affected the measured species concentration, and for this reason this matter was investigated further. Figure 3.17 below shows the effect of time delay in measuring the concentration of species in a mixture of external and internal standard (80% IS: 20% ES). Such a mixture was used at the start of the day to test the constancy of FID detection (ensuring constancy of retention times over a campaign of tests). The mixtures were collected directly from the gas bottles, emptied into separate bags to ensure the gas was at atmospheric pressure, and 80ml of IS and 20ml of ES mixtures were taken via a syringe and 10ml was subsequently injected into the gas inlet of the GC-FID. 24 hours later, the same syringe contents were injected into the FID.
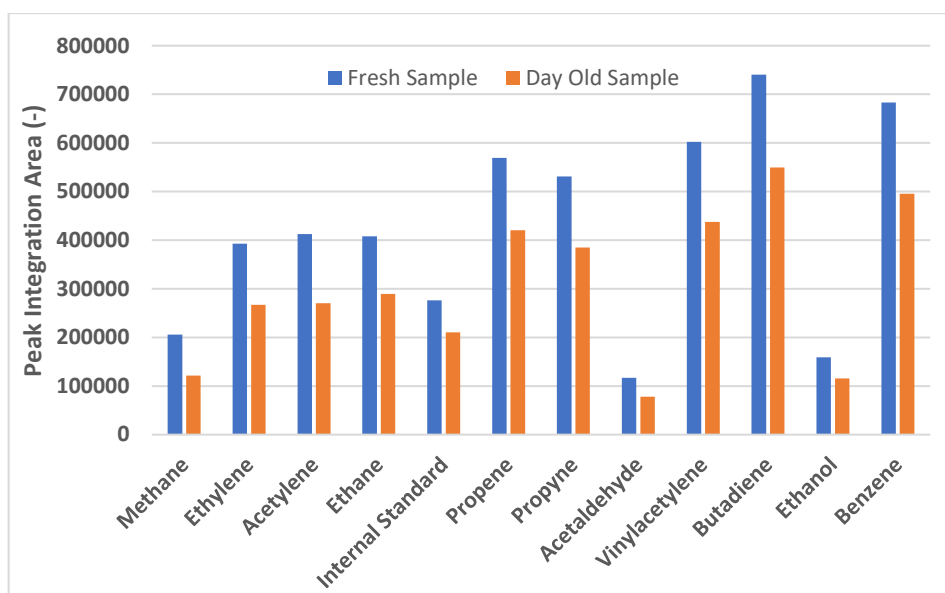
Figure 3.17: Component peak integration comparison between fresh sample and day-old sample

Table 3.9: Percentage integration decrease of individual components and overall average*

Species	Integration area % drop over 24hrs
Methane	41
Ethylene	32
Acetylene	34
Ethane	29
Internal Standard	24
Propene	26
Propyne	27
Acetaldehyde	33
Vinylacetylene	27
Butadiene	26
Ethanol	27
Benzene	27
Average	**30**

Figure 3.17 and Table 3.9 illustrate the effect of time on concentration of the individual species in the calibration gas. An average decrease of 30 % was noted over 24 hours, equating to a decrease of approximately 1.25%/hr. It is pertinent to note here that the most significant decrease was noted in the lighter species, in general, such as methane and acetylene. A potential factor here is that, as opposed to sample condensation - which would affect heavier species, chiefly benzene, to a greater extent - the most significant factor behind concentration decrease over time may have been escape of the species from the syringe itself. Acetaldehyde was also noted to decrease to a greater extent than species with similar retention times. This could have been due to the fact that, because the integration area for oxygenated molecules was lower, the calculation possessed more error. Overall, a drop of 1.25%/hour of sample was not deemed significant, however, every effort was made to inject samples within an hour of extraction in order to minimise error, as the calculated decrease in sample concentration in one hour assumes a linear decrease in concentration.

4. Effect of molecular structure of lignocellulose-derived furans on combustion and emissions in a compression ignition engine

As outlined in Chapter 2, there remains an appreciable knowledge gap in the use of 2nd generation biofuels in compression ingition engines. Fuels resembling diesel-based molecules have been synthesised from this form of biomass,[36,82,116] but the following results were obtained from combustion of blends of diesel (and in some cases butanol) and furan based molecules that are more easily obtained from 2nd generation biomass.

Screening of a variety of bioderived molecules was performed in order to improve our understanding of how this class of molecules respond when combusted in light-duty compression-ignition engines. The molecules tested were selected based on their potentially more economic and less energy intensive production routes, compared to more conventional alternative diesel fuels that contain long-chained hydrocarbons. Furthermore, reducing carbon emissions is possible through the use of these 2nd generation biofuels that are, by nature, carbon neutral, and the fact that the sources are from non-edible, lignocellulosic feedstocks means that competition with food resources is negated. In addition, the changes in combustion that the presence of these molecules influence will impact on the ultimate emissions produced; these emissions, such as nitrous oxides (NO_x) and particulates are known to have detrimental health effects on humans, and the use of biofuels has been shown to have various effects on these outputs. As a result, the primary aim of the following results is aimed at evaluating the effect of using the chosen 2nd generation fuels on combustion and emissions.

4.1. Experimental procedure

4.1.1. Blending of test fuels

A range of fuel molecules, illustrated in Table 4.1, theoretically attainable from biomass, were tested as fuel blends with diesel in the aforementioned CI engine; either in 50:50 volume ratios or 10% in a 70:20:10 volume ratio blend with diesel and butanol.

Furfural (99%), Furfuryl Alcohol (98%), 2-Acetylfuran (99%), Furan (99%), 2,3-Dihydrofuran (99%), 2,5-Dihydrofuran (97%), Tetrahydrofuran (99.9%), 2-Methylfuran (99%), 2,5-Dimethylfuran (99%), 2-Ethylfuran (99%), 2-Methyltetrahydrofuran (99%), 2-Methyltetrahydrofuran-3-one (97%) were all purchased from Sigma Aldrich. 1-Butanol (99%) was purchased from Alfa Aesar and the zero FAME content fossil diesel used was purchased from Haltermann Carless.

Furanic species are hazardous chemicals, therefore all blending was performed within a fume cupboard and subsequent utilisation i.e in the filling and refilling of the fuel system, was undertaken using a full face respirator, nitrile gloves and disposable lab coat.

Blending was performed on a volumetric basis; for example, a 50:50 blend of 200mL would therefore include 100mL of fossil diesel and 100mL of test fuel. Given that some test fuels, particularly heavily oxygenated molecules such as furfural, are highly viscous and polar in nature, a homogenous mixture was not immediately formed when these were added to the fossil diesel and butanol mixture. Subsequently, a magnetic stirrer bar was employed for all blends to ensure that each component had dissolved. It should be noted here that butanol was primarily used for its ability to dissolve the insoluble oxygenated fuels into the diesel fuel; its use as a blending component in diesel fuel is limited due to its low cetane number (15.92).[384]

Stirring was performed for at least 5 minutes or until no visible separation was evident after the mixture was allowed to settle for 1 hour. Before engine tests, the blends were observed and photographed to ensure no separation had transpired before the test fuel was introduced
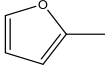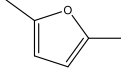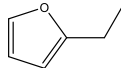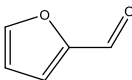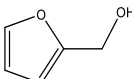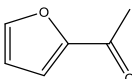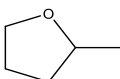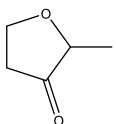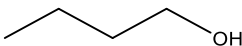
to the engine fuel system. Figure 4.1 below indicates the effect that a lack of stirring had on the blending ability of the furan fuel in fossil diesel.

Figure 4.1: Comparison of 50:50 furfuryl alcohol blend with diesel having formed a homogenous mixture (a) and a visibly separated mixture (b)

Table 4.1: Molecular structure and properties of test fuels (table continues onto the following page)

Molecule	Abbreviation	Boiling Point (°C)[385]	Density (g/ml)[385]
Furan	none	31	0.936
Methylfuran	MF	63	0.91
Dimethylfuran	DMF	92	0.903
Ethylfuran	EF	92	0.912

Tetrahydrofuran	**THF**	66	0.889
2,3-Dihydrofuran	**2,3-DHF**	54	0.927
2,5-Dihydrofuran	**2,5-DHF**	66	0.927
Furfural	**FF**	162	1.16
Furfuryl Alcohol	**FA**	170	1.135
Acetylfuran	**AF**	168	1.098
Methyl-tetrahydrofuran	**MTHF**	78	0.86
Methyl-tetrahydrofuran-3-one	**MTHF-3-one**	139	1.034
n-butanol	**none**	118	0.81
Diesel	**none**	150-380	0.85

4.1.2. Engine operation

For all tests, engine conditions were kept consistent to ensure useful comparison across different blends and molecules, as shown in Table 4.2. Intake temperatures were maintained at 120°C using an inline air heater (Secomak 571), which was placed 330mm upstream of the intake manifold. This temperature was employed to ensure the successful ignition of all test fuels at the engine conditions utilised, while maintaining consistency across samples to ensure comparisons were valid. All engine tests were conducted from a control room- no personnel was allowed to enter the test cell during engine operation.

Table 4.2: Engine operating conditions

Engine Condition	Steady-state Value
Engine Load	4 bar IMEP
Engine Speed	1200 rpm
Injection Pressure	550 bar
Injection Timing	10 CAD BTDC (except for diesel:furan and Diesel: MF blend combustion)
Air Inlet Temperature	120°C

In order to maintain a constant engine load of 4 bar IMEP, the injection duration was varied between fuels and also between specific tests of the same fuel. This relatively low engine load was used so as to ensure results were more representative of city driving; air pollution is particularly pertinent in urban environments. Furthermore, lower engine loads were hoped to emphasise the impact of fuel molecular structure on combustion emissions; higher engine loads and the higher temperatures associated with these could obscure the subtleties of combustion variances between blends. Moreover, the low amounts of fuel available meant that high injection durations were not feasible for the collection of multiple data points. Table 4.3

shows the mean value, and coefficient of variation (COV), of injection durations required when combusting different fuel blends. Overall, these differences could be attributed to two factors; firstly, different fuel molecules possess different calorific contents for a given mass; more heavily oxygenated fuels tend to possess lower energy densities and therefore required longer injection durations to maintain the same engine load. Secondly, the physical properties impacted the injection system itself, for example, a highly viscous fuel, such as furfuryl alcohol (FA), required a longer injection period since the greater frictional forces present between the fuel and injector components necessitated longer injector opening times for the release of the same mass of fuel. Moreover, blends with poor lubricity may have resulted in increased friction between injector components and thus delaying needle movement relative to the control signal.

Table 4.3: Average injection timings for each fuel blend

Fuel Blend	Average Injection Duration (μs)	Injection Duration COV (%)
Furan	762	0.95
MF	757	1.62
DMF	697	2.23
2,3- DHF	684	0.42
2,5- DHF	657	0.72
THF	668	0
MTHF	753	2.89
10% DMF	880	4.95
10% MTHF	860	3.40
10% EF	801	2.36
10% FF	696	0.66
10% FA	713	0.80
10% AF	701	0.24
10% MTHF-3-one	740	0.96
Diesel	666	3.99 (Overall) 1.53 (Average Daily)

4.2. Results and discussion

4.2.1. Combustion characteristics

4.2.1.1. Degree of saturation
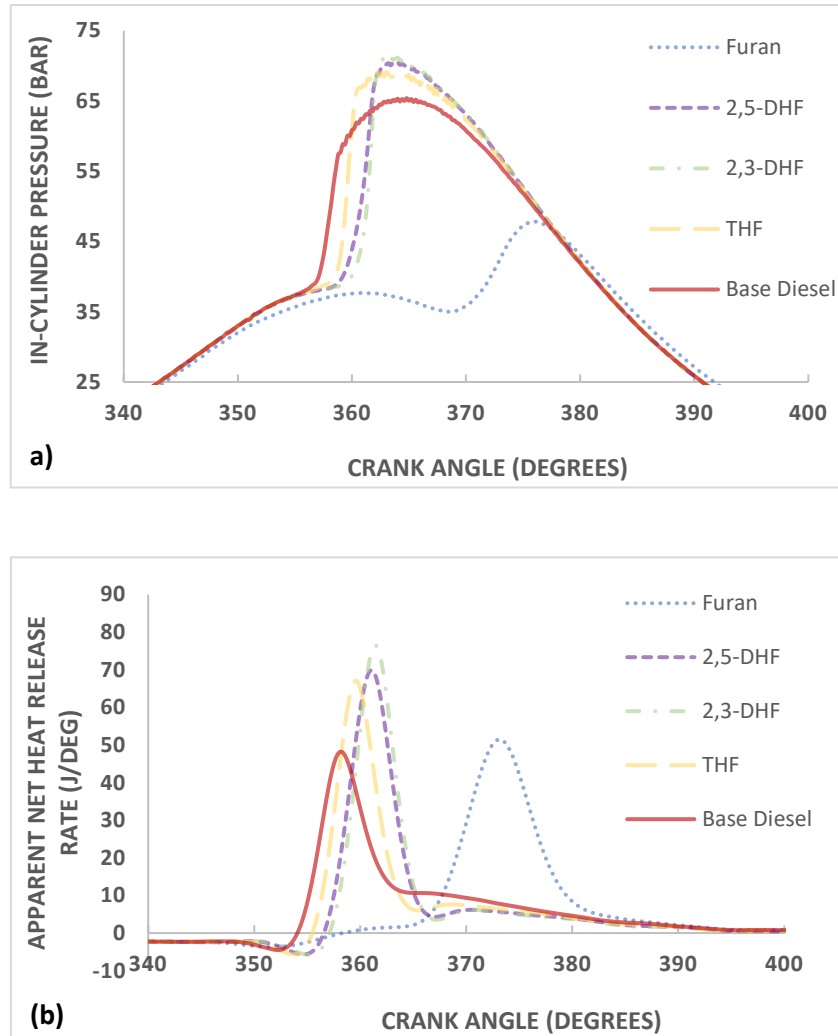
Figure 4.2: In-cylinder pressure (a) and apparent heat release rate (b) of 50:50 furan:diesel blends and base diesel, comparing the degree of saturation. Injection timings were held consistently at 10° BTDC (except for the furan blend, where injection was retarded to 19° BTDC to enable combustion)

Figure 4.2 shows the in-cylinder pressure and corresponding heat release rate of the various 50:50 furanic fuel:diesel blends, comparing the saturation of the molecule; with furan fully unsaturated (aromatic), DHF partially unsaturated and THF fully saturated.

The in-cylinder pressure indicates an earlier release of energy in the case of diesel only compared to the 50:50 furanic fuel:diesel blends, with the combustion retarded approximately 2 crank angle degrees (CAD) in the case of THF and the two DHF blends. Meanwhile furan:diesel combustion did not begin until well into the expansion stroke, and once full ignition commenced a significantly lower in-cylinder pressure was reached (Figure 4.2a). Apparent from the heat release of the furan:diesel blend (Figure 4.2b) is that initial combustion commenced at a timing similar to the other blends, but an appreciable increase in heat release is not noted until after 365 CAD. It is postulated that combustion begins in the case of furan:diesel from radicals created purely from the diesel fraction; the aromatic molecule may not have produced radicals readily, and in fact acted as a radical sink. Polyaromatic hydrocarbons are known to quench reaction rates by acting as a sink for hydrogen atoms,[386] and their stability means that they persist for long periods of time, therefore it is not unreasonable to expect a similar phenomenon for these aromatic furan species. Eventually however, with escalating temperatures, furan decomposition begins, the ring opens, releasing radicals, and rapid premixed combustion ensues. Aromatics contain extremely stable π bonds, which makes H-abstraction difficult. Boot[194] notes, however, that once H-abstraction has occurred, and the ring has opened, the BDEs of the molecule decrease and combustion can ensue more rapidly. This may also explain the apparent 2-stage combustion occurring in the case of furan, indicated clearly in Figure 4.2b by a slight rise in heat release at 355 CAD, before more significant heat release commences at approximately 366 CAD, at which conditions it is suggested the furan component is able to burn.
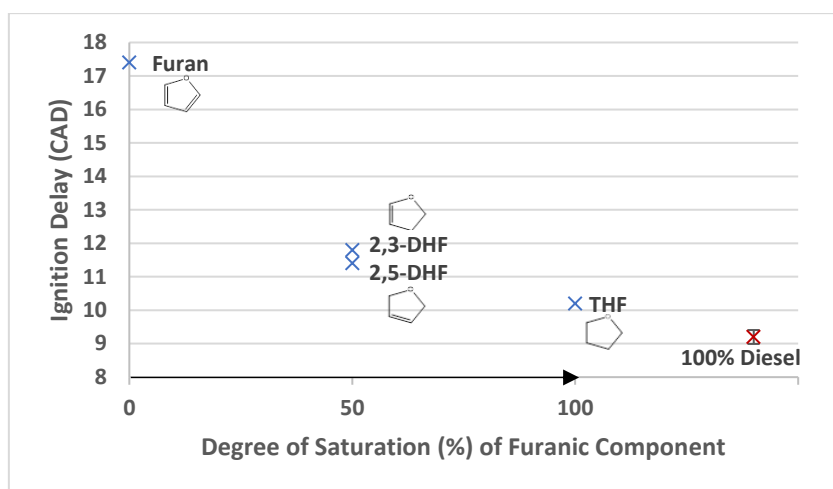
Figure 4.3: Duration of ignition delay of 50:50 vol:vol blends of fossil diesel and furan

molecules of varying degrees of saturation, and of unblended reference diesel

The ignition delay period is defined by the duration (in CAD) from the timing of fuel injection (referenced as the time that the signal is sent to the injector) to the time at which combustion commences (when net heat release becomes positive). Figure 4.3 shows the ignition delay of the 50:50 furan blends and reference diesel, where saturation of the furan molecules increases from left to right. Immediately apparent is that a greater degree of saturation reduces the duration of ignition delay. This is in agreement with previous studies[181,192] whereby a greater degree of saturation has been observed to increase the propensity of a molecule to auto-ignite. The least saturated molecule tested, furan, exhibited the longest ignition delay of 17.4 CAD, while THF, which is fully saturated, possessed an ignition delay of 10.2 CAD (Figure 4.3). Boot[194] explains that H-abstraction on olefins (unsaturated species) produces allyl radicals, which contain delocalised pairs of electrons and therefore are highly stable, slowing down the overall reaction rate. Moreover, Fan[227] provides comparisons of the bond dissociation energies (BDEs) of C-H groups for furan, both dihydrofurans and THF; it is noted that the highest BDE, and therefore most difficult H-abstraction, is present in furan. A more saturated molecule also possesses a greater number of hydrogen atoms that may be extracted, therefore the size of the radical pool during the combustion of a more saturated molecule has the potential to be

greater. The extended delay period of furan was such that the injection timing needed to be retarded to 19 CAD in order for ignition to occur close enough to TDC that stable combustion could ensue, illustrated in Figure 4.2b.

All test blends exhibited longer delay periods than neat diesel, which was anticipated given that the oxygen present within the furan molecules will likely have a negative impact on the rate of early-stage low temperature combustion reaction such as H-abstraction and isomerization. However, it is apparent from these results that the aromaticity has a larger effect on ignition delay than the presence of oxygen within the blends; a difference of 1 CAD exists between base diesel and the THF:diesel blend, but an increase in delay of 1.2-1.8 CAD was observed between the THF:diesel blend and partially unsaturated DHF:diesel blends. A study by Eldeeb[224] compared the ignition delay times of a furan-based molecule- DMF- and the hydrocarbon isooctane in a shock tube study at temperatures from 1000-1400K, concluding that the latter was considerably more reactive as iso-octane undergoes unimolecular decomposition, which generates radicals early on, while H-abstraction by O_2 is the dominant reaction pathway in the case of DMF.

The difference found in ignition delay between the position isomers, 2,3-DHF and 2,5-DHF, was small, at only 0.4 CAD, therefore any conclusions based upon this are stressed as only tentative predictions. According to Sudholt's study;[88] the location of the double bond is important in dictating the cetane number as a result of the change in bond dissociation energies around the rest of the molecule. In the case of 2,3-DHF, it is stated that H-abstraction will first occur on the opposite side of the molecule from the double bond, which links positions 4 and 5, mainly at the saturated C2 position because the hydrogen atoms at the C1 position are partially stabilised by the lone pairs of electrons on the oxygen. For 2,5-DHF, Sudholt notes that the BDEs are lower for comparable positions 2,3-DHF, which could explain the slightly lower ignition delay in the case of 2,5-DHF in the current study (Figure 4.3). However, it was also suggested that while the position of the double bond in 2,5-DHF results in easier H-abstraction, the subsequent radical is unreactive, which would then hinder further early stage

combustion reactions. For this reason, the cetane number calculated by Sudholt was higher in the case of 2,3-DHF. While this does not agree with the observed shorter ignition delay of the 2,5-DHF blend (Figure 4.3), these cetane numbers were calculated for pure fuels, and thus the impact of blending with diesel in the current work, and any synergies in the low temperature reaction kinetics of the furans and diesel hydrocarbons, are not accounted for. Furthermore, the ignitability of the fossil diesel is likely to dominate, therefore any differences in auto-ignition between the dihydrofuran blends used here were likely obscured as the differences in calculated cetane number are small.

4.2.1.2. Number and length of alkyl branching
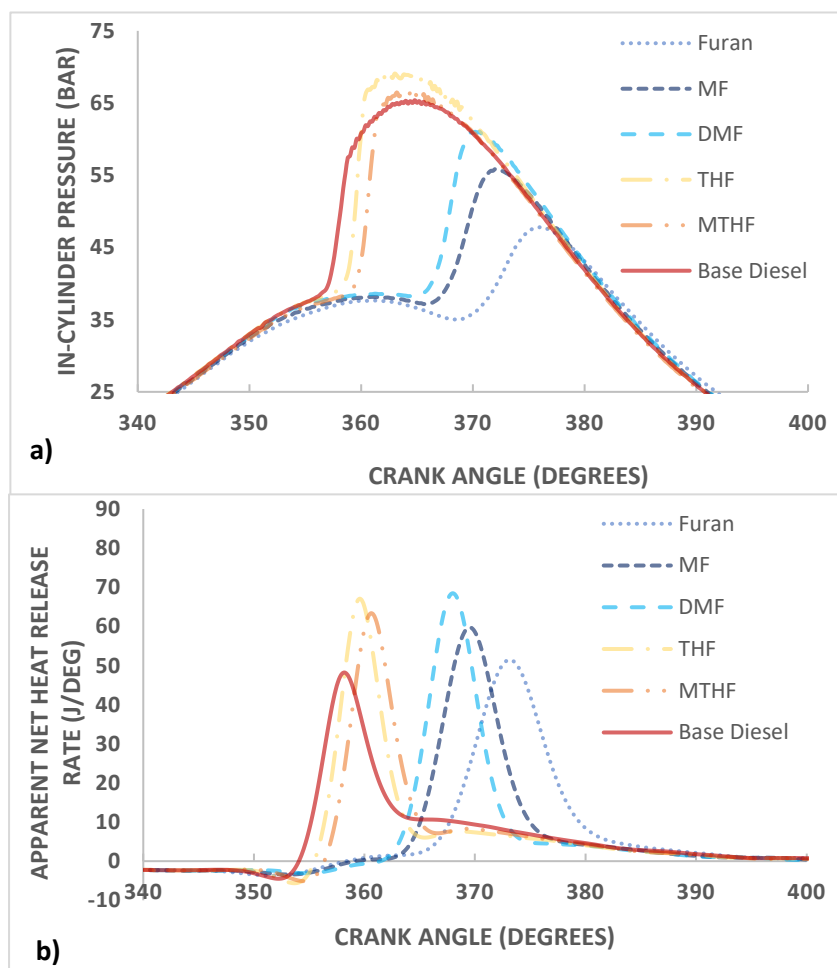
Figure 4.4: In-cylinder pressure (a) and apparent net heat release rate (b) of 50:50 furan:diesel Blends, comparing the level of molecular branching

A comparison of the furan molecules, with slight differences in branching are shown in Figure 4.4. Apparent from both in-cylinder pressure and heat release rates is that there was a clear distinction between saturated and aromatic molecules, but the combustion performance was improved with the addition of alkyl branching with heat release commencing at more favourable conditions (closer to TDC) in the case of DMF compared to MF and furan. From the results of furan, MF and DMF illustrated in Figure 4.4b, it is postulated that the slightly destabilising effect of alkyl chains on an aromatic ring, as well as the easier hydrogen abstraction from the alkyl carbon, likely allowed for a greater pool of radicals to form in the ignition delay phase where early stage combustion reactions occurred.[88] Furthermore, the additional alkyl chain(s) allow for a greater range of reaction pathways in the oxidation or decomposition of these aromatics; early studies concluded that the loss of CO was the only process in furan and MF decomposition, but other pathways were possible in DMF decomposition.[387] More recent investigations determined that H-addition onto the carbon adjacent to the oxygen in furan to produce acetylene was possible while, in MF, H-abstraction from the methyl group was dominant, and DMF possessed a high tendency to produce 1,3-cyclopentadiene and benzene- soot precursors.[388–390] Ultimately, the presence of alkyl chains not only improves reaction rates with lower bond dissociation enthalpies,[88] but also increases the number of potential reactions. However, despite the improvement in ignition with alkyl branching, the in-cylinder pressure (Figure 4.4a) indicates combustion is still only occurring in the expansion stroke for the aromatic furan blends, therefore peak pressures and heat release rates are relatively low. The higher peak HRR and peak pressures in the combustion of a more branched molecule are not replicated in the case of saturated THF and MTHF however, though it is suggested that the benefit of adding a methyl branch is not as apparent in fully saturated THF, which possesses good ignition quality, compared to an aromatic that is highly resistant to ignition.

MTHF might be expected to produce higher heat release rates given the slightly longer ignition delay period allowing for more premixing. Since the chemical properties are very similar, the physical properties of the two molecules should also be considered. The lower volatility of MTHF, coupled with a slightly higher density/viscosity, can be observed in the heat release rate traces in Figure 4.4b. MTHF possesses a slightly longer delay period, but this does not see greater premixed combustion and therefore a higher pHRR. The fact that this is not the case here indicates that, potentially, the mixing rate of MTHF is poorer than that of THF; the more gradual slope of the decreasing trace (between approximately 353 and 355 CAD in the Figure 4.4b HRR trace) for MTHF indicates that this vaporisation period is not as rapid.
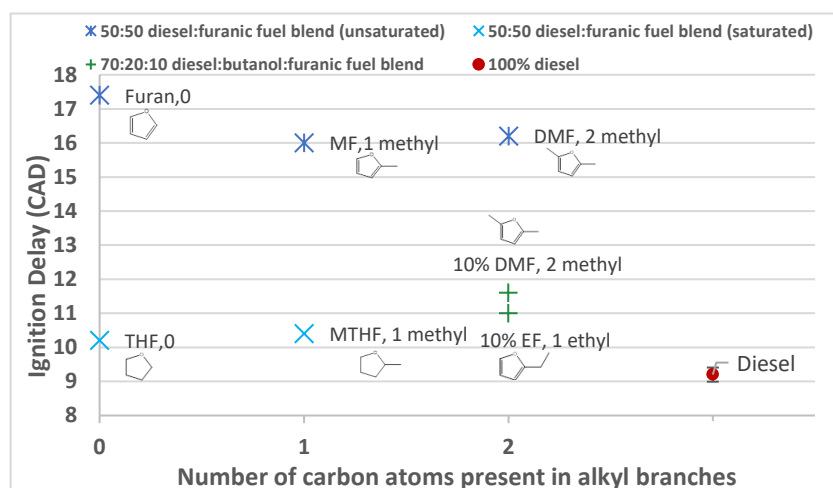
Figure 4.5: Duration of ignition delay, comparing the level of molecular branching, in both 50:50 (blue star) and 70:20:10 (green cross) blend ratios to diesel (red dot)

Figure 4.5 shows the ignition delay periods of furanic fuel:diesel blends and furanic fuel:butanol:diesel blends, comparing the number and length of alkyl branches present on the furan ring. From furan to MF to DMF, there is an increase in branching, and a slight decrease in ignition delay by 1.4 CAD from furan to MF (it should be noted that an earlier injection timing

was used for the furan:diesel and MF:diesel blends in order to reach stable combustion conditions). In the case of the fully saturated furan derivatives, addition of a single methyl branch increased slightly the duration of ignition delay of MTHF relative to THF by 0.2 CAD. Comparing the 10% furan molecule blends, ethylfuran possessed a 0.6 CAD shorter delay period than DMF.

Ultimately, the hydrogen atoms on any side chain of a furan species are considerably easier to remove than on the stable furan ring itself, therefore H-abstraction occurs here initially and, as a result, the ignition delay period is expected to decrease when alkyl chains are applied.[120] The delay period of DMF is longer than that of ethylfuran because the BDEs of the two alkyl branches are equally strong in DMF, whereas, in ethylfuran, Sudholt indicates that the carbon atom between the end of the alkyl chain and the ring carbon will be very reactive (with a BDE of 351 kJ/mol, compared to 360.9 kJ/mol as the lowest BDE in 2-MF). These results are in agreement with Eldeeb's comparative investigation, where ethylfuran was found to ignite up to six times faster than DMF.[224] This suggests that the second carbon on the alkyl chain has a significant effect on the propensity for a furan species to ignite, and any furan-based designer molecule should possess at least two carbons on a side chain. Under oxidative conditions, Sudholt suggests that the most prevalent reaction pathway for a furan species is an addition reaction and subsequent ring opening into alkenes, rather than hydrogen abstraction. Since H-abstraction is not the major reaction pathway, adding an additional methyl chain (therefore more H-abstraction sites) may not have a considerable effect.

The ignition delay of THF and MTHF is very similar, 10.2 and 10.4 respectively (Figure 4.5). While Sudholt notes that ignition behaviour is dictated by the side chain of a THF molecule, this does not hold true between THF and MTHF, since the difference in BDEs is not significant between methyl and ring carbons, and the addition of a methyl chain does not alter the C-H bond strength of the ring carbons relative to base THF[88]. For all THFs, it is claimed that hydrogen abstraction first occurs on the carbon connected to the oxygen and any side chain present. Ultimately, hydrogen abstraction occurs at either the C2 or C5 position in THF,

and primarily the C2 position in 2-MTHF. Since the location of radical attack is unchanged in

MTHF relative to THF, the reaction pathway and rate is likely very similar for both molecules,

and therefore the ignition delay is not significantly affected.

4.2.1.3. Effect of oxygenated side chains
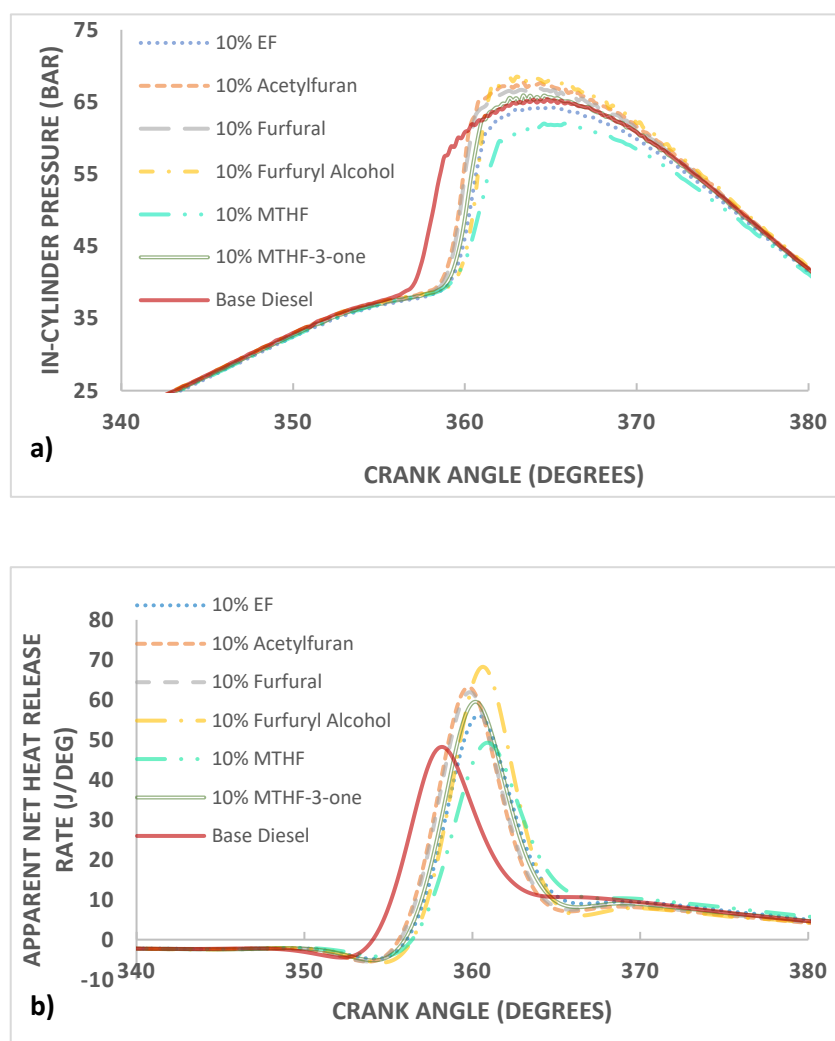
Figure 4.6: In-cylinder pressure (a) and apparent net heat release rate (b) comparison of 70:20:10 diesel:butanol:furanic fuel blends, comparing various oxygenated functional groups

The trend between possessing different oxygenated functional groups is more subtle than

that of the saturation or degree of branching; as can be seen in Figure 4.6, the most notable

distinction is between the base diesel test and all of the blends tested, which are grouped. The

readily visible longer ignition delay of the blends clearly allowed for a greater amount of premixed combustion and therefore a higher pHRR. Unlike the 50:50 blends, these blends consisted primarily of diesel (70 vol%), which allowed pHRR to occur at approximately TDC, despite the likelihood of the furan component exhibiting undesirable combustion traits. Likely the main reason for only small differences between these blends is the fact that only 10% of the fuel was varied between each blend (as opposed to 50% of each blend in the previous tests). Despite this, there are some notable effects; in the case of furfural and furfuryl alcohol, a carbonyl group is replaced by an alcohol group and, while this may not seem a considerable change in 10% of the fuel, it is clear that the alcohol has an extended period of premixing, indicated by the longer period before positive heat release and a greater premixed combustion fraction.
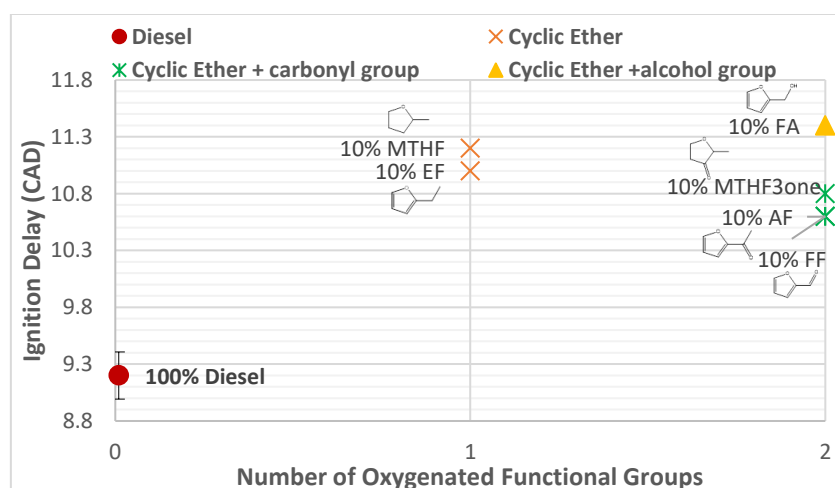
Figure 4.7: Duration of ignition delay, comparing various oxygenated functional groups within 70:20:10 diesel:butanol:furanic fuel blends and pure fossil diesel

Figure 4.7 shows that the ignition delay of furfural and acetylfuran, possessing two oxygenated functional groups, exhibit a shorter delay time than ethylfuran, containing only a single oxygen atom as an ether linkage within the aromatic ring. The same relationship is shown when comparing saturated MTHF to MTHF-3-one, where the latter possesses an

additional oxygen atom in the form of a carbonyl group. However, furfuryl alcohol exhibited an appreciably longer delay period than ethylfuran, highlighting the differing impact that dissimilar oxygenated functional groups have on low temperature kinetics. In general, the delay period of a straight chain oxygenated molecule is greater than that of straight chain hydrocarbon of the same length.[391,202] The greater electronegativity of the oxygen atom (due to a greater proton number compared to a carbon atom for the same number of orbitals) has a knock on effect throughout the rest of the molecule, and therefore the bond dissociation energies of all C-H bonds.

Ethylfuran possessed a longer ignition delay than acetylfuran (Figure 4.7); the latter the same structure as ethylfuran but with the addition of a carbonyl group on the first carbon on the alkyl chain. Moreover, furfural also possessed a shorter delay period than ethylfuran, despite, in the former, the loss of one carbon atom where hydrogen abstraction may occur (and expected to reduce the delay period). A difference of 0.4 CAD in the delay period is not substantial enough to draw any certain conclusions, but a decrease in ignition delay of the same magnitude can also be noted when considering MTHF-3-one relative to MTHF, where the change of molecular structure is again the addition of a carbonyl group, in this case on the ring itself. Despite the observation of only a minor decrease, it is significant that the delay period does not increase, as one would expect with the addition of an oxygen. Furfuryl alcohol, however, possess a significantly longer delay time than both ethylfuran and furfural. This decrease in ignition delay from an alcohol to an aldehyde has been attributed to the high reactivity of the latter species. Aldehydes are intermediates in the low temperature reactions of alcohol, which essentially reduces the number of reaction stages required for complete combustion of the oxygenated molecule. A further tentative suggestion here is that the delay period of furfural is not increased, relative to single-carbon ethylfuran, because there is no hydrogen connected to the additional oxygen in acetylfuran or furfural (the additional oxygen is double bonded to the carbon only), while peroxy radicals are known to be easily formed from these functional groups, increasing reactivity.[392] The same argument potentially explains why

the ignition delay period of furfuryl alcohol is significantly higher than furfural and acetylfuran; a hydrogen atom is directly bonded to the oxygen on the alkyl chain. However, when considering AF and FF relative to EF, one would assume a change in BDEs on the remaining hydrogens in the molecule from the addition of a carbonyl group; Koivisto *et al*[391] studied a variety of carbonyl molecules in their propensity to ignite, finding that the ignition delay increased between an alkane and a ketone of the same chain length. In the test blends employed in the current study however, the molecule is predominantly cyclic rather than a straight chain and, potentially, the additional oxygen has a more destabilising effect on the overall molecule compared to ethylfuran. In essence, oxygens generally inhibit early stage combustion reactions when added to straight chain alkanes, but appear to promote them when added to aromatics and stable ring structures. The electron withdrawing effect of the oxygenated side chain likely disrupts the π bonding that makes aromatic rings highly stable and unreactive. Furthermore, it is important to note that hydrogen abstraction is not the only process that dictates ignition delay; isomerization through chain branching is an important pathway that increases the radical pool, and it has been shown that oxygenated species can hinder this in straight chain molecules.[391] Again, the change in the molecular characteristics created by the addition of a C=O bond to a furan may enhance this relative to an alkylfuran.

Tetrahydrofurans (THFs) and furan differ in their aromaticity, Figure 4.7 shows that the effect of a carbonyl group on ignition delay in both THF and furan ring structures is the same, suggesting both ring structures are relatively stable species that can be disrupted by the addition of an oxygen (carbonyl) group. In MTHF-3-one, the carbonyl group is directly connected to the ring structure and, as in acetylfuran and furfural, this carbonyl group is not connected to any hydrogens itself, therefore does not inhibit hydrogen abstraction from a specific location. A further consideration is that, unlike in the case of furfuryl alcohol, hydrogen bonding is not possible in the carbonyl (C=O) group molecules. This increase in intermolecular force between molecules could also inhibit fuel atomisation and ignition; more polar fuels tend to possess higher viscosities. In the case of MTHF-3-one, the carbonyl group directly

connected to the ring will likely alter the BDEs throughout the structure as it is a small cyclic molecule. The electronegativity of the two oxygens on either side of the molecule will draw electrons away from the centre of the molecule, plausibly making the hydrogens located there more easily abstracted.

4.2.1.4. Effect of butanol

MTHF and DMF were both used as 50:50 blended fuels with diesel and as 10% blends in 20% butanol and 70% diesel. This enabled comparisons to be made across the two ranges of fuels tested, as well as the effect of butanol on the ignition and combustion characteristics to be evaluated. The effect of butanol on diesel combustion relative to neat diesel is already well established at a range of engine conditions, outlined in Babu's review,[201] however the study here can give some insight into the effect of butanol on combustion relative to the furans tested. Butanol as a diesel fuel extender has been shown to improve diesel combustion characteristics to an extent.[201,203] However, high levels of butanol (greater than 40%[29]) see long ignition delays due to the low cetane number of the alcohol, and so it was desirable that the butanol concentration be minimised. The ratio of 70:20:10 was selected based on the solubility of the furan fuels in diesel- for some of the molecules, double the amount of butanol was required to successfully solvate the furan- rather than the applicability of butanol itself. A further point to add is that, as can be seen in Table 2.2, the injection duration required to be increased significantly during the 10% DMF and 10% MTHF blend tests. This suggests that the butanol in particular possessed very poor lubricating properties and the injection of fuel was less consistent for these tests.
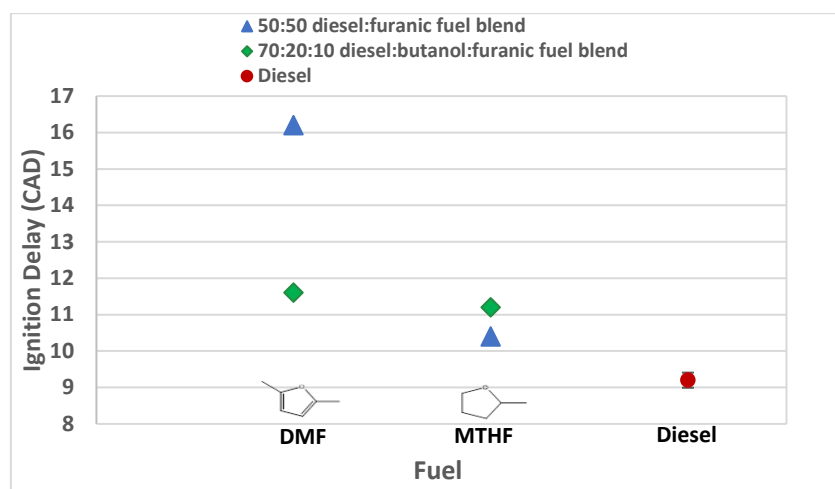
Figure 4.8: Comparison of the duration of ignition delay between DMF and MTHF 50:50 and 70:20:10 blends, as well as fossil diesel

Comparing the MTHF blends, Figure 4.8 illustrates that the ignition delay in the 50:50 blend is slightly lower, which is extremely promising; despite the lower percentage of diesel in this blend, the propensity of this blend to ignite was actually increased slightly when MTHF replaced butanol (and a percentage of the fossil diesel).

The opposite trend is observed when comparing 50 vol% DMF to 10 vol% DMF fuel and 20 vol% butanol. The 50:50 blend here possessed an extremely long ignition delay period of over 16.2 CAD, whereas the 10% blend with additional butanol exhibited a delay period of 11.6 CAD. The additional diesel can help explain the shorter delay, but it is also possible the butanol is having a positive effect relative to the DMF fraction it replaces. Overall, it can reasonably concluded that, relative to butanol, MTHF has a greater propensity to ignite, therefore a higher cetane than butanol (Sudholt calculated the cetane number of MTHF at 22,[88] while the derived cetane number of butanol is 15.92[384]) and hence can be considered, along with other tetrahydrofurans, as a viable diesel blender from a purely combustion perspective. However, fully unsaturated furans, such as DMF (calculated cetane number of 10.9)[88] ignite poorly compared to butanol. The very stable aromatic ring is difficult to break down in early stage combustion, therefore its ignition delay is very high compared to butanol.

4.2.2. CO emissions
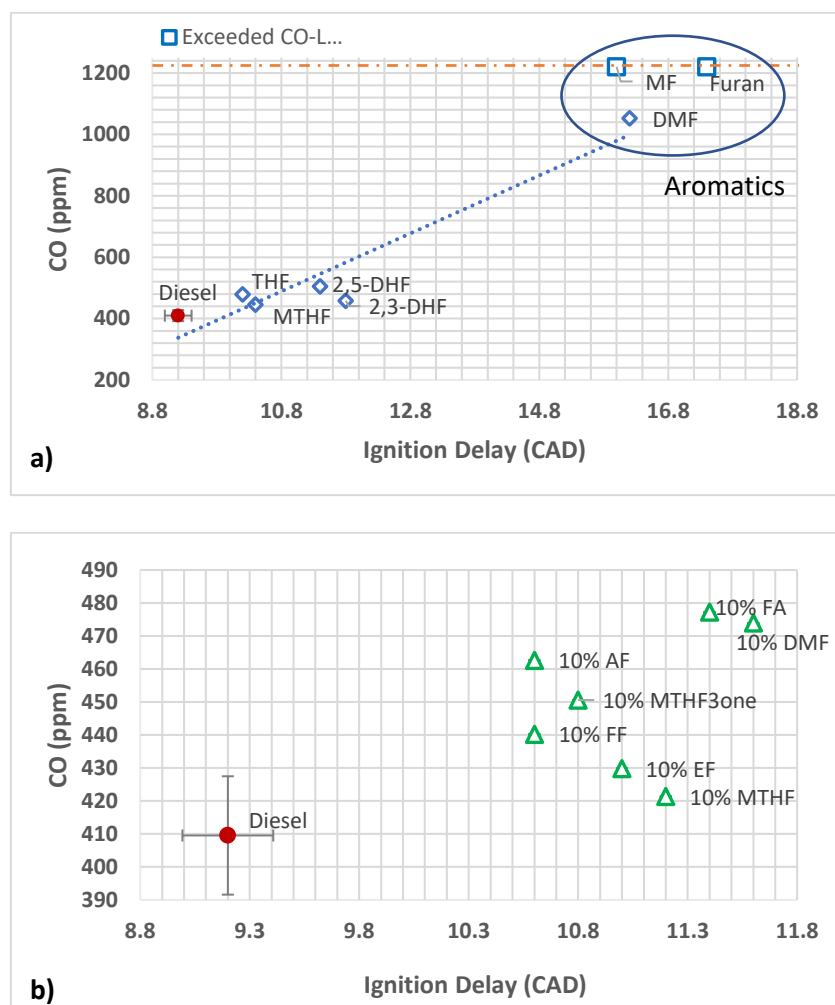
Figure 4.9: Exhaust CO levels (ppm) with varying ignition delay of a) 50:50 blends and b)

70:20:10 diesel:butanol blends

Figure 4.9 shows the CO emissions of the furan blends and reference diesel, relative to ignition delay. The emissions of CO are a strong indication of the degree to which complete combustion is occurring; higher CO emissions indicate more incomplete combustion.

Figure 4.9a indicates that the levels of CO emitted during the furan:diesel combustion were over twice as high as both DHFs and THF (the CO emissions of the furan:diesel blend

exceeded the CO upper detection threshold), suggesting that the combustion performance was very poor, in agreement with the late combustion phasing. It is pertinent to note the considerable jump in CO emissions, and therefore combustion efficiency, between the partially unsaturated DHFs and full unsaturated furan, with the CO emissions of 2,3-DHF in fact 20ppm lower than THF despite the lower degree of saturation. The shorter ignition delay of THF could potentially result in higher levels of incomplete combustion products, relative to 2,3-DHF, due to lower levels of air premixing, potentially enhancing the presence of fuel rich zones where CO will form. This effect may have been slightly counteracted, however, had the ignition delay of the DHF blends been long enough for fuel to have become overdiluted; this could result in greater incomplete combustion due to the lower temperatures and quenching effect of the relatively cold cylinder walls, if fuel had become impinged here. This reasoning could also explain the lower CO emissions of pure diesel, which exhibited a shorter delay period than any of the blends yet. Despite the reduced time for air-fuel mixing, CO emissions are lower, thereby suggesting that overdilution in the extended premixing period is the primary mechanism of incomplete combustion.

Figures 4.9a also shows that unbranched furan and MF (one methyl branch) produced the highest CO emissions of all fuels tested (both exceeded the maximum threshold detectable, likely due to the very poor combustion quality exhibited by both (Figure 4.4), followed by DMF (two methyl branches), which produced approximately 40ppm higher CO emissions than EF (one ethyl branch) in the 10% blend tests (Figure 4.9b). This reinforces the conclusion that, among the furanic fuel blends tested, the levels of CO emitted do not follow the trend of reduced CO with shorter ignition delay. A further factor to consider is the magnitude and timing of peak in-cylinder temperature. Figure 4.10 shows the magnitude and time of occurrence of the calculated maximum in-cylinder global temperature for each of the blends tested. Apparent from Figure 4.10, as could be expected, are higher temperatures when this peaks occurs closer to TDC, earlier in the expansion stroke.
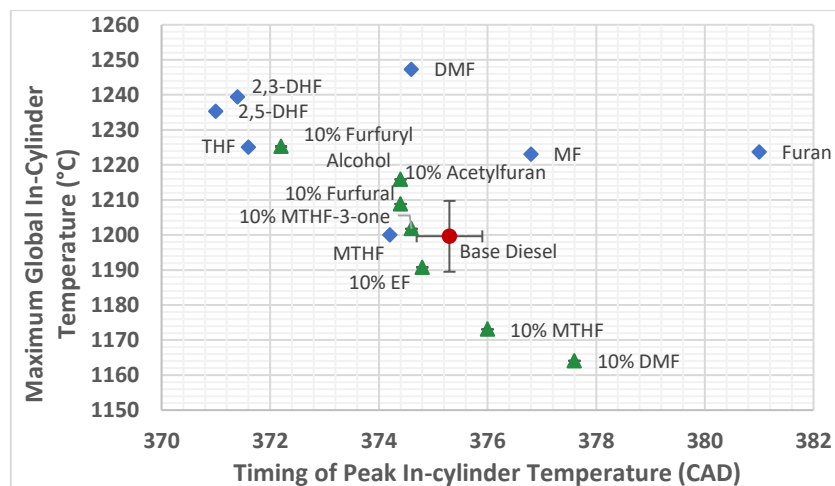
Figure 4.10: Magnitude and time of occurrence of calculated maximum in-cylinder temperature

an of 50:50 furanic fuel:diesel blends and 70:20:10 diesel:butanol:furanic fuel blends

It can be seen from Figure 4.10 that furan exhibited a relatively late timing of peak in-cylinder temperature compared to the other 50:50 diesel:furanic blends (and the lowest pHRR, as seen in Figure 4.2b), and emitted higher levels of CO than all other fuels tested, with the potential exception of the 50:50 MF:diesel blend (which also exceeded the CO detector threshold- Figure 4.9). EF combustion meanwhile yielded higher cylinder temperatures than DMF in the 10% tests (the 10% DMF test saw the lowest peak temperatures of any blend) and slightly lower CO emissions. Lower temperatures can be expected to see increased incomplete combustion and CO formation. Furan, MF and DMF all displayed two stage combustion, as shown in Figure 4.4b, whereby diesel reacts in the initial stage and the furan species only acts initially as a diluent of the diesel, before being able to burn as the flame propagates (the flame initiated by the diesel component). With these long ignition delays the fuel is likely to become impinged on the cylinder walls, where temperatures are reduced relative to air-fuel mixture, likely contributing to a further increase incomplete combustion products such as CO and hydrocarbons. Figure 4.9a shows that between THF and MTHF, as with ignition delay (Figure 4.5), there is little difference in the level of CO emissions formed, most likely due to the similar

BDEs and reaction pathways of both of these molecules, despite the addition of a methyl branch.

Figure 4.9b indicates that furfural and acetylfural blends exhibited higher CO emissions than ethylfuran, following the trend of higher incomplete combustion products with a shorter ignition delay and period for premixing. Figure 4.10 indicates that all of the oxygenated alkylfurans (2 oxygen atoms within the structure) exhibited higher peak temperatures during their combustion than ethylfuran, which could be due to pHRR occurring closer to TDC, resulting in higher temperatures (indicated in Figure 4.10) through reduced heat transfer to cylinder walls. Furfuryl alcohol's long ignition delay did not result in a decrease in CO emissions, as was observed when considering ethylfuran, acetylfuran and furfural. Nor does FA exhibit a low peak in-cylinder temperature that could imply incomplete combustion (Figure 4.10). In fact, the 70:20:10 DMF blend displayed a longer delay period than FA, yet produced lower levels of CO (Figure 4.9b). The physical properties of furfuryl alcohol therefore need to be considered; its density is much higher compared to DMF, and its viscosity was noted to be higher when blending, which will likely result in poorer atomization of the more dense and viscous alcohol and greater fuel impingement on the cylinder walls. Further, this impinged fuel could be released in the expansion stroke when it is not able to fully oxidise due to the lower temperatures present during this combustion phase.

The physical properties of these different molecules can also help explain the difference in CO emissions between the MTHF and MTHF-3-one blends. The shorter delay period in the case of the latter would have reduced mixing time, thus resulting in larger fuel rich zones with potential to form CO, however, given that the ignition delay difference is very small (Figure 4.7), it may not account for the increase in CO of MTHF-3-one shown in Figure 4.9b of 30 ppm. More likely, since MTHF-3-one was more viscous, the injection of this blend forms more oxygen deficient zones, from reduced atomisation, where CO will form from incomplete combustion.

4.2.3. NO$_x$ emissions
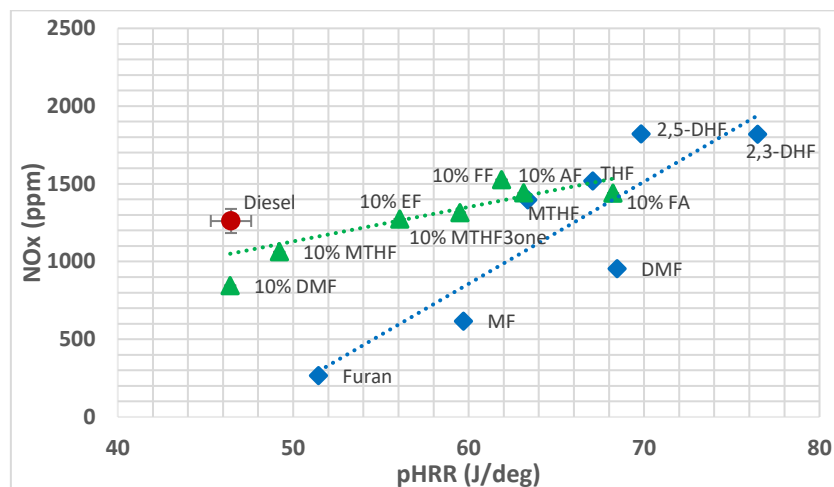
Figure 4.11: NO$_x$ emissions relative to peak heat release rates of 50:50 blends (blue diamond), 70:20:10 blends (green triangle) and fossil diesel (red circle)

Figure 4.11 shows the exhaust levels of NO$_x$ for the furan blends and reference diesel, relative to pHRR. Immediately apparent is the significantly lower level of NO$_x$ emissions in the case of the furan blend, relative to all other fuel blends tested, while the highest NO$_x$ levels were emitted by the partially saturated DHF blends. The levels of NO$_x$ produced show a clear trend of increasing with peak HRR. NO$_x$ is predominantly formed via the thermal oxidation of nitrogen, rates of which are strongly dependent on temperature, and this is also sensitive to the duration for which sufficiently high temperatures are present. Considering the effect of furan saturation, it can be seen that this acts on NO$_x$ levels predominantly via the duration of ignition delay. The higher NO$_x$ emissions in the case of DHF (Figure 4.11) are postulated to be due to the longer ignition delay of the dihydrofurans compared to THF (Figure 4.3). However, the significantly prolonged ignition delay of the furan:diesel blend does not elevate NO$_x$ emissions due to much later occurrence of maximum in-cylinder temperature and ensuing poor combustion quality, as indicated by the observed high CO emissions (Figure 4.9).
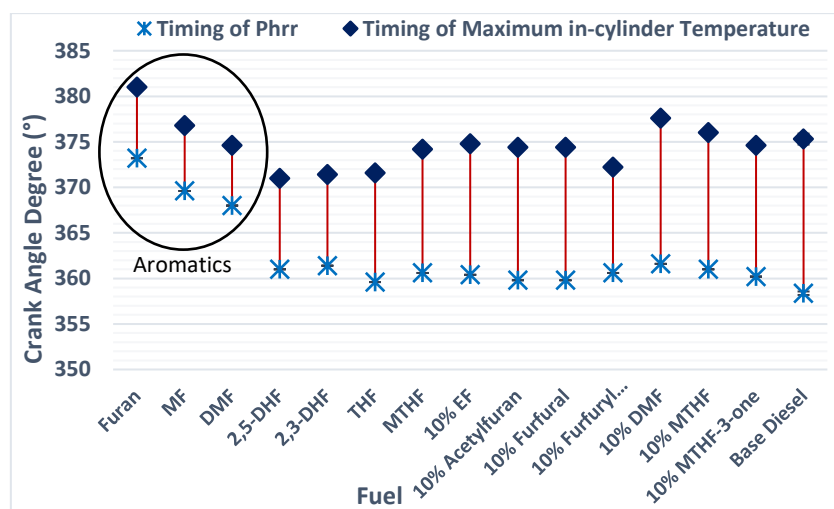
Figure 4.12: Timing of pHRR and peak in-cylinder temperatures of all blends

Combusting the furan:diesel blend likely resulted in conditions unsuitable to produce substantial NO_x, as a result of the apparent quenching of diesel radical reactions resulting from the presence of the aromatic furan molecule. From Figure 4.12, it can be seen that while the calculated maximum in-cylinder temperature of the furan:diesel blend was comparable to the other 50:50 blends tested, it occurred far later in the expansion stroke. It is suggested that, despite sufficiently high maximum temperatures, due to rapid reductions in temperature during the expansion stroke, these were present for too short a period of time for substantial NO_x to be formed. Figure 4.12 demonstrates not only that peak heat release and peak temperatures occurred far later in the furan blend compared to other blends, but also demonstrates that a longer duration between pHRR and peak temperatures tends to result in higher NO_X. In the case of furan, which emitted the lowest levels of $NO_X,$ this duration is approximately 8 CAD, whereas for fossil diesel the interval is 17 CAD. Therefore, despite furan combustion displaying a higher peak temperature than diesel (Figure 4.10), it is the latter which produces higher NO_X emissions (Figure 4.11).

Figure 4.11 clearly shows that, for the 50:50 diesel:furanic fuel blends, emissions of NO_x increased as number of methyl branches attached to the aromatic ring increased (furan, MF and DMF), with ethylfuran producing higher levels than DMF. NO_x output was, however,

comparable between THF and MTHF, within the margin of error indicated by the vertical error bars of the diesel result. The higher NO_x emissions of DMF relative to MF can be likely attributed to the higher in-cylinder maximum temperature observed in the case of the former (Figure 4.10) and this is likewise the case when comparing ethylfuran to DMF and THF to MTHF.

It can also be seen in Figure 4.11 that 70:20:10 diesel:butanol:furanic fuel blends containing additional oxygen (AF, FF and FA) displayed higher NO_x emissions than ethylfuran. This observation is consistent with the trends of peak heat release rate (Figure 4.6) and maximum in-cylinder temperatures (Figure 4.10), with the exception of furfural, which emitted levels of NO_x higher than furfuryl alcohol, despite a lower in-cylinder temperature. From Figure 4.12, it can be noted that the timings of pHRR and peak temperatures occur at almost identical timings for these FF and FA blends, indicating that the longer delay of FA did not result in a retarded release of energy. Longer delay periods tend to result in higher cylinder temperatures as a result of greater duration for premixing, which can explain the higher temperatures during furfuryl alcohol combustion compared to ethylfuran, but does not explain why acetylfuran and furfural also produced higher temperatures than EF, since the delay period of these was shorter (Figure 4.7). One tentative suggestion is that the greater density of more oxygenated AF and FF (see Table 4.1) allows for more enhanced mixing rates due to greater spray momentum, allowing for a greater premixed combustion phase that causes a higher pHRR.[393] The additional oxygen may also account for the observed increase in the average cylinder temperatures (Figure 4.10). The reason for this is twofold, firstly the adiabatic flame temperature of oxygenated fuels tends to be higher,[394] and secondly, locally the combustion of these blends may be more complete due to the increase in fuel-bound oxygen.

Figure 4.11 shows higher NO_x emissions from MTHF-3-one relative to MTHF, despite comparable, if not shorter, ignition delay and can likely be attributed to an earlier pHRR closer to TDC (Figure 4.12) and, potentially, a greater rate of mixing in the case of the more dense MTHF-3-one blend.[395]

4.2.4. Particulate emissions
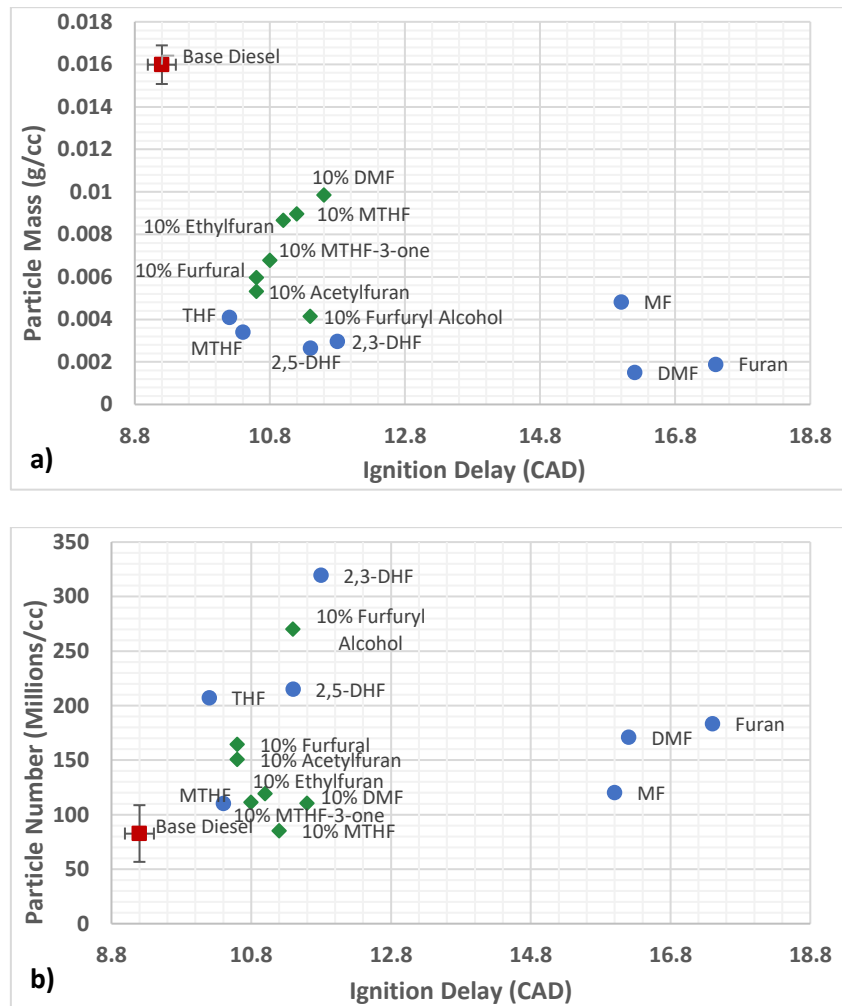
Figure 4.13: Exhaust emissions of a) particle mass and b) particle number of 50:50 blends (blue circle), 70:20:10 blends (green diamond) and diesel (red square), relative to ignition delay

Figure 4.13a and 4.13b show the total mass of particulate matter and total number of particles emitted relative to the ignition delay of the 50:50 diese:furanic fuel and 70:20:10 diesel:butanol blends. The most evident trend in Figure 4.13 is the difference between the particulate output of the furanic blends and base diesel; the latter possesses a particle mass a factor of four times greater than the furans, but a significantly lower particle number. It is

likely that the significant difference in ignition delay is the reason for this as the onset of combustion therefore begins earlier, allowing more time for particle formation and growth than the test blends before the exhaust stroke, increasing particle mass while decreasing particle number. The shorter ignition delay during diesel combustion also leads to the formation of more pyrolysis products in fuel rich zones within the combustion chamber, therefore it is possible that there is a greater rate of soot formation initially. Moreover, displacement of fossil diesel, which generally contains a significant proportion of aromatic and unsaturated molecules, will likely have reduced the number of species that are able to readily form soot; either through direct growth to larger aromatic species or via decomposition to short chain unsaturated precursors.

There is evidently an effect of the degree of saturation on the particle mass emitted in the exhaust, increasing from 0.00189 ug/cc in the case of unsaturated furan to 0.0041 ug/cc with fully saturated THF, an amount greater than the indicated standard deviation error bars of the observed PM emissions of diesel combustion across the testing period. The particulate mass emitted by the DHF blends was within this range (Figure 4.13a). THF possessed the shortest delay period so, as with the CO emissions, there is less time for a homogenous fuel-air mixture to be formed, and thus likely a greater presence of fuel rich zones that will likely form particulates. In general, however, aromatic fuels are expected to produce greater particulate mass, since aromatics themselves are soot precursors. Moreover, Karavalakis[396] notes that aromatics are more difficult to vaporize than paraffins, meaning they are more susceptible to becoming trapped on cylinder walls and in cylinder deposits. In the current study, an effect of aromatics does not seem to be prevalent in increasing soot formation. These experiments involve furan as the aromatic, which contains oxygen; the presence of the oxygen in the furan will potentially inhibit the formation of soot precursors; aromatic hydrocarbons that are normally present in fossil diesel fuel- such as benzene- do not possess this oxygen and form these precursors more easily. Substituting 50 vol% of the diesel is therefore anticipated to result in a reduction in these known soot precursors. However, previous studies have noted that furan

is prone to forming acetylene- one of the building blocks for PAHs- while DMF's major decomposition products include cyclopentadiene and benzene, which are also precursors to particulates.[223] Alexandrino *et al*[397] noted that the formation of soot, and precursors such as ethylene and acetylene, increased when using DMF relative to other oxygenated fuels, such as ethanol or methyl formate. However, the pyrolysis conditions used may not be reflected in a combustion engine. Important to note also is the impact of engine load. Xiao[398] conducted CI combustion studies into the use of DMF in diesel blends and noted that DMF decreased 1,3-butadiene and benzene emissions while increasing acetaldehyde production. However, engine load played a major part in the observations; at lower loads, DMF addition decreased the concentration of soot but, at high engine loads (1.13MPa BMEP), the DMF blends saw higher particle size distributions than pure diesel. It is suggested that, at lower loads, the dilution of diesel is the dominant role of DMF, while at higher loads and temperatures, DMF is able to contribute to the formation of soot in the mechanism explored in more controlled pyrolysis studies by the likes of Alexandrino.[336,397]

In terms of particle mass (Figure 4.13a), there is little difference between the two dihydrofurans, but 2,3-DHF produced a considerably higher particle number (Figure 4.13b), greater than all other fuels tested. It is not clear why this occurs, but one could suggest the 2,3-DHF forms more soot later in combustion, relative to 2,5-DHF; these particles therefore do not have time to grow in size due to the rapidly decreasing temperatures at this stage of combustion. It has already been noted that the diesel seemingly dominates the early stage of combustion in these blends (to a significant extent in the case of the furan:diesel blend) until temperatures are high enough for the furanic component to also ignite (Figure 4.2b). Therefore in the latter stages of a combustion cycle, the furanic molecule may dictate the formation of particulates. Fan[227] notes that the reaction pathway of 2,5-DHF will initially yield stable furan, which is less likely to form particulates, while 2,3-DHF produces large amounts of propene and propene radicals, and these could be responsible for the formation of more soot particles.[189] While THF produces greater particulate mass than both DHF molecules (Figure 4.13a), it

produces fewer particles, suggesting these particles are generally larger, and this is confirmed by the measured particle size distribution (see Appendix Figure D1a). One hypothesis is that there is potentially a greater degree of soot oxidation occurring during the combustion of the dihydrofurans owing to the slightly higher in-cylinder temperatures (Figure 4.10) relative to THF, which can be attributed to the longer ignition delay of the former (Figure 4.3). Furthermore, since ignition (and thus combustion) occurs slightly earlier in the THF:diesel blend relative to that of DHF, particles form earlier. As a result, the fuel spray is less dispersed, there is more time for the particles formed to collide and grow into larger particles via coalescence and agglomeration, and particle formation can occur when the piston is closer to TDC at lower volume, and therefore higher density, making particle collisions more likely.

The increase in branching of DMF compared to furan and MTHF compared to THF saw a decrease in both particle mass and number. Figure 4.13 shows that the methylfuran blend produced a greater amount of particulate mass than either the furan of DMF blends, but the lowest particle number of the full aromatic 50:50 blends. The trend in ignition delay (furan> MF/DMF>EF) does not explain this result, and in this case the level of particulates formed cannot be solely attributed to the amount of mixing allowed to occur before combustion commences. Although, the higher soot emissions during MF combustion compared to DMF could be attributed to overdilution and fuel impingement on the cylinder walls due to the significantly extended ignition delay period of MF. The aforementioned poor combustion quality of furan and methylfuran likely dominates the formation of particulates relative to other fuels tested. The earlier injection timing of the furan blend (19 CAD BTDC) relative to MF (17 CAD BTDC) could explain the significantly higher particulate mass produced by methylfuran compared to furan (Figure 4.13a). The peak temperatures reached during combustion of both blends were very similar (Figure 4.10), but this temperature occurred earlier with the MF:diesel (Figure 4.12). With in-cylinder temperatures being higher earlier in the expansion stroke, more fuel would be available to pyrolyse and form soot relative to furan:diesel combustion.

Comparing DMF and EF, the latter emitted slightly lower particulate mass in the 70:20:10 blends (Figure 4.13a). This is likely due to the very long delay period shown by the DMF blend (Figure 4.5), which may have resulted in overmixing, which concurs with the CO emission observed (Figure 4.9b). The higher particle number exhibited by ethylfuran (Figure 4.13b) suggests that the particles emitted from the DMF:butanol:diesel blend were larger (indicated in Appendix Figure D1b in the Appendix), and potentially formed earlier. In addition to overdilution, it is suggested that the molecular structure of DMF could be responsible for the relatively higher emission of particulates compared to EF. Hoang *et al*[13] reviewed the current knowledge of DMF combustion, outlining that unimolecular decomposition is a major pathway in the breakdown of the molecule, with initial bond breaking at the C-H site on the methyl carbons and subsequent ring-opening resulting in 1,3-butadiene as a major product, a well-known soot precursor. A study by Song[221] meanwhile described the main products of EF decomposition as primarily 2-vinylfuran, 2-furylmethyl and vinylketene, and suggest that the hydrocarbons formed in the pyrolysis of DMF are more likely to form soot precursors.

An appreciable difference in particulate mass emissions between THF and MTHF can be seen in Figure 4.13; the THF blend produced 0.0041 ug/cc, while MTHF produced 0.0034 ug/cc. This could partially be explained by the slightly shorter delay period observed for THF (Figure 4.5). However, since the difference in ID is only small, other explanations are warranted. Some of the trends noted in these experiments could potentially be explained by the difference in volatility between molecules. A more volatile fuel (the boiling point of THF is 66°C, while the boiling point of MTHF is 80.2°C) could result in a fuel vapour cloud forming close to the injector nozzle, which will create local temperature hot spots in this area and high soot formation due to the relatively fuel rich zone.

Figure 4.13a also shows that the mass of particulates was consistently lower for the molecules with greater oxygen content. This oxygen will play a role in the particulates' oxidation phase, while the higher temperatures exhibited in the combustion of these fuels would enhance oxidation rates further compared to ethylfuran. Furfuryl alcohol combustion displayed the

lowest particle mass overall; acetylfuran and furfural blends produced slightly higher PM emissions, though less than EF. This could suggest a greater ability for oxygen bonded to carbon and hydrogen to aid in the oxidation of soot particles, as is the case in alcohols. The C=O bond is difficult to break, whereas oxygen in the alcohol likely becomes more readily available for oxidation earlier during combustion. The particulate number exhibits the opposite trend, whereby the lowest particulate number is emitted by the DMF blend (1 oxygen atom), while the highest is found in furfuryl alcohol combustion. Hellier *et al*[33] reviewed the effect of various oxygenated functional groups on soot formation, and concluded that the carbon bonded to the oxygen in a ketone group did not contribute to soot formation, while the carbon connected to a hydroxyl group in an alcohol was involved in particulate formation. So, while particulate mass decreased due to enhanced oxidation in FA, it is suggested that this blend formed more soot initially, thus a greater number of particles were detected. Both FA and DMF possessed a very long delay period in which fuel impingement may occur, but the particle number was considerably lower in the case of DMF combustion (Figure 4.13b). The reason for this is potentially due to the poorer combustion quality exhibited when using the DMF blend; furan itself is an aromatic that is difficult to open, and DMF does not possess any polar groups that can destabilise the ring and significantly inhibit this effect. Furthermore, temperatures appeared far higher using the furfuryl alcohol blend compared to the DMF blend (Figure 4.10), which would likely promote the initial formation of the pyrolysis products. Physical properties of these molecules also need to be considered. The greater hydrogen bonding of furfuryl alcohol, compared to DMF, can be reasonably expected to increase blend viscosity, an attribute that reduces air entrainment and atomisation, leading to larger fuel droplets and therefore more localised pyrolysis zones to form soot.

The delay period of furfural/acetylfuran was similar to that of ethylfuran, but the more oxygenated former species produced a higher PM number. This could again be attributed to the increased viscosity of these fuels that make atomization more difficult and therefore fuel rich zones more prevalent. Meanwhile, the higher cylinder temperatures during AF/FF/FA

combustion, relative to EF, could also result in higher levels of soot being formed initially (due to an enhanced kinetic effect) before these oxygenated alkylfurans see an enhanced oxidation phase and considerably reduce the particulate mass. The same explanations can explain the apparent trend when comparing MTHF and MTHF-3-one; the fuel with greater fuel-bound oxygen (MTHF-3-one), greater viscosity and maximum calculated peak in-cylinder temperatures, produces lower levels of particulates on a mass basis, approximately 0.0068 ug/cc compared to 0.009 ug/cc (Figure 4.13a).

A final consideration is the increase in boiling points noted in the more oxygenated species (Table 4.1). For example, the boiling point of FA is 170°C, whereas the boiling point of DMF is just 92°C. Considering the boiling point of butanol- 118°C - the blend of diesel, butanol and FA contains components of vastly different volatilities. It has been shown that ternary blends of this type undergo micro-explosions, a phenomenon in which a volatile fuel component (butanol in this instance) becomes trapped inside the bulk fuel droplets, superheating to form bubbles that eventually 'explode' and disperse the parent fuel droplet.[395,399] This aids in fuel atomisation, reducing fuel-rich zones and thus could help account for the reduction in particle mass seen in more oxygenated furanic fuel blends. It is also suggested that, in addition to physical fuel effects and fuel bound oxygen increasing soot oxidation, oxygen atoms could inhibit stages of soot formation by disrupting aromatic ring growth on a molecular level. Isotope tracing experiments have indicated that carbons bonded to oxygen atoms are less likely to be involved in soot formation- forming CO and CO_2 more readily- while the increase in species, such as OH radicals, that comes with an increase in oxygen content, has been indicated to limit PAH growth.[400,401]

4.3. Conclusions

The screening of the various biomass-derived molecules as blends with diesel and butanol has helped to determine viable bio-derived molecules that could be investigated more extensively, with the following specific conclusions drawn.

21. The ring structure of the bioderived molecule needed to be saturated, or at least only partially unsaturated, for stable combustion and to avoid excessively long durations of ignition delay period. The long ignition delay of aromatic furan, MF and DMF 50:50 blends, meant combustion occurred very late in the expansion stroke.

22. The long ignition delay of blends containing stable aromatic species was not only detrimental to the overall combustion quality (observed by the high carbon monoxide emissions of these blends) but also meant that soot was formed very late, allowing less time for soot oxidation, resulting in a high particulate number.

23. This late combustion also meant that temperatures required for thermal NO_x formation were not attained for a significant duration, therefore furan, MF and DMF blends produced the lowest of these emissions of all fuels tested.

24. The greater ignition quality of EF relative to DMF suggests that the presence of two carbons within an alkyl chain is particularly beneficial to the ignition quality of a cyclic molecule. Comparing THF to MTHF; the addition of one carbon to the ring did not make a notable difference to ignition delay or the resulting emissions of CO or NO_x, suggesting future tests should look into the use of longer alkyl chains from a ringed structure.

25. The addition of a carbonyl group to the furan/THF structure was observed to shorten the ignition delay, increase CO and NO_x emissions, while decreasing the particle mass and increasing particle number. Alcohol group addition to a furan/THF molecule exacerbated these trends compared to the carbonyl group, producing even lower emissions of CO and particle mass (and a higher number). An extended ignition delay

and impact on the fuel physical properties of the alcohol potentially explains this trend, as well as the fact that alcohols are more effective in oxidising particles than carbonyl equivalents.

26. All test blends displayed the same trait in particulate emissions (decreasing mass and increasing number). The substitution of a significant volume of diesel is likely the major cause at these load conditions, as the hydrocarbons present in diesel are prone to forming soot in fuel rich zones of the fuel jet. However, it has been shown that DMF, for example, also forms soot precursors during thermal decomposition.[120] Therefore, other factors, such as the presence of fuel-bound oxygen and an extended ignition delay causing a reduction in the time available for particle formation and growth, could contribute to this trend.

Despite the increased processing required to reach a saturated THF (as opposed to furan) from platform chemicals such as HMF and furfural, the combustion quality and emissions means that the processing penalty upstream is required to secure a viable diesel blending component. Other than greater molecular saturation, the presence of a carbonyl group on the ring structure or on an alkyl chain from that structure improves combustion quality; increasing ignition propensity while decreasing particle mass. The following investigation utilises these findings by employing another range of novel bioderived fuels in a diesel engine as blends and pure fuels.

5. Combustion and emission characteristics of lactone fuels in a compression ignition engine

As discussed in Section 2.1.6 and 2.2.2.5, lactones are a promising class of bio-derivable molecule that possess favourable characteristics for use in diesel blends. While they differ from conventional biodiesel in their cyclic nature, they possess the ester functionality that could be advantageous in reducing the amount of particulate emissions produced (at least on a mass basis). The investigation of furans outlined in Chapter 4 also indicated that the addition of an exocyclic oxygen group to a cyclic molecule can help to improve the ignition quality of the fuel in a contrasting way to the addition of an oxygen to an aliphatic molecule, such as is the case for the fatty acid esters that comprise conventional biodiesel.[181] An advantage to lactones is their variety. Numerous ring sizes can be obtained with various number and lengths of side chains, as well as differing degrees of saturation. However, while the variety of lactones that can be obtained from biomass is promising, a screening process is required to determine the type of molecule that may be most applicable to diesel applications. From the previous results (Chapter 4) it is possible to streamline the selection process slightly. For example, a lactone that is fully saturated is likely to be the most viable candidate as this saturation has been shown to reduce the ignition delay of the fuel, as well as the NO_x emissions, compared to an equivalent molecule that is partially saturated. As a result, the lactones tested in the following study were fully saturated.
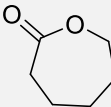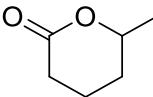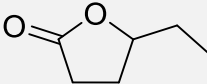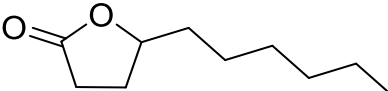
5.1. Introduction to test fuels

The first series of lactones considered, the structures of which are shown in Table 5.1, were used to compare the impact of the ring size and overall carbon number on blending with fossil diesel and the ignition quality. ε-caprolactone (εCL), is a seven membered lactone (six

carbons) with no side chains, δ-hexanolactone (δHL) also possesses 6 carbons but one of these carbons is branched from a six membered ring, while γ-caprolactone (γCL) takes this further by extending the branch to an ethyl chain at the expense of the ring size (five membered).

The comparison of these molecules enabled the impact of the ring size and presence of alkyl chains to be determined while keeping the overall carbon number constant (C6). The fourth lactone tested here, γ-decalactone (γDL), differed by possessing ten carbons (C10). However, as with γ-caprolactone, the cyclic structure consists of four carbons and an oxygen. The purpose of including this molecule was to compare the relative effect of adding further carbons to the chain off the same ring. Naturally, the ignition delay was expected to decrease, but if the combustion was dominated by the ring structure then the chain length would likely not have been noted to make a considerable difference to the ignition quality.

Table 5.1: Physical properties of three C6 lactones and C10 lactone (γDL) tested in blends
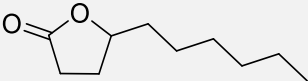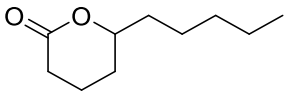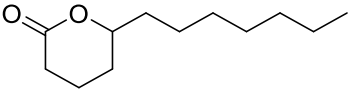
Lactone	Abbreviation	Structure	Boiling Point (°C)	Density (g/cm³)*	Viscosity (mPa)***
ε-caprolactone	εCL		98	1.030	7.44
δ-hexanolactone	δHL		111	1.037	4.53
γ-caprolactone	γCL		219	1.023	3.00
γ-decalactone	γDL		281	0.948	7.50

*atmospheric temperature
**preliminary test results obtained with a Brookfield digital rheometer (Model DV-III)*

Four lactones were also tested with the prediction of igniting as pure components; it was anticipated that a greater number of carbons overall would result in a reduction in the ignition delay period. The tested molecules' structures and physical properties are supplied in Table 5.2 below.

Table 5.2: Structures and physical properties of C10 and C12 lactones tested as pure fuels

Lactone	Abbreviation	Structure	Boiling Point (°C)	Density (g/cm³)*	Viscosity (mPa)* **
γ-decalactone	γDL		281 (760mmHg)	0.948	7.50
δ-decalactone	δDL		283 (760mmHg)	0.954	11.2
γ-dodecalactone	γDDL		130-132 (1.5 mmHg)	0.936	14.6
δ-dodecalactone	δDDL		304 (760mmHg)	0.942	15.0

*atmospheric temperature
**preliminary test results obtained with a Brookfield digital rheometer (Model DV-III)

5.2. Experimental procedure

5.2.1. Blending of test fuels

The solubility of the blended lactones (Table 5.1) in fossil diesel fuel varied significantly. To maintain consistency, and as was the practice with the blends tested in Chapter 4, a constant blend ratio was utilised for all tests which reflected the maximum blend ratio possible for the poorest blending fuel. Table 5.3 below specifies the volume ratios used for all lactone blends tested.

Ideally the molecule could be blended without the addition of a co-solvent, as this would obscure the combustion characteristics of the molecule, though this was determined to be impossible. Butanol was selected again due to its frequent use in diesel blend studies and the improvement in emissions this molecule can bring when utilised in low quantities.[10-11] A study by Yang utilised butanol in a blend with both diesel and GVL, which determined little change in engine power when utilising higher percentages of oxygenated fuel, with major reductions in HC emissions and smoke opacity.[402] In the current study however, the proportion of lactone relative to butanol was maximised so as to be able to observe the effects of varying lactone molecular structure.

εCL was noted to blend poorly with diesel. When diesel was combined in a 50:50 volume ratio with the lactone species, a single phase solution could not be formed. The size and polarity of a molecule are the main attributes in dictating the solubility of a molecule. Ester molecules tend to be polar and given the rule of 'like- dissolves-like', with diesel being a non-polar solvent, poor blending was not unexpected. The large ring and shape of this molecule are also likely reasons for the poor blending properties in diesel; the ring shape means that it cannot form the necessary Van de Waals forces with diesel molecules, which tend to be long chains of alkanes, rendering it poorly soluble.

As in the case of ε-caprolactone, δ-hexanolactone was noted not to be insoluble in fossil diesel fuel. Moreover, the blending properties were poorer relative to εCL, such that all blend ratios were dictated by δHL solubility. Since the polarity of the various lactones is likely to be very similar, the overall surface area and the orientation in which the diesel molecules may be able to fit around the lactone molecules could explain the observed difference in solubility. The solubility of γCL was found to be higher than that of δ-hexanolactone, therefore not following a trend of ring size or side chain length. The longer chain of γCL compared to δHL may present enough non-polarity for diesel molecules to be able to interact to the extent necessary for the lactone to become solvated more effectively than the methyl branched δHL. Comparing εCL to δHL though, the former is a more compact structure, which would be beneficial to its

solubility. γ-decalactone could be blended in 50:50 ratios without butanol in the diesel fuel, however, to maintain consistency, the same blend ratios were used for all tests. The enhanced solubility of γ-decalactone is due to the long side chain of the lactone, producing a degree of non-polarity within the molecule that allows the formation of intermolecular forces with diesel fuel molecules, which are typically made up of long aliphatic chains.

Table 5.3: Lactone blending ratios

Diesel Volume	Butanol Volume	Lactone Volume	Lactone Volume %
150ml	50ml	100ml	33

A 50vol% diesel:butanol blend was also tested in this study to assess the relative effects of replacing butanol with the various lactone molecules.

5.2.2. Engine operating conditions for lactone blend combustion

The engine was operated at conditions similar to those described in Chapter 4; a constant engine load of 4 bar IMEP and a constant engine speed of 1200 rpm. However, where in Chapter 4 the furan blends were tested at a constant start of injection, the lactones blends were tested at only constant start of combustion timing, with the start of injection varied according to the ignition delay of that fuel so that the start of combustion always occurred at TDC.

A constant injection pressure of 550 bar was utilised for all tests, with the injection duration and timing modified for each fuel to maintain a constant engine load of 4 bar IMEP and start of combustion at TDC. A summary of these injection parameters is outlined in Table 5.4 below, with diesel injections at the start and end of a testing day supplied to highlight any major changes in injector performance across a day.

Table 5.4: Injection parameters for the blends tested (4 bar IMEP, 1200 rpm)

Fuel	Average Injection Duration (µs)	COV of Injection Duration (%)	Injection Timing (CAD BTDC)
Base Diesel (Start)	593	0.3	9.6
ε-caprolactone	658	0.99	14.5
δ-hexanolactone	659	0.37	14.3
γ-caprolactone	648	0	14.2
γ-decalactone	637	0.11	12.6
Butanol	638	0.23	14.6
Base Diesel (End)	594	0	9.8

5.2.3. Engine operating conditions used for pure lactone fuels

The pure lactone fuels were tested under the same engine load and speed conditions as those of the lactone blends. For these pure fuels, both constant injection (CInj) and constant ignition (CIgn) tests were utilised. This was decided due to the fact that, because pure fuels were tested, a greater range of ignition delays was anticipated, and it was important to discern whether differences in combustion characteristics were caused by combustion phasing or the fuel chemistry.

A summary of the injection properties is supplied in Table 5.5 below. It was noted that these values were consistent across all tests and fuels, likely due to the effective lubrication of the high viscosity lactone fuels.

Table 5.5: Injection durations and timings of pure lactone fuels and base diesel tests (4 bar IMEP, 1200 rpm, SOI = 10 CAD BTDC for CInj tests)

Fuel	CInj Average Injection Duration (µs)	CInj COV Injection Duration (%)	CIgn Average Injection Duration (µs)	CIgn COV Injection Duration (%)	CIgn Injection Timing (CAD BTDC)
Diesel	592.5	0.25	591	0.15	9.6
δ-decalactone	691	0.18	694.5	0.28	12.6
γ-dodecalactone	678.5	0.27	679.5	0.30	9
δ-dodecalactone	679	0.37	685.5	0.12	10
γ-decalactone	687	0.71	694	0.26	11.8

5.3. Diesel-butanol-lactone blend results

5.3.1. Combustion characteristics
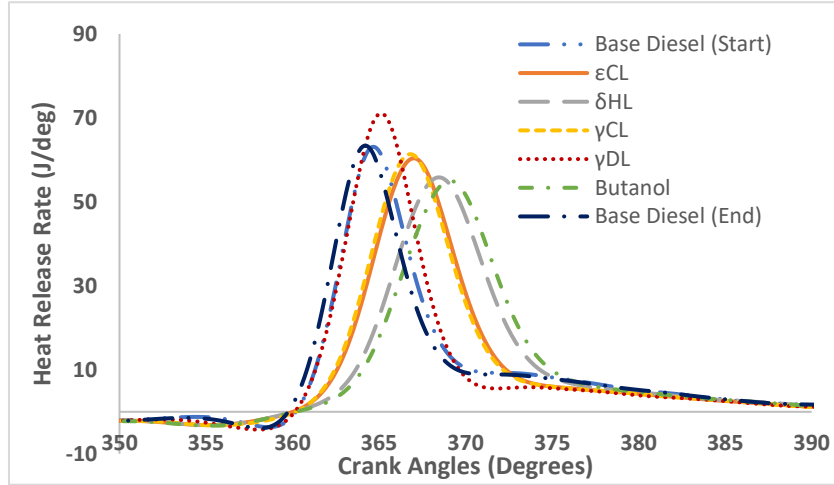
Figure 5.1: Apparent net heat release rates during combustion of diesel-butanol-lactone blends and base diesel at 4 bar IMEP, 1200 rpm and constant start of combustion at TDC

Figure 5.1 shows the apparent net heat release rates of the various diesel-butanol-lactone blends, compared to fossil diesel. The tests were conducted at constant ignition conditions, which ensures that heat release occurs at similar in-cylinder volumes. Heat release during diesel combustion at the start and end of a test day are shown to highlight the range of experimental variation; apparent from Figure 5.1 is the subtle difference in the heat release rates of base diesel start and base diesel end, suggesting the variation in heat release between the lactone blends to be attributable to the fuel composition and not drift in engine performance. Of the fuels tested the sharpest rise in heat release rate is seen in the case of base diesel start and base diesel end, followed by γDL and with the slowest increase in heat release rate apparent during combustion of the δHL and the butanol only blend. Interesting to note is that the γDL blend exhibited a higher peak heat release rate than base diesel, owing to the longer ignition delay that allows more time to form a homogenous fuel-air mixture (observable from the start of injection, indicated by the negative HRR slope in Figure 5.1, occurring just after

350 CAD). γCL and εCL produce peak heat release rates of comparable magnitude, and occur slightly later compared to those exhibited by the base diesel and the γDL blend. More rapid combustion is expected in the case of γCL, given that the ethyl chain will likely help produce the radicals necessary to fully open the lactone ring and enhance flame propagation. However, it is unclear why similar combustion phasing was exhibited by εCL given the absence of an alkyl chain to provide readily available sites for hydrogen abstraction.

Relative to δHL (with one methyl branch), the lack of any side chains in εCL might be expected to reduce ignition quality and combustion stability. Figure 5.1 indicates that this is not the case, with δHL exhibiting a lower magnitude and later timing of pHRR, suggesting that the structure of δHL harms combustion. Since both injection and ignition timings were similar for both molecules, it is likely that initial radical formation is not the pathway that is hindered, and δHL derivatives may result in more chain terminating reactions. δHL combustion appeared similar to that of the diesel:butanol 'control' blend, with both blends resulting in relatively unstable combustion. Butanol has been commonly employed in diesel testing[29]- under a range of conditions- but blend ratios greater than 20vol% have been shown to result in poor combustion efficiency- high CO emissions.[204]
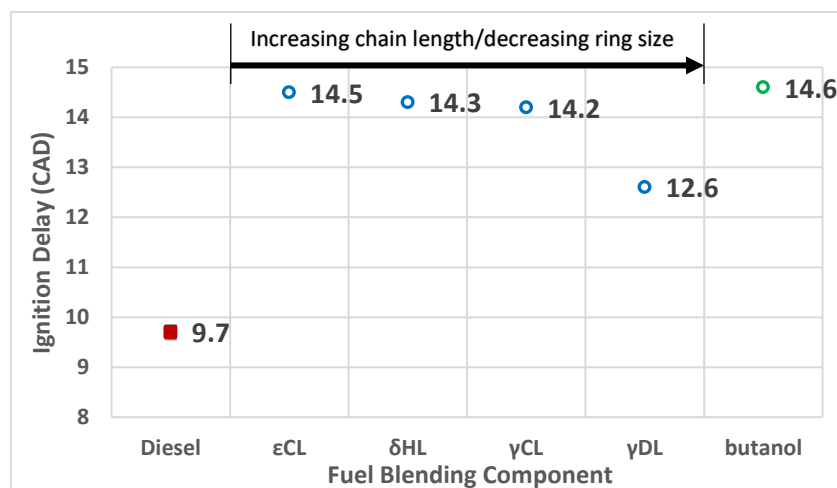
Figure 5.2: Duration of ignition delay of the lactone and butanol blends, and base diesel, at constant engine speed and IMEP and variable injection timing for constant start of combustion

Figure 5.2 shows the duration of the ignition delay period during combustion of the lactone and butanol blends and also the base diesel results. Immediately apparent in Figure 5.2 is the consistent repeatability in measurement of ignition delay as signified by the minor error bars calculated from the standard deviation of all base diesel repeats. The lactone/butanol blends all exhibited longer delay periods than the base diesel. Given the fact that the longest delay period was exhibited by the butanol blend, it is apparent that all the lactones tested possessed higher ignition quality as a blending component than the short chain alcohol. This is expected, given the low cetane number (15.92) of butanol[384] and the higher carbon number of the lactones compared to the four carbons in butanol. With a variation of only 33% of the blend content, it can be seen that the duration of ignition delay is not changed significantly between the three C6 lactones (ε-caprolactone, δ-hexanolactone, γ-caprolactone), with the longest ignition delay exhibited by εCL and the shortest by γCL, indicating a trend of decreasing ring size and longer side chain length reducing the duration of the delay period. With a further increase in the length of the side chain at constant ring size (γ-decalactone relative to γ-caprolactone) the delay period is reduced more substantially (12.6 CAD from 14.2 CAD). Recalling again that only 33% of the blend content is varied between the lactone blends, and yet the delay period decreases by over 1 CAD, suggests that γ-decalactone is a highly ignitable fuel compared to the other lactone tested in these blends.

5.3.2. Gaseous emissions
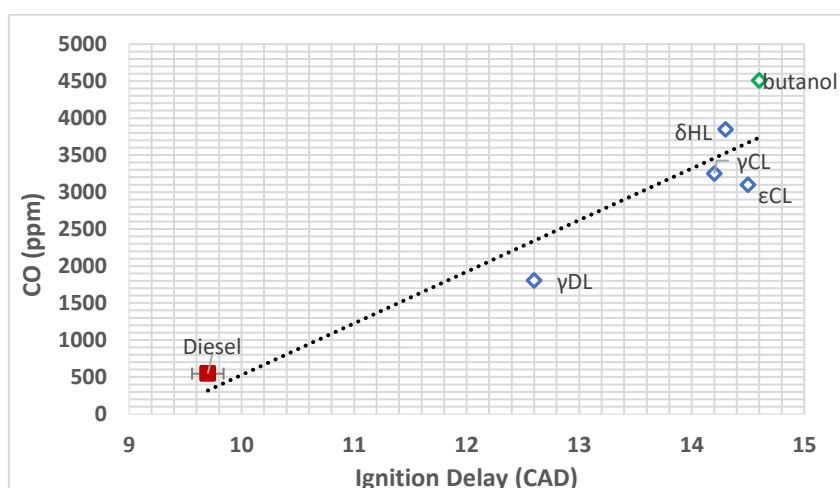
Figure 5.3: Exhaust gas concentrations of CO and duration of ignition delay during combustion of the lactone blends and base diesel

The combustion efficiency can help illustrate, to a large degree, the compatibility of a given fuel with a compression ignition engine. The extent to which combustion is incomplete is indicated by Figure 5.3, which shows the exhaust gas concentrations of CO at varying durations of lactone blend ignition delay and where higher emissions of CO imply more incomplete combustion. Figure 5.3 indicates a positive trend of CO emissions with increasing ignition delay. With increasing duration of ignition delay it is likely that the fuel becomes increasingly overdiluted with inert nitrogen, and thus complete combustion does not occur. This excessive ignition delay is largely attributed to the butanol within the blend (the diesel:butanol blend possesses the highest CO emissions), although the 6-carbon lactones are also responsible given their relatively low carbon number and high oxygen content, and therefore low ignition propensity (Figure 3.2). This extended delay period not only causes overdilution, and therefore lower combustion temperatures- reducing reaction rates and therefore the proportion of complete combustion- but also increases the likelihood of fuel impingement on the cylinder walls; the fuel may remain unreacted long enough to reach the quench zone and the relatively cold cylinder walls.

The higher density of these lactones (see Table 5.1) compared to diesel (with a density of approximately 0.85 g/cm^3) is a property that has been shown to increase lift-off length of fuel sprays, thus increasing the likelihood of droplets reaching the walls.[395] The lactone also possess higher viscosities than diesel itself (diesel viscosity: ~ 1.35 mPa s)[403], making fuel atomisation poorer and resulting in a greater proportion of fuel-rich, oxygen deficient zones where CO may form. A further physical property to consider though is the boiling point; ε-caprolactone and δ-hexanolactone are relatively volatile, with boiling points of 98°C and 111°C respectively. It is therefore postulated that, for these lactones and butanol in particular, fuel penetration into the chamber is relatively low. As discussed in relation to furan fuels in Chapter 4, this reduced penetration could see a vapour cloud close to the injector tip that is responsible for incomplete combustion due to a lack of oxygen entrainment.

γ-caprolactone possesses a boiling point of 219°C, far higher than the other two C6 lactones. However, this blend produced levels of CO similar to those during combustion of ε-caprolactone, therefore physical properties do not entirely explain the trends in CO emissions-ignition delay is a clear contributor. δ-hexanolactone sees the highest CO emissions and therefore degree of incomplete combustion. Since the delay period decreases from the largest to smallest ring, the ID does not fully explain the difference in CO emissions, which increase from seven to five to six-membered rings, though these differences are relatively minor. A tentative suggestion, however, is that, because δ-hexanolactone possesses the highest density, this fuel spray possesses the greatest momentum during injection and is most likely to become impinged onto the cylinder walls when coupled with the long ignition delay periods observed in these C6 lactone and butanol blends.
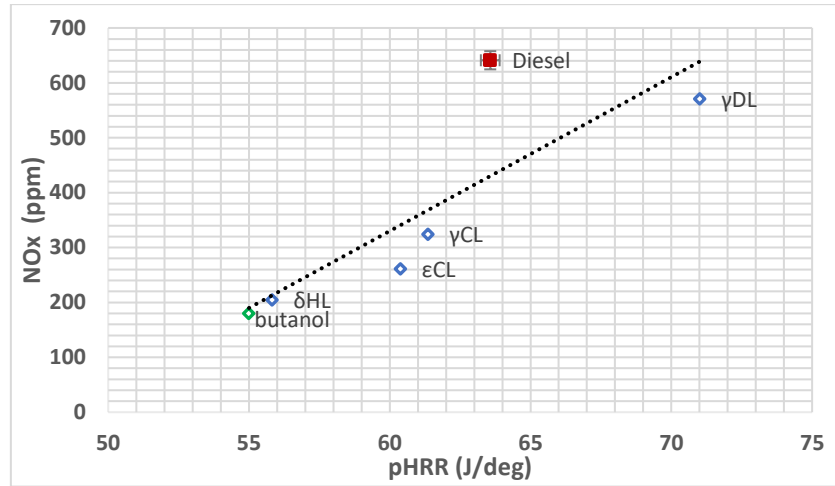
Figure 5.4: Trend between nitrous oxide emissions and peak apparent heat release rate

Figure 5.4 shows the exhaust levels of NO_x relative to the peak apparent net heat release rates during combustion of the lactone-butanol-diesel blends and base diesel at constant IMEP and start of combustion at TDC. Indicated is the significantly lower NO_x concentrations emitted by the lactone blends compared to the base diesel, which consistently produced approximately 640 ppm; the error bars show plus and minus one standard deviation, and indicate the high degree of repeatability in NO_x measurement during diesel combustion. The lowest NO_x levels were observed for the butanol blend and can likely be attributed to the more unstable combustion in the case of this blend- noted by the high CO emissions (Figure 5.3)- and thus could be expected to yield lower in-cylinder temperatures on average. Given the fact that NO_x emissions are formed from the oxidation of nitrogen- and therefore rates of formation increase with increasing temperature- this decrease in temperature corresponds to lower NO_x.
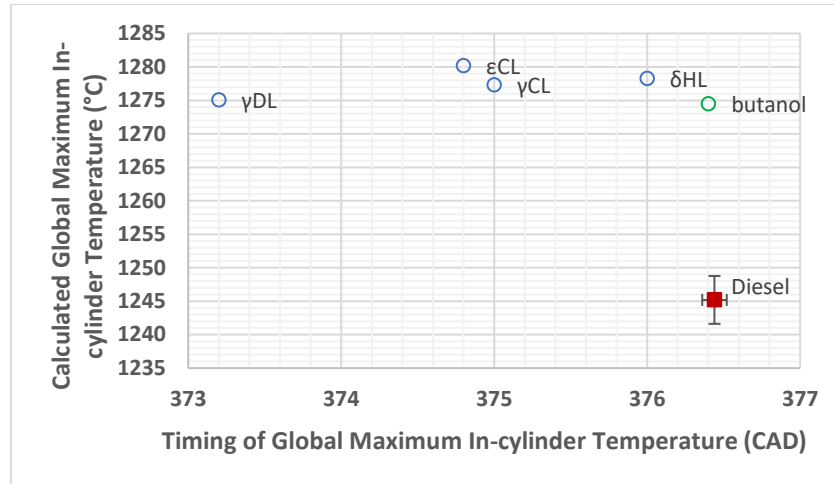
Figure 5.5: Magnitude and timing of calculated maximum global in-cylinder temperature of blended lactone-butanol-diesel fuels and base diesel

Figure 5.5 shows the calculated maximum global in-cylinder temperature and time of occurrence for the lactone blends and base diesel. Contrary to the lower temperatures suggested by the NO_x emissions (Figure 5.4), Figure 5.5 indicates that the butanol blend exhibited comparable maximum in-cylinder temperatures when compared to the lactone blends, and at a timing equivalent to that of base diesel. Also illustrated is the considerably lower maximum in-cylinder temperatures experienced during diesel combustion compared to the lactone blends. However, the timing of the peak HRR and maximum global temperatures, shown in Figure 5.6 below, offers potential reasoning for higher NO_x during diesel combustion as compared to the lactone blends. Figure 5.6 shows that the duration between peak heat release rate and maximum in-cylinder global temperature is approximately 12 CAD. Comparing this to butanol blend combustion, where the difference is closer to 7 CAD, suggests more sustained combustion in the case of diesel and therefore the temperatures necessary for NO_x formation are likely prolonged.
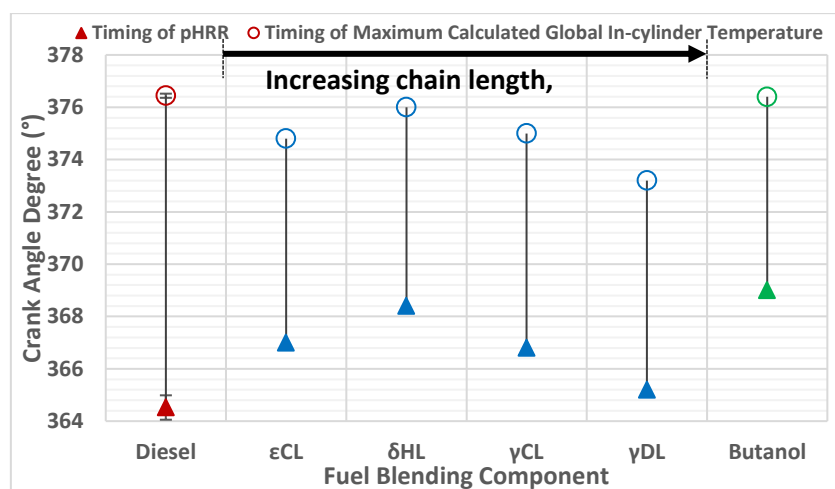
Figure 5.6: Time of occurrence of peak HRR and peak calculated global in-cylinder temperature of fuel blends and base diesel

Higher pHRR and a longer duration of sustained high combustion temperatures, also helps to explain why the blend of γ-decalactone produced the highest NO_x emissions of any of the lactone blends tested, despite having the shortest ignition delay period that often results in lower NO_x emissions due to a reduction in premixed combustion. The strong ignition properties of γDL enabled pHRR to occur earlier in the expansion stroke (compared to other test blends), shown in Figure 5.1 and 5.6, where higher cylinder pressure conditions may be attained. Thus, high temperatures could be maintained with reduced cylinder volumes reducing rates of heat transfer to the exposed wall surface area. While the advanced combustion phasing in the case of yDL is beneficial to combustion efficiency, resulting in a reduction in incomplete combustion products such as CO (as noted in Figure 5.3), the higher temperatures result in higher NO_x (Figure 5.4)

Considering the C6 lactones, the longest delay period and highest maximum in-cylinder temperatures are observed with ε-caprolactone, though γ-caprolactone produced higher NO_x emissions. A shorter delay period generally reduces fuel-air premixing and therefore the potential magnitude of pHRR (thereby reducing energy release and temperature). However, as shown in Figure 5.4, however, NO_x emissions are in agreement with pHRR, while the period

between pHRR and peak temperature (Figure 5.6) is marginally longer in the case of γ-caprolactone. The increase in NO_x emissions seen in the case of γ-caprolactone may also be explained by an improvement in combustion quality as a result of the ethyl chain on this lactone, as indicated by the shorter duration of ignition delay (Figure 5.2). The ethyl chain, and the radicals that may be produced from this, may have helped to sustain higher combustion temperatures, offsetting the effect of butanol within the blends; the butanol diesel blend emitted the lowest NO_x levels (Figure 5.4), attributable to its poor combustion properties (Figure 5.1 and 5.2) and delayed time of peak heat release rate (Figure 5.6).

It consistently appeared that δ-hexanolactone possessed significantly unfavourable combustion characteristics compared to the other C6 lactones, with pHRR and peak in-cylinder temperature occurring later (Figure 5.6), despite a shorter ignition delay to that of εCL, and higher CO emissions produced (Figure 5.3). The lower NO_x emissions produced with this blend continue this trend of poor combustion. Injection timings were similar for all C6 lactones as a result of the similar ignition delay period, and the start of combustion commenced at 360 CAD in all cases. The physical properties shown in Table 5.1 do not appear to reflect major discrepancies in volatility and density, but important to note is that the blending of δ-hexanolactone was the poorest of all lactones, despite it seemingly representing a mid-point between ε-caprolactone (no side chain) and γ-caprolactone (ethyl chain), suggesting that competing molecular characteristics are at play. One hypothesis is that the structure of δ-hexanolactone, and or its subsequent decomposition products, is not conducive to combustion, potentially inhibiting initiation or propagation reactions. Six-membered ring structures are the most stable cyclic molecules,[145] and therefore, while the methyl group may allow for some release of radicals, it could be that this ring structure is the most difficult to open of the lactones tested, and the reactants produced from the methyl chain are not sufficient in breaking this ring early in the premixed combustion phase.

5.3.3. Particulate emissions
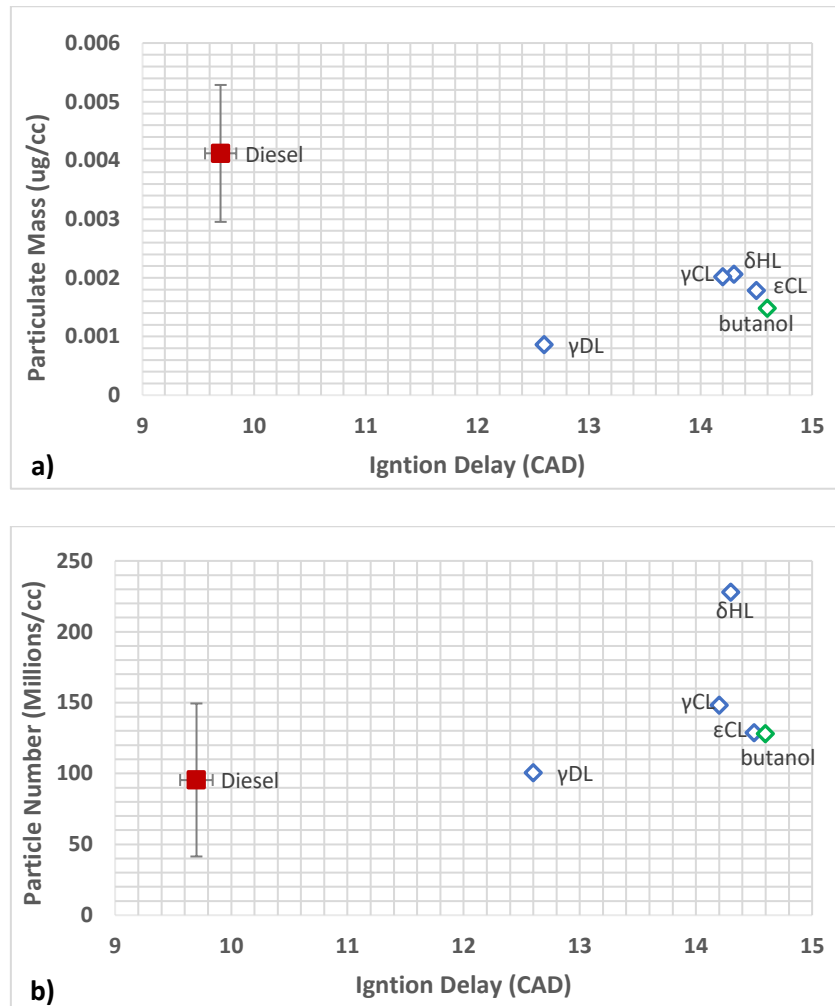
Figure 5.7*:Trend between particle mass (a) and particle number (b) with ignition delay of lactone and butanol blends and base diesel (start and end)*

Figure 5.7 indicates that the daily drift in particulate formation was noted to be a general decrease over the day. Potentially this occurred as a result of more consistent engine conditions after a period of running i.e. higher oil temperatures and a well lubricated injector, therefore conditions became more favourable for complete combustion. This drift is also reflected in the error bars in Figure 5.7, which encompass a significant range of results that includes the majority of the results of the blended fuels. Therefore, the following conclusions

are stressed as suggestive. Notwithstanding the range of error presented, it can be seen from Figure 5.7 that all of the lactone-butanol-blends emitted a significantly lower level of particulate mass relative to diesel only combustion, which is in line with the extended ignition delay that could allow for greater fuel-air mixing and a reduction in fuel-rich zones in which particulate formation is prevalent.

As noted in the previous chapter, the particulate mass and number output from the combustion of 'biofuels' contrast significantly with the emissions from purely fossil diesel combustion; the particulate mass generally decreases substantially, while the particle number increases as a result of the formation of more, smaller particles in the case of the blends. A significant contributor to the reduction in particle mass (other than the aforementioned extended ID) is likely the oxygen present in the lactones, which seemingly increased rates of oxidation of particulates post-formation, rendering particulates exhausted smaller. It is also likely that the phasing of soot formation is shifted slightly with the longer ignition delay period seen in these bio-derived molecules, not only decreasing particle mass but increasing number. The formation of particulates occurs later in the blends, therefore there is less time (and also a greater in-cylinder volume) in which the particles are able to form and grow.
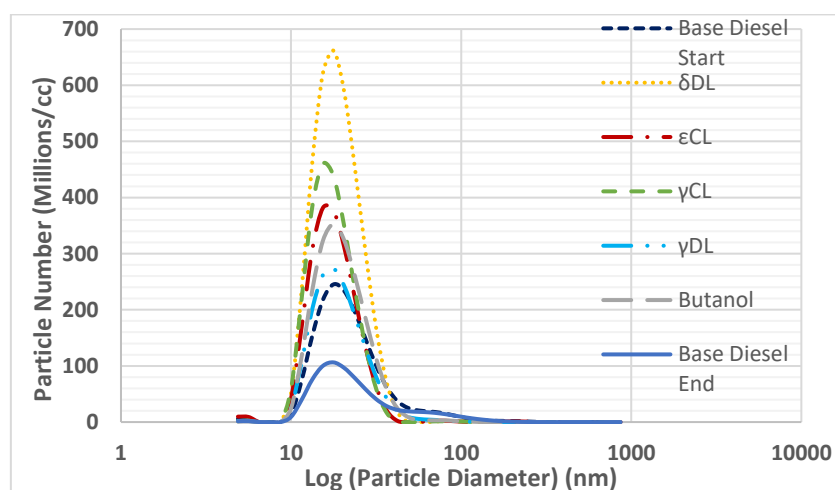
Figure 5.8: Particle size distribution of lactone and butanol blends and base diesel (start and end)

The reduced soot agglomeration and coagulation afforded by the retardation of combustion in the case of the blends can be seen from the particle size distribution plot in Figure 5.8. Also apparent is the significant increase in small particles of δHL in particular. Comparing the C6 lactones tested to the butanol:diesel blend, an increase in particle mass and number (although the particle number output of butanol and ε-caprolactone were very similar) was noted in the case of the lactones (despite an increase in oxygen content) which is counter to the view that the poor combustion quality of butanol (Figure 5.1) may lead to the formation of more incomplete combustion products (Figure 5.3). This may be due to the combustion of the butanol diesel blend being too unstable, with an excessive ignition delay, to the extent to which particulates are not formed in great amounts since local temperatures were not sufficient to produce pyrolysis products. Another potential explanation is that the structure of the lactones is more inclined to result in greater particulate formation, the higher carbon number providing greater availability of reactants for soot precursors. Alcohols, as has been discussed in Section 2.2.2.3, are one of the most effective oxygenated fuels in reducing particle formation, most likely due to the single carbon-oxygen bond that renders the oxygen more available to oxidise soot particles and reduce the particle mass.[83,372] The particle mass of all C6 lactones was similar, the main difference in particle emissions is in the case of δ-hexanolactone which produced the highest particle number. As with CO emissions (Figure 5.3), it is not clear why δHL has the greatest tendency to form incomplete combustion products compared to the other lactones, and the aforementioned stability of this 6-membered ring structure and the subsequent late release of energy could be the reason. Another theory put forward is that the chemical structure of this 6-membered ring lactone is slightly more likely to produce soot precursors. Until recently, soot particles were thought to consist predominantly of six-membered ring species (benzenoids),[404] but studies have realised the potential of five-membered rings (pentagonal) to be major factors in the morphology of soot particle, especially introducing 'curvature' into the carbon nanostructures and becoming prevalent in incipient soot

particles.[405,406] Given that the structure of δHL is that of five carbons within the cyclic ester moiety, and the addition of a methyl chain, it is tentatively suggested that the breakdown of this molecule has a higher tendency to form these five-membered rings that are effective in amalgamating PAHs. It is not unreasonable to expect that the carbons within the ring of δHL do not always separate if the ring structure is not broken until well into the expansion stroke. More certain is the shift in combustion with δHL (and butanol), which results in pHRR occurring later in the expansion stroke (Figure 5.1 and 5.6). Therefore, a likely cause of the higher particle number for a given mass is that the particles have less potential to agglomerate at these higher volume conditions, closer to the exhaust stroke. The difference between δHL and butanol in terms of particle number, however, is the strong oxidative capability of the alcohol, which reduces overall particle mass and number.

The reduced particle mass and slightly reduced particle number produced by γ-decalactone, compared to the other lactone blends, is a surprise given the significant increase in carbon number of this lactone. Likely, this is due to a combination of the higher combustion temperatures (Figure 5.5) that enhance the rate of soot oxidation, reducing particle mass. Furthermore, γDL's boiling point is significantly higher than in the other blends, potentially increasing lift-off length, which tends to see a reduction in particulate emissions as this increases the available oxygen entrained, thereby lowering the premixed equivalence ratio.[407] Moreover, when a tertiary fuel blend is combusted, and possesses vastly different boiling points, it can undergo a micro-explosion phenomena.[204] The more volatile component- butanol in this case- will vaporise within the bulk droplet and essentially 'explode', fractionating the main fuel droplet more effectively and reducing pyrolysis regions.

5.4. Pure lactone fuel results

From the lactone blend study it was apparent that a long alkyl chain attached to the ring of a lactone was highly effective in reducing the ignition delay period, the CO emissions, and both particle mass and number. Furthermore, the ability to blend the high carbon number molecules- with non-polar side chains- in higher ratios than the C6 lactones, and without butanol, is advantageous from both a combustion perspective (butanol is a poor compression ignition fuel) and in looking at the impact this fuel could have on reducing the reliance on fossil fuels. A 50:50 blending ratio would be achievable, however tests were subsequently conducted to assess the viability of the C10-C12 lactone fuels (Table 5.2) as pure components without the presence of diesel fuel. Not only would this enable the combustion performance of the individual fuels to be determined more accurately, but successful combustion would indicate the lack of need for conventional diesel molecules to be used in compression ignition engines in the future.

5.4.1. Combustion characteristics

Constant injection timing and constant ignition timing tests were possible in this set of experiments, due to the stable combustion traits that all test fuels displayed. In tests involving blends (Chapter 4 and Section 5.3), fuels varied considerably in their ignition quality, meaning that combustion was not stable with SOC at 360 CAD and/or consistent injection timings often resulted in late-stage combustion that made meaningful comparisons difficult to draw. At constant injection (CInj) conditions, are fuels experienced equivalent physical conditions during the ignition delay period while, for constant ignition (CIgn) combustion, all fuels were exposed to the same conditions at the start of combustion.
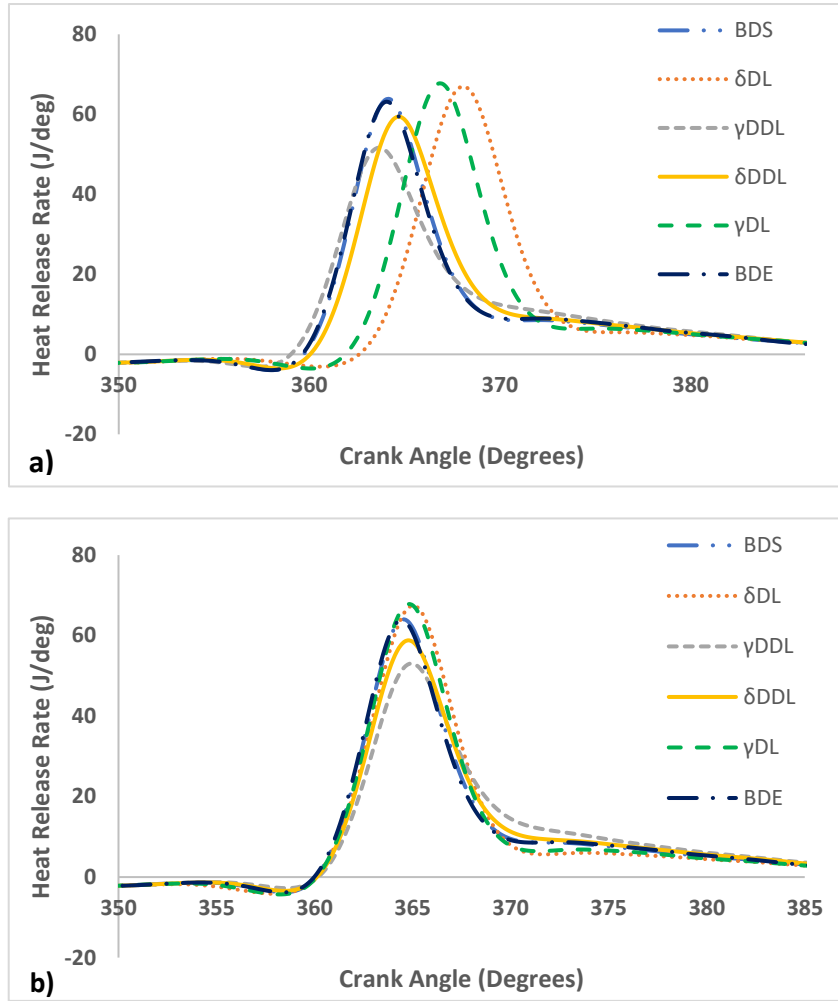
Figure 5.9: Apparent net heat release rates during combustion of lactone fuels and diesel fuel (start and end) at constant injection (a) and constant ignition (b) conditions at 4 bar IMEP, 1200 rpm and constant start of combustion at TDC

From Figure 5.9, comparing base diesel start and base diesel end it is apparent that the engine drift in terms of heat release was negligible. Figure 5.9 also shows that three out of the four pure lactones tested exhibited longer ignition delays than the base diesel. The exception being in γ-dodecalactone. The reduced premixing time of this C12 lactone can be seen to reduce pHRR compared to diesel. Its isomer, δ-dodecalactone, displayed a slightly longer delay time than diesel, though produced a slightly decreased pHRR, indicating that mixing was

less efficient for this fuel. Table 5.2 shows boiling points of the lactone fuels (γ-dodecalactone's b.p was not available at atmospheric conditions), indicating that δ-dodecalactone possess a boiling point over 300°C. This low volatility was potentially detrimental to fuel vaporisation,[395] resulting in reduced premixing of fuel and air and therefore lower pHRR, and more of the fuel being burnt in the diffusion-led combustion phase relative to diesel. The two C10 lactones, as pure fuels, resulted in marginally longer delay periods than diesel, and thus resulted in higher pHRR. The aforementioned low volatility of δ-dodecalactone was not as pertinent in these C10 molecules of lower atom number.

Comparing constant injection and constant ignition experiments, it can be seen that the γ-dodeclactone test registered a pHRR earlier than that of diesel when injection was constant, but marginally later when ignition timing was maintained; in both cases the magnitude was lower. With constant injection timing, the shorter delay period of this lactone naturally resulted in an earlier pHRR, as combustion has been advanced slightly. During constant ignition tests however, the lactone injection was retarded slightly to compensate for the rapid ignition, thus delaying pHRR relative to diesel (diesel injection timing was similar for both CInj and CIgn tests).

A similar analysis can be made when comparing δDL to γDL. The former possesses a longer delay period- 0.6-0.7 CAD longer- and so when injection timings are changed to normalise ignition timing, the phasing of δDL and γDL combustion converge, indicating little change in the actual combustion rates of the 2 lactones once ignition reactions have initiated. However, δDL has more time to mix with air, so the fact that the pHRR does not increase suggests there is more unreacted fuel, or incomplete combustion, from this fuel compared to γDL.
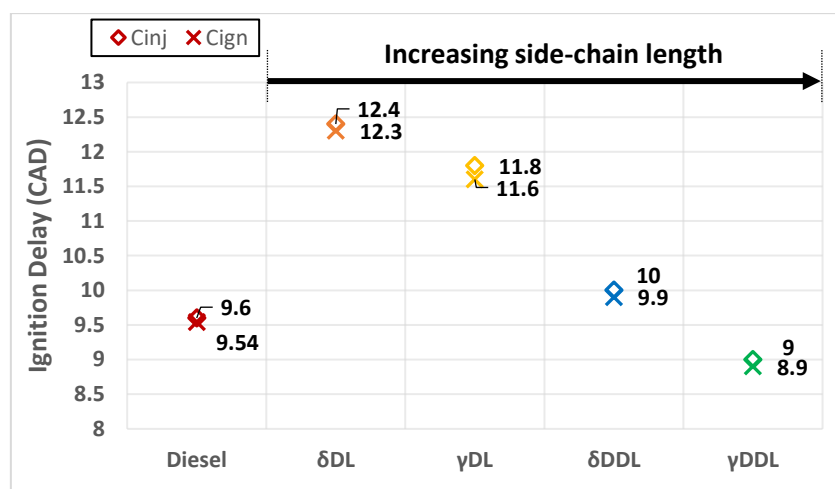
Figure 5.10: Duration of ignition delay of lactone fuels and base diesel (diesel results are calculated averages) at constant engine speed and IMEP and variable injection timing for constant start of combustion

The durations of ignition delay shown in Figure 5.10 enables some conclusions to be drawn from the use of a pure lactone fuel in a compression ignition engine. First of all, it is apparent that these lactones, despite possessing oxygen that tends to increase the delay period of a fuel molecule,[83,202] exhibit encouraging ignition properties relative to diesel. It was noted in Chapter 4 that, when utilising unsaturated furans in 50:50 blend ratios with diesel, the ignition delay was extended to over 16 CAD, causing combustion to become unstable due to initial energy release occurring at larger volumes where in-cylinder pressures and temperatures were relatively low; changes to the injection timing and duration were unable to improve combustion stability. Figure 5.9 indicates, however, that none of the pure lactones tested possessed delay periods long enough for combustion to become unstable. The shortest delay period was noted in the test of γ-dodecalactone, possessing a delay period of 9 CAD at constant injection timing, which was even lower than that of fossil diesel (Figure 5.10). It can be seen that the gamma-lactones have shorter ignition delays than the delta analogues, with γ-dodecalactone possessing a delay period of approximately 9 CAD, while δ-dodecalactone exhibiting a longer delay period of 10 CAD. Naturally, the 10 carbon lactones are slightly less

susceptible to ignition with a shorter chain lengths and overall atom number, but a delay period of between 11.8 and 12.4 for γ-decalactone and δ-decalactone respectively is still promising considering no fossil diesel was used. These results indicate the importance of the increasing chain length of the side chain in increasing ignition propensity and, likely, the resulting combustion quality; these are more of an influence on the delay period than the size of the ring, which likely breaks apart at a later phase after which enough radicals have been formed from the side chain for ignition to ensue.

5.4.2. Gaseous emissions
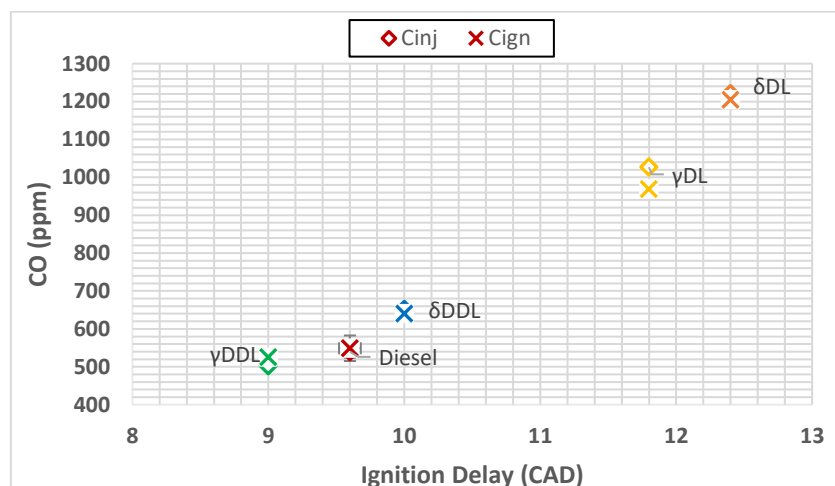
Figure 5.11: Relationship between carbon monoxide emissions and ignition delay of pure fuels at constant injection and constant ignition conditions

Figure 5.11 indicates that, for the pure lactones, CO emissions follow a trend of increasing ignition delay, in agreement with the tests outlined in Chapter 4. The same reasons are put forward in explanation; a greatly extended ignition delay potentially leads to combustion at lower temperatures from overdilution and heat release during the expansion stroke; also, an increased viscosity fuel (Table 5.2 indicates the high viscosity of the lactones tested as pure

fuels) leads to poor atomisation, thus larger fuel droplets, impeding fuel-air mixing which can result in incomplete combustion through a lack of oxygen available. Poor fuel vaporisation also increases the chance of droplets reaching the cylinder wall and becoming impinged on the cold surface, where complete combustion is unlikely.

At both constant injection and constant ignition timings, δ-decalactone emitted the highest levels of CO and exhibited the longest duration of ignition delay (Figure 5.11). γ-dodecalactone, with a delay period even shorter than that of diesel, displayed slightly lower CO emissions than the fossil fuel, implying that the reduced premixing time available in the case of the lactone did not result in excessive fuel-rich zones favouring CO formation. The inclusion of oxygen in this molecule has been shown as advantageous in reducing CO emissions[188] relative to diesel, with the occurrence of oxygen deficient zones reduced.

Constant injection and ignition tests yielded very similar results. For the fuels possessing longer delay periods than diesel, the constant injection tests produced slightly higher levels of CO, as combustion was retarded slightly (ignition began *after* 360 CAD), and potentially a reduced proportion of complete combustion occurred. In the case of γ-dodecalactone, constant ignition tests meant an injection timing slightly delayed compared to constant injection timing.
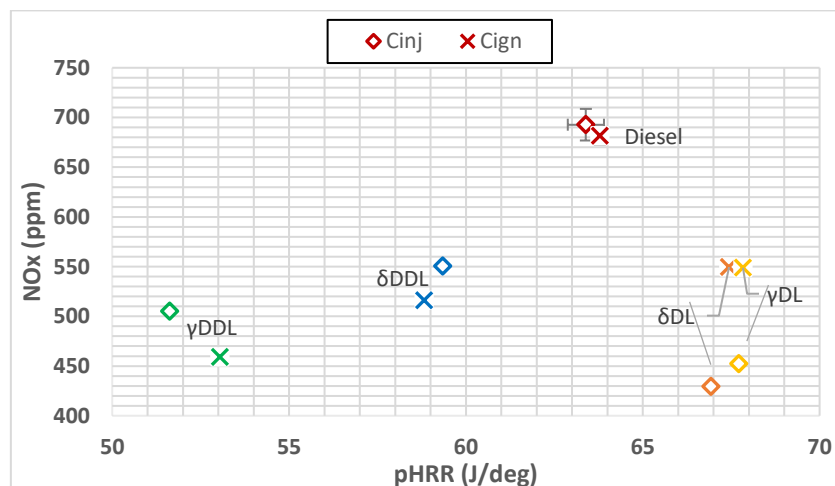
Figure 5.12: Exhaust gas nitrous oxide emissions and peak heat release rates for pure lactones and base diesel at constant injection and constant ignition conditions
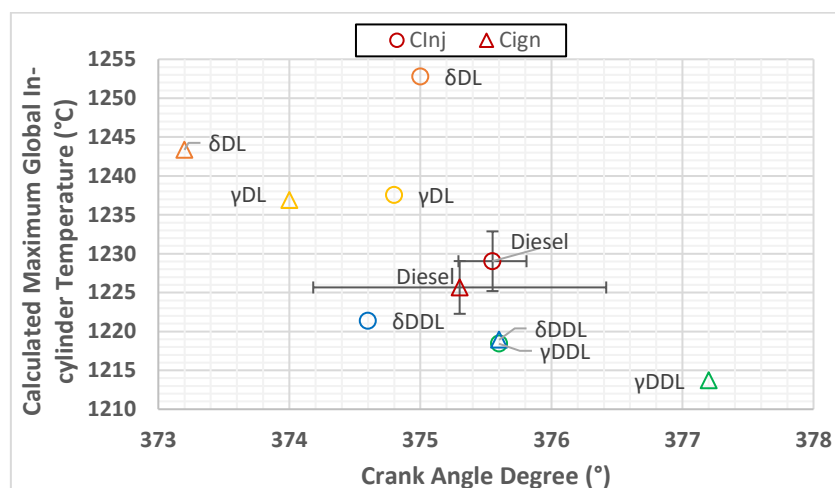
Figure 5.13: Magnitude and timing of calculated maximum global in-cylinder temperature of pure fuels and base diesel at constant injection and constant ignition conditions

Clear from Figure 5.12 is that the emissions of NO_x from the diesel tests are consistently higher than that of the lactones, despite the pHRR of lactone combustion being comparable, if not higher, than diesel (Figure 5.9); as discussed in the context of the lactone-butanol diesel blends (Figure 5.4) NO_x emissions tend to relate to the magnitude of pHRR and resulting temperature. Figure 5.13 illustrates that the maximum magnitude of in-cylinder temperatures for diesel lay in the middle of those determined for the lactones, though the error bars suggest a significant degree of uncertainty. Instead of looking at in-cylinder temperatures themselves, it may be more informative to look at the timing of pHRR and peak temperatures (Figure 5.14).

Figure 5.14 shows that for constant injection testing, the timing of pHRR is earliest in the case of diesel and γ-dodecalactone, which could explain why diesel produces the highest concentration of NO_x (Figure 5.12); potentially, temperatures sufficient for NO_x formation were sustained for longer before exhausting the contents of the cylinder, alluded to in Figure 5.14 by the long duration between pHRR and peak in-cylinder temperature. γ-dodecalactone did not emit as much NO_x as diesel combustion however, despite the timing of the lactone pHRR being earlier than that of diesel in the constant injection tests, resulting in an even longer

duration between pHRR and peak global temperature. This can be attributed to the lower magnitude of pHRR and peak temperature as a result of the shorter ignition delay period in the case of γ-dodecalactone.

The two C10 lactones went against the trend of increasing NO_x with pHRR (and maximum in-cylinder temperature). The combustion phasing again helps to explain this, with the shortest duration between pHRR and peak temperature seen during combustion of these two fuels (Figure 5.14). The CO emissions of the C10 lactones were also the highest of all fuels tested (Figure 5.11), suggesting a reduced combustion efficiency. From the HRR shown in Figure 5.9, it can be seen that almost all of the heat release during combustion of the C10 lactones occurs in the premixed phase, and it is possible that there is insufficient quantities of fuel left in diffusion-led combustion to sustain the high temperatures necessary for NO_x formation.
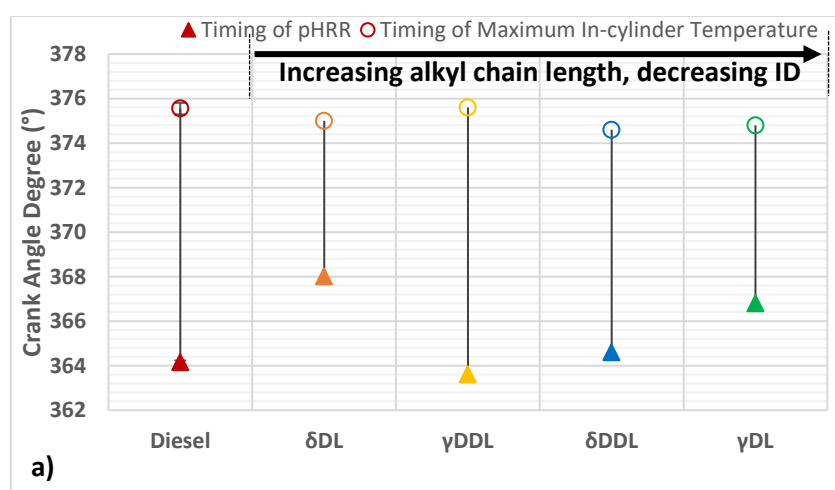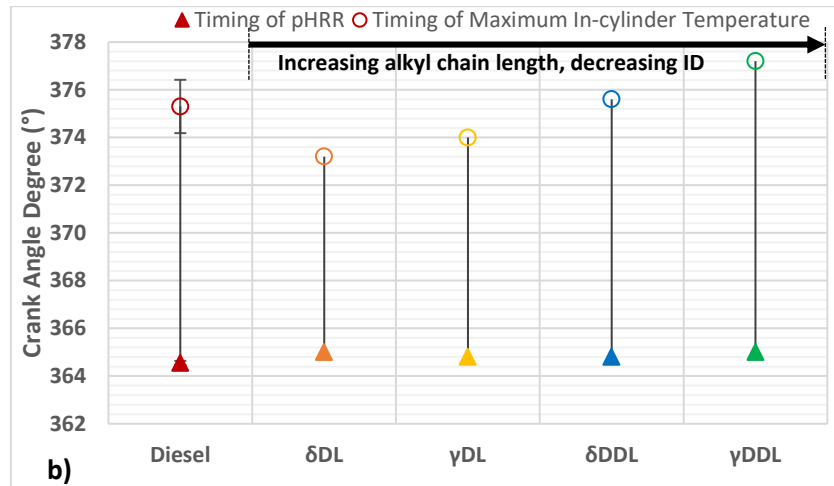
Figure 5.14: Comparison of timings of pHRR and peak in-cylinder temperature of pure fuels at constant injection (a) and constant ignition conditions

A final note to make is the contrast in NO_x emissions when comparing constant injection and constant ignition tests. Whether CInj or CIgn NO_x emissions are higher depends on the ignition delay of the respective fuels. Since the ignition delay of diesel was such that CInj and CIgn injection timings occurred at approximately the same time (Table 5.5; 9.6 CAD BTDC for CIgn, 10 CAD BTDC for CInj), there was little difference in NO_x emissions from diesel at these two timings. However, when the ignition delay was significantly lower than that of the reference diesel, as in γ-dodecalactone (Figure 5.10), constant ignition results saw far lower NO_x emissions (Figure 5.12), which is likely because ignition was forced to occur later. In the case of CInj, ignition occurred while the fuel-air mixture was still undergoing compression, and likely this release of energy during the compression stroke saw significant NO_x formation due to higher temperatures forming earlier and thus increasing time for the thermal NO_x formation mechanism to occur. In the case of the C10 lactones, constant injection tests resulted in lower NO_x exhaust concentrations (Figure 5.12). CInj tests saw ignition occur later than the CIgn experiments, into the expansion stroke, where lower pressures meant that the majority of energy was released at less favourable conditions for thermal NO_x to form. The fact that δ-

decalactone and γ-decalactone exhibited very similar levels of NO_x under constant ignition conditions, suggests that the difference in NO_x emissions between the two fuels is almost entirely due to the differences in the premixing phase, and that the two fuels' molecular breakdown is very similar once initiation reactions have begun.

5.4.3. Particulate emissions
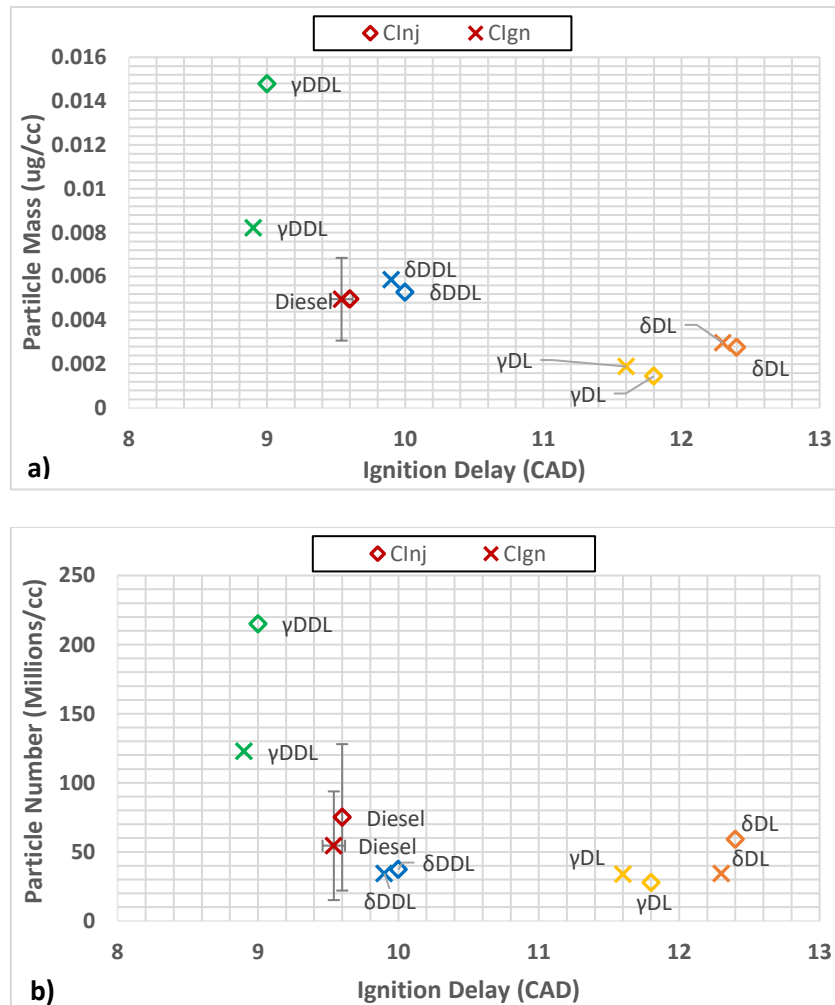
Figure 5.15: Relationship between particle mass (a) and particle number (b) and ignition delay of pure fuels at constant injection and constant ignition conditions

Important to note in Figure 5.15 is that the drift of the DMS instrument was significant, meaning conclusions as to the effect of the fuel itself are difficult to draw, noted by the major error bars.

Overall, both particle mass and particle number seemingly followed a general trend of decreasing ignition delay, likely caused by reduced mixing durations increasing inhomogeneities in the fuel-air mixture. Compared to previous investigations involving combustion of blends, these pure lactone fuels behaved more comparably to diesel and did not possess significantly prolonged ignition delays (and therefore phasing), meaning that the particle mass and number follow similar trends. This is in contract to the results from the previous chapter and in the studies of lactone blends, where the biofuels saw a significant reduction in soot emissions on a mass basis, but an increase in the particle number, suggesting smaller particles are formed from both an increase in oxidation, or because particles are formed later and thus see a reduction in accumulation mode particles from the shift in combustion phasing.

Notwithstanding the error bars shown, Figure 5.15a shows that the emissions of particulate mass are reduced in the case of γ-decalactone and δ-decalactone compared to diesel, but increased in the case of γ-dodecalactone. This was likely due to the short ignition delay. The longer ignition delay of the C10 lactones (Figure 5.11) is also likely responsible for the lower particle mass emitted relative to diesel, however the higher oxygen:carbon ratio compared to the C12 lactones and diesel probably decreases particle mass. Meanwhile particle numbers are comparable between the C10 lactones and diesel (and the error bars suggest comparisons of these relatively small differences in PN cannot be made).

Other than the reduced ignition delay resulting in less time for premixing of the fuel-air mixture, it is suggested that a potential reason for the observed higher particle mass of the C12 lactones (Figure 5.15a) is the length of the side chains present. It is not established how the lactones studied break down during combustion, but the particulate mass in this instance is in keeping with the number of carbons on the side chain of the molecule, increasing from γ-

decalactone (six carbons on the side chain) to δ-dodecalactone (seven carbons) to γ-dodecalactone (eight carbons). Diesel fuel consists of numerous species, including long chained alkanes, therefore it is not surprising that the PM emissions of the lactones and diesel fuels are comparable, especially if one of the first stages of the molecular break-down of a lactone involves separation of the side chain from the ring, or a ring opening reaction, which would provide ample potential for soot precursors to form from radical attack on these long-chained alkyl chains. Pyrolysis products have been shown to increase as the chain length of a molecule increases- even when keeping overall carbon numbers constant, likely as a result of the weaker bond dissociation bonds of a longer molecule.[408]

It is difficult to draw conclusions from the particle number given the extent of the drift from the start to the end of testing. Comparable emissions of particle number are not unexpected though, given that the ignition delay period of the lactones and the diesel fuel was similar, thus combustion phasing has not shifted to favour the formation of more smaller particles during oxygenated fuel combustion

Constant injection and ignition tests of the same fuels saw considerable variation of particle mass and number some cases (Figure 5.15a and 5.15b). Notwithstanding the evident variability in the measurement of particulates, and as highlighted in the discussion of NO_x emissions, constant injection testing of γ-dodecalactone saw combustion commence in the compression stroke. These lower volume conditions are likely to increase pyrolysis in inhomogeneous regions of the fuel-air mixture, relative to CIgn combustion. With a retarded injection timing (CIgn), combustion begins at TDC, meaning the cylinder volume is increasing as energy is released and this therefore reduces the likelihood of regions suitable for pyrolysis occurring.

The most notable feature from these results is that (unlike previous biofuel combustion results obtained in Chapter 4 and in the lactone blends) particulate emissions for long chained lactones are comparable to that of pure diesel. One of the main advantages put forward for biofuels is their reduction of this type of emissions that is well-documented to cause health

issues. In order to better understand how these lactones break down and form soot precursors, such as acetylene and aromatic rings, further investigations are required.

5.5. Conclusions

From the results outlined in Chapter 4, saturated cyclic esters- lactones- were predicted to yield positive combustion characteristics in a compression ignition engine. Therefore, low-carbon number lactones were tested in diesel:butanol blends to obtain their effectiveness as diesel fuel extenders. The following conclusions can be drawn from the findings obtained.

- The combustion of the three C6 lactone blends saw a significant increase in ignition delay, relative to fossil diesel, likely due to the low carbon number of the biocomponent, bringing the blend's ignition quality in line with that of an equivalent butanol blend.

- Levels of CO emitted by the C6 lactones were primarily influenced by the extended duration of ignition delay relative to reference diesel. All of the lactones emitted higher levels of CO than reference diesel, likely to be attributable to fuel over-dilution and impingement.

- NO_x emissions followed a general, expected, trend with pHRR, as higher pHRR generally correlates with higher, more sustained temperatures that are necessary for NO_x formation. The butanol blend produced the lowest levels of NO_x due to the poor combustion quality, and therefore low in-cylinder temperatures. γ-decalactone produced the highest pHRR, with a slightly longer ignition delay causing greater premixed combustion, but lower NO_x, than diesel. This was potentially caused by the later onset of pHRR and earlier timing of peak temperature, suggesting more fleeting high temperatures.

- Emissions of particulate mass were reduced relative to reference diesel for all of lactone blends, compared to diesel. γ-decalactone registered the lowest mass of all

blends, due to the presence of oxygen combined with the higher combustion quality allowing for higher temperatures and therefore enhanced soot oxidation.

- Ultimately, γ-decalactone, despite being blended with butanol, exhibited good combustion characteristics for a diesel fuel. Ignition delay was not increased to the extent that that high amounts of incomplete combustion products were formed, while the lactone oxygen content and higher peak heat release resulted in lower particle mass, and similar particle number, to diesel.

It was then shown, for the first time, the operation of a diesel engine, without modification, using 100% bio-derived lactone fuels. The C10 and C12 lactones tested here can be derived from first generation biomass and, more recently, investigations have outlined potential pathways to obtain the molecules from 2nd generation sources also. From the experimental results presented, the following conclusions can be drawn.

- Ultimately, all of the longer lactones showed promising ignition quality, equivalent to that of diesel, but the C12 lactones, in particular, appeared not to alleviate the emissions of particulates, relative to diesel, although instrumentation drift made conclusions difficult to draw.
- NO$_x$ emissions decreased for all lactones compared to diesel, which was explainable by either the magnitude or timing of peak HRR and peak global in-cylinder temperatures; no evidence of an impact of differing physical properties was apparent.
- C10 lactone combustion likely resulted in overdilution and fuel impingement, caused by a relatively long ignition delay, observed by an increase in CO emissions that indicated greater incomplete combustion.
- C10 lactones, due to their slightly lower ignition quality compared to the C12 lactones and diesel, resulted in a lower particle mass and similar number to diesel combustion emissions.

While these combustion experiments were insightful in understanding the effectiveness of a lactone fuel in a diesel engine, there remains limited understanding in the decomposition of these types of molecule, and the role of oxygen, in the formation of pollutant pyrolysis products. As a result, the purpose of the next chapter is to use GC and FID techniques to detect initial fuel breakdown and the products formed therein. Ultimately, it is hoped that lactones can be used as possible diesel fuel extenders, but the potential benefits i.e. reducing emissions of particulates, are not clear; particulate mass and number are similar for both pure lactones and fossil diesel, despite similar ignition delay. It is important therefore to investigate the molecular breakdown of lactones, with the aim of realising a viable lactone candidate that may be used in compression ignition engines.

6.   Decomposition of C10 fuels and formation of gaseous soot precursors in a tubular reactor, with proof of concept in a compression ignition engine

So far in this work, a range of potential biofuels have been tested in an engine to determine combustion characteristics and emissions, the results of which are presented in Chapters 4 and 5. The use of biofuels is advantageous in utilising a renewable energy source, but also because the presence of oxygen in the molecule generally sees a decrease in particulate emissions.[409] In the tests conducted in this project, the particle mass decreased, though particulate number tended to increase (Figure 4.14 and Figure 5.7). One hypothesis previously suggested was that the observed delayed combustion phasing (Figure 4.2, Figure 5.1 and Figure 5.9), with the use of biofuels, reduced the time available for particle coagulation and agglomeration. Moreover, the presence of oxygen in the fuel may enhance oxidation of soot particles, but this will generally only affect particle mass (Figure 4.14 and Figure 5.7) , whereas the particle number will likely remain constant, or decrease but to a lesser extent (Figure 5.15)

In addition to shifted combustion phasing, a potential cause of greater particle number for biofuels is that the molecular structure of the fuel itself is more prone to forming particles. It is important to understand whether this is the case as, if so, additional after-treatment steps may be needed should biofuels become more widespread in the future, before electrified vehicles dominate the fleet. A deeper understanding of the fuel's breakdown is therefore required, and this has led to the development of an empirical procedure for analysing molecular breakdown, the results of which are discussed in this chapter.

The use of a tubular reactor under pyrolysis conditions is beneficial as it can concentrate species that would be present in an engine, but likely at much lower levels. This is because, in an engine, the presence of oxygen limits pyrolysis to fuel rich zones within the fuel-air mixture, thus limiting the overall concentration in the cylinder gas of such species. As outlined in Section 2.3.5, the premixed region of the reaction zone will burn at approximately stoichiometric

conditions. Oxygen-deficient regions, as highlighted in Dec's model, are those in the fuel-rich side of the reaction zone, around the edge of the fuel jet region.[156] Using controlled pyrolysis conditions in a tube reactor allows for a more fundamental and controlled approach, whereby fuel can be injected into an oxygen free, high temperature zone, and sampled after selected reactor residence times.

Sampling gaseous emissions from an engine naturally introduces more variation in local reaction conditions than when sampling from a pyrolysis furnace, with local temperatures potentially higher, pressures of up to 60-70 bar even at relatively low loads, and oxygen being present in the charge gas. However, as already highlighted in Section 2.3.6.2, in-cylinder sampling has been performed since the 1970s, and numerous studies can be found on its use as a method of determining soot and NOx concentrations at varying engine timings.[338,339,343] As is the case in research performed by Kittelson *et al*,[345,346,350] the in-cylinder sampling technique performed here has the advantage of having little effect on the actual combustion, with extremely short sampling valve opening durations and tiny amounts of cylinder gas removal that would not adversely affect the results compared to normal engine operation. The semi-continuous nature of the sampling also means that gaseous sample gas mixing averages out cycle to cycle variation before the sample is analysed. Previous work by the UCL research group[369,374,410] has made use of the same principle and technique (outlined in Section 3.5). The work by Ogbunuzor found similar conclusions to those of previous in-cylinder sampling studies in relation to the formation of soot over the combustion cycle, validating the method. Also highlighted in that work was the dominance of gaseous soot PAH species relative to soot-bound PAH species, especially at earlier phases of combustion, in the premixed region. However, not performed in this work was the sampling of the gaseous precursors outlined in Section 2.3.5. The relative abundance of these species could help in explaining the fluctuating relationship found between engine phasing and soot/PAH concentration, as relative rates of
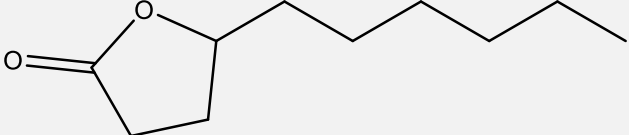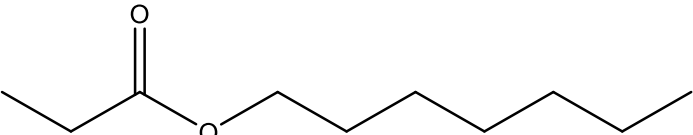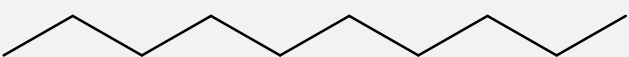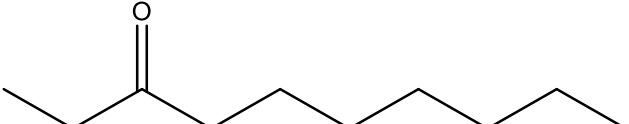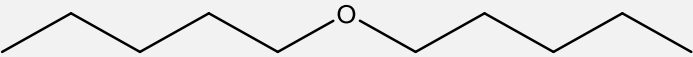
reaction between precursor formation and consumption (and soot formation and oxidation) vary as in-cylinder conditions change.

The in-cylinder sampling results herein provide a proof of concept onto the technique of sampling gaseous soot precursors from a diesel engine; difficulties associated with implementing the in-cylinder sampling technique and the complexity of taking samples and developing a suitable GC-FID method meant that findings from the engine itself are stressed as preliminary. Particular focus will be given to the effect of using an oxygenated fuel- heptanone- and a model diesel fuel surrogate- heptane. The results from the furnace will be discussed as well to note major changes observed between engine and furnace derived species. In future work, it is hoped that the novel biofuels discussed up to this point - chiefly lactone fuels - could be used in the engine with in-cylinder sampling, with the results then combined with those from the pyrolytic reactor in order to enhance our understanding into the effect of these fuels on soot formation and eventual emissions.

6.1. Introduction to tested molecules

Given that the reactor studies provide a more fundamental study than the engine experiments outlined in Chapters 4 and 5, the focus of the reactor study was on one lactone. Additional molecules were included in the experimental study with their structure associated with that of lactone but altered systematically so that certain lactone molecular functionality was altered or removed. The aim was to determine what- if any- modifications to the lactone molecule could reduce the amount of soot precursors released from the breakdown of this biofuel. Table 6.1 indicates the tested molecules.

Table 6.1: Tested C10 molecules

Molecule (abbr)	Structure	*Functionality*
γ-decalactone (GDL)		*Lactone-Cyclic Ester*
n-heptylproionoate (n-HP)		*(Straight-chain) Ester*
Decane		*Base Hydrocarbon*
Decanone		*Ketone*
Di-n-amyl ether		*Ether*

In addition to the lactone envisioned as a potential replacement for diesel fuel (based on its comparative ignition delay period (Figure 5.10) and heat release profile (Figure 5.9), as well as a reduction in particle mass (Figure 5.15) relative to diesel) a straight chain version, n-heptylpropionate (n-HP), was also tested. This molecule was utilised in an effort to understand the method of breakdown of the lactone molecule. If the pattern of precursor formation was very similar for both, but with the straight chain version forming these species at slightly lower temperature conditions, it provides evidence that the biofuel molecule firstly opens up into a straight chain intermediate under pyrolysis conditions. The other molecules in Table 6.1 (decane, decanone and di-n-amyl ether) were selected in order to test various oxygenated functionalities and the potential effect of these on the formation of the precursors. It was also envisaged that the pattern in which the various fuel molecules break down as the temperature

increases would also be revealed. It was also aimed to characterise the potential of these functional groups to oxidise intermediate species, before these were able to react further and form the first aromatic ring.

As highlighted in Section 2.3.6.1, the exact mechanism of benzene and subsequent PAH growth into soot particles is not fully understood- even in the context of a relatively simple ethylene flame combusting under controlled conditions. In the context of an engine or with more complex fuels, the knowledge is even more sparse. However, the literature reflects a focus on a few C2-C4 species and radicals responsible for benzene formation (though it should be noted that, potentially, benzene may not always be the first aromatic ring formed, and formation of phenylacetylene or naphthalene could overlay benzene production).[304] However, benzene's stability and volatility make it a good indicator of a fuel's propensity to form soot, and the extensive research already completed to determine its formation from known precursors make it the most interesting species on which to focus attention onto, by comparing its relative abundance to those of lighter species, such as acetylene and vinylacetylene. Sampling radical species is extremely complex given their instability. Valencia and Ruiz differentiate between ordinary flame radicals (OSRs), such as methyl and ethyl radicals, and resonantly stabilised radicals (RSRs), which are stabilized by delocalised unpaired electrons and include species such as propagyl and allyl radicals.[411] However, even with greater stability, the lifetime of all radicals is fleeting and thus, unless measurements are able to be taken in real time, are not detectable. As a result, in the experiments presented in this chapter, it was decided that focus would be given to the stable species associated with these radicals. In addition to methane, C2 species, namely acetylene, ethylene and ethane were detected; acetylene is naturally of particular interest due to the aforementioned research into this species and its role in the formation of the first ring and in PAH growth. C3 species, specifically propene and propyne, were also investigated, as well as butadiene, vinylacetylene (C4s) and benzene. Cyclopentadiene- corresponding to the PAH-forming cyclopentadienyl radical- is discussed, however, the retention time of this species was unknown since its instability meant that its

inclusion in the external standard was not possible. Two oxygenated intermediates-acetaldehyde and ethanol- were included in these investigations, not because of their relevance to soot formation, but because it was envisaged that their presence may help understand the breakdown of oxygenated molecules and potentially their release in the engine exhaust, in addition to the more abundant CO and CO_2 oxygenated products/intermediates. The influence of an oxygenated fuel on these types of emissions, when the air-derived oxygen is removed, is unclear.

6.2. Experimental procedure

6.2.1. Furnace temperature

Initial testing on the tubular furnace, using the experimental setup outlined in Section 3.6, was aimed at determining conditions suitable for initial fuel decomposition by pyrolysis, so as to capture the very first species formed. Given that the primary fuel of interest was γ-decalactone, this fuel was initially tested at a furnace set-point temperature of 650°C-corresponding to an actual local reactor temperature of 568°C at the sampling point- with the aim of detecting gaseous precursors. However, from the chromatogram shown in Figure 6.1 below, it can be seen that species were not formed in sufficient amounts for accurate determination of concentrations; the only significant peak observed was that of the internal standard at 9.8 minutes (equating to 100ppm). At a higher temperature of 800°C, a greater abundance of species was detected, and therefore this furnace temperature-corresponding to a reactor actual temperature of 678°C, was used as the lowest set-point temperature for the remaining fuels. In order to evaluate how pyrolysis might proceed as furnace temperatures were increased, two further furnace temperatures- increasing in 100°C increments- were also used. 900°C furnace temperature corresponded to a reactor temperature of 775°C, while 1000°C equated to a real reaction temperature of 879°C.
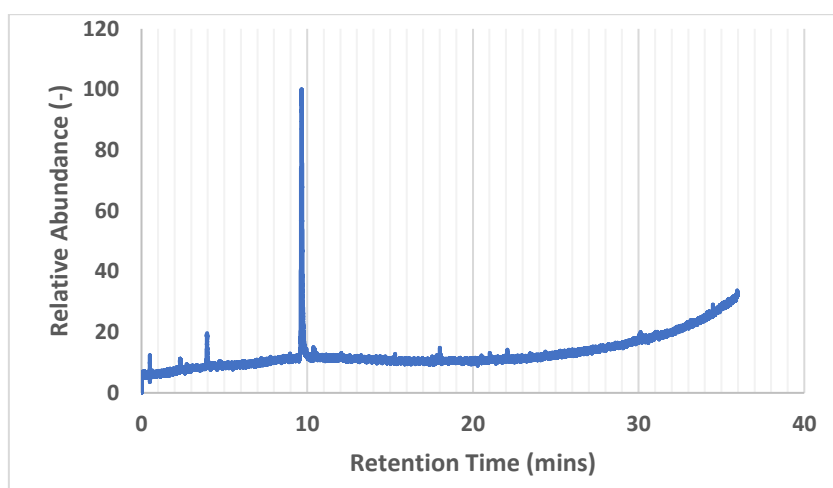
Figure 6.1: Chromatogram of FID response to sample collected during γDL pyrolysis at 650°C furnace temperature (568°C reactor temperature)

6.2.2. Fuel-feed capillary temperature

A further temperature consideration was that of the capillary used to deliver the fuel into the nitrogen flow. With the baseline fuel- n-heptane- the 98°C boiling point was considered low enough such that the nitrogen stream, heated to 400°C, would effectively vaporise the fuel. However, with the highest boiling point fuel- γ-decalactone, boiling point 281°C- it was necessary to consider whether the fuel would fully vaporise. Initially, the capillary was heated to 190°C, about 90°C below the boiling point of γ--decalactone, but the resulting chromatogram- indicated in Figure 6.2a below- suggested that there was a potential issue with the injection system, as the species concentrations were sensitive to capillary temperature. It was observed that when the capillary was heated to 220°C, to be approximately 60°C below the boiling point, the resulting chromatograph (Figure 6.2b) indicated effective vaporisation of the fuel. Therefore, for the remaining C10 fuels, injection temperatures were set approximately 60°C below the respective boiling points on the molecules. Table 6.2 summarises the capillary heating for each fuel.
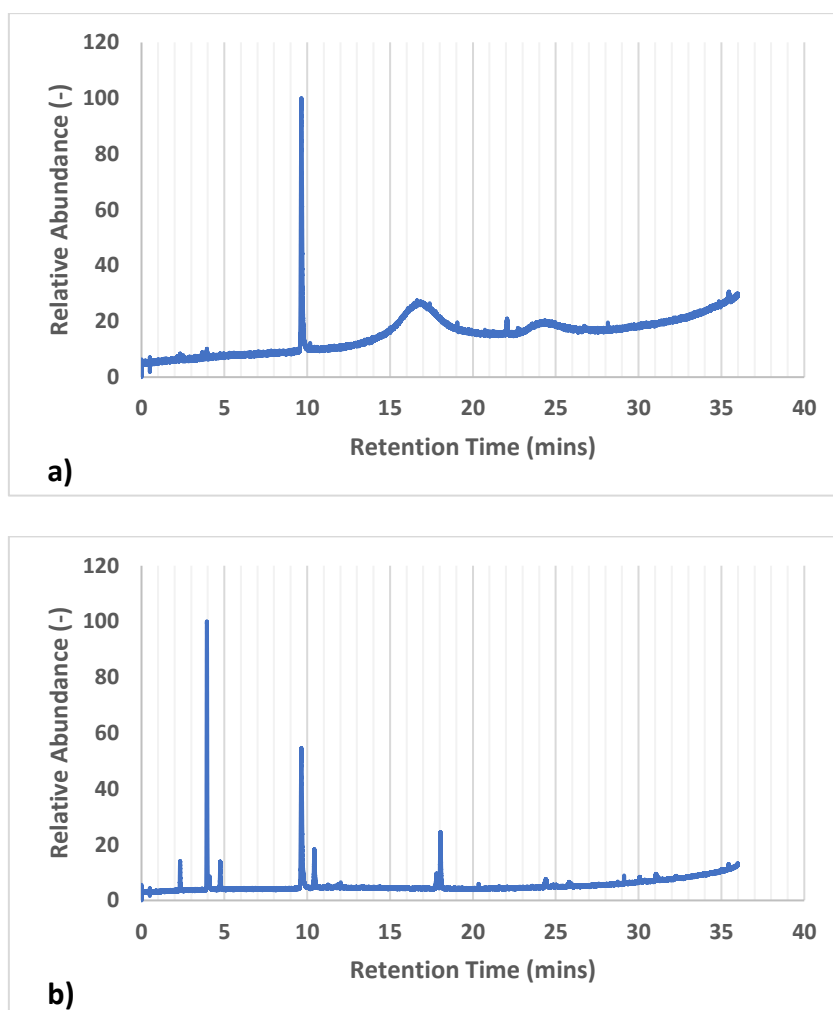
Figure 6.2: Comparison of γDL pyrolysis sample analysis (678°C reaction temperature) when using 190°C (a) and 220°C (b) capillary heating

Table 6.2: Summary of tested molecules' boiling points and corresponding capillary heating values

Molecule	Boiling Point (°C)	Capillary Heating (°C)
Heptane	98	Room temperature ~ 25
Decane	174	114
γ-decalactone	281	221
n-heptylpropionoate	210	150
3-Decanone	203	143
Di-n-amyl ether	188	128

Another parameter to consider was the residence time in the furnace. It had been noted in previous experiments[373] that shorter residence times saw greater range in the concentration of detected species. Initially, a relatively short residence time was employed, so as to observe a greater range in species, as more intermediates with lower stability would likely be sampled from the furnace. A greater range of species would provide a better indication as to the fuel molecular breakdown, as less time would be available for reactions to be completed. However, it was noted that, even with a fairly short residence time, species concentrations were too variable to give meaningful results. As a result, the residence time was increased to 1494/T and the results here proved more stable, but also resulted in a wide range of products providing insight into the species formed during the fuel pyrolysis.

6.2.3. Fuel flow rate

The injection of fuel was set at a flow rate to maintain consistent injection of carbon into the reactor. A set rate of 5000ppm of carbon was selected, which, given the difference in density and carbon number of the various molecules selected, meant different fuel flow rates

were required for each fuel. Table 6.3 below summarises the flow rates of each of the fuels tested.

Table 6.3: Fuel flow rates injected into nitrogen flow at reactor inlet

Molecule	Fuel Flow Rate (ml/min)
Heptane	0.0875
Decane	0.0815
γ-decalactone	0.0751
n-heptylpropionoate	0.0824
3-Decanone	0.0791
Di-n-amyl ether	0.0848

6.2.4. Heptane baseline tests

With the furnace residence time, furnace temperature and capillary temperatures set, heptane was run both at the start and end of this campaign of tests (lasting a period of approximately 4 weeks) at the three furnace temperature conditions (start and end tests were repeated to give 3 result for each temperature). This was done in order to provide a set of baseline results which could subsequently be used to detect any obvious changes in furnace operation. As results with heptane were also available from the engine, a comparison of the furnace and engine results is provided in the Section 6.4.3.
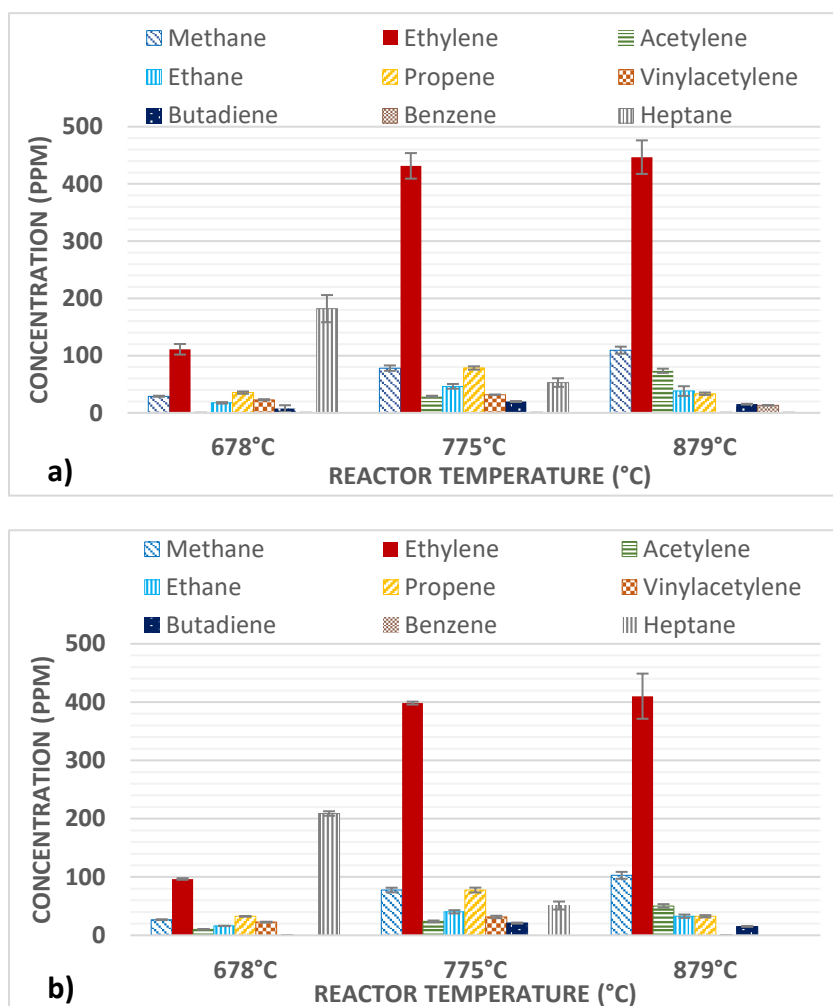
Figure 6.3: Comparison of heptane start (a) and end (b) soot precursor concentrations obtained under varying temperature pyrolysis conditions

Figure 6.3 indicates the results obtained from heptane pyrolysis at the beginning of the overall testing period, and at the end. Overall, the results suggested good repeatability in the detected species concentrations, with the majority of species concentrations in the final heptane test being within the margin of error (calculated from the standard deviation of 3 test points at the same condition) of the initial heptane tests. One of the most variable species concentrations was n-heptane, the fuel itself, particularly at 678°C during the start test. This could be attributed to the testing procedure becoming more consistent over time, but overall it

is not unexpected that the fuel (given that at this condition it remains at relatively high concentrations) was observed to fluctuate. Small differences in pyrolysis product concentrations likely stemmed from larger variations in the fuel concentration from which the lighter species were formed; it was the aim to measure intermediate stable species concentrations while the fuel molecule was still undergoing pyrolysis. Variations in the flow rate of cooling air used to freeze the reaction and minor irregularities in sampling were likely to have been reflected most apparently in variations in the fuel concentration, given that this molecule continued to decrease as time or temperature increased. As can be seen from the result in Section 3.6.5, the furnace temperature itself varied (standard deviations of +/- 8-25°C were noted, depending on furnace temperature), which could also account for some of the variation in fuel concentration. The resultant species concentrations were more consistent, especially those formed at lower concentrations, which were likely to have been formed from terminating reactions and therefore, once they formed, they remained relatively stable and not susceptible to further reactions.

As with the absolute concentrations, the pattern of molecular breakdown- from the start to the end of testing- was also consistent in heptane, indicating no leaks in the system that could allow oxygen into the reactor and alter reaction pathways. One discernible variation, however, was the decrease in acetylene concentration at 879°C during the end test (Figure 6.3b) compared to the starting test (Figure 3.6a). Perhaps a clue in explaining the discrepancy was the existence of another variation at this test condition; the presence of benzene. One could predict that, in the start test, the presence of benzene and higher concentrations of acetylene suggests that pyrolysis conditions were more favourable, and therefore the reactions leading to benzene were more prevalent. An alternative theory is that the higher concentrations of ethylene and acetylene in the initial test, coupled with the presence of benzene, implies that these species have reacted with each other species to a greater extent in the end test. Potentially, benzene could have been formed in quite low concentrations during heptane pyrolysis and was quick to react with C2 molecules, particularly acetylene, and grow to larger

molecules that could not be detected using this GC column. The HACA mechanism- chiefly involving the reaction of phenyl radicals and acetylene- is known as a dominant reaction pathway in the formation of PAHs and soot,[302] therefore it could be expected that a concurrent decrease in the concentrations of benzene and acetylene are observed at high temperatures. Smith[286] notes that a major benzene pyrolysis product is acetylene; the higher concentration of acetylene and the presence of benzene in the heptane start test, compared to the end tests, suggests that consumption of benzene was not due to its own pyrolysis (into acetylene), and more likely to have been a result of ring growth. Overall, the decrease in ethylene, acetylene and benzene observed from the end test may have been due to interconnected reactions between these molecules (or radical analogues of these i.e. ethyl and phenyl radicals).

Ultimately, the similarities between the two tests gives provides confidence that changes in results generated using different fuels were relatively small and unlikely to have been caused by changes in the operating conditions of the furnace or sampling probe. For subsequent analysis of heptane pyrolysis, more focus will be given to the start test sample, given that end results are more likely to have been impacted by constant use of the equipment e.g. a column with a degree of sample saturation.

One of the immediately apparent features of these results is the decrease in heptane as temperature increases. An initial heptane concentration of 5000ppm was injected into the furnace, and the resulting output of approximately 200ppm (4%) suggests that the majority of fuel had already broken down as is to be reflected in the detection of gaseous species, or has combined to form PAHs and potentially soot. Naturally, the sum of concentrations of the gaseous species highlighted here- also considering their lower carbon number- does not account for the remaining 96% of carbon atoms initially injected, therefore growth into larger species is clearly a factor, though outside the scope of this investigation. By far the most abundant species detected was ethylene. Likely, this was derived from ethyl radicals that are particularly prevalent in hydrocarbon pyrolysis[297] and were key in the formation of the first aromatic ring.[299] It is postulated that the reaction to ethylene from either ethyl or recombined

methyl radicals is relatively fast, but subsequent reactions from ethylene are much slower. Leigh[412] notes the rapid formation of ethylene from ethyl radicals in the pyrolysis of propylbenzene, while Pant and Kuzru's study[413] into heptane pyrolysis confirmed ethylene as the main product, formed from ethane by dehydrogenation from hydrogen free radicals as well as butyl radical unimolecular decomposition.

Methyl and ethyl radicals may have been particularly abundant as the sample was taken during the early stages of pyrolysis, forming stable ethylene, ethane and acetylene through methane radical recombination (MMR), and methane itself when recombining with hydrogen radicals.[414] Davidson *et al's*[415] study into heptane and iso-octane pyrolysis in shock tubes noted a rapid rate of conversion of the fuel to methyl radicals, accounting for 14% of the carbon in n-heptane during decomposition at temperatures of 1100-1600K. Aribike observed that the main products of heptane pyrolysis were methane, ethylene, propene, 1,3-butadiene and butene, with secondary products including ethane, propane and benzene.[416]

At 678°C, it is clear that temperatures were not sufficiently high for a great number of gaseous precursors to form and accumulate; a significant proportion of those that were formed had likely already been consumed to form PAHs and soot at the point of sampling. At higher temperatures however, with further fuel molecular breakdown and thus a greater radical pool, the gaseous precursors were more likely to be expressed as intermediate species. Pertinent to this discussion, though, is that the difference in stable species concentrations between 678°C and 775°C was far more apparent than that between 775°C and 879°C, and could suggest the overcoming of certain thermodynamic barriers that initially restrict the formation of less saturated species; Shukla[299] noted that acetylene is only formed in hydrocarbon pyrolysis at high temperatures. Once acetylene is formed, it is postulated that a greater number of higher order hydrocarbons are attainable in the reactor, likely due to this species' involvement in addition reaction with radical species to form C4 species and PAHs.[14,288,299,304] Given that acetylene is prone to these addition reactions, its presence suggests a build-up in which its formation begins to offset its consumption in reactions with other hydrocarbons, such as C4

species, and subsequent cyclisation into benzene. This reaction with C4 species could explain why this increase in acetylene coincides with a decrease in 1,3-butadiene at higher temperatures. However, Glassman notes that 1,3-butadiene can also be formed from acetylene.[288] It is postulated that the increase in acetylene from 678°C to 775°C contributes to the increase in 1,3-butadiene concentrations but, at higher temperatures, with an abundance of both acetylene and 1,3-butadiene, the addition reaction between the two molecules (or their radical derivatives) is favourable, forming aromatic species. The relative lack of 1,3-butadiene at higher temperatures would mean a lack of available species in which the acetylene could have combined and formed aromatics, causing further accumulation of acetylene as temperatures increased.

Figure 6.3 illustrates that concentrations of ethane, propene, vinylacetylene and 1,3-butadiene all follow the same pattern, that is to say that concentrations initially increase from 678°C to 775°C, but then decrease again at 879°C. Most prevalent of these species is propene, which is not unsurprising, given the explanations provided by Wang that highlight the importance of C3 propargyl species on the formation of benzene production, and therefore soot formation.[304] Propargyl coupling is seemingly one of the most common reactions for benzene formation.[14,299,301,303] Aribike concurs with these trends, noting an increase in methane and ethylene as heptane is converted, while propene passed through a peak in concentration.[416] The abundance of this precursor would substantiate the hypothesis that it is involved significantly in the formation of pyrolysis products, and the same can be said for vinylacetylene. Unlike propene however, vinylacetylene disappears completely at 879°C, from approximately 30ppm at 775°C, and the subsequent formation of small amounts of benzene could imply that this is one of the main products of vinylacetylene consumption. The fact that this species disappears completely though signifies that its contribution to aromatics is only present at lower temperatures and, at higher temperatures, the formation of vinylacetylene is less favourable than other reactions, such as the formation of acetylene or PAH growth. Butadiene is only ever formed in very low concentrations and, other than benzene, was the

least abundant species measured. This suggests that the formation and consumption rate of butadiene and benzene are likely very similar, and only at specific temperatures (between 678°C and 775°C) does formation outweigh consumption. Aribike's observations differed slightly in the case of butadiene, where a gradual increase in conversion was observed with increasing temperature, though their experiments did not reach the maximum temperatures used here.[416] Butadienyl radicals are highly important in forming the first ring via the reaction of acetylene, while the reaction between butadiene and vinyl radicals, followed by hydrogen elimination, has been proposed as a major pathway in the formation of benzene.[311] The study by Westbrook and Pitz on the influence of oxygenated hydrocarbons on soot formation found that butadiene represented a significant species in the fuel rich environment, but that the concentrations were appreciably lower than ethylene, acetylene, propyne, and propene.[189]

The low production of ethane, especially compared to ethylene, is somewhat surprising given the greater reactivity of ethylene, but again can potentially be explained by relative reaction rates. While ethylene may be consumed at a faster rate than ethane, the formation of ethylene is much higher, something that is likely attributable to the high competition for hydrogen radicals that mean fully saturated species are not formed in great quantity. Ethane is actually the only fully saturated species detected in these tests (methane is fully saturated but 'unsaturated' methane is a radical species, and therefore highly likely to recombine with other species to form C2 species, such as ethylene), and is unique in this respect, probably because of its low carbon number reducing the reactions required for its formation. The rapid consumption of ethane is possible at higher temperatures though, hence the decrease in concentration at 879°C- at these temperatures, even a relatively stable C2 saturate is susceptible to radical attack. Chakraborty and Kunzru's investigations into high pressure heptane pyrolysis yielded different trends in ethylene and ethane production, suspected to be due to the lower temperature and higher pressure environments favouring formation of ethane by bimolecular reaction between ethyl and hydrogen radicals over the formation of ethylene from dissociation of ethyl radicals.[417]

A feature of the chromatograms obtained during heptane pyrolysis is the lack of higher hydrocarbons formed as a direct result of molecular decomposition i.e. no pentane or hexane was detected from the removal of one or two carbon atoms from heptane. Chakraboty[417] noted that pentene and hexene were formed in appreciable amounts in high pressure heptane pyrolysis, though Aribike, while detecting 1-pentene, noted it as a secondary product compared to the lighter hydrocarbons species.[416] It is possible that the conditions utilised here were not applicable to detection of these species in significant amounts. The absolute temperature naturally impacts the rate of fuel breakdown, but the presence of heptane shows that reaction of the fuel is still ongoing, and therefore the lack of C6 or C5 'fragments' suggests that the residence time may have been too long to detect intermediate species between the fuel and stable gaseous precursors; essentially, once the heptane molecule has begun to decompose, this decomposition, forming C1-C2 radicals, is rapid. A further tentative suggestion is that any resulting C6 and C5 species will possess an extremely reactive group[418] and may recombine on other large fragments, or indeed undergo cyclization to form cyclic and/or aromatic molecules that could not be detected on the column. Cyclopentadiene is a known precursor to aromatic rings, with potential to form benzene from its reaction with ethylene and subsequent hydrogen and methyl removal, or naphthalene via the reaction of two cyclopentadienyl radicals (formed from unimolecular dissociation of cyclopentadiene). However, its apparent lack of potency in the chromatograms here suggests its reactions towards higher order aromatics significantly outweigh its formation from allyl radicals and acetylene.[14] Furthermore, Kim *et al*[419] highlight cyclopentadiene's high reactivity and ability of self-recombination as reasons for its importance in the formation of larger PAHs (which cannot be explained by the HACA mechanism alone) and this reactivity may limit the accumulation of this (and other C5) species.

Overall, it is suggested that once that activation energy required to initially breakdown a heptane molecule is overcome, subsequent reactions to the precursors are extremely fast. Even at the low residence times attainable here, these species are potentially too short-lived to be detected- higher carbon number aliphatic molecules are more reactive than their lighter

analogues- and once hydrogen abstraction has commenced, the radicals that are formed combine quickly, and methane and ethylene appear as the main initial products.

6.2.5. In-cylinder sampling

Section 3.5 highlights the general procedure for collecting in-cylinder samples of gaseous emissions, while Section 3.7 explains the principle behind gas chromatography, coupled with flame ionisation to produce the chromatograms used to analyse species abundance. The following section describes the engine conditions used for collection of gaseous samples, the chromatograms analysing the composition of which are supplied in Section 6.4. It is important to note here that the Section 6.4 is intended to demonstrate proof-of-concept, in that this sampling mechanism can be used to detect gaseous species abundance. Future work is therefore envisioned to continue this application with a wider variety of fuels, engine conditions, and sampling times.

6.2.5.1. Engine operation

Two C7 fuels were combusted within the research engine outlined in Section 3.1. Heptane (anhydrous, 99%) and 2-Heptanone (99%) were purchased from Merck, and the low volume fuel system (Section 3.2.2) was employed for the high pressure injection of these fuels.

The engine conditions and sampling valve timings, corresponding with the chromatograms shown in Section 6.4.3, are outlined in Table 6.4.

Table 6.4: Engine operating conditions used during in-cylinder sampling collection during heptane and heptanone combustion

Engine Condition	Steady State Value
Engine Load	5 bar IMEP
Engine Speed	1200 rpm
Fuel Injection Pressure	550 bar
Fuel Ignition Timing	360 CAD (TDC)
Sampling Timings	- 370 CAD (10 CAD ATDC) - 420 CAD (60 CAD ATDC)

In the results outlined in Section 6.4, constant engine load and ignition timings were employed (by varying injection durations and timings respectively), as this meant that conditions within the cylinder between heptane and heptanone were comparable, and any differences in soot precursor output should be predominantly due to the molecular structure. However, it is recommended that constant injection duration and timing conditions should also be employed in future (i.e, varying engine load and SOC). The reason being that while the temperature of the in-cylinder contents would vary, approximately the same volume of fuel would be injected, making soot precursor abundance potentially more comparable across different fuels.

6.2.5.2. Sampling extraction

As already outlined in Section 3.5, gas-tight syringes were used to collect samples using a septum placed inside the control room. The sampling valve was first run for 1 minute to purge the heated line leading to the septum and to ensure the sample collected was representative of the contents of the engine cylinder at the sampling timing desired. Important to note is that

the voltage supplied to the sampling valve was for each test varied to ensure sufficient opening duration and valve flow gap. The voltage varied depending on the sampling time desired (e.g. higher pressure in-cylinder conditions necessitated greater voltages) but also the condition of the sampling valve (warmer conditions helped increase valve poppet movement, although it was also observed that this could sometimes lead to sluggish operation, likely as a result of O-ring expansion). As a result, exact voltages and voltage signal timings are not reported; the values were constantly varied to maintain the opening timings desired.

The manual ball valve placed downstream of the septum was gradually closed until the syringe plunger started to move due to sample line pressure, a sample of approximately 20cm^3 was collected and the syringe sealed and removed. After relieving a small volume to allow any residual gauge pressure to reduce, a known volume of internal standard was introduced to both gain an approximate quantification of the concentration of the species in the chromatogram, and to ensure FID response was consistent across samples. This mixture was finally injected into the gas sampling inlet of the GC, and the program outlined in Section 3.7 was run.

6.3. Pyrolytic reactor results using C10 fuels

6.3.1. Pyrolysis of decane

The C10 fuels tested within the pyrolytic reactor were pertinent in regards to discerning molecular breakdown, specifically of γ-decalactone- a model bioderived lactone molecule previously evaluated to produce good combustion quality and a reduction in soot mass. The remaining C10 fuels were selected based on their similarities and differences from the lactone, in order to elucidate the effect of various characteristics of molecular structure on pyrolytic breakdown. The explanation of n-heptane pyrolysis provided in the previous section can be applied to the discussion of these C10 molecules as well, but more important is the comparison

between molecules and the relative abundance of the precursors produced by the pyrolysis of these molecules.
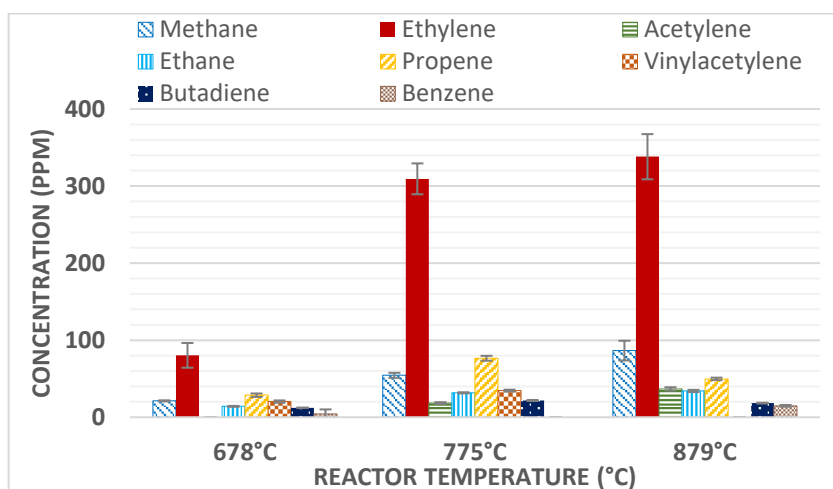
Figure 6.4: Soot precursor concentrations detected using decane under varying pyrolysis temperatures

Decane was tested as a simple, straight chain, fully saturated C10 hydrocarbon. It produced, predictably, a very similar set of results (Figure 6.4) as its C7 counterpart, heptane (Figure 6.5), though its breakdown appears to have been marginally delayed as, at 879°C, ethane concentrations are still rising, acetylene concentrations do not exceed those of methane at the highest temperatures, and butadiene is still fairly prevalent (Figure 6.5c). Also, benzene is detected in relatively high concentrations at 879°C. Potentially, benzene formation is greater in the pyrolysis of decane. Alternatively, benzene growth to PAHs may not be as rapid as in the case of heptane; or, the radicals formed in heptane pyrolysis favour the direct formation of aromatics other than benzene, such as phenylacetylene and naphthalene formed from C2 and C5 intermediates respectively.[304] It is stressed that the latter suggestion is a tentative one; while literature[420] indicates that bond dissociation energies (BDE) of C-H bonds are weaker at the end of molecules compared to the centre (therefore a longer molecule will see a lower minimum BDE compared to a shorter one), there is little indication as to the expected species formed in the pyrolysis of different carbon number n-alkanes.
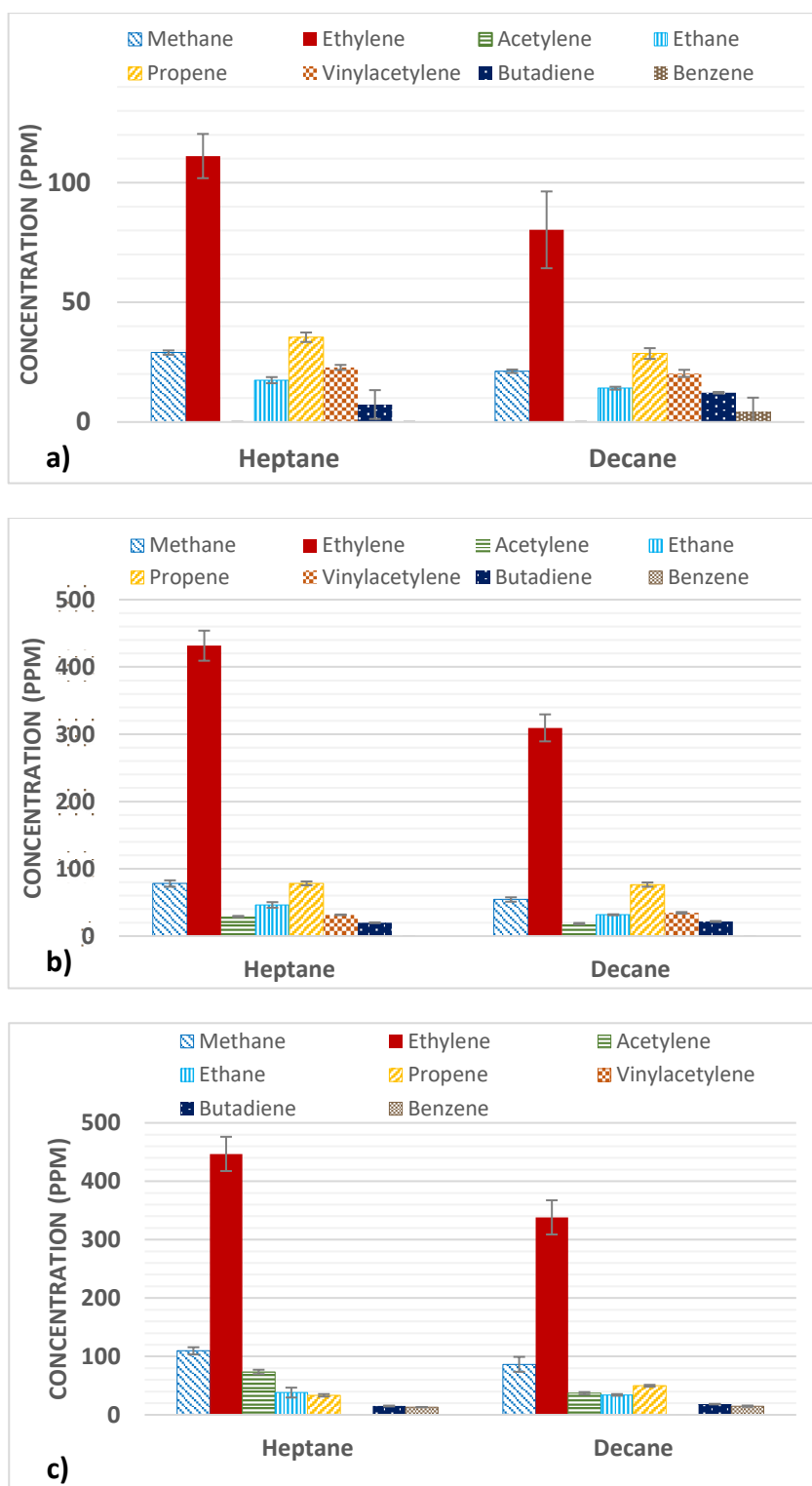
Figure 6.5: Comparison of pyrolysis products produced from heptane and decane at (a) 678°C, (b) 775°C and (c) 879°C

Injection rates of the test fuels were controlled such that the concentration of carbon atoms in the nitrogen flow was maintained constant with molecules of differing carbon numbers. Therefore, the primary difference between heptane and decane is in the bond enthalpies and the differences in relative species abundance noted here is likely attributed to this fact. Xin and Liu[408] conducted density functional theory (DFT) analysis on C4-C7 hydrocarbons, determining that the bond dissociation enthalpies of both C-H and C-C bonds decrease as the carbon number increases, noted from an increase in hydrocarbon fragments- including radical species- when using a C6, isohexane, compared to a C4, isobutane. The longer chain length of decane will therefore see an increase in fragments compared to heptane. This trend in BDEs has been used to explain why longer hydrocarbon exhibit shorter ignition delays in an engine, with the lower BDEs making it easier for radicals to form in the relatively low-temperature premixing phase.[202] However, these explanations appear to contradict with the fact that decane's pyrolysis is delayed compared to heptane, concluded from the lower concentrations of ethylene and the fact that concentrations of species such as ethane have not begun to decrease at the maximum (879°C) temperature. It is suggested that a greater chain length potentially provides greater scope for reactions towards PAHs, as radicals generated will perhaps, on average, possess greater carbon number and more easily recombine to form species above the detectable range, hence the slightly lower concentrations of C1-C6 species observed in the decane tests compared to heptane.

A comparison of absolute concentrations of species between fuels is not the primary aim of this investigation; a more important questions is whether the reaction mechanism is significantly changed- the presence of different species would indicate this- but it is apparent that between heptane and decane this is not the case. The same features remain; ethylene is the most abundant species- increasing substantially from 678°C to 775°C, then again by a small amount at 879°C (Figure 6.5)- while concentrations of methane and acetylene increase with temperature and C3 and C4 species increase up to a point, after which consumption reactions appear favourable, and their abundance decreases.

6.3.2. Pyrolysis of γ-decalactone and n-heptylpropionate (cylic and straight chain ester)
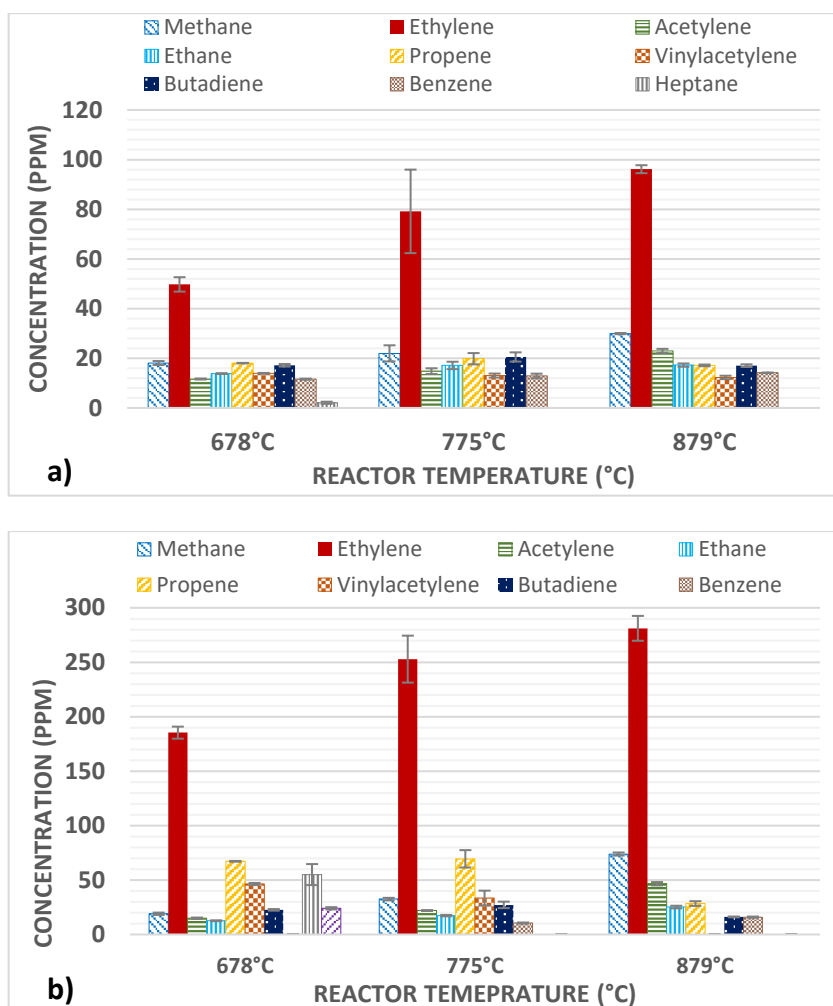
Figure 6.6: Soot precursor concentrations detected using (a) γ-decalactone and (b) n-heptylpropionate under varying pyrolysis temperatures

The primary fuel of interest here is γ-decalactone, the pyrolysis product concentrations of which are provided in Figure 6.6a. Surprisingly, the precursor output consisted of largely the same pyrolysis peaks as decane and heptane, with some small traces observed at retention times of 22.0, 24.3 and 30.0 minutes that were not present in the external standard (see appendix Figure D4). The peak at 24.3 was hypothesized to be cyclopentadiene, as this was also present in small amounts in other samples, and will be discussed in more detail in Section

6.3.4. The species at 22.0 was potentially a contaminant, as this also appeared in a test using the external standard only. While the species detected themselves are not considerably different to those of unoxygenated decane (Figure 6.4), the lower soot precursor concentrations are promising when considering the fact that this could be a potential fuel molecule, and therefore reduced soot precursor formation is desirable (note y-axis of Figure 6.6a). The reduced formation could be due to the oxygen present within the molecule. This could result in more oxidising reactions to form either CO or CO_2, or the C-O bond could remain intact, thereby reducing carbon available to form soot, as alluded to in Eveleigh's investigations.[401] It is important to compare this result to that of n-HP (Figure 6.6b), as this is a straight chain version of the lactone molecule and could help elucidate the mechanism of fuel breakdown.
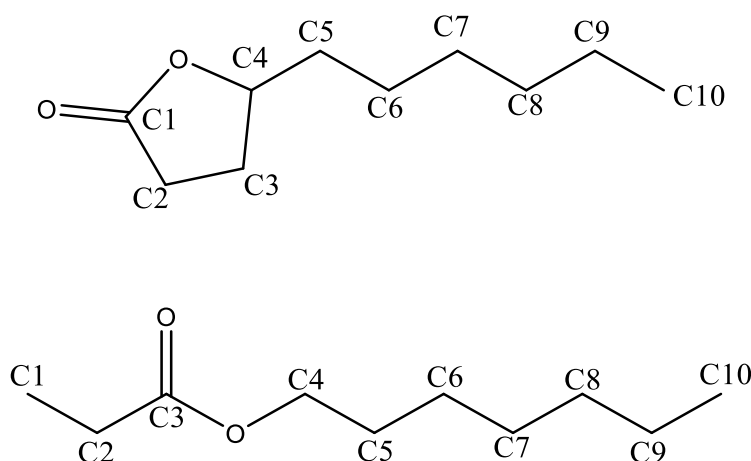
Figure 6.7: Molecular structure of cylic ester, γ-decalactone (above), and straight chain ester, n-heptylpropionoate (below), with carbon numbers labelled

In the case of n-HP, as indicated in Figure 6.6, the output differs compared to γDL, suggesting that the two molecules do not break down via the same pathway. This may have been expected if the lactone's first reaction was ring opening at the C4 position, shown in

Figure 6.6 above. Given that there are more species present in Figure 6.5 in the case of the straight chain ester, this suggests a different pathway. In the following paragraphs a comparison will be made of the results for n-HP and γDL, and their implications for first ring formation; the results for n-HP and γDL will first be compared with those for the hydrocarbons, in order to highlight the influence of molecular oxygen on soot formation pathways. For both esters, overall concentrations are lower than for decane and heptane (Figure 6.5) at 775°C and 879°C - maximum ethylene concentrations for decane were approximately 320ppm at 879°C, but for n-HP, this maximum was only 260ppm, and even lower- at approximately 105ppm- for γDL. However, at 678°C, n-HP saw far higher precursor concentrations than in decane, suggesting a much earlier onset of molecular breakdown, undoubtedly caused by the influence of oxygen in the ester that reduces bond dissociation enthalpies- increasing radical formation- of adjacent C-C and C-H bonds. The destabilising effect of oxygen also appears to yield a greater range of precursors for a given temperature; in the γDL graph, benzene concentrations are significant across the temperature range, while the concentration of vinylacetylene does not completely disappear at 879°C in the same way as it does during the decane pyrolysis. Nevertheless, the overall pattern of precursor abundance remains similar for these fuels compared to hydrocarbons, in terms of the relative formation and consumption of methane through to butadiene. The fact that hydrocarbons form much larger amounts of ethylene compared to other precursors could suggest that the oxygen atoms present likely increase the potential type of radical species formed, and this in turn leads to a gradual increase in benzene formation. McEnally and Pfefferle[302,421] noted a similar trend, in this case in comparing branched alkanes to linear analogues, whereby the branched species produced more benzene due to higher formation of propene (C3) and butene (C4) species, whereas the linear chains were more prone to forming ethylene. In n-hydrocarbons, it is suggested that a build-up of ethyl species inhibits subsequent recombination to eventually form benzene but, in oxygenated fuels, the oxygen is able to increase the rate of ethylene (derived-radical) consumption, yielding C3 and C4 species that are necessary in forming the first aromatic ring.

Comparing the oxygenated fuels specifically (Figure 6.6), the higher concentration of species in the case of n-HP could be a result of its molecular structure. γDL oxygen atoms are likely more reactive than those in n-HP (since the latter's oxygen groups are protected in the centre of the molecule) making the former's oxygens able to interact and consume/oxidise more radical species. Furthermore, an increase in steric hindrance caused by the longer chained n-HP (in the case of γDL, 4 carbons are in a cyclic structure that shortens the overall length of the molecule) could also be the reason for fewer oxygen-radical reactions. Oxygen atoms at one side of the molecule also makes γDL more polar, which effects the physical properties of γDL. In terms of species present, both γDL and n-HP differ from other fuels in producing a suspected C6 aliphatic and heptane respectively (see appendix Figure D4 and D5), specifically at lower temperatures (though n-HP pyrolysis generated significantly higher concentrations of higher order aliphatic compared to γDL). Concentrations of the potential C6 species, using γDL, were only 2ppm at 678°C, but were over 150ppm when using the straight chain ester. As seen from the heptane experiments initially, heptane is not completely consumed at 678°C (Figure 6.3), with about 10% of the overall input remaining. This could be an indication of the fact that a straight chain ester would potentially detach at the C-O ether linkage and be able to restabilise itself to heptane, before this heptane itself is pyrolyzed further at higher temperatures.

One major difference is the existence of acetaldehyde in n-HP pyrolysis (Figure 6.6b), albeit at low concentrations that mean that γDL may also have formed this species, but in levels that were too low for detection. The formation of a C2 aldehyde is surprising, as it would potentially require the complete breakdown of the molecule to form ethyl radicals that may be partially oxidised. Alternatively, the aldehyde species may form from C=O bond in the ester, however, even if the C=O bond remains intact during molecular decomposition, the product would likely form CO or CO_2, rather than compete with hydrogen radicals to form the aldehyde species. Studies performed investigating ester pyrolysis and combustion have suggested that the C=O remains intact to form CO or CO_2.[372,422,423] Instead, the C-O bond in the ether is more

likely broken to form a C3 aldehyde radical. However, since heptane is also detected in the output, this would suggest that the other side of the ether linkage is also broken, yielding a highly reactive oxygen radical that could be responsible for the aldehyde species upon reaction with ethyl radicals, which are evidently present (inferred from the abundance of ethylene as a product). Breaking the C-O bond of the ester moiety would be expected to form a reactive C3 species; this may be inferred from the relatively high concentration of propene seen in Figure 6.6b, specifically at lower temperatures in which the molecule was still undergoing decomposition.

6.3.3. Effect of ketone and ether moiety
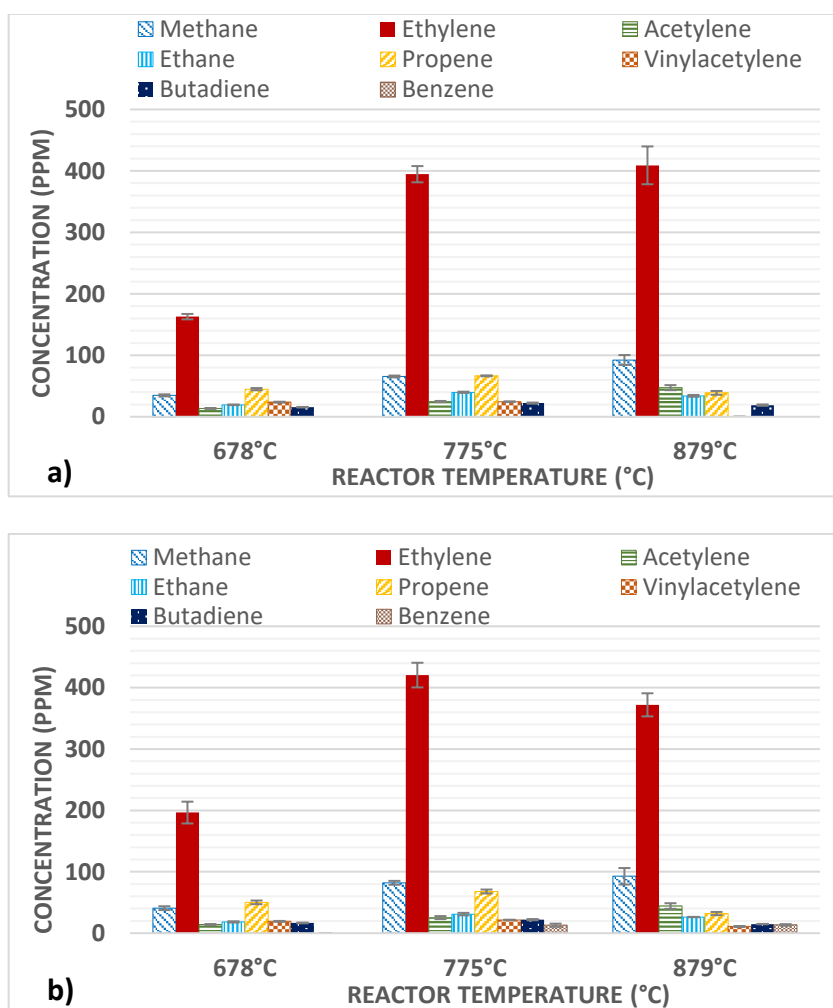
Figure 6.8: Soot precursor concentrations detected using (a) 3-decanone and (b) di-n-amyl ether under varying pyrolysis temperatures

The output of decanone and di-n-amyl ether are now discussed to better differentiate the roles that the oxygen, as ketone and ether moieties, might play in molecular breakdown and precursor concentration. Relative to n-HP, the former removes the ether linkage that is potentially responsible for the variation seen between the esters and decane, while the latter maintains the ether linkage but removes the C=O group, a bond that has been hypothesised as not breaking under pyrolytic conditions.

An ether linkage placed at the same location as that in the ester molecule (between the 3rd and 4th carbon- propoxyheptane) was not commercially available, therefore an ether was used in which the oxygen was located at the centre of the molecule, between the C5 and C6 positions, making it symmetrical. Given the level of interrogation into molecular breakdown, an observable difference in precursor concentration as a result of moving the ether linkage is likely. However, the difference is assumed relatively minor, compared to the difference between an ether and an alcohol, for example. Zhang *et al*[124] noted the sooting tendency of dimethyl ether (DME) was notably lower than that of the alcohol structural isomer, ethanol, with a likewise reduction in the detected precursors- C_2H_2, C_3H_3, C_4H_2, C_4H_4, C_5H_5, C_6H_6 during diethyl ether (DEE) pyrolysis. The location of the ether is still protected by multiple carbons on each side in di-n-amyl ether, therefore an ether linkage at the 5th carbon would likely possess similar breakdown characteristics to those of an ether linkage at the carbon 3 position.

As observed in Figure 6.8, di-n-amyl ether output does not appear to produce any acetaldehyde, suggesting that this aldehyde species was attributable to the C=O moiety in the ester molecule, rather than a reactive oxygen radical formed by breaking either side of the ether linkage. The high concentration of C3 species produced in n-HP pyrolysis (Figure 6.6b), relative to the other gaseous species detected, suggests that, the C-O bond breaks, resulting in a 3 carbon molecule. However, the fact that the ether linkage was in the centre of the tested ether, as opposed to being between the C3 and C4 positions as it is in n-HP, could have changed the reaction pathway sufficiently to avoid the production of any of this aldehyde.
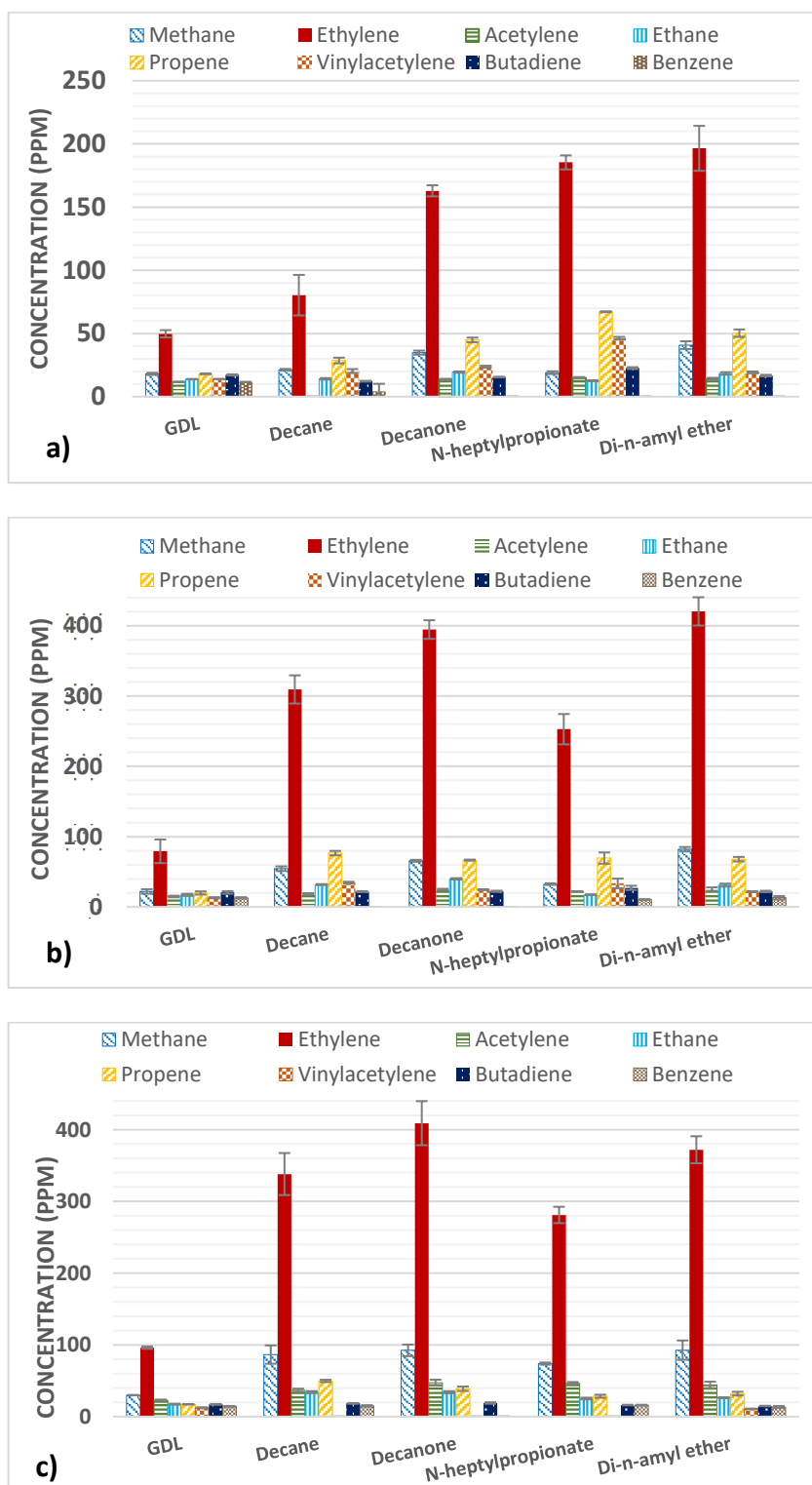
Figure 6.9: Comparison of pyrolysis products produced from all C10 fuels at (a) 678°C and (b) 775°C and (c) 879°C

Pertinent in the results obtained from the ketone and ether pyrolysis tests is the high concentration of ethylene- a greater amount than that found in the purely hydrocarbon C10 of decane (Figure 6.9a). This could be a possible indication of a crossover point in molecular structure, whereby a single oxygen is enough to destabilise the molecule and thus become more prone to forming soot precursors, but further oxygen means that these species start to decrease, relatively, through oxidative means. This factor would potentially explain why, at 678°C, di-n-amyl ether produces the highest concentration of ethylene, with decanone and n-HP also producing levels of ethylene of over 100ppm while decane pyrolysis at this condition saw approximately 70ppm of ethylene (Figure 6.9a). However, at 879°C, the pattern shifts and decane, decanone and di-n-amyl ether are observed to have appreciably higher levels of ethylene compared to n-HP (Figure 6.9b). Oyeyemi performed a computational study, using BDEs and multireference configuration interaction (MRCI) of species formed from molecular breakdown of various oxygenated molecules, and found that species formed from the decomposition of aldehydes were far more multiconfigurational than those formed from the same cleavage site in acids and esters.[425] This was postulated to be due to the additional oxygen atom in esters able to negate somewhat the charge from radical sites formed from C-C or C-H cleavage. Potentially, the greater multiconfigurational ability of decanone decomposition product explains why precursor concentrations are highest for this fuel (with the exception of heptane) at 879°C.

The pattern of precursor concentrations for decanone and di-n-amyl ether is similar to that of decane. That said, the ether differs as ethylene concentrations peak at 775°C, with the concentration at 879°C being approximately 50ppm lower (Figure 6.8b). This would agree with the previous statement that the ether molecules are very prone to molecular breakdown as, by 775°C, ethylene had already reached its peak, whereas in other molecules the rate of ethylene formation is always greater than rate of consumption under the measured temperatures. However, the lack of benzene presence here would indicate favourable conditions for

formation of PAHs as a result of potential combination of the species formed from di-n-amyl ether breakdown and the level of temperature. As stated in Wang's review,[304] naphthalene or substituted phenyl groups can form before benzene, and it is possible that the radicals formed in this ether's breakdown are preferential in these reaction schemes. For example, Golea[426] determined that the reaction of two 5 carbon species- indenyl and cyclopentadienyl radicals- was the dominant reaction in the formation of the PAH phenanthrene. Five member rings are likely to be preferentially formed in this di-n-amyl ether breakdown, since the ether linkage splits two 5 carbon chains, and the C-O bonds are likely the most susceptible to cleavage. This is in contrast to measurements in both γDL and n-HP molecules, where benzene is noted at virtually all temperatures (Figure 6.6). It is possible that the additional oxygen is able to destabilise the molecular configuration further, making it more susceptible to forming species such as acetylene and propargyl radicals that are the most important in forming benzene.[426]

Also notable in the comparison between these single oxygen molecules, compared to decane, is that the ethylene concentration increase afforded by the oxygenated fuel is slightly compensated by a partial decrease in propene and vinylacetylene concentrations, at temperatures of 775°C and 879°C (Figure 6.9). During decane pyrolysis, it appears propargyl formation and the resulting reaction to benzene and PAHs is a significant pathway. Considering the oxygenated fuels, ethylene formation is enhanced and therefore ethylene derived radicals represent a major reaction pathway to benzene. However, the relatively low concentrations of species at 678°C for decane suggests that, rather than the reaction chemistry differing significantly, it is primarily the delayed breakdown of the unoxygenated decane that is responsible.

This could also be a factor when comparing decanone and di-n-amyl ether to the ester molecules. At 775°C and 879°C, while the concentration of ethylene is much lower in the double oxygen ester, the amount of propene is more comparable, and in fact higher at 775°C (Figure 6.9). Potentially, at this temperature, the phase of molecular decomposition in n-HP centres on the oxygen atoms bonded to the C3 carbon, and thus forms a significant amount of

C3 radicals. On the other hand, since decanone has no ether linkage- and merely a ketone group that does not interfere with the carbon chain itself- the main species present is ethylene, matching a pattern similar to that of decane, and suggesting a relatively minor impact of the decanone oxygen content in changing the reaction pathway at this temperature.

Di-n-amyl ether produces the highest methane and ethylene concentrations at 775°C (Figure 6.9b), slightly higher than that of decanone and relatively similar to that of the hydrocarbons, heptane and decane. However, while the ether has appeared to reach maximum overall gaseous precursor concentrations at 775°C, the concentration of methane and acetylene is still rising slightly at 879°C (Figure 6.8). Again, the conclusion is that the ether, like the ketone, does not significantly change the reaction pathway in the same way as the esters, but in the ether's case, molecular breakdown is able to commence at lower temperatures compared to the more stable hydrocarbon. Surprisingly, the presence of oxygen in the chain was not reflected in the presence of differing species in the output chromatograms, but it is possible that trace amounts of species may have been seen at lower temperatures than 678°C (a discussion surrounding other detected species can be found in Section 6.3.4 below). However, it is suggested that the oxygen in this ether was more influential in precursor abundance than the oxygen in the ketone group of decanone; di-n-amyl ether possessed the highest concentration of ethylene at 775°C, but a ~50ppm lower value at 879°C- which could be indicative of oxidation at these temperatures or enhanced dehydrogenation to form acetylene, which increases with temperature. Given an earlier onset of molecular breakdown in di-n-amyl ether, it is possible that the radical pool is larger at equivalent conditions, increasing dehydrogenation of ethylene. An enhanced oxidation rate may be inferred from the n-HP results, which see an initial range of concentrations in-line with those of the single oxygen molecules at 678°C, but lower at 775°C and 879°C (Figrue 6.9). Meanwhile ethylene concentrations during n-HP pyrolysis were approximately 50ppm lower than decane at these temperatures while, at 678°C, they far exceed the decane precursor concentrations.

6.3.4. Other detected species

A small number of species, other than those already highlighted in Figure 6.3-6.9, were generally found in trace amounts from the FID output and their identity could not be ascertained from the external standard gas mixture; the discussion above focussed on species that could be identified in abundance. However, some mention should be given to some specific chromatograms, which can be seen in the Appendix Figures D4-D6, where the presence of some species provides further potential indications of the way the molecules being considered break down.

As mentioned, a peak at 24.3 minutes was often detected in the chromatograms- all fuels presented this peak at the 678°C furnace temperature- but traces were also observed at 775°C, suggestive of a species that forms relatively early in molecular breakdown or PAH formation, but which relatively quickly reacts further to form heavier species. This peak is suggested as cyclopentadiene, the only primary PAH precursor not included in the external standard due to its instability. There were three primary factors to indicate this peak identity. Firstly, the consistency of its presence indicated that the 24.3 peak represented a common pyrolysis product.[405,427,428] Secondly, the retention time of 24.3 minutes can be expected to represent a C5 species, lying almost directly between the C4 species of butadiene (18.0) and the C6 of benzene (31.0). Finally, the species in which this peak was observed in highest concentrations was di-n-amyl ether. This symmetrical C10 ether is highly likely to produce C5 species, as the C-O bonds are most susceptible to splitting, therefore it would be reasonable to expect the peak seen here to represent the most prevalent C5 precursor molecule. Assuming that this is the case, it should be noted that this species was detected in the pyrolysis of all other molecules at 678°C, indicating that a reaction pathway involving cyclopentadiene is a key feature in the formation of aromatics.[304] Only the ether produced this in trace amounts at 775°C. Another factor observed was that the 24.3 peak was more prevalent in the hydrocarbons, heptane and decane, than in the oxygenated fuels (with the exception of the aforementioned ether). It could be inferred from this that, unless the oxygen is positioned in

such a way to promote the formation of C5 radicals, the oxygen atoms are either able to reduce the amount of cyclopentadiene formed or are able to effectively oxidise this species to a greater extent than species such as ethylene, which possess greater oxidative stability.

Another feature, replicated for all fuels tested, was the presence of a small amount of species at 11.4 and 11.7 minutes at 879°C conditions only. The former was identified as propyne, and it is postulated that the 11.7 peak represents another C3 species- potentially propadiene (allene) another aromatic precursor.[429] It is suggested that the greater radical pool allowed by the higher temperatures causes an accumulation of C3 species, which are formed at a faster rate than they can react. In the same way that acetylene (a triple bonded C2 aliphatic) is observed at higher temperatures relative to ethylene (a double bonded C2), tripled bonded propyne concentrations and that of two-double bonded allene can be observed against the more saturated and stable propene.

The final observation relevant to an unidentified peak is pertinent to γDL pyrolysis specifically. While it was noted that n-HP produced a high amount of heptane, γDL produced only a minor amount at 678°C, indicating a significant difference in molecular breakdown between the two. However, γDL was noted to produce species at approximately 30.4, though the exact timing and concentration varied. While the identity of this peak is not known, one hypothesis is that it represents a C6 species aliphatic, generated by the total detachment of the hexyl side chain from the lactone ring. However, the fact that this peak varied in abundance means that this prediction is only theoretical, while the slight variations in retention time observed (from test-to-test) suggest the potential of similar, but distinct, species to form, rather than a single molecule consistently. One potential cause of this apparent variability is that the species formed is highly reactive, and in fact could continue to reduce in concentration between the time of sampling to the time of analysis. The reactivity of these species increases with carbon number, though the existence of heptane in n-HP pyrolysis means that the long chained aliphatic formed from γDL is not able to reliably restabilise itself into hexane in the same way a C7 radical formed from n-HP can form heptane. While a small hexane peak could be

identified in one test, this was not observed in repeat results. It is suggested that other peaks in this region are caused by more unsaturated species, such as hexene. Assuming that the side chain detaches, a radical species forms with high reactivity at one end, and it is possible that one product of this is 1-hexene.

6.4. In-cylinder sampling results

The following chromatograms were obtained using the same GC-FID (column, oven temperature ramp rates etc) as that utilised for the analysis of samples drawn from the tubular reactor. The initial task in applying this methodology was to determine the consistency of internal standard across samples. Important to note here is the result of sampling during heptane combustion at a time of 370 CAD (Figure 6.10b), where the measured concentration of internal standard is indicated by the magnitude of the peak at a retention time of 9.6 minutes and labelled 'I.S'. The dilution of the internal standard was intentionally not consistent across all samples; this particular sample was diluted with just 1/6th IS, whereas other samples were diluted to a slightly greater extent i.e. 80% sample and 20% internal standard. Correcting for the differing dilution levels, however, did not produce the expected integration of the IS in this sample; the integration value of the IS in the heptane sample taken at 370 CAD sample was three times lower than expected. The reasoning for this is unclear, as it is unlikely the FID sensitivity would have dropped to this level and recovered without changes to the experimental set-up. A handling error may be responsible. For example, if the extraction of sample and internal standard was not performed at the same atmospheric conditions, equal volumes would result in differing mass concentrations. This was likely a greater issue in the engine, compared to a the reactor, as pressure fluctuations were higher when sampling from the cylinder. However, the significant deviation from the expected value suggests a more fundamental issue.

As the cause of this disparity in IS concentration could not be resolved during this study due to technical issues, quantitative comparisons across samples and between furnace results are not possible, however, a qualitative appreciation of the relative abundance of species can be made. The technical issues which hindered resolution of the apparent variation in IS concentration included inconsistencies in valve opening times, potentially explained by general degradation of the valve stem which hindered vertical movement, as well as malfunction in the engine fuel injection system that necessitated a repair period lasting several months. However, while exact species concentrations were not available, it was possible to make some insightful observations from the results.

b)

c)
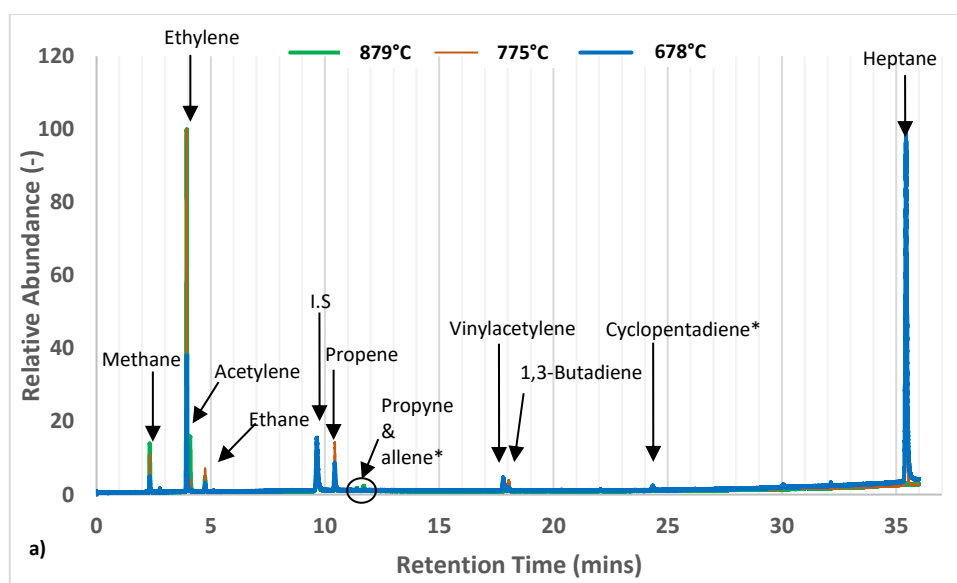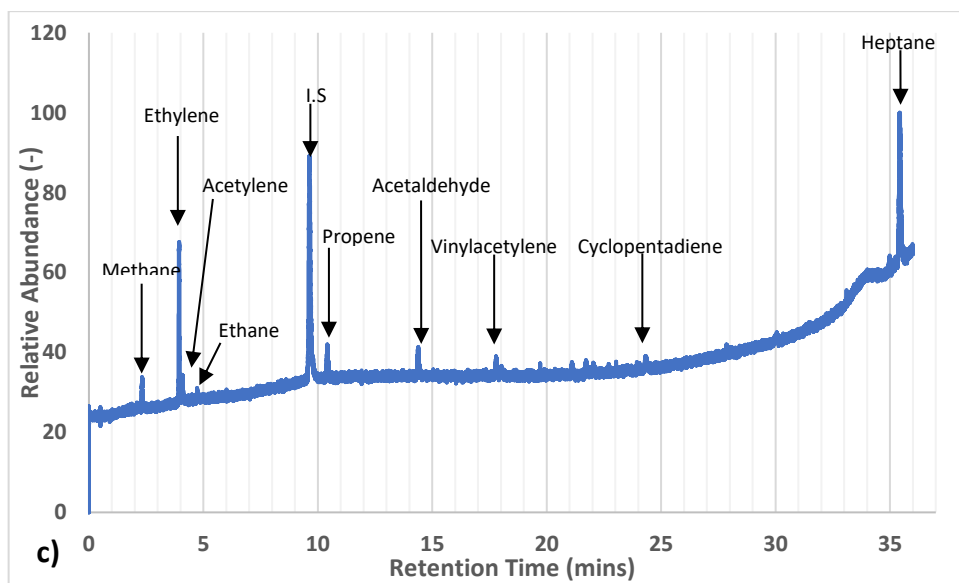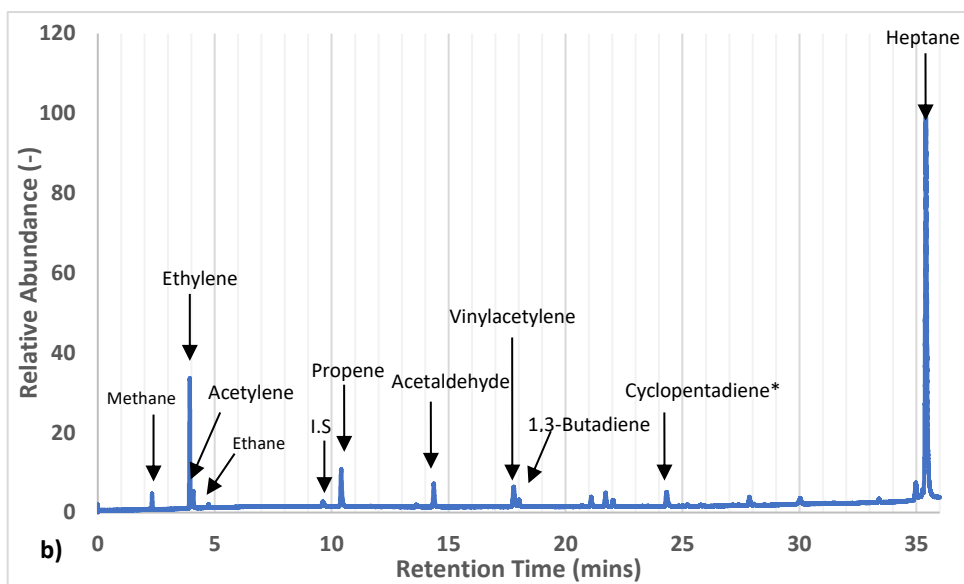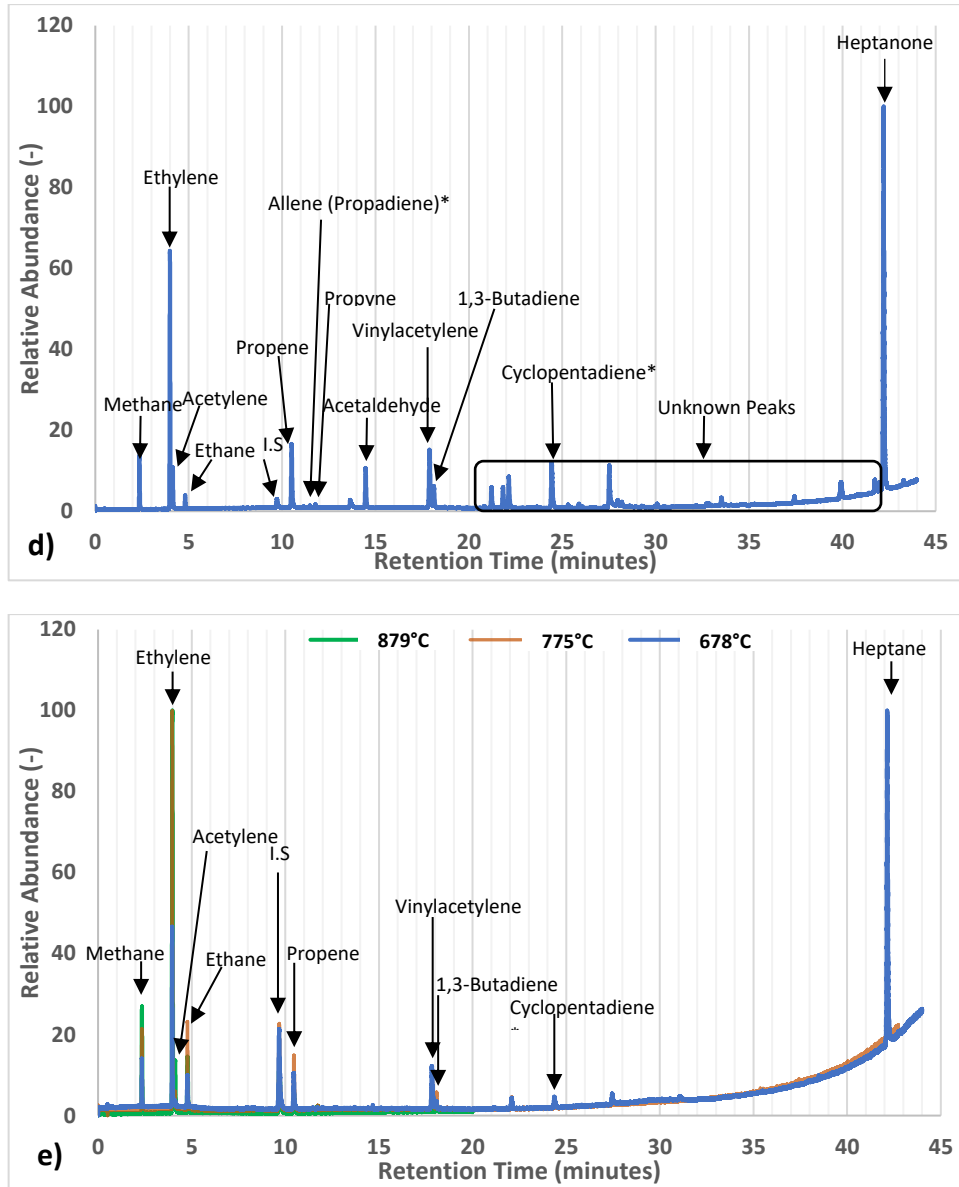
Figure 6.10: Chromatograms of heptane pyrolytic reactor samples at 678°C, 775°C and 879°C furnace temperature (a), and in-cylinder samples taken during combustion at 370 CAD (b) and 420 CAD (c), and heptanone combustion at 370 CAD (5 bar IMEP, SOC= TDC) (d) and heptanone pyrolytic reactor samples at 678°C, 775°C and 879°C furnace temperature (e)

Table 6.5: Integrated peaks from chromatograms of heptane combustion, comparing species and their integration at 370 CAD and 420 CAD sampling times

SPECIES	370 CAD		420 CAD	
	Peak (mins)	Integration Area	Peak (mins)	Integration Area
METHANE	2.321	31290.82	2.324	3385.65
ETHYLENE	3.931	216401.5	3.938	17347.59
ACETYLENE	4.081	28829.19	4.086	3027.1
ETHANE	4.736	15787.74	4.729	989.94
INTERNAL STANDARD	9.628	16851.78	9.635	53928.44
PROPENE	10.404	103822.3	10.415	7876.05
ACETALDEHYDE	14.368	59436.8	14.386	5859.51
VINYLACETYLENE	17.784	71903.78	17.79	4587.89
BUTADIENE	18.024	20767.08		
N/A	21.097	25222.3	21.711	2685.05
N/A	21.71	39565.71	21.711	2732.55
N/A	22.027	19789.83	22.043	3029.6
CYCLOPENTADIENE	24.318	52391.02	24.321	4109.84
N/A	27.86	29099.35		
N/A	30.044	29283.04	30.054	2638.97
N/A	34.98	54784.85	34.982	3365.88
HEPTANE	35.41	1410384	35.424	34292.94

Table 6.6: Integrated peaks from chromatograms of heptane and heptanone combustion, comparing species and their integration at 370 CAD sampling time

	HEPTANONE		HEPTANE	
	Peak (mins)	Integration Area	Peak (mins)	Integration Area
METHANE	2.363	174851	2.321	31290.82
ETHYLENE	3.996	852337.8	3.931	216401.5
ACETYLENE	4.149	160532.9	4.081	28829.19
ETHANE	4.81	52190.11	4.736	15787.74
IS	9.719	60224.19	9.628	16851.78
PROPENE	10.509	341570.3	10.404	103822.3
PROPANE/ALLENE	11.489	25852.79		
PROPYNE	11.786	23790.32		
N/A	13.64	60237.64		
ACETALDEHYDE	14.469	202366.7	14.368	59436.8
VINYLACETYLENE	17.892	393564.7	17.784	71903.78
BUTADIENE	18.132	108036.1	18.024	20767.08
N/A	20.83	29956.98		
N/A	21.212	119501.6	21.097	25222.3
N/A	21.829	127822.8	21.71	39565.71
N/A	22.136	200415	22.027	19789.83
CYCLOPENTADIENE	24.435	328649.6	24.318	52391.02
N/A	25.891	22749.28		
N/A	27.515	297902		
N/A	27.972	73764.47	27.86	29099.35
N/A	28.182	44937.2		
N/A	30.079	28531.43	30.044	29283.04
N/A	33.525	28180.51		
N/A	37.428	34043.97		
N/A	39.932	125372.3		
N/A	41.738	56582.08		
N/A	41.992	25860.59		
FUEL	42.201	2235974	34.98	54784.85
N/A	43.282	32258.72		

6.4.1. Effect of sampling time on soot precursor concentration

The preliminary results outlined above enable some potential conclusions to be drawn when comparing species collected for different fuels and at different sampling times, while also providing some clarification of the methodology that will be useful to employ in future work. One of the clearest examples of this is that the sampling time of 420 CAD (Figure 6.10c) produced a relatively noisy and distorted chromatogram. This is likely due to this timing producing samples that consisted primarily of accumulation mode particulates, and very few gaseous precursors. This concurs with results obtained previously in the group,[374] which suggested a high abundance of PAHs at 40 CAD, and a subsequent cessation of PAH formation by 55 CAD, in which oxidation is prevalent. Gaseous species that were present in this sample might also have been diluted due to absorption onto particulate species.. As a result, it is suggested that future testing utilises sampling times which are at earlier combustion phasing.

One of the primary deductions from the test at 420 CAD sampling time was that species concentrations detected were low, suggested by both the internal standard peak representing the most abundant species (see Table 6.5) and the high levels of noise. Also apparent was that there existed some fuel in the sample (indicated by the peak at 35 minutes retention time in Figure 6.10c), indicating that, even during late stage combustion, fuel is not completely combusted. One potential explanation for this remaining fuel was postulated by Ogbunuzor to be a result of in-cylinder swirl or fuel impingement.[374] The fate of this unreacted fuel could be that it is burnt in late stage combustion, or passes into the exhaust unreacted. Levels of all species were relatively low, explainable by the fact that, at this timing, calculated global in-cylinder temperatures were approximately 800-900°C, and therefore molecular breakdown of heptane was reduced compared to earlier engine timing; at 370 CAD global temperatures were close to their maximum, at approximately 1200-1300°C. This, coupled with the fact that the remaining heptane fuel itself existed in fairly low concentrations (apparent through comparison

of the heptane peak to that of the IS), likely accounts for the low abundance of light hydrocarbons.

Comparing the 420 CAD sample to a sample taken at 370 CAD (i.e. 10CAD ATDC), the concentrations of species were appreciably higher at 370 CAD (Figure 6.10b), based on the strong peaks and relative abundance of internal standard (though, for the reasons highlighted previously, exact concentrations have not been reported). Moreover, a greater number of species could be detected. However, Table 6.5 indicates that only two species detected in heptane combustion at 370 CAD were not detected at 420 CAD. In all, 6 species were unidentifiable, ranging between retention times of 21-35 minutes. These are suggested to signify C5-C6 aliphatic hydrocarbon molecules, though oxygenated species could also be stable enough to be detected. Surprisingly, the simplest aromatic, benzene, was not detectable at either sampling condition. As noted in the reactor experiments, benzene is only formed in low concentrations relative to the majority of its precursors, suggesting its formation into PAHs is a rapid step in soot formation, aided by the abundance of potential reactants, such as acetylene. With a residence time orders of magnitude shorter in an engine than that encountered in the reactor under pyrolytic conditions, it is suggested that benzene reacts with addition groups, like acetylene, as soon as it is formed, given the relative abundance of acetylene and other addition groups. Meanwhile, Sun *et al*[430] noted high concentrations of biphenyl radicals formed during benzene pyrolysis, suggesting the recombination of phenyl radicals as a major reaction pathway, forming the biphenyl species that would not be detected within these chromatograms. Additionally, it is suggested - though further investigations are needed - that the conditions in an engine are less prone to forming benzene molecules, instead forming higher order aromatics that can be produced directly from aliphatic precursors i.e the combination of cyclopentadienyl radicals;[419] this cyclopentadiene species was more consistently observed in both the pyrolytic reactor and engine experiments. Ethylene was the primary gaseous precursor detected, though the concentration of acetaldehyde was also significant, relative to other detected species, and a notable amount was still present at 420

CAD, suggesting this species is relatively stable throughout the diffusion-led combustion phase. This molecule itself is not a major soot precursor, therefore its consumption is likely due to decomposition[431] into CO and methane. The high presence of C3 species suggests that routes involving these species, referred to by Shulka[299] and Wang[304], are significant in the breakdown of heptane under the conditions experienced in the engine combustion chamber.

The significant abundance of fuel at 10 CAD ATDC suggests that the original heptane molecule is still in the early phase of premixed combustion. During these tests, the start of combustion was maintained at 360 CAD by adjusting the engine injection timing, therefore the sampling time of 370 CAD meant that a relatively low cylinder volume was sampled from, containing an abundance of fuel. Despite the prevalence of heptane molecules, there is also a large abundance of precursor species; the majority of these are hydrocarbons, but one of the most abundant species detected was acetaldehyde, an oxygenated aldehyde species.

At 370 CAD, ethylene is the most abundant hydrocarbon species, with lower levels of methane, acetylene, ethane, propene, vinylacetylene and 1,3-butadiene found (Figure 6.10b). This pattern reflects that of the pyrolysis tests conducted in the tubular reactor (Figure 6.10a). By 420 CAD (Figure 6.10c), abundance of all species had reduced in the late stage combustion phase, due to lower fuel concentrations and lower temperatures, such that new pyrolysis products were less prevalent, and soot agglomeration was dominant.

6.4.2. Effect of oxygenated functionality on precursor abundance

Considering the oxygenated fuel, 2-heptanone, more gaseous species were detected during combustion than with heptane at the same sampling time, as shown in Table 6.6 and Figure 6.10d, where heptanone produced 27 observed individual species (other than itself or the internal standard) compared to just 14 during heptane combustion (Figure 6.10b). These additional species were non-identifiable. However, the appearance of this multitude of peaks is postulated to be due to a combination of oxygenated precursors and species that were formed as a result of the oxygen present in heptanone, but themselves do not contain oxygen.

The latter is suggested because in heptane combustion the availability of oxygen from the air would likely mean that oxygen concentration is not a limiting factor (sampling occurred between fuel injector sprays where oxygen deficient regions are more limited), therefore the presence of oxygen within the molecule is not expected to correlate with a significant increase in oxygenated precursors within an engine. It is possible that the carbonyl group, positioned at the C2 position, is able to destabilise the molecule by lowering equivalent bond enthalpies, thus facilitating an earlier release of radicals.

While absolute concentrations are not considered, an apparent fact is that, overall, the pattern of precursor formation and consumption is broadly similar for heptane and heptanone combustion and pyrolysis, agreeing with the results obtained from the furnace, which suggested similar breakdown products despite changes to the fuel molecular structure. Ethylene is the dominant species detected, while acetylene has begun to form, even at this early stage of combustion. Propene meanwhile, represents a significant pyrolysis product during combustion of both fuels. A difference noticed with heptanone combustion was that it appeared to form intermediate species, propyne and (postulated) allene, indicated in Table 6.6. However, Figure 6.10a shows a small amount of these same peaks at the highest reactor temperatures employed during heptane pyrolysis. This implies a greater abundance of C3 fragments as temperatures increase and signifying that both C7 fuels have the potential to form propyne and allene. It is important to note that these aforementioned C3 species presented in very low concentrations during heptanone combustion, and thus their presence does not suggest a significant difference in reaction pathway between the ketone and n-heptane. Heptanone, like heptane, also forms acetaldehyde, but given that heptane does not contain oxygen atoms, this suggests that this is formed from air-derived oxygen, as opposed to the oxygen within heptanone, and is the first indication of a differing reaction pathway during combustion in the engine compared to pyrolysis in the tube reactor.

6.4.3. Comparison between engine and reactor results

Comparisons between the engine and the furnace are qualitative and speculative, as the amount of fuel injected per cycle is not known. However, as between the comparison of heptane and heptanone in the engine, any apparent difference in reaction pathways should still be discernible from the results. Overall, the major difference between the reactor and engine samples appears to have been an increase in the number of precursors in the engine during the early stage of combustion, as observed in Figure 6.10a compared to Figure 6.10b and Figure 6.10d compared to Figure 6.10e, though these additional species existed in relatively low abundance. The shorter residence time within the engine may be expected to have reduced the number of reactions occurring, but it is likely that this shorter residence time reduced potential for stabilising reactions. It is suggested that, within the pyrolysis reactor, a greater range of species form initially than seen in the chromatograms but have sufficient time to react further into the stable intermediates identified (methane, ethylene etc) before the reaction is frozen during sampling. Furthermore, the additional role of air present in engine combustion was likely a cause for the greater number of species to be present. A final consideration is that, as shown in Figure 6.10a and Figure 6.10e, the number of species detected in the pyrolytic reactor was greatest at 678°C. It is therefore postulated that the precursors detected in the engine were mostly formed from relatively low temperature zones within the cylinder, for example impingement regions on the walls or over diluted air-fuel regions.

While these additional species could not be identified, the significant formation of acetaldehyde within the engine, as mentioned, was likely derived from the air-oxygen, since heptane possesses no fuel-bound oxygen to contribute to this. Furthermore, heptanone pyrolysis within the oxygen-deficient reactor produced no acetaldehyde (Figure 6.10a), again implying that this aldehyde species was not formed from fuel-bound oxygen. The likelihood is that the C=O bond in heptanone was not generally broken during pyrolysis, as noted in Section

6.3.3, where decanone also saw no acetaldehyde formed, and instead remained intact with the carbon-oxygen group responsible for forming CO or CO_2. The only fuel species noted to produce acetaldehyde in the tubular reactor was an ester, which contained an ether linkage which was likely the cause for this aldehyde to be present at low concentrations and under relatively low temperatures; a free radical oxygen might have become liberated and able to combine with C2 radicals to form a stable aldehyde. Given the lack of an ether oxygen in heptanone this route would not have been possible, whereas, during engine combustion, oxygen from the air could have supplied the necessary reactants for acetaldehyde formation.

Ultimately, it is clear that the samples taken from the reactor were less complex than those from the engine for both heptane and heptanone, with a greater range of peaks detected under the same GC conditions in the case of the engine cylinder sample. However, the results indicate that the tubular reactor was a powerful tool in mimicking pyrolysis reactions within a combustion engine. While some peaks were absent in the pyrolyser, unidentified peaks at 22.1 minutes from heptanone (Figure 6.10d and Figure 6.10e) and 30.0 minutes from heptane (Figure 6.10a and Figure 6.10b) in both cases suggest that even species at low abundance in an engine can also be detected in the more controlled conditions of the tubular reactor. Overall, the presence of air oxygen in the combustion engine is postulated to create a greater availability of oxygen-containing free radicals that can facilitate the generation of a greater range of species. Notwithstanding this, the presence of well-known gaseous precursors, leading to the aromatic molecules, has been clearly identified under both reaction conditions.

6.5. Conclusions

6.5.1. Reactor results summary

Overall, while the precursor concentration in oxygenated molecules is initially much higher than hydrocarbon fuels in the pyrolysis reactor, as temperatures increase the difference starts to converge, with ester fuels reducing the gaseous hydrocarbon concentrations to a greater

extent than ethers, which in turn are more effectual than the ketone. Whether this is due to the oxygen disrupting and competing with certain free radical reactions, which ultimately leads to benzene, or because the oxygen atoms are oxidising more stable hydrocarbon species (RSRs or the molecules detected in the spectra) is not clear. Likely, there is contribution from both, because concentrations of the majority of species decrease, though some precursor formation is clearly disrupted more than others. For example, the concentration of acetylene detected during the pyrolysis of decanone, di-n-amyl ether and n-HP remains similar between molecules as temperature is increased. However, concentrations of propene, vinylacetylene and butadiene are reduced to a greater extent with the ester functionality included.

Comparison of the molecular breakdown of the two esters is difficult, as the concentration of the precursors under γDL pyrolysis is significantly reduced overall and the cause for this is not fully understood. The presence of the oxygen atoms from the C1 carbon in γDL, as opposed to the more central C3 carbon in n-HP, is likely a major reason in explaining a greater oxidative ability of the lactone compared to the straight chain isomer. Furthermore, the overall reaction mechanism of the two fuels appears to have been changed- illustrated by the significant amount of heptane formed in n-HP pyrolysis, as well as the presence of acetaldehyde- indicating that the lactone's ring moiety does not open early on in pyrolysis to form a straight chain ester.

Furthermore, γDL differs from all other species in that it is the only fuel to produce higher amounts of butadiene than vinylacetylene at 678°C. Other fuels begin to preferentially form butadiene at higher temperatures, therefore it is not known whether a difference in reaction mechanism is responsible, or an early onset of decomposition afforded by the lactone. The former is suggested when also considering that concentrations of butadiene are greater than that of propene- a feature not replicated by other fuels at any other temperatures- and the concurrent presence of a potential C6 aliphatic. This preference for butadiene formation is proposed to originate from the 4 carbon membered ring of the lactone, and would indicate that these carbons are able to liberate themselves, both from the hexyl side chain (generating the

C6 aliphatic) and from the ester oxygen groups. Potentially, butadiene is preferably formed compared to vinylacetylene, as the latter is more unsaturated, and the original carbons in the lactone ring are fully saturated.

This possible difference in molecular breakdown of the lactone compared to the straight chain ester is potentially advantageous; any soot-reducing properties of the lactone are not diminished by ring-opening to form a species with two carbon chains acting as protective groups (as in the case of n-HP). If the increase in butadiene formation and presence of a C6 aliphatic is caused by separation of the ring and the side chain, followed by the formation of oxygen radicals, then a reduced production of soot upon use of this fuel, compared to current biodiesel fuels that utilise long chained esters, is envisioned.

6.5.2. In-cylinder sampling results summary

As a demonstration of the utilisation of this in-cylinder sampling valve, the results outlined in Section 6.4 indicated great promise in the continued investigation of potential soot precursor formation within a combustion cycle. The comparison with the more controlled tubular reactor setup indicated that the samples taken were representative of the early stage pyrolysis of these fuels, supported by the significant levels of fuel detected at 370 CAD. The sampling mechanism was effective in drawing gas from the cylinder and maintaining significant levels of precursor species.

As a starting point, heptane and heptanone comparisons were made to note any major differences in soot formation between the two fuels. As with the reactor results, no major differences in molecular breakdown were noted between the hydrocarbon and its ketone analogue. Future work should investigate more complex molecules, such as lactones and other bioderived oxygenated molecules that represent promising biofuels, and where the relative benefit in reducing overall soot formation is not fully understood. Additional sampling timings should also be employed in further investigations, in order to provide a more detailed

picture of the formation and consumption of these precursors, relative to the PAHs they form

and, ultimately, the respective tailpipe particulate emissions.

7. Aspiration of aqueous ammonia with pilot injection of diesel in a compression ignition engine

7.1. Motivation

The biofuels tested herein are envisioned as providing potential solutions to the need for reducing carbon emissions and the release of harmful exhaust gas emissions from on-the-road vehicles. For the most part, utilisation of these fuels would centre around heavy duty vehicles, since the electrification of most vehicles appears to be the future of the transport sector, but heavy duty machinery still requires diesel fuelled power units.

However, while the infrastructure of electric charging points may be conceivable in a developed country, many countries rely on internal combustion engines for transport through sparsely populated environments with few households or industry- one of the main advantages of the ICE is its far-reaching capability, with market penetration in extremely remote locations.[153] Transport of hydrogen fuel to filling stations could potentially be performed in a not dissimilar way to that of fossil petrol and diesel now, although it is a more hazardous and complex material to deal with, and therefore its use in the developing world may be limited. One potential use of hydrogen is in marine applications, in ocean tanker engines for example.[432] This industry could make significant use of hydrogen fuel since the issues associated with transporting the fuels to less developed environments are not present, and the ability to use electricity alone is not feasible for transport ships. Safety, however, is still a problem here. Large amounts of hydrogen on ships crossing oceans, facing harsh conditions, is unlikely to see large investment. Hydrogen also possesses a very low energy density (10 kJ/l) at atmospheric conditions, therefore options such as compression, liquification or the use of metal hydrides have been explored as ways of boosting this density.[433] Unfortunately,

compression does not enhance the energy density to high enough levels to be used as long term storage (4.5 GJ/m^3 required), while liquified hydrogen requires extremely low temperatures that are expensive to maintain. Metal hydrides meanwhile require temperature/pressure swings for adsorption and desorption, and are in themselves expensive. A potential solution to this is the use of ammonia. Bicer and Dincer[432] published a life cycle analysis of using ammonia as a maritime fuel, noting that even the partial use of these fuels could see a significant reduction in total GHG emissions. while also citing the ease of transporting ammonia through pipelines, by railway and by ship as another major benefit of using this as a marine fuel over hydrogen itself. Furthermore, ammonia spills are deemed less hazardous than spills of heavy oils that are normally used on ocean tankers. Moreover, only moderate pressures and atmospheric temperatures are required for ammonia to be in a liquid phase, making transportation and storage much simpler.

A common theme in literature is the suggested use of blends of ammonia (Section 2.2.2.6), either with other hydrogen derived fuels or in combination with a small amount of fossil fuel, acting as pilot injected ignition and combustion promoters. To this end, this study presents testing of pilot ignited aqueous ammonia in a light duty diesel engine in order to provide insights into its feasibility as a sustainable fuel for combustion engines, potentially in the heavy duty and marine sectors.

The study by Reiter and Kong provided a comprehensive investigation of compression ignition engine operation using both diesel and ammonia.[249] However, despite advantages relative to H$_2$, ammonia remains difficult and dangerous to handle and so, for the current study, a solution of ammonium hydroxide (NH$_4$OH) was instead used to investigate the potential contribution to energy release during combustion when ammonia is present in this form. Ammonium hydroxide is synthesised by saturating water with ammonia, and could be a simple way of utilising ammonia within combustion engines (providing the water does not inhibit any combustion or result in excessively high pollutants) without the need for compression or

cooling of ammonia itself. However, the injection of ammonium hydroxide can be expected to alter emissions characteristics beyond that which can be accounted for by the ammonia itself. A series of experiments were undertaken in a single cylinder diesel engine investigating combustion and emissions characteristics where a range of engine loads were achieved by varying the relative proportion of intake air aspirated ammonium hydroxide solution and direct injected fossil diesel fuel.

7.2. Experimental procedure

In order to reduce any potential reactions, or indeed phase separation, between NH_4OH and diesel, mixing of the two fuels and subsequent injection through the same injector was deemed undesirable. Further, the Delphi injector used for diesel injection was not compatible with NH_4OH due to its very poor lubricity, while the constant evaporation of ammonia into the gaseous phase may have caused injection problems. Therefore, a system using a pilot direct injection of diesel was employed alongside aspiration of the ammonium solution. The fossil diesel utilised was of zero FAME content and obtained from Haltermann Carless, while the 28% NH_3 Ammonium hydroxide solution was sourced from Sigma-Aldrich (boiling point: 38°C, melting point: -58°C, density: 0.9 g/ml at 25°C, vapour pressure: 2160 mmHg at 25°C).

For all engine experiments, ammonium hydroxide was aspirated into the engine air intake manifold via a port fuel injector, while the fossil diesel fuel was direct injected and supplied by a conventional common rail circuit. Given the constant evaporation of ammonia from this solution, however, it was important to minimise the potential escape of ammonia via an open lid. A pressure vessel containing the ammonium solution was pressurised to 2 bar and connected via a short length of pipe to a Bosch gasoline fuel injector installed into the air intake of the diesel engine. Initial attempts were made to blend a fuel with a high cetane number, diethyl ether (DEE), with the aqueous ammonia in an attempt to achieve autoignition of the

ammonia in the absence of pilot ignition. This, however, did not achieve ammonia combustion as it was noted that DEE and ammonium hydroxide were not miscible.

Therefore, for all experiments reported in this work, fossil diesel was direct injected at a constant injection timing of 10 degrees BTDC and 550 bar injection pressure, so as to reach in-cylinder conditions at which the intake air aspirated aqueous ammonia contributed to heat release during combustion. Table 7.1 summarises the conditions of the pilot ignited ammonium hydroxide engine tests. Diesel and aqueous ammonia injection durations during each test are outlined in Table 7.1, while the engine speed was maintained at 1200 rpm for all tests.

Initially, during diesel-only combustion, engine load was maintained at the desired value by adjusting diesel injection durations on the fly. Ammonium hydroxide was then aspirated into the engine in order to increase the engine load by 0.5 bar and 1 bar, during which time the diesel injection duration was maintained at the rate that corresponded with contributing 4 bar IMEP (645µs). Diesel injection was then lowered at maximum load (D4A1: 5 bar IMEP), where ammonium hydroxide was contributing to 20% of the energy contribution, and the ammonium hydroxide aspiration rate was held constant as the overall engine load was lowered (a 2750µs injection duration). This thereby increased the proportion of energy released by the aqueous ammonia, relative to diesel (A1D3.5: 22% NH_4OH energy contribution, A1D3: 25% NH_4OH energy contribution).

Both the frequency and duration of opening of the PFI injector supplying aqueous ammonia could be controlled but, for ease of comparison, only the duration was altered, while the frequency was kept to a low value of 1.9Hz. Injector calibration was performed by bench testing the injection set-up, using water rather than NH_4OH due to similar physical properties, but greater hazard, of handling ammonium hydroxide (full face masks were used when ammonium hydroxide was exposed to the atmosphere). A fixed injection frequency and varying durations were output from the injector driver and measured using an oscilloscope, timed for 1 minute,

and the quantity of water remaining in the vessel subtracted from the original volume. This enabled flow rates to be calculated for a given injector pulse duration (see appendix Table B1).

Initial tests were performed with injection of fossil diesel only, with the injector opening duration set so as to maintain a constant engine IMEP of 4 bar, 4.5 bar and 5 bar. In following experiments, the level of ammonium hydroxide aspirated into the intake manifold was gradually increased so as to increase the engine IMEP by 0.5 bar and then 1 bar (4.5 bar and then 5 bar overall respectively). Subsequently, the amount of diesel injected was gradually reduced, while maintaining a constant level of ammonium hydroxide aspiration, such that the engine load was reduced to 4.5 bar and then 4 bar IMEP. This was to allow a comparison to be made between combustion at equivalent engine loads, but with differing energy contributions from the aqueous ammonia and fossil diesel.

Table 7.1: **Overview of test conditions**

Test	Diesel Injection (us)	Ammonia Injection (us)	Inlet Temperature (°C)	Diesel Load (bar IMEP)	Ammonia Load (bar IMEP)	Ammonia Load Contribution (%)	Abbreviation
1	662	0	83.1	4	0	0	*D4 (Start)*
2	692	0	83.8	4.5	0	0	*D4.5*
3	730	0	84.1	5	0	0	*D5*
4	645	1400	74.8	4	0.5	11	*D4A0.5*
5	645	2750	36.1	4	1	20	*D4A1*
6	611	2750	28.5	3.5	1	22	*A1D3.5*
7	582	2750	27.3	3	1	25	*A1D3*
8	639	0	28.0	4	0	0	*D4(ST)*
9	643	0	83.1	4	0	0	*D4(End)*
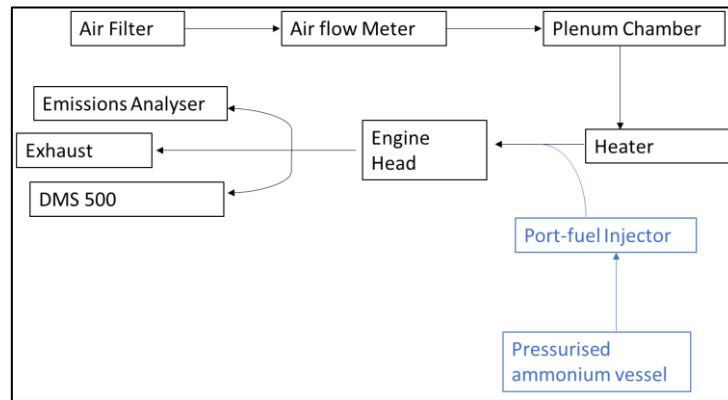
Figure 7.1: Schematic of air intake system

Intake air temperatures were raised utilising an inline air heater (Secomak 571), placed approximately 260mm prior to the port injector, and 330mm upstream of the intake manifold. The temperature was set to 80°C using a PID control system, though the actual inlet temperature, as indicated in Table 7.1, varied depending on the injection rate of ammonium hydroxide. As seen from Figure 7.1, port fuel injection was placed downstream of the heater, to remove any risk of accidental ammonia ignition in the intake. It was noted though that, due to ammonium hydroxide injection, the air temperature reduced to atmospheric levels once it had reached the manifold, necessitating the diesel test D4(ST), that utilised pure diesel combustion at the same air intake temperatures. Ammonium hydroxide port fuel injection was achieved using a Hartridge (HK852) signal unit to send a signal of set frequency and duration that released ammonium solution into the intake manifold at a pressure of 2 bar. It was assumed that chemical interaction between ammonium hydroxide and lubricant oil was negligible, due to high turnover rate and relatively low concentration of ammonium hydroxide present in the air manifold.

7.3. Results and discussion

7.3.1. Ignition delay
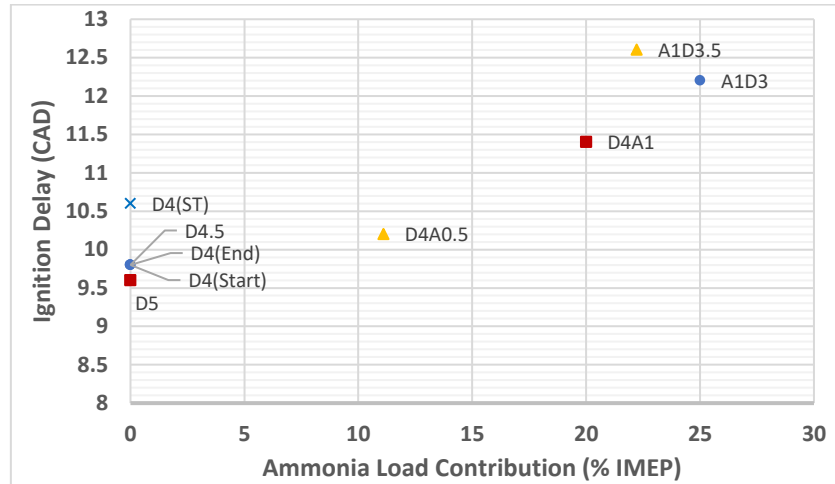
Figure 7.2: Ignition delay during Diesel-led combustion at varying engine loads and ammonia contributions. Blue circle (4bar), Yellow triangle (4.5bar), Red square (5bar)

Figure 7.2 shows the observed ignition delay at each of the fuel and load combinations tested (Table 7.1). Immediately apparent from Figure 7.2 is a significant increase in the duration of ignition delay as more of the engine load is attributed to the combustion of ammonia, both at constant engine load and where the diesel fuel injection duration was held constant. One of the most notable features of the aspiration of aqueous ammonia was its effect on the intake air temperature; the intake temperature for all tests was set at 80°C (except for the D4(ST) test), however the ammonium hydroxide injection occurred downstream of the heater and the evaporation of this solution lowered the intake air to almost room temperature just prior to the engine intake valves. This reduced intake- and thus compression- temperature would naturally see a decrease in the rates of the early stage combustion kinetics, which dictate the ignition delay period, and have a knock-on effect on the combustion conditions itself. Since this reduction in the intake temperature was noted during all tests with aspirated aqueous ammonia, and would therefore obscure any notable effect on the ignition delay period

attributable to the ammonia itself, a test was also performed at 4 bar IMEP for diesel only with no heating of the air intake (D4(ST) test). As illustrated in Figure 7.2, with reduced intake air temperature the ignition delay increased from 9.8 (D4(Start)) to 10.6 (D4(ST)) for the diesel only tests at constant load. While this indicates that a significant proportion of the ignition quality of the air fuel mixture may be due to the temperature of the intake air, this delay period is still less than that of the ammonia and diesel test conducted at the same load condition (A1D3). As noted extensively in the literature, ammonia possesses high resistance to autoignition- the autoignition temperature of ammonia is 651°C compared to 225°C for diesel[262]- far greater than that of other hydrogen carrier fuels such as methanol or diatomic hydrogen, and so it is likely that the extended ignition delay of diesel-ammonia combustion is attributable to the ammonia itself. It is also interesting to note that the ignition delay variability seen in Figure 7.2 is minimal when comparing engine load changes for the same fuel, for example the ignition delay of diesel only combustion varies from 9.8 CAD to 9.6 CAD at 4 bar to 5 bar IMEP respectively, which can likely be attributed to the higher in cylinder temperatures at the higher load condition.

An initial study by Gray confirmed that combustion of ammonia through means of compression alone was not feasible given the compression ratios and elevated inlet temperatures required for only moderate performance.[155] The notable reduction in temperature of the inlet air is due to the water in the ammonia solution used. Pure ammonia is a toxic gas and thus carries a considerable safety risk. This toxicity also means that care needs to be taken to avoid ammonia slip, whereby ammonia enters the atmosphere with other pollutants via the engine exhaust; catalysts may be used in this case, and since these are already present in modern powertrains for road transport, it may not add considerable cost. The use of ammonium hydroxide solution may mitigate some of these toxic effects, however, the use of this ammonia source has been shown here to have a negative impact on the ignition quality of the direct injected diesel fuel, attributable to the very high heat capacity and dilution of the

reacting mixture, and potentially limiting the contribution to engine IMEP. It is apparent, however, that the air intake temperature is not the only reason behind the change in ignition delay- the high resistance of ammonia to autoignition is clear.

7.3.2. Heat release rate
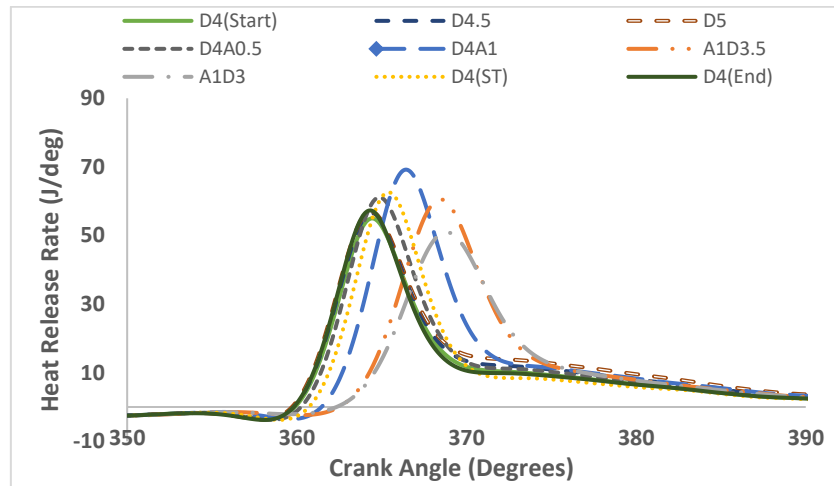
Figure 7.3: Apparent net heat release rate during co-combustion of diesel fuel and aspirated aqueous ammonia at varying engine IMEP

The heat release rates shown in Figure 7.3 indicate that combustion phasing was retarded as a greater proportion of ammonia was responsible for energy release. Initially, it can be seen that a change in the engine load from 4 to 5 bar IMEP when using diesel only saw little change in combustion phasing (from D4(Start) to D4.5 to D5); the peak heat release rate (pHRR) is generally dictated by the ignition delay period, which was similar for all 3 engine loads, while a slight difference was noted in the diffusion controlled combustion phase. This is expected since more energy is released at higher loads and limited energy increase is attributable to the premixed combustion phase given that the ignition delay period (and therefore the amount of fuel and air mixed prior to the start of combustion) is very similar in these cases.

It can also be seen in Figure 7.3 that, from the difference between D4(Start) and D4(End), the engine drift from the start of the day to the end was minimal in terms of heat release, while

the delayed phasing of the D4(ST) test condition also highlights the effect of operating the air intake at atmospheric conditions. In general, ignition delay and heat release rate can be expected to reduce and increase slightly from the start to end of a testing day, due to higher oil and coolant temperatures and better lubrication of the injector through sustained use of diesel. The fact that this potential engine drift is not apparent here gives more certainty towards the impact gauged from ammonium hydroxide aspiration. The cooler inlet air reduces reaction rates and thus extends the ignition delay period, leading to higher peak heat release. Comparing the heat release rates of D4(ST) and A1D3, it is apparent that the addition of ammonia delayed the start of combustion considerably; in general, a longer delay period sees a higher peak heat release rate but it can be seen that the substitution of diesel fuel for energy release from aqueous ammonia resulted in an appreciable decrease in the values of peak heat release. In the case of A1D3, energy release occurs later into the expansion stroke at higher volume conditions and this likely results in greater heat losses due to the larger exposed surface area of in-cylinder wall. This retardation was very pronounced, and resulted in a lower combustion stability that can be observed from the large coefficient of variation (COV) of engine loads calculated for this test, as shown in Table 7.2 below. Indicated by the COV values is an increase in combustion instability with an increasing ammonium load contribution and decrease in overall engine load.

Table 7.2: Coefficient of variation (%) of base diesel tests at varying loads, compared to tests conducted using 0.5 bar and 1 bar ammonium load contribution

Test	COV (of IMEP) (%)
D4 (Start)	1.05
D4.5	0.84
D5	0.74
D4(ST)	0.97
D4 (End)	0.94
D4A0.5	1.10
D4A1	0.96
A1D3.5	1.15
A1D3	1.55

Figure 7.3 also shows heat release rates at 4.5 bar IMEP and at 3 different conditions; with diesel only (D4.5), diesel contributing 4 bar IMEP and aspirated aqueous ammonia 0.5 bar (D4A0.5), and when aqueous ammonia is contributing 1 bar and diesel 3.5 bar (A1D3.5). Apparent from the heat release at this condition is that when increasing the amount of aspirated aqueous ammonia from zero to a contribution of 0.5 bar IMEP, the ignition delay and the peak rate of heat release rate both increase. As the contribution of ammonia was further increased to 1 bar IMEP, the ignition delay increased, but the peak rate of heat release began to decrease. This suggests that there was sufficient diesel injection in the D4A0.5 test to maintain reaction rates such that the dual fuel charge ignited without extending the delay period significantly relative to diesel only combustion. As a result, the peak heat release rate increases in line with the longer delay period in the case of the D4A0.5 test. In addition to greater heat losses, the lower peak heat release rate of the A1D3.5 can likely be attributed to the extended duration of ignition delay resulting in an over-dilution of the diesel fuel in air. Similar

observations have been made in Reactivity Controlled Compression Ignition (RCCI) experiments employing methanol, another premixed fuel with low ignition quality, in combination with diesel fuel.[434]

5 bar IMEP conditions, with and without the use of ammonia, are outlined. In this case, the load appears to be high enough that in-cylinder conditions are suitable for ammonia to contribute effectively towards energy release (compared to when the total load is set to 4 bar IMEP, with ammonia also contributing 1 bar). The delay period is extended in the D4A1 test, and therefore a higher pHRR is observed compared to the D5 test, as a result of the longer period allowed for premixing of fuel and air. A further observation is that, when the engine load is increased using ammonia, the difference is observed primarily in the premixed phase. When comparing pure diesel combustion at 5 bar (D5), and combustion at 5 bar utilising 1 bar IMEP from ammonia, the premixed burn fraction was increased, from approximately 56% to 63%. Furthermore, increased ammonia combustion contribution saw the extent of the premixed fraction extend further to 67% for the A1D3.5 run and 65% for the A1D3 test. Naturally a greater proportion of the diesel is combusted in the premixed phase due to the longer delay period, but it is suggested that ammonia combustion is also more prevalent in the premixed phase.

7.3.3. CO emissions
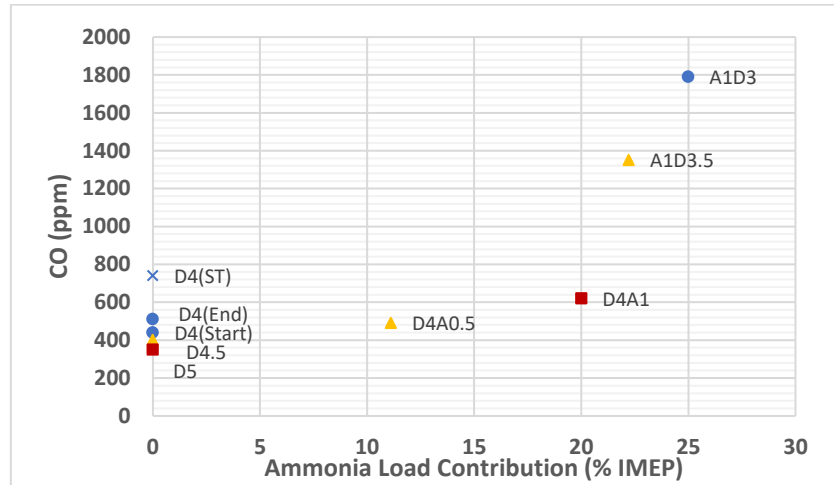
Figure 7.4: Carbon monoxide concentrations in the exhaust gas at various engine loads and ammonia injection rates. Blue circle (4bar), Yellow triangle (4.5bar), Red square (5bar)

Figure 7.4 shows that, for all engine loads, as the amount of aqueous ammonia supplied was increased- with a concurrent reduction in the duration of the diesel injection- levels of CO in the exhaust increased. This is contrary to the study of Grannell *et al*[256] with gaseous ammonia in an SI engine, where an increased proportion of fossil fuel seeing higher CO emissions. While the study by Reiter of CI combustion of ammonia and diesel/biodiesel did not measure CO emissions, a similar trend in HC emissions to the one seen here in CO concentration was noted, and postulated to be due to lower combustion temperatures.[249]

A further related explanation is that the extended ignition delay period observed with increasing proportions of aqueous ammonia present, potentially increased fuel impingement on the cylinder walls and thus levels of incomplete combustion. When the duration of diesel injection is reduced, temperatures are lowered further and, eventually, saw unstable combustion in the case of the A1D3 test, indicated by the highest COV in IMEP shown in Table 7.2. Considering the diesel only experiments, CO levels reduce at higher loads, primarily as a result of higher combustion temperatures, rather than the trend noted in SI combustion[256] whereby the CO output is far more sensitive to the actual amount of fuel carbon injected (with

dissociation also likely an important factor in CO formation and typically absent during CI combustion). While, in the case of the diesel only tests, higher engine loads see a decrease in CO emissions, the same trend is not apparent where higher levels of aspirated aqueous ammonia were used to increase the power output (Figure 7.4), suggesting that the resultant reduction of in-cylinder temperature dominates the CO emissions and produces an apparent reduction in diesel fuel combustion efficiency.

One potential contributor to the increased CO emissions with increasing presence of aqueous ammonia is the reduced intake air temperature caused by the increase in heat capacity of the charge gas that the ammonium hydroxide affords; not only does this lead to the aforementioned extended ignition delay through reduced reaction rates it will likely also impair the efficiency of fuel air mixing, which could see an increase of overly lean or rich regions within the combustion zone, and therefore greater CO formation. However, as can be seen from the D4(ST) result in Figure 7.4 with an intake air temperature of 25°C, this reduced temperature sees only a 0.03% increase in CO emissions compared to D4(Start) and D4(End), as opposed to the 0.14% increase with aspiration of aqueous ammonia at the same load of 4 bar IMEP (A1D3). This observation suggests that a decreased inlet air temperature alone is not sufficient to explain the observed increase in CO concentration. Furthermore, there appears to be a linear increase in CO emissions when reducing the duration of diesel injection from 645μs to 582μs (D4A1 to A1D3), which is a more considerable increase than seen when gradually adding ammonia to a fixed quantity of diesel. It may be inferred from this, again, that a minimum engine load, or duration of diesel injection, is required for the aspirated ammonia to contribute effectively to the combustion process and energy release. It is suggested that when the duration of diesel injection is too low, combustion does not propagate effectively through the premixed aqueous ammonia and the combustion efficiency of the direct injected diesel, resulting in significantly elevated levels of CO in the exhaust (Figure 7.4).

7.3.4. NOx emissions
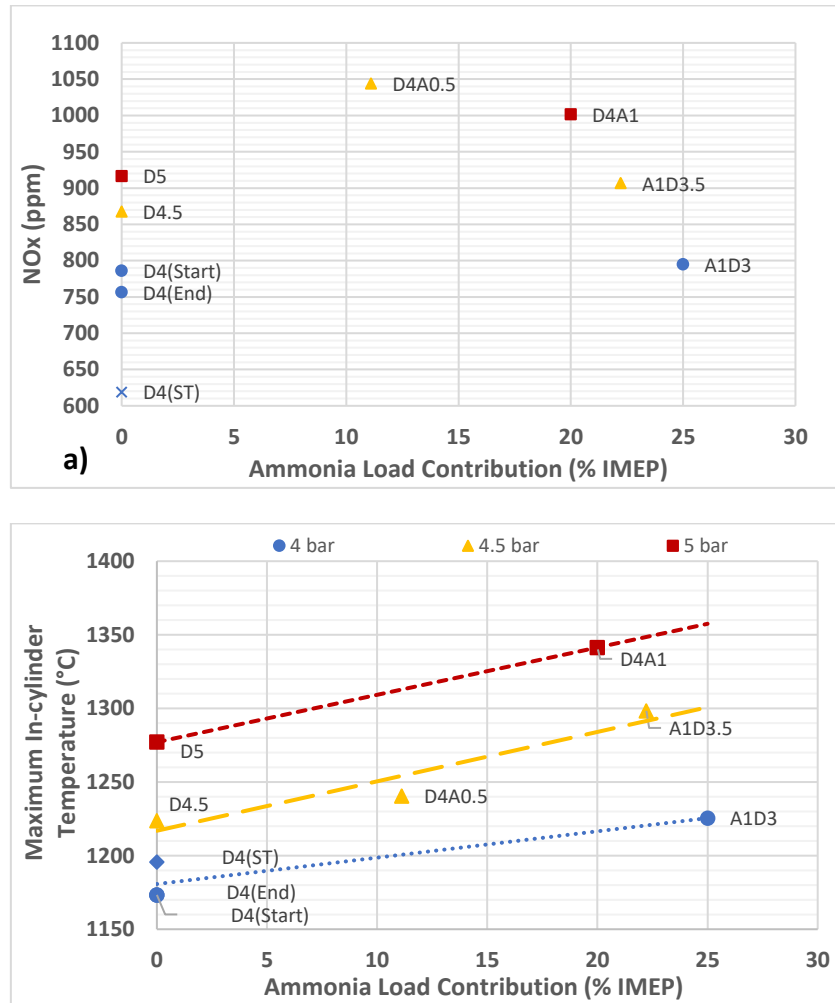
Figure 7.5: (a) NOx concentrations in the exhaust gas at various engine loads and ammonia injection rates. Blue circle (4bar), Yellow triangle (4.5bar), Red square (5bar) and (b) peak in-cylinder global temperatures calculated at various engine loads and ammonia injection rates. Blue circle (4bar), Yellow triangle (4.5bar), Red square (5bar)

The aforementioned higher temperatures at higher engine load can also be inferred from Figure 7.5a with an increase in NOx emissions at higher load conditions with the use of diesel alone, while the calculated maximum global in-cylinder temperatures shown in Figure 7.5b further support this assumption. Maximum in-cylinder temperatures were calculated assuming

the ideal gas law applies (see appendix A); it is assumed that the molar flow into the cylinder is constant, therefore the molar flow of ammonium hydroxide replaces the same moles of air, thus changing the mass. The new mass flow rate of air, with the addition of the mass flow of ammonium hydroxide, sees an overall reduction in mass flow rate relative to charge gas comprising air alone. An increase in temperature and NO_x with engine load are to be expected given the longer fuel injection with increasing load and thus higher combustion temperatures where rates of NO_x formation are highly temperature dependent.[435] Figure 7.5a shows an initial increase in NO_x levels with the aspiration of aqueous ammonia, relative to the diesel only test at the same engine load. This is in line with maximum in-cylinder temperature, illustrated in Figure 7.5b, though the small temperature increase alone observed in the D4A0.5 test, relative to D4.5, is unlikely to explain the large increase in NO_x emissions of just under 200ppm. In the case of the D4A0.5 test, the slightly longer ignition delay period (Figure 7.2) and higher pHRR (Figure 7.3) relative to diesel only at the same load, would likely cause the slightly higher in-cylinder temperatures. However, it is postulated that, in the case of ammonia combustion, NO_x is influenced by nitrogen in the ammonia when there is no appreciable change in maximum temperature, as is the case when comparing the tests at 4.5 bar IMEP with 0 and 12 % load contribution from the aspirated ammonia, D4.5 and D4A0.5 respectively. Moreover, it is suggested that the calculated global temperatures (which assume ideal gas behaviour of the cylinder contents) are inherently unlikely to show complete correlation with NO_x given that locally hotter regions are not discernible. In the case of the D4A0.5 test, NO_x levels are higher than in diesel only combustion at 5 bar (Figure 7.5a), D5, despite a significantly lower maximum in-cylinder temperature (Figure 7.5b). This indicates an effect beyond maximum global temperature in explaining NOx emissions during diesel and aspirated ammonia combustion. There is some potential that the nitrogen content of the aspirated ammonia itself contributes to NO_x formation. Wang and Herreros[258] noted that an increase in ammonia increased NO_x levels during experiments in a diesel engine, and the ratio of NO_2 to NO also increased. Reiter,

however, observed relatively low levels of NO_x emissions with the use of ammonia at levels of energy displacement up to 60% (after which the influence of fuel-bound nitrogen in the NH_3 molecule becomes prevalent), as a result of the lower combustion temperatures when NH_3 is aspirated.[249] Ryu,[262] meanwhile, observed an increase in NO_x with combustion of ammonia in an SI engine, attributed to the presence of fuel bound nitrogen. Grannell also noted a contribution of fuel-bound nitrogen, but highlighted the lowering of adiabatic flame temperature that ammonia affords as the main driver of trends in NO_x emissions during combustion.[256] Furthermore, Duynslaegher stated that, when using ammonia in an SI engine, the 'nitrogen monoxide concentration was very low due to relatively low combustion temperatures', implying little impact of nitrogen in the ammonia molecule on the type of nitrogen emissions in the exhaust.[250]

The influence that the ammonium solution aspiration has on the stoichiometry of the combustion mixture may also play a role in explaining the discrepancy in NO_x levels and peak in-cylinder temperature. While diesel combustion occurs predominately at stoichiometric conditions, ammonia combustion will occur at more lean conditions, having been delivered to the combustion chamber as a homogeneous mixture with the intake air. Reiter and Kong observed that, with a diesel energy contribution of greater than 60%, the BSFC of ammonia increases substantially, suggesting this could be due to the injected ammonia burning under conditions that were 'too lean' when concentrations were too low.[249] As stated previously, the D4A0.5 test- with only 12% of engine load attributable to the aspirated ammonia- produced slightly higher NO_x than the D4A1 test at higher 5 bar IMEP and ammonia providing 20 % of the engine load. This may be inferred as an indication of a peak level of ammonia injection in exacerbating NO_x emissions; ammonia levels are sufficient for appreciable NO_x formation from the fuel bound nitrogen, but any decrease in temperature arising from a decrease in stoichiometric diesel combustion and increase in lean premixed ammonia combustion is insufficient to reduce thermal NO_x (but this is the case when ammonia contributes greater than

20% of the total load). This could potentially explain why the maximum temperature observed in the D4A0.5 test was less than 20°C higher that of pure diesel and over 50°C when ammonia contributed 1 bar out of 4.5 bar IMEP; ammonia was overdiluted at the lower injection rate. Moreover, a study by Talibi $et\ al$,[243] utilising pure hydrogen in tandem with pilot injected diesel, showed that NO_x levels varied markedly- especially at earlier phases of combustion- depending on whether a sample was taken within the diesel spray or in between sprays. Within a spray the absence of air likely resulted in lower burn rates, while the hydrogen concentration was low. Between sprays, where hydrogen and diesel were mixed more homogenously, the high flame temperature of hydrogen in addition to heat release from diesel combustion was reflected in higher NO_x. Also observed was a threshold of hydrogen energy contribution, after which flame temperatures exceeded the amount required for NO_x formation, but below which the hydrogen-air mixture was overlean and elevated NO_x emissions relative to diesel only combustion were not observed.[243] It is again suggested that- in the current study- despite a slight decrease in maximum global temperature, the D4A0.5 test was possibly an 'optimal' condition to run the engine at for stable combustion, with both thermal and fuel-bound NO_x prevalent.

It has been noted before, but at this point may be pertinent to mention again, that NO_x formation requires both high temperatures and sufficient time at these conditions. Figure 7.6 indicates the time of occurrence of both maximum in-cylinder temperatures and peak heat release rates, with the interval between these two events tentatively suggested to correlate with the duration of high temperature conditions. Comparing the tests at 4.5 bar IMEP, diesel only combustion (D4.5) sees pHRR occur at 364.4 CAD and the maximum temperature is observed at 380.4 CAD, while during the D4A0.5 run, with 12 % of the engine IMEP contributed by the aspirated aqueous ammonia, the pHRR is shifted slightly later to 364.8 CAD and the maximum temperature are seen slightly earlier, at 379.6 CAD. Furthermore, when the contribution of ammonia is increased further (A1D3.5) to 22 % of IMEP, the time of pHRR is

retarded even further to 368.4 CAD, but the timing of maximum temperature was relatively unchanged, at 380 CAD. The shorter interval between peak heat release and maximum temperature when ammonia is injected at greater levels explains why the NO$_x$ levels may not be directly linked to peak in-cylinder temperatures, as these temperatures are present for a shorter duration than diesel only combustion.
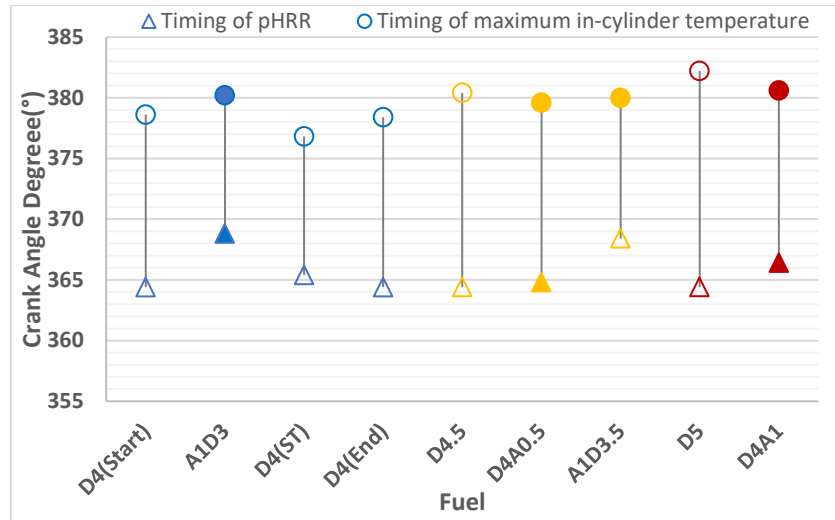
Figure 7.6: Timing of peak in-cylinder temperatures and peak heat release rate detected in tests conducted at various engine loads and ammonia injection rates (blue= 4 bar, yellow= 4.5 bar, red= 5 bar; hollow markers signify diesel only combustion)

7.3.5. Particulate emissions
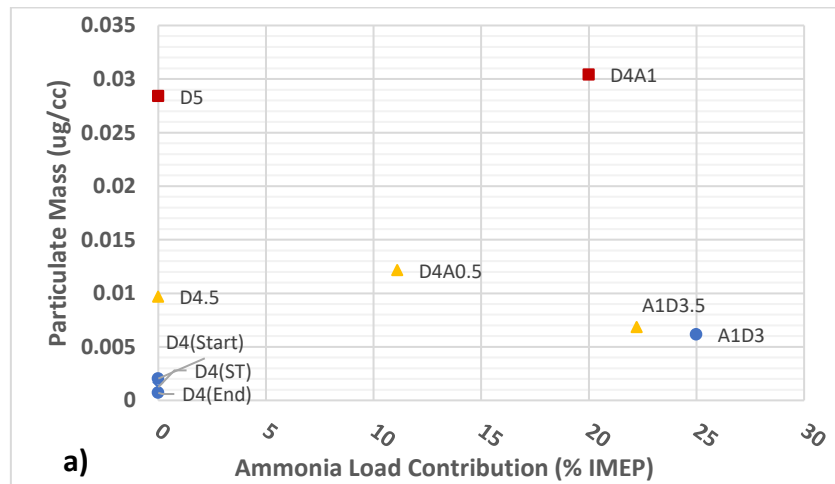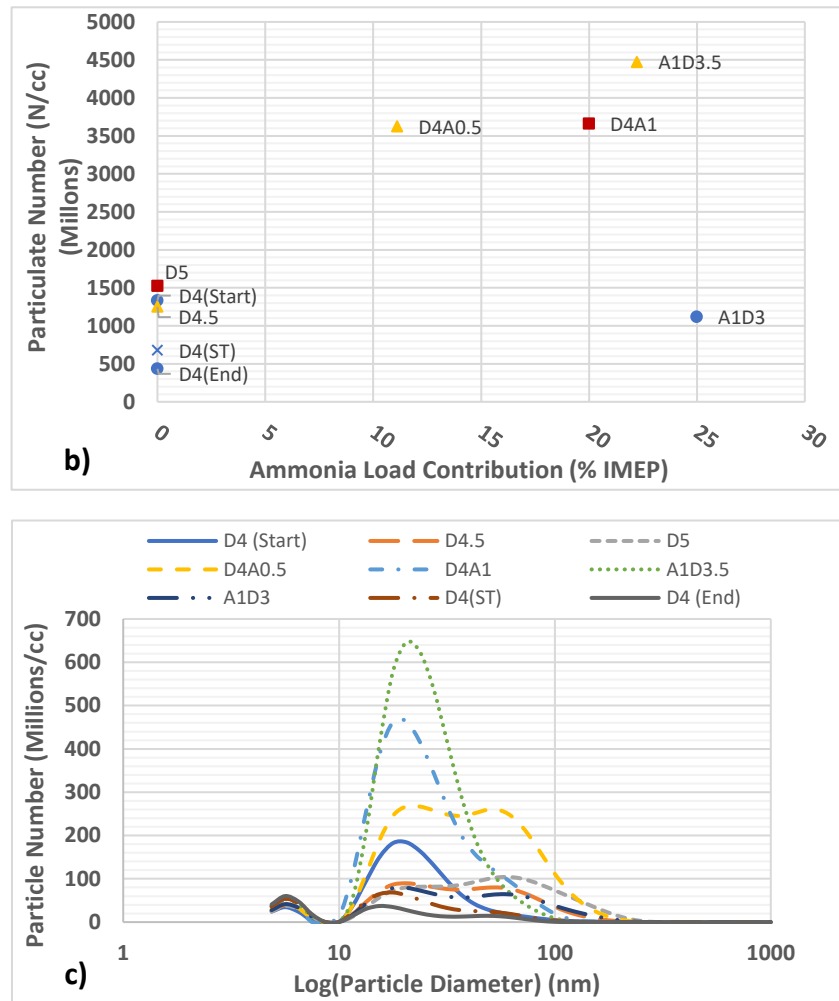
Figure 7.7: Particulate mass (a) and number (b) emissions, and size distribution (c) in the exhaust gases of tests conducted at various engine loads and ammonia injection rates. For (a) and (b), Blue circle (4bar), Yellow triangle (4.5bar), Red square (5bar)

Particulate emissions are not often reported during combustion testing with ammonia. However, Reiter and Kong published further results to their 2008 paper with soot emissions recorded,[436] observing a decrease in soot concentration as diesel was displaced with ammonia during combustion. However, they also state that soot emissions are increased if combustion temperatures are too low, with reduced rates of soot oxidation. For instance, 80:20 diesel: ammonia combustion saw higher emissions of soot than 100% diesel, since there was

still sufficient carbon within the fuel mix to produce soot, but the lower combustion temperature from the 20% ammonia reduced soot oxidation rates. The particulate mass and number measured during the current study is plotted in Figure 7.7. The first observation is the general increase in particle mass as IMEP increases. This is expected given the increase in the duration of diesel injection and therefore fuel carbon available to undergo pyrolysis and form particulates. Upon aspiration of ammonia to increase the engine load from 4bar- D4(Start)- to 4.5 bar IMEP (D4A0.5), the particulate mass and number increased, despite no change in hydrocarbon fuel input. Relatively, the particle number appeared to increase to a greater extent than that of the mass, potentially attributed to the longer ignition delay period, reducing the time subsequently available for particulate agglomeration. With regards to the increase in particle mass, this could be attributed to the increasing proportion of ammonia (and water) within the cylinder and the subsequent dilution of available air, though it was estimated that the reduction of air in the charge gas was slightly less than 4% during peak ammonium hydroxide injection. The same pattern is observed when comparing the tests at equivalent load conditions; the particulate mass increased relative to pure fossil diesel (D4.5 compared to D4A0.5) combustion. The cooling effect of aqueous ammonia aspiration on the air inlet from 80°C (diesel only test) to atmospheric temperature (diesel and ammonia test) could also be a cause for the increased particulate mass, as this may have had a negative impact on fuel vaporisation, resulting in a worsening of fuel droplet atomisation within the fuel spray and therefore more favourable conditions for soot formation in this instance. Figure 7.7 shows that diesel-only combustion, with the intake air temperature reduced to atmospheric temperature (D4(ST)), decreased the particulate number to a greater extent than the addition of ammonia (A1D3) relative to the initial diesel test at 4 bar IMEP, D4(Start) (with intake air at 80°C). This suggests that the extended ignition delay resulting from a lower intake air temperature is likely the most influential factor in the observed reduction in particulate number and that, potentially,

the aspiration of aqueous ammonia counteracts this to an extent, as indicated by the general increase in particle mass and number.

As seen from the CO emissions (Figure 7.4), the supply of aqueous ammonia becomes detrimental to complete combustion after a rate of aspiration equivalent to 20 % of the engine IMEP. This is also apparent from the particulate output, which requires more stable combustion for formation, compared to CO, to supply the temperatures needed for fuel pyrolysis. Particle mass (and number) initially increase with the addition of ammonia, likely due to combustion remaining efficient and the ammonium solution diluting the oxygen availability, promoting greater fuel pyrolysis. Comparing the tests conducted at 5 bar IMEP, where aspirated aqueous ammonia contributed to 1 bar IMEP of engine load (Figure 7.7b), the particle number also increases (D4A1 relative to D5), as there is still sufficient combustion stability for particulates to form.

From the particle size distribution shown in Figure 7.7c, a major observation to note is the decrease in particulates formed from the start to the end of the testing day, an expected trend as engine warm-up contributes to more efficient combustion. Furthermore, it is clear that the increase in particle number observed from ammonium hydroxide incorporated combustion is due to the increase in number of smaller particles, which would concur with the theory that delayed combustion, caused by an increase in the ignition delay period and subsequent extension of the premixing duration, results in a reduction in agglomeration mode particles, compared to nucleation mode. It is tentatively postulated that a proportion of the ammonia solution supplied is passing through unreacted, without contribution to energy release, and emitted in the exhaust; droplets of unreacted ammonium solution could be a cause of the increase in particle number (but a more minor effect on particulate mass) seen as ammonia aspiration is increased; ammonium salts are considered $PM_{2.5}$ material.[437] The particle distribution of A1D3.5 appears to support this hypothesis, with a marked increase in smaller particles. Since the particle spectrometer assumes a constant particle density, if these particles

were indeed ammonium hydroxide derived, and therefore of distinctly lower density than that assumed, then this could also explain why the particle mass is lower for this test than that with only 12 % contributed from ammonia to the same engine load (in addition to the fact that the particles measured were smaller). Unburnt hydrocarbons, containing carbonyl groups, can react with ammonia, forming nitrogen-containing organic compouds.[437] Furthermore, if a proportion of ammonium hydroxide is passing into the exhaust, it is suggested that chemical reactions between ammonia and reactive groups on the surface of the particulates are possible. These reactive species could be inorganic material, such as PAHs or, more likely, polar volatile organic compounds (VOCs) containing oxygen.[438] If these reactive groups are removed from the bulk surface, a decrease in particle size can be expected.

While the shift towards smaller particles is noted from D4A1 to A1D3.5, a further reduction in load to 4 bar IMEP (A1D3) does not continue the trend of greater ammonium hydroxide injection leading to smaller particles that are potentially less dense than the assumed value. However, the reduction in engine load may see different factors dominating and, compared against the D4(ST) test, the particulate output across the whole size range also increases for the A1D3 test. The expected increase in smaller particles may not be prevalent at this engine load where ammonia is making up 25 % of combustion energy contribution, since the lower load conditions result in lower temperatures that are potentially below the threshold required for significant fuel pyrolysis. This test sees the most dilute stoichiometry of diesel carbon to air, and so the fact that the particle number (and mass) increases would concur with the results at 4.5 bar and 5 bar, where ammonia injection sees an increase in particulate formation, most especially in the nucleation mode.

7.4. Conclusions

This study presents experiments utilising intake aspirated aqueous ammonia and direct injection diesel co-combustion in a compression ignition engine, investigating the potential of the ammonia solution to usefully a proportion of the energy provided by diesel fuel and the impact on exhaust emissions of doing so. From the findings of the engine experiments and modelling presented, the following conclusions can be drawn:

- Ignition of the aspirated aqueous ammonia was achieved, and contributed a maximum of 25% of the total engine load at 4 bar IMEP, albeit resulting in a significantly extended ignition delay period relative to diesel only combustion.

- Exhaust CO emissions increased near linearly with the proportion of engine load provided by aspirated aqueous ammonia, despite a concurrent reduction in the fuel carbon present. A similar increase in engine cycle to cycle variability was also observed, suggesting greater combustion instability with increasing levels of heat release contributed by the premixed aspirated ammonia relative to direct injected diesel.

- Levels of NO_X in the engine exhaust increased initially with the level of aqueous ammonia present, but decreased at ammonia engine load contribution levels greater than 20 %. The initial increase in NO_X may be attributable to the increasing levels of fuel-bound nitrogen present from ammonia, however, at higher levels of aspiration this impact was offset by greater combustion instability and lower temperatures.

- A general increase in both particulate mass and number, as ammonia load contribution was increased, was observed. An especially significant increase in the number of nucleation mode particles was seen as ammonia injection increased, suggestive of the presence of ammonia solution droplets, until the 25% load

contribution from ammonia at 4 bar IMEP, at which it is suggested diesel was too dilute and combustion temperatures were too low to continue this trend.

8. Conclusions and potential future work

8.1. Summary

A summary of the previous chapters is compiled herein. The novelty of this work ranges from the use of previously untested fuels, to the use of a sampling technique to detect light hydrocarbons in the cylinder of a compression-ignition engine. In the case of the latter, the findings were not exhaustive, with significant setbacks encountered due to equipment failure and lab closures as a result of the pandemic. As such, recommendations for potential future work will also be made, making use of the original concept tested in the current study.

8.1.1. Literature review

Conclusions from the literature review (Chapter 2) are as follows:

- 2nd generation biofuels are an emerging technology that show high promise in reducing global GHG emissions and in representing a source of sustainable fuel that does not impede on agriculture and food production.

- A vast range of oxygenated fuels have been tested as blends in combustion engines. Alcohols represent a promising option based on availability i.e. ethanol and butanol, but while particulate mass reduced upon use of this fuel, combustion efficiency decreases, due to the relatively low calorific content, and NO_x emissions tend to increase.

- Recent investigations have therefore expanded into more exotic bio-derived molecules, including furans (cyclic ethers) and lactones (cyclic esters). Through the use of relatively simple hydrolysis and dehydration steps, fuel blending components MF and DMF can be synthesised from hemicellulose and cellulose respectively. These fuels have been tested in both gasoline and diesel fuelled engines.

- One of the major benefits of utilising these fuels is that their use tends to decrease the tailpipe particulate emissions (without the use of post-treatment). These particulates are formed via a complex process; unsaturated radical species form from fuel decomposition, which precedes growth to aromatic species and then PAHs through pathways such as the HACA mechanism.

- The role of oxygenated fuel molecules on the formation of soot particulates is still under research, but one of the main effects is the ability of fuel-bound oxygen to assist in the oxidation phase of soot; post formation. Hence, particulate mass generally decreases, but particle size tends to shift towards smaller (nucleation mode) forms, which can be more harmful to humans.

- Studies into the formation of particulates and their precursors, PAHs, under pyrolysis conditions and in engines, have implied a complex relationship between the initial fuel molecule and the method and degree of particulate formation. Chemical and molecular factors are often masked by the effects on the fuel physical properties, which can be more influential in determining overall particle emissions.

8.1.2. Second generation biomass-derived fuel blend combustion

The first series of fuels tested were based on their relative ease of production from 2nd generation biomass. The subsequent effect on combustion of these molecules can be found in Chapter 4:

- High blend ratios of relatively low carbon number furans could be used in a compression ignition engine while sustaining effective combustion.

- However, the biofuel molecule needed to possess a degree of saturation, as opposed to aromaticity, for it to ignite with diesel. Aromatic furan, MF and DMF, displayed 2 stage combustion, in which the biofuel component was ignited late in the combustion cycle.

- An increase in saturation decreased ignition delay and the formation of the incomplete combustion product, CO. NO_x emissions were highest with partially saturated DHF due to the longer ignition delay, compared to THF, but more stable combustion compared to aromatic furan.

- Particulate emissions on a mass basis decreased substantially when substituting 50% diesel with the biofuel. Particle number increased, likely due to the later onset of combustion and thus a reduced soot agglomeration and coagulation phase.

- The addition of methyl branches assisted in decreasing the ignition delay slightly, but the propensity to ignite increased markedly when utilising an ethyl branch, as opposed to two separate methyl branches.

- Addition of another oxygenated functional group decreased particle mass further, and again increased the particle number, suggesting the enhanced oxidation allowed for particle breakup. Alcohol group addition increased the ignition delay relative to the base alkylfuran, whereas a carbonyl group, placed either on a side chain or on the ring itself, decreased the delay period.

8.1.3. Combustion and emissions characteristics of lactone fuels in a diesel engine

The next series of fuels tested were lactones, which can also be sourced from 2nd generation biomass, although current sourcing is generally from 1st generation oils. These were chosen based on the molecular characteristics highlighted above that reduced particulate emissions as well as the ignition delay period. The results are surmised below:

- Blended C6 lactones- ε-caprolactone, δ-hexanolactone and γ-caprolactone- displayed promising ignition qualities, relative to butanol, an alcohol often employed in diesel blending experiments.

- Ignition delay decreased as the length of the side chain increased, but combustion was seemingly more stable in both ε-caprolactone and γ-caprolactone, compared to the methyl branched δ-hexanolactone which possessed the highest CO emissions and particle number. A similar trend was noted in literature, wherby methylfuran possessed higher sooting tendencies compared to furan and dimethylfuran.

- The C10 lactone, γ-decalactone, within the diesel-butanol blend, possessed excellent ignition quality, while also reducing particle mass significantly. All blends produced lower particle mass than base diesel.

- Two C10 and two C12 lactones were employed- based on their potential to be derived from biomass- as pure fuels in the diesel engine. Despite significant differences in physical properties compared to diesel, stable combustion was observed, with ignition delay approximate to that of base diesel.

- The high carbon number and long alkyl chains of the C12 lactones likely explain the relatively high particulate output of these fuels, which was comparable to diesel. C10 lactones showed greater alleviation of particulate emissions, likely due to a combination of lower carbon number and extended ignition delay relative to diesel.

8.1.4. Pyrolysis of C10 fuels in a tubular reactor

Based on the success of utilising a pure lactone fuel within the research engine, efforts were made to increase the understanding of the breakdown of this molecule, particularly in relation to its pyrolysis and subsequent inception of aromatic precursors and subsequently soot. A tubular reactor was employed here to enable more controlled conditions to expose the test fuels:

- C10 fuels underwent pyrolysis at three different pyrolysis conditions, with constant residence times and carbon flow rates.

- Detected patterns of light hydrocarbons, ranging from methane to benzene, were similar for all fuels, regardless of structure, but variations in species and abundance could be observed.

- Carbonyl addition to an hydrocarbon did not appear to change the reaction pathway of fuel decomposition, with the C=O bond likely unbroken during pyrolysis.

- The ether, di-n-amyl ether, appeared to reduce particulate emissions relative to the ketone equivalent, but did not see a major change in reaction pathway. However, both straight chain ester and cyclic ester (γ-decalactone) produced unique species at lower temperatures.

- Esters reduced the emissions of all precursors relative to the other fuels tested. The cyclic lactone is suggested to initially break the bond between ring and alkyl chain (forming a cyclic and straight chain intermediate), resulting in a differing reaction pathway to the straight chain version.

- A sampling valve was installed in the research engine and successfully utilised in sampling these gaseous precursors within the cylinder itself during combustion. While results were stressed as preliminary, initial experiments indicated comparable patterns of precursor formation, with some additional species detected that are postulated to form as a result of air-derived oxygen.

8.1.5. Utilisation of a hydrogen carrier in a compression ignition engine

While biofuels possess advantages such as carbon neutrality, and a decrease in particle formation, these fuels contain carbon. Therefore CO_2, a greenhouse gas, is emitted as a by-product. As a result, a fuel source containing no carbon was tested within the research engine:

- An investigation was undertaken in the use of aspirated ammonium hydroxide and pilot injected diesel. Ammonium hydroxide is a potential hydrogen carrier, and carries advantages over hydrogen and ammonia gas in both storage and safety aspects.

- Increasing levels of ammonium hydroxide aspiration increased CO emissions, and initially increased NO_x emissions before combustion temperatures became too low to form thermal NO_x. Initial NO_x increase was postulated to be due to fuel-bound nitrogen from the ammonium hydroxide.

- Particulate emissions increased in both mass and number with an increased proportion of ammonium hydroxide load contribution (at the same load conditions). This could have been caused by ammonia derived particulates, or have been as a result of a reduction in concentration of intake oxygen, limiting particle oxidation and increasing oxygen deficient zones within the combustion chamber.

8.1.6. Overall conclusions

Oxygenated biofuels are potentially beneficial from an upstream and downstream perspective, decreasing the use of fossil fuels and decreasing the formation of harmful particulate emissions. The experimental investigations presented highlight the varying effect on combustion that a wide selection of novel fuels can possess. The substitution of diesel with a biofuel was likely a major factor in reducing pyrolysis products as a result of the reduced carbon atoms and aromatics available from the fuel. Variations in the ignition delay of the fuel were also an influence on the resulting combustion and emissions, with the bioderived molecules extending this period, often reducing particle mass but increasing number due to the retardation of the combustion event. The potential to source long chain cyclic esters from 2nd generation sources was shown, and their ability to be used as pure fuels was demonstrated. The molecular breakdown of these fuels, and their subsequent formation of particulate precursors, was investigated. A reduction in these gaseous precursors was observed upon use of these esters within a tubular reactor. Esters possess two oxygens by definition, and so the amount of pyrolysis products was reduced relative to a base hydrocarbon. However, lactones with a high enough carbon number were shown to produce comparable particulate

emissions to diesel in an engine. Pyrolysis studies implied a reduced formation of soot precursors for γ-decalactone breakdown and a different pathway to that shown in the straight chain analogue, implying detachment of the alkyl chain, as opposed to ring opening, as the main mechanism of decomposition. As a result, an increase in alkyl side chain length is seemingly directly linked to the increased formation of particulates.

The pattern of precursor formation appeared to be similar in a range of C10 fuels under pyrolysis conditions. Therefore, the impact on ignition delay and physical properties is still likely to be the predominant reason for the difference in emissions produced in an engine. Preliminary investigations using in-cylinder sampling suggested major pyrolysis products formed within an engine were comparable to those formed within a pyrolysis reactor.

Ammonium hydroxide represents a zero-carbon hydrogen carrier, reducing both GHG emissions and, potentially, carbon-based particulate emissions. Its aspiration did not alleviate the production of harmful emissions, however, ammonia acted as an additional energy source provided enough diesel injection was supplied for initial flame propagation.

8.2. Future work

This study has investigated a considerable range of potential future fuels, from easy-to-obtain 2nd generation furans, to a hydrogen carrier, ammonium hydroxide. However, while trends in emissions and combustion characteristics have been realised, the next step is optimisation. For example, it was shown that introducing saturated furans was positive in reducing particulate mass, but the particulate number increased, while emissions of CO and NO_x were marginally exacerbated. It is believed that tuning of the blend ratio may alleviate the production of CO and NO_x, which were both postulated to have increased due to an extended ignition delay leading to fuel impingement (producing CO emissions) and a high pHRR (generating high in-cylinder temperatures, and therefore NO_x). If the blend ratios of the bio-

component was reduced slightly, benefits in particulate mass reduction and fossil fuel utilisation could be maintained while, potentially, the reduction of ignition delay could reduce gaseous emissions.

This same principle of optimisation is also hoped to enhance the understanding of introducing ammonium hydroxide solution into the intake manifold of diesel engines. Preliminary studies suggested that ammonia could contribute effectively towards combustion, but appeared to increase emissions in the process. Future investigations could consider the use of an ammonium hydroxide blend with a higher cetane number, bioderived component that could overcome the reduction in combustion temperatures generated by the introduction of water into the charge gas. This reduction in combustion temperatures meant that, at higher ammonium hydroxide aspiration, combustion became unstable and the formation of incomplete combustion products increased.

Finally, it is hoped that the preliminary studies into the use of an in-cylinder sampling valve indicate the effectiveness of this technique in sampling gaseous soot precursors. Only heptane and heptanone components were tested here however, and so it is believed worthwhile to investigate the precursors formed during the combustion of lactone fuels, and other C10 molecules tested in the tubular reactor. Not only will the comparison between engine and reactor be useful in confirming the general differences, but one of the main advantages of the use of these lactones is a reduction in particle mass; it is therefore important to discern whether this effect is merely in the oxidation phase or whether the breakdown of these fuels affords lower precursor abundance within an engine. Sampling at a greater number of combustion timings would achieve this in forming a picture of precursor abundance from the start to the end of the biofuel combustion event.

8.3.   Contributions to knowledge

To summarise the work, the following contributions to knowledge are explicitly stated herein:

- Chapter 4 represents the first systematic study into the use of 2nd generation-derived furanic biofuels within a diesel engine, comparing molecular attributes: the degree of saturation, the level of alkyl branching, and the types of oxygenated functional groups present in the molecule.

- The results of the furan study indicated lactones as a desirable fuel source. All lactones tested in this study represented never-before-tested molecules within a combustion engine, and the use of some lactones as pure fuels represents a potential breakthrough in the types and sources of next generation biofuels.

- Utilising a tubular reactor and an in-cylinder sampling technique, molecular decomposition of lactones was analysed in detail by studying the abundance of gaseous hydrocarbons formed from fuel pyrolysis. Decomposition of the C10 molecules utilised has not been previously reported, and represents a novel means of determining the sooting tendency of a molecule on a chemical level.

- Chapter 7 utilised a novel hydrogen carrier- ammonium hydroxide- in conjunction with pilot injected diesel to show the potential of aqueous ammonia as an additional fuel source to a CI engine. Previous studies have utilised gaseous ammonia for this; the novel use of aqueous fuel was deemed a far safer employment of this fuel source.

Appendix A

Indicated mean effective pressure (IMEP)

During this work, the engine load is stated in terms of the indicated mean effective pressure. The IMEP is a measure of the work done by the engine per unit of swept volume; it is therefore independent of the size and number of the cylinders, as well as the speed of the engine. It is In order to calculate this, first the work performed per cycle is needed:

$$imep \left[\frac{N}{m^2}\right] = \frac{W_{c,i} \ (indicated \ work \ output \ [Nm] \ per \ cylinder \ per \ mechanical \ cycle)}{V_s \ swept \ volume \ per \ cylinder \ [m^3]} \qquad \text{(Eq A.1)}$$

$W_{c,i}$ is defined as:

$$W_{c,i} = \int p \ dV = - \int_{intake} p dV + \int^{compression} p dV - \int_{expansion} p dV + \int^{exhaust} p dV \quad \text{(Eq A.2)}$$

And V_s is found using equation A.3:

$$V_s = A_{bore}(m^2) * Stroke \ Length \ (m) \qquad \text{(Eq A.3)}$$

Heat release rate (HRR)

Heat release rates indicate the amount of heat necessary to add to the cylinder gases to cause the observable changes in pressure. The (apparent) heat release rate is therefore calculable by using the in-cylinder pressure and the volume of the cylinder at that time, given the position of the piston. The latter parameter can be found using the equation:

$$V = V_{clear} + [A_{bore}(l_{con} + r_{crank} - \sigma)] \qquad \text{(Eq A.4)}$$

where V is the clearance volume, l_c is the length of the connecting rod, r_{crank} is the crank radius, σ is the stroke position:

$$\sigma = r_{crank}\cos\theta + \sqrt{l_{con}^2\, r_{crank}^2 \sin^2\theta} \qquad \text{(Eq A.5)}$$

where θ is the crank angle with respect to TDC.

Using the value of V from equation A.4, heat release rates can be acquired:

$$\frac{dQ_n}{dt} = \frac{dQ_{com}}{dt} - \frac{dQ_{ht}}{dt} = p\frac{dV}{dt} + \frac{dU}{dt} \qquad \text{(Eq A.6)}$$

where dQ$_n$/dt is the amount of heat released by combustion minus the heat transfer from the system and U is the sensible internal energy of the system. This equation can be further iterated by assuming an ideal gas (hence this is an 'apparent' heat release calculation).

$$\frac{dQ_n}{dt} = p\frac{dV}{dt} + mc_v\frac{dT}{dt} \qquad \text{(Eq A.7)}$$

Substituting the ideal gas law, pV=mRT and eliminating T:

$$\frac{dQ_n}{dt} = \left(1 + \frac{c_v}{R}\right)p\frac{dV}{dt} + \frac{c_v}{R}V\frac{dp}{dt} = \frac{\gamma}{\gamma-1}p\frac{dV}{dt} + \frac{1}{\gamma-1}V\frac{dp}{dt} \qquad \text{(Eq A.8)}$$

where γ is the heat capacity ratio c_p/c_v (= 1.4 for air)

In-cylinder Temperature

Maximum mean apparent in-cylinder temperatures were calculated assuming the ideal gas law applies. Therefore:

$$pV = mRT \qquad \text{(Eq A.9)}$$

The pressure (p) is known, while the volume corresponding to that pressure is also known from equations A.4 and A.5. R is a constant while m refers to the mass of charge gas within the cylinder at that time. It is assumed that the mass of fuel injected has a negligible impact on the total mass of charge gas. Therefore, the mass of charge gas is the value corresponding to a full cylinder volume of air (assuming atmospheric pressure and temperature), with a 95% volumetric efficiency.

The volume of air can be converted to moles using the molar volume constant i.e 0.024m³:

$$no.\,of\,moles\,(n) = \frac{Volume\,(m^3)}{Molar\,Volume\,(\frac{m^3}{mol})} = \frac{0.49945 * 10^{-3} * 0.95}{0.024} = 0.019792 mol$$

which can then be converted to mass using the molar mass of air (28.97 g/mol):

$$Mass\,(m) = no.\,of\,moles * Molar\,Mass = 0.0198 * 28.97 = 0.573g = 0.000573kg$$

This value for mass was maintained for all maximum global in-cylinder temperature calculations.

Appendix B
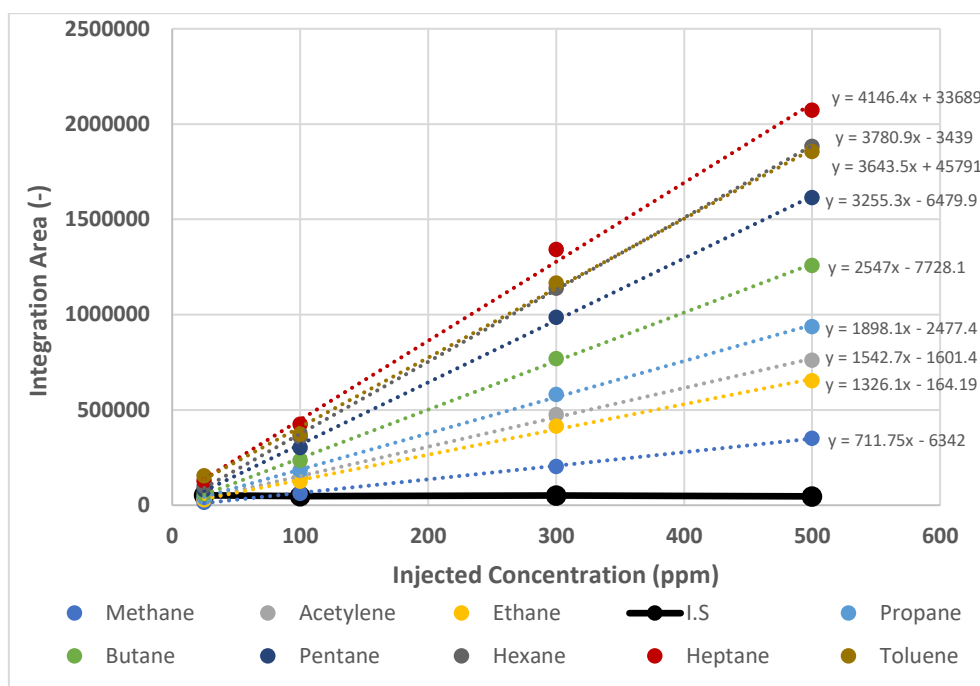
Figure B1: Calibration curve of gas mixture containing 1000ppm of all species plotted, diluted with nitrogen and constant volume of internal standard (IS)
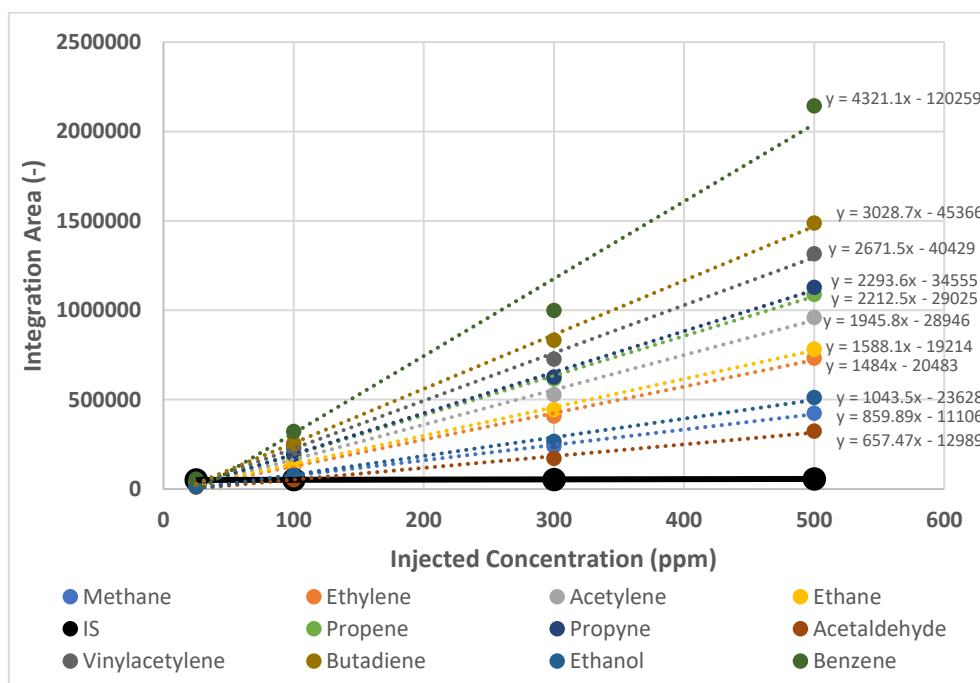
Figure B2: Calibration curves of external standard species at 25ppm, 100ppm, 300ppm and 500ppm concentrations, conducted at the start of pyrolysis testing

Table B1: **Port fuel injector calibration**

Injection Duration (µs)*	Time Elapsed (mins)	Water Injected (ml)	Flow Rate (ml/s)**
1200	2	17	0.14
1200	2	18	**0.15**
1200	2	19	0.16
2750	2	40	**0.33**
2750	2	38	0.32
2750	2	43	0.36

Measured using an oscilloscope to detect output signal from Hartridge control box
** *Median values in bold used as reference flow rates*

Table B2: Instrumentation uncertainty

Measurement Type	Measurement Purpose	Manufacturer	Instrumentational Error
Piezoresistive pressure transducer	In-cylinder pressure	Kistler	$\pm$0.18%
Shaft encoder	Combustion timing	Leine&Linde	$\pm$0.03%
Dynanometer	Engine speed	David McClure Ltd	$\pm$2%
Infrared	CO/CO_2 emissions	Horiba	$\pm$1%
Chemiluminescence	NO_x emissions	Horiba	$\pm$1%

Table B2 highlights the error present in some of the major equipment used in the current research. It is apparent that the instrumental error was relatively minor; for example, the variation of the in-cylinder pressure of 0.18% (combined with the the shaft encoder resolution) would have resulted in slight errors in the calculation of engine load, in-cylinder temperature and heat release rate. However, as noted by the error bars in the figures related to these parameters, the test-to-test variability observed was significantly greater than this; for example, in Figure 4.10, the maximum in-cylinder temperature varied by approximately +/-10°C (with absolute values of approximately 1200°C, equivalent to 0.8%), while Figure 5.4 shows a variation in heat release rate of approximately +/-0.3 J/deg, which is 0.5% of the absolute values of 64 J/deg. It is clear that test-to-test variation is greater than the instrumentation error (emissions results tended to vary during repeat tests by over +/-2%) signifying that hardware uncertainty itself did not unduly result in invalid conclusions throughout the research.

Appendix C

Figure C 1: Delphi 6-hole fuel injector
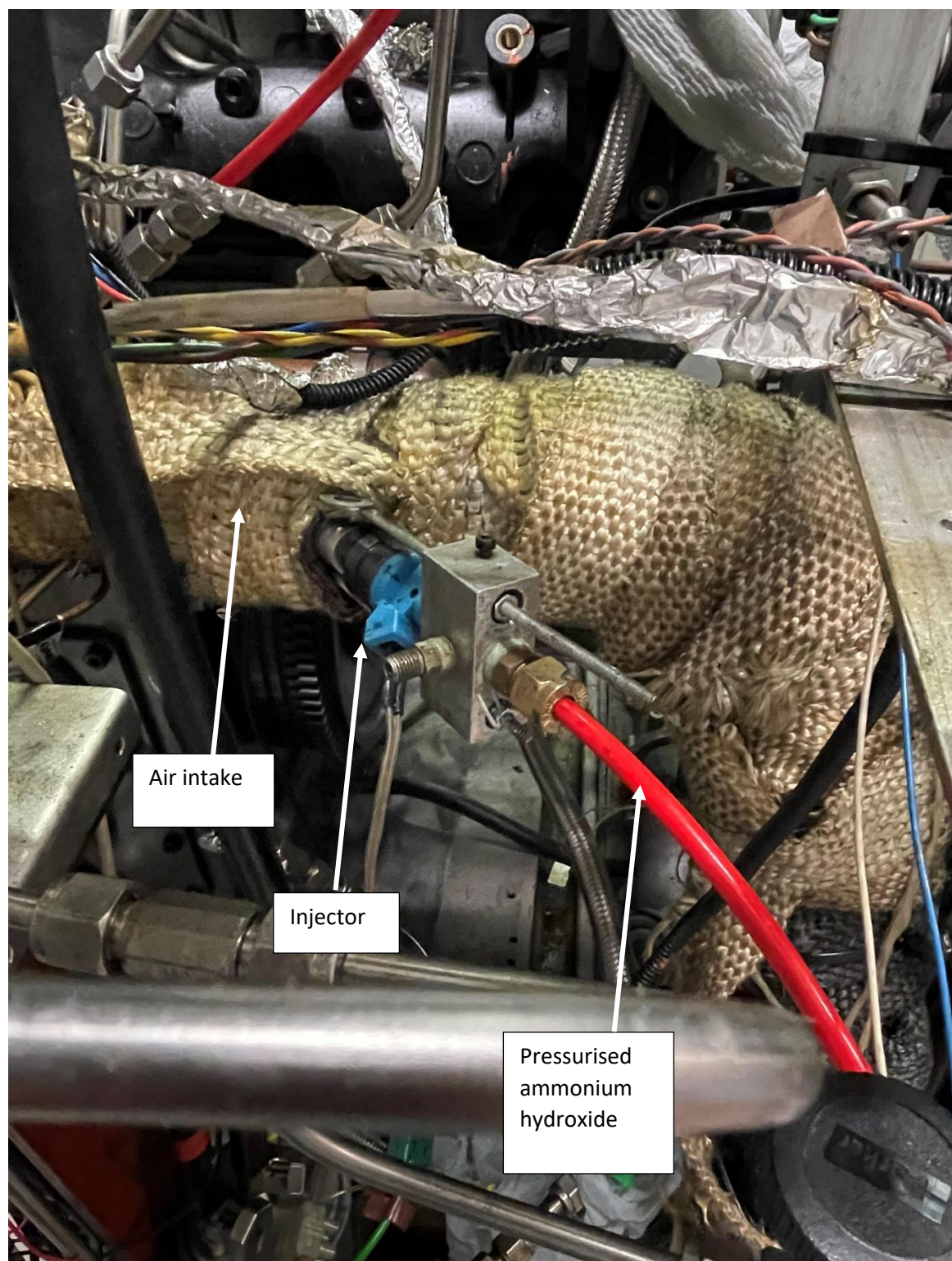
Figure C2: **Port fuel injector used during ammonium hydroxide aspiration**

:
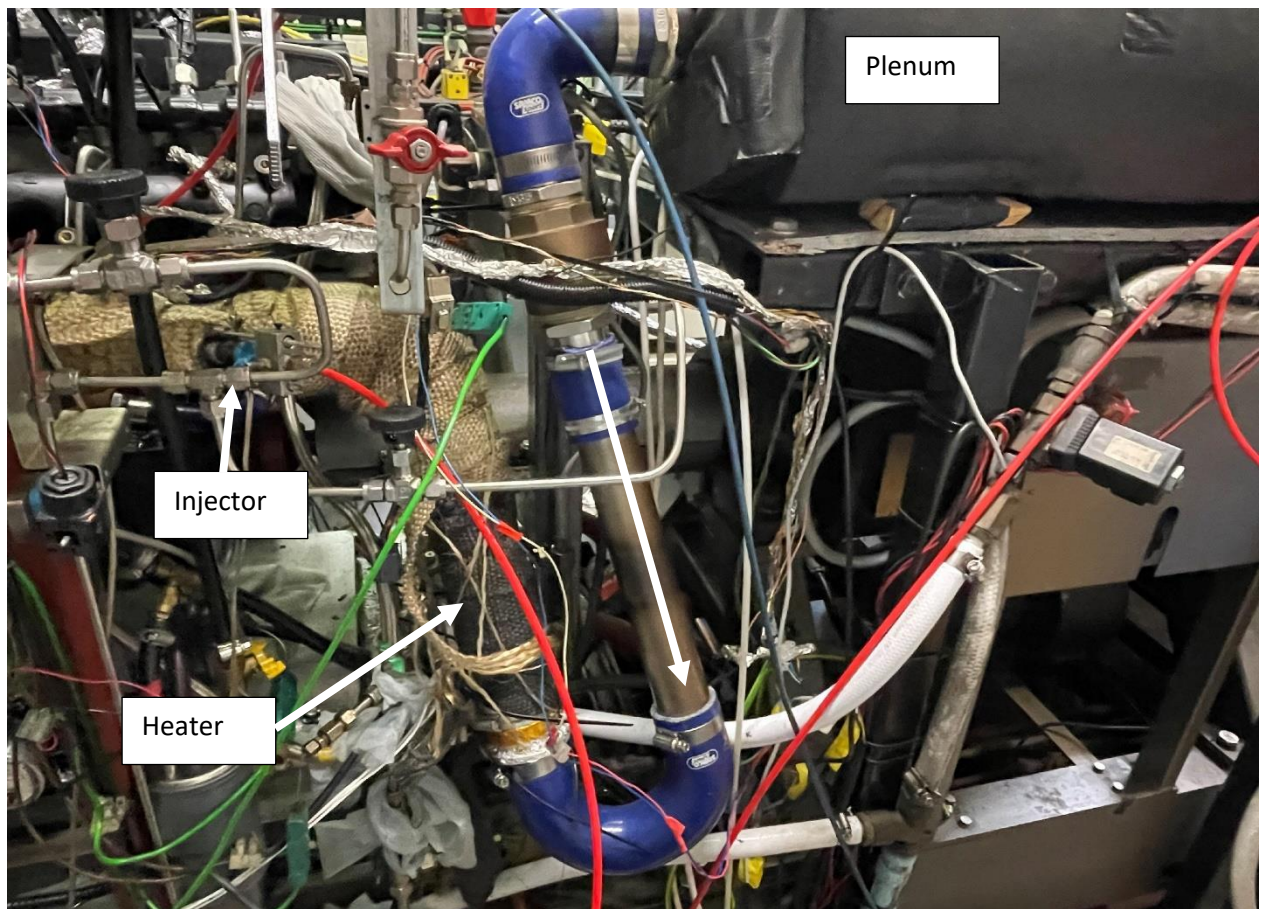
Figure C3: Inline heater of air intake

Figure C4: Port fuel injector
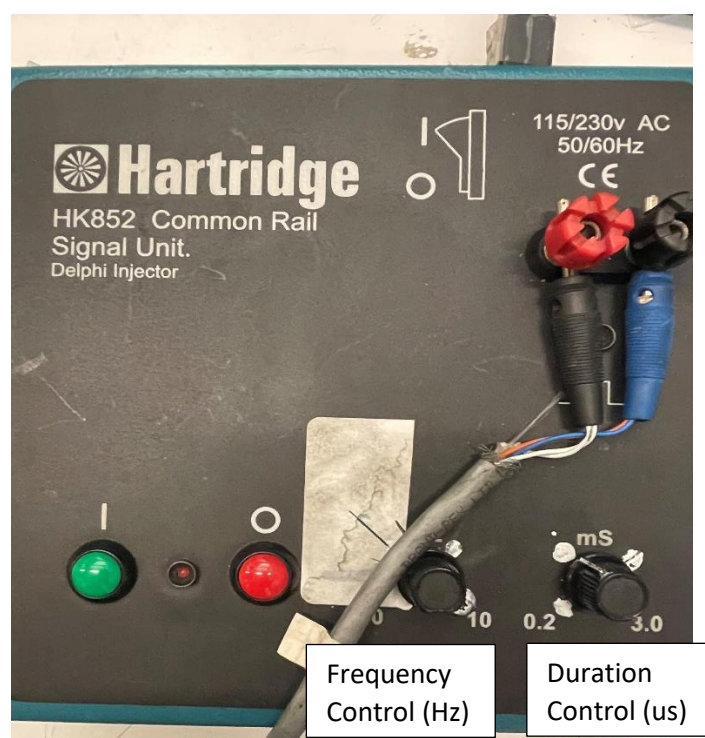
Figure C5: Hartridge controller used to send controlled pulse to port fuel injector (based on frequency and duration)

Figure C6: Syringe pump used for injection of fuel samples into furnace
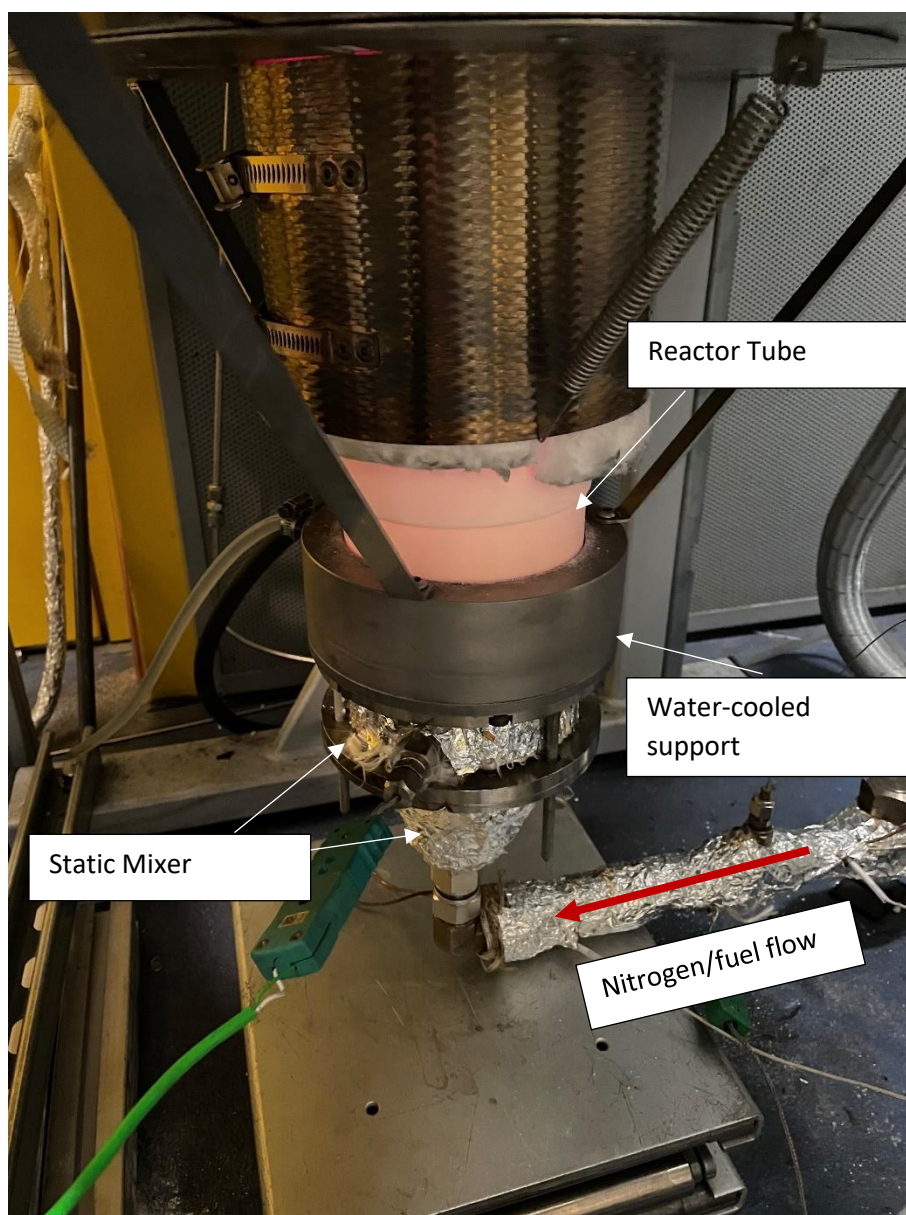
Figure C7: Furnace inlet

Figure C8: Glass syringe used for sample collection and injection during furnace and sampling valve studies involving the GC-FID

Hammer

Proximity sensor
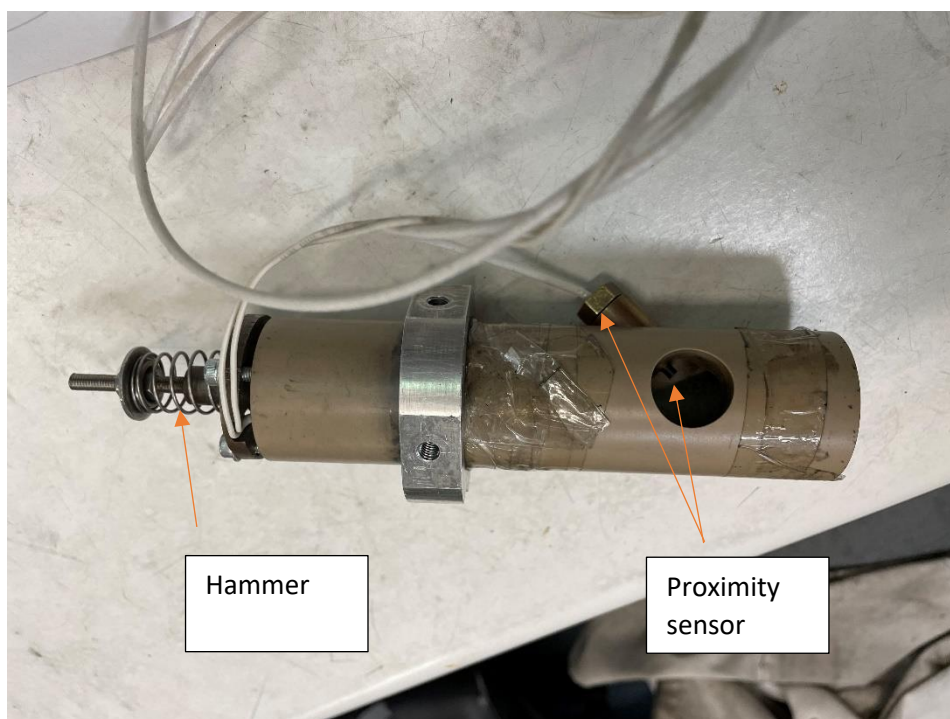
Figure C9: Sampling valve magnet housing
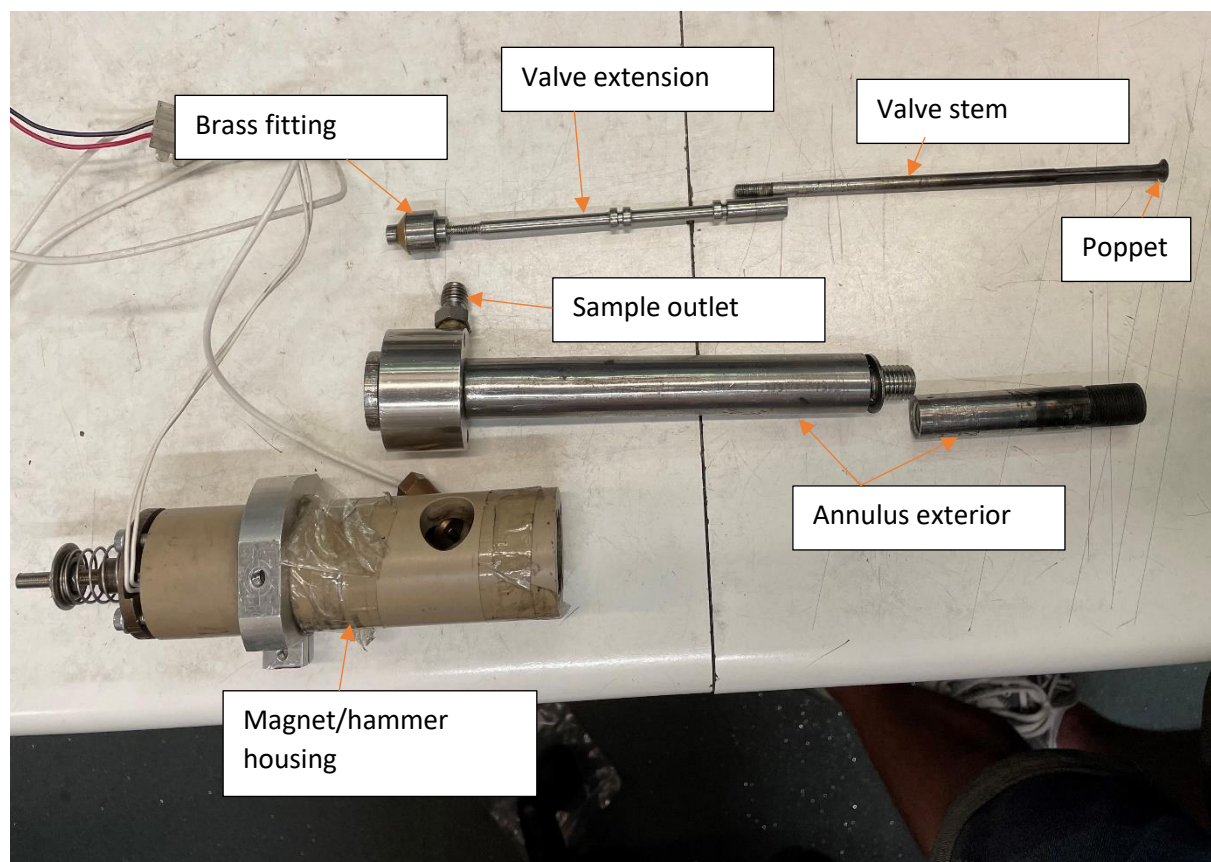
Figure C10:: Disassembled sampling valve

Figure C11: Engine exhaust sampling ports

Appendix D
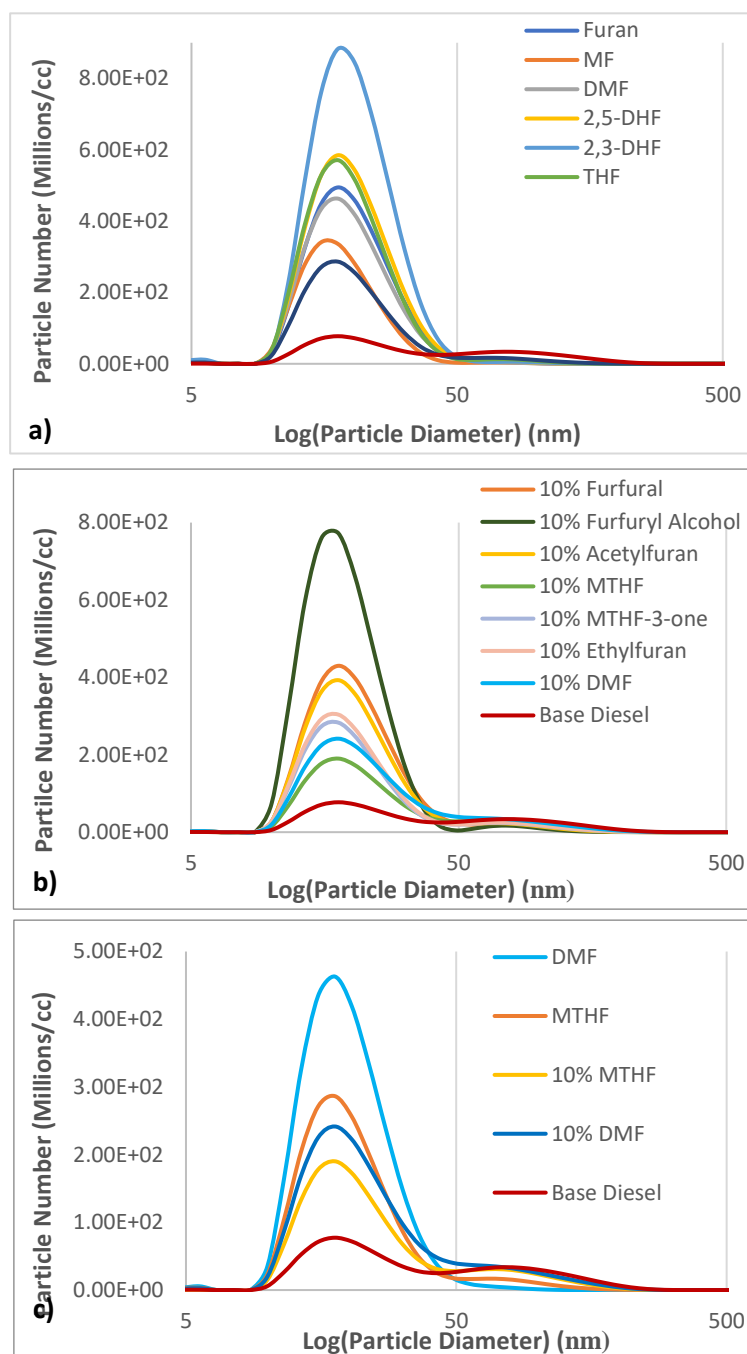
Figure D1: Particle size distributions of 50 :50 diesel :furan blends (a), 70:20:10 diesel: butanol blends (b) and DMF and MTHF with both blend ratio (c)
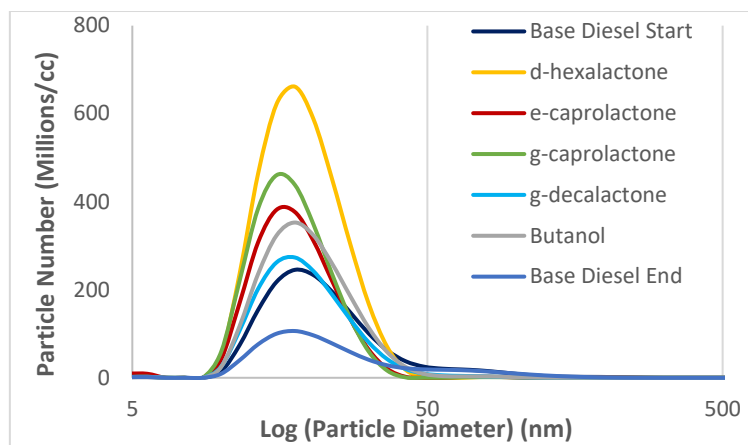
Figure D2: Particle size distribution of lactone-butanol-diesel blends and base diesel
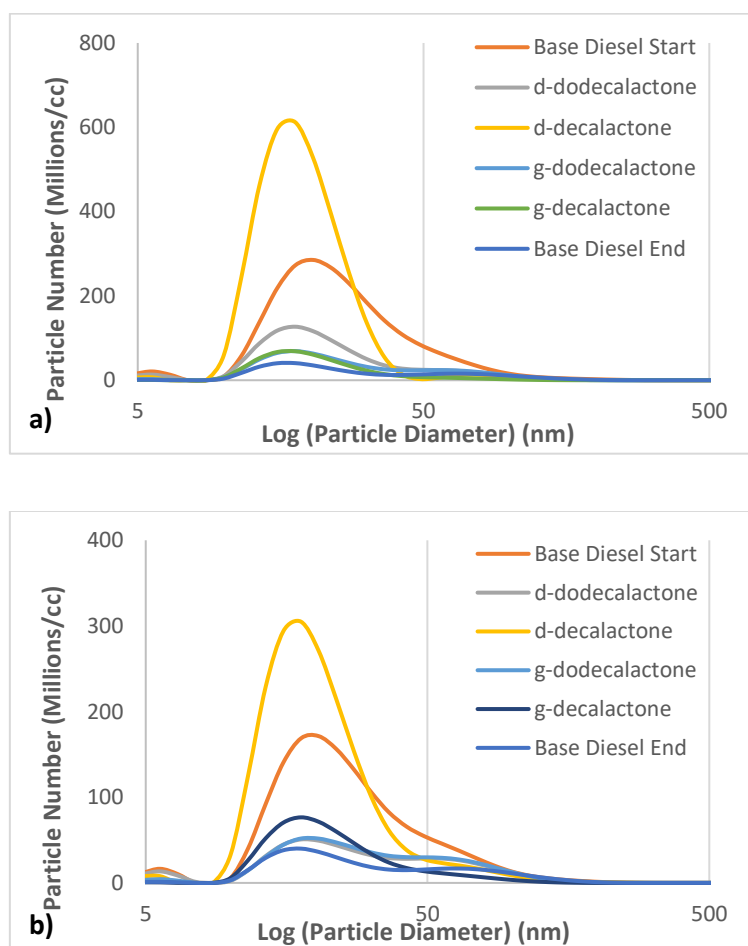
Figure D3: Particle size distributions of C10/C12 lactones and diesel at (a) constant start of injection and

(b) constant start of ignition
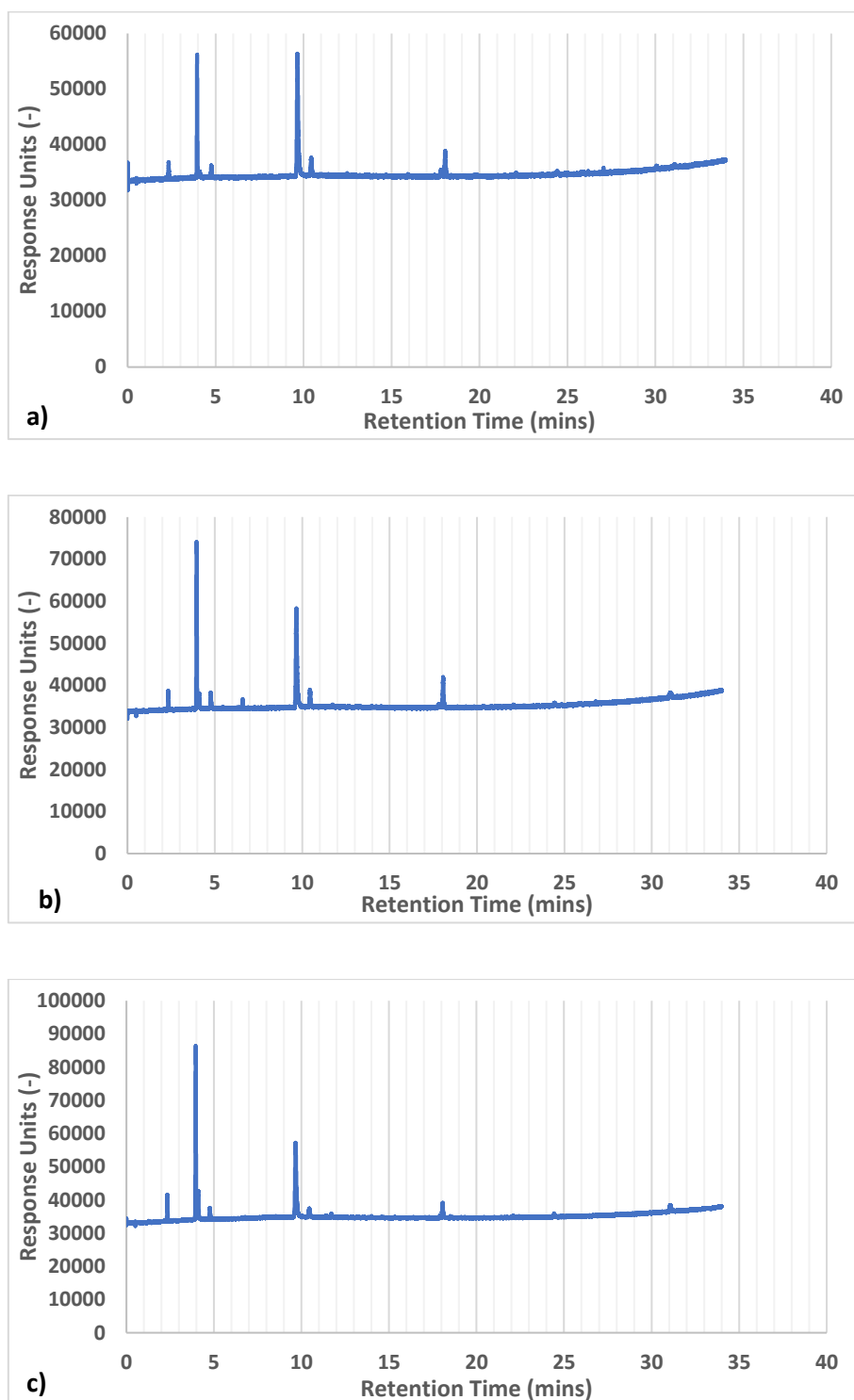
Figure D4: GC-FID chromatograms of samples taken from pyrolytic reactor using γ-decalactone at reaction temperatures of a) 678°C, b) 775°C and c) 879°C
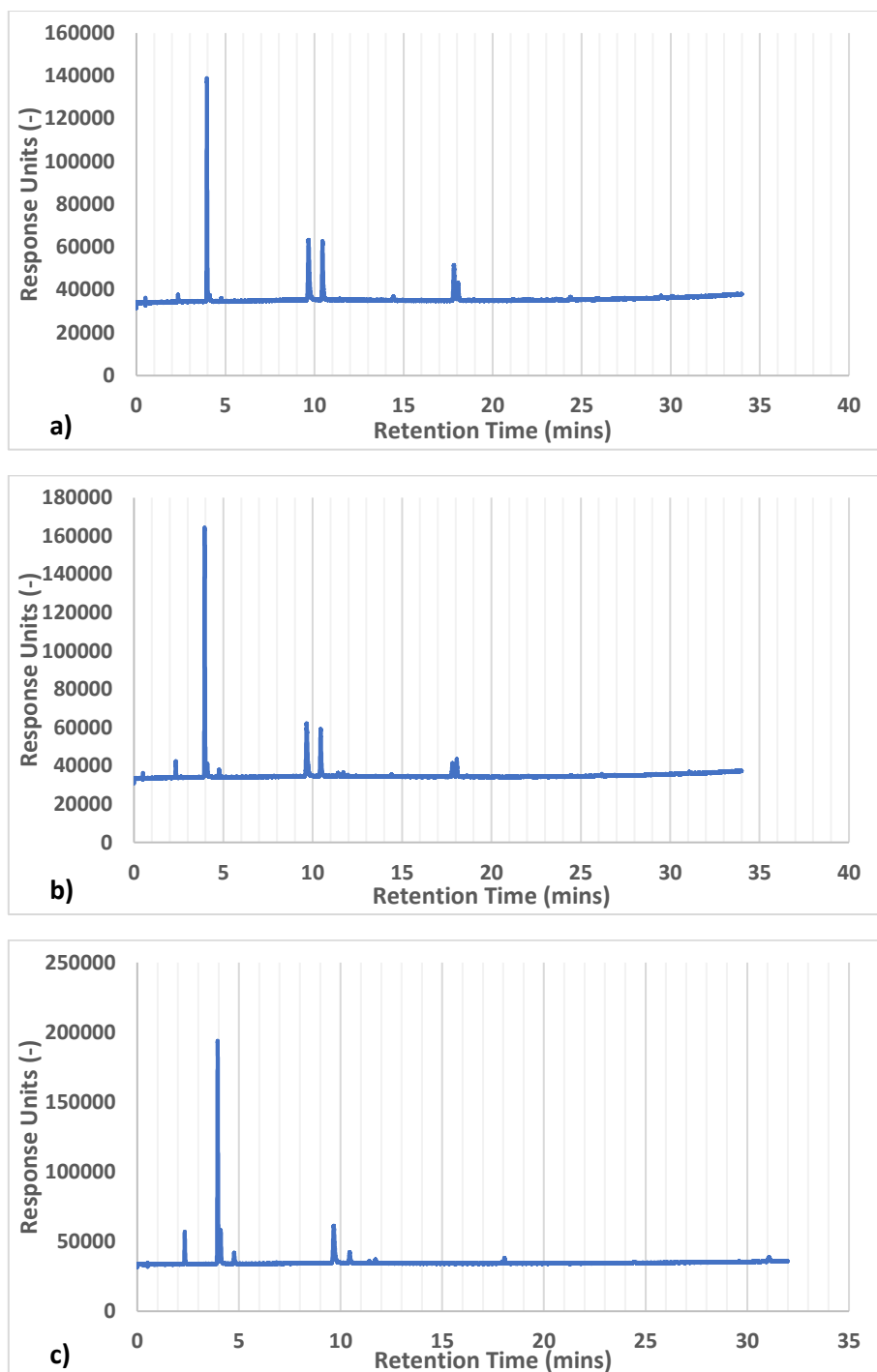
Figure D5: GC-FID chromatograms of samples taken from pyrolytic reactor using n-heptylpropionate at reaction temperatures of a) 678°C, b) 775°C and c) 879°C
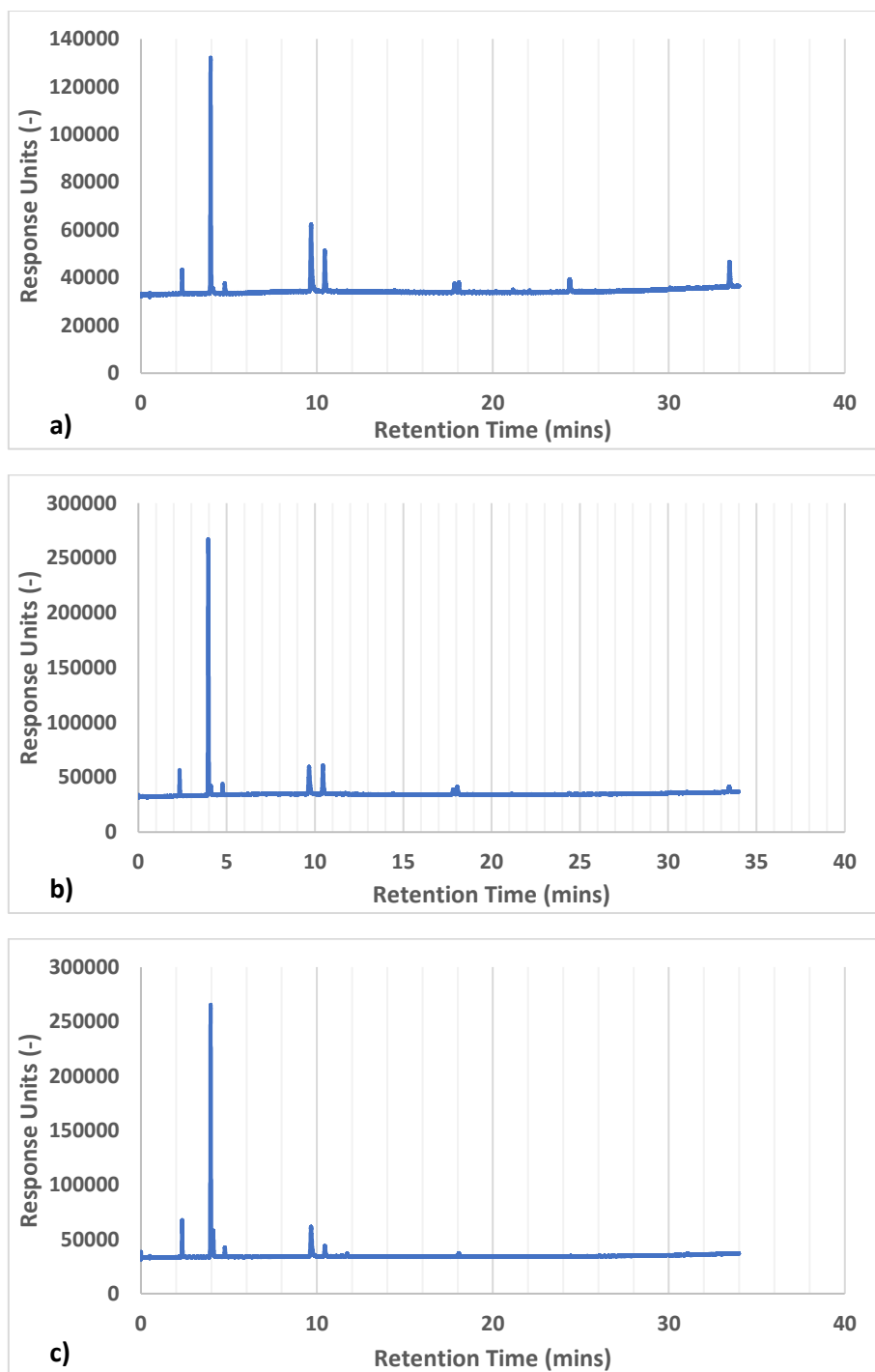
Figure D6: GC-FID chromatograms of samples taken from pyrolytic reactor using di-n-amyl ether at

reaction temperatures of a) 678°C, b) 775°C and c) 879°C
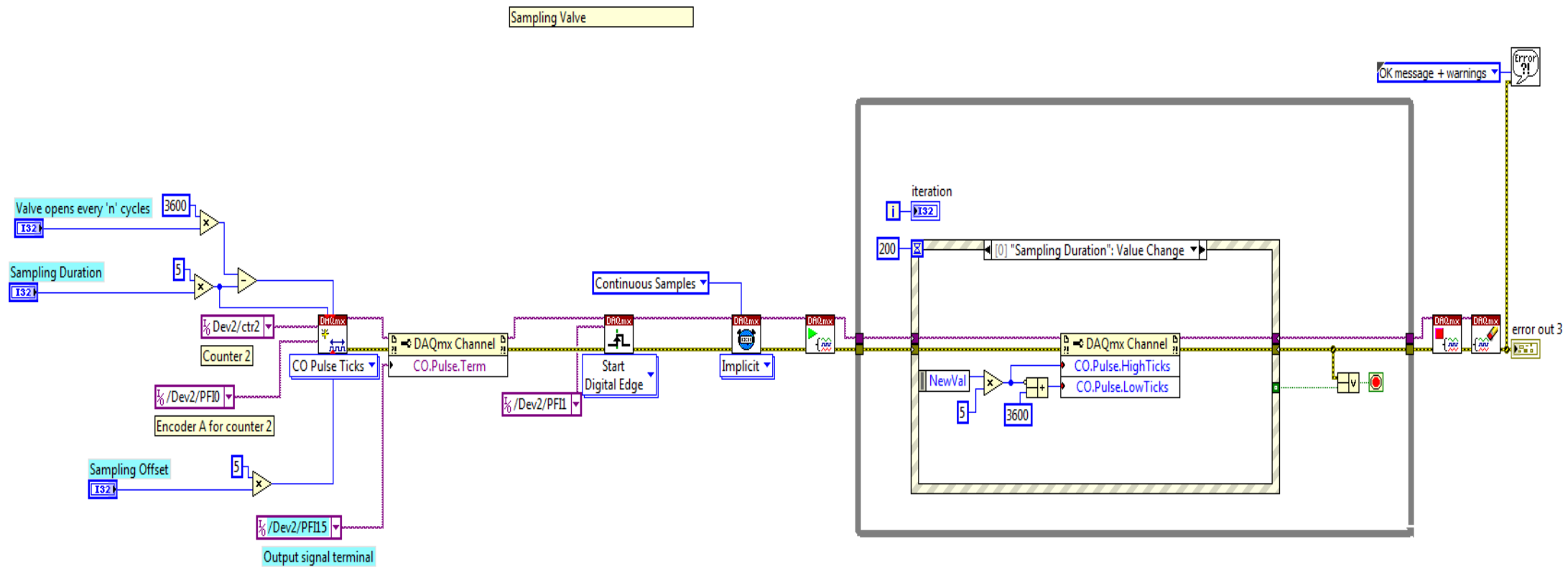
Figure D7: Sampling valve Labview code

Appendix E

BOC

F-SG-0007 R18

QUOTATION

To:	James Frost	Prepared by:	Karen Rowsome
Company:	University College London		Business Development Advisor
Account number:	TBC	Date:	01.09.2020
Email Address:	james.frost.17@ucl.ac.uk	Quote number:	516203995
Tel number:	n/a	NME ref. number:	516195169
Your reference:	Email Enquiry	Page 1 of:	2

BOC Special Products, 10 Priestley Road, The Surrey Research Park, Guildford, Surrey, GU2 7XY

Tel: 0800 02 0800   Fax: 0800 136601

VISIT OUR WEB SITE AT **www.boconline.co.uk**

Item 1

GRAVIMETRIC HYDROCARBON STANDARD

Components	Quantity	Unit	Calibration and Measurement Capability Expressed as an Expanded Uncertainty (k=2) Relative Uncertainty (%) * (see note)	Price
Methane	1000	ppm	+/- 1.0	£ 1,519.61 per cylinder
Ethane	1000	ppm	+/- 1.0	
Ethylene	1000	ppm	+/- 1.0	
Acetylene	1000	ppm	+/- 1.0	
Ethanol	1000	ppm	+/- 1.0	
Acetaldehyde	1000	ppm	+/- 1.0	
Propene	1000	ppm	+/- 1.0	
Propyne	1000	ppm	+/- 1.0	
1,3-butadiene	1000	ppm	+/- 2.0	
Vinyl acetylene	1000	ppm	+/- 2.0	
Benzene	1000	ppm	+/- 1.0	
Nitrogen	Balance			

Note: * The expanded measurement uncertainty values assigned to the certified component concentrations are calculated after filling and analysis. The calculation takes into account the impurity uncertainties from the raw materials and the filling and analytical uncertainties. These values may occasionally be larger than the Calibration and Measurement Capability values quoted above.

Material number:	TBC-HC	
Cylinder size:	AL* (1530mm x 250mm - 50 liquid litre capacity)	
Nominal pressure (bar):	61 @ 15°C	
Contents:	3.11m³	
Valve outlet:	BS4	
Shelf-life:	12 months	
Certification basis:	Molar	
Cylinder Rental: *(Per Month)*		£ 4.26 per month

Note: The actual pressure in the cylinder supplied may vary slightly from the nominal pressure quoted.

Figure E1: Quote and chromatograms (from BOC) of external standard gas mixture

BOC
A Member of The Linde Group

F-SG-0007A-R12

QUOTATION

To:	James Frost	Prepared by:	Naomi Barry
Company:	University College London		Business Development Advisor
Account number:	TBC	Date:	10.08.2020
Email address:	james.frost.17@ucl.ac.uk	Quote number:	516172265
Tel number:	N/A	NME ref. number:	516137559
Your reference:	Email Enquiry	Page 1 of:	2

For Order Placement and Enquiries   Tel: 0800 02 0800   Fax: 0800 136601
E-mail: specialproducts@boc.com

Item 1	HP1500 Series Single Stage Regulator	Price
	For use with non corrosive and mild corrosive gases and mixtures up to N6.0 purity.	
		£507.18 each
	Bar stock stainless steel body and hastelloy diaphragm	
	Click to view web page	
	Material Description: HP1501S.GE-BS4	
	Material Number: 851357	
	Max. Inlet Pressure: 26 bar (GE)	
	Outlet Pressure Operating Range: 0.1 – 5 bar	
	Flow Rate: Cv = 0.06	
	Inlet Connection: BS4	
	Inlet Options: None	
	Outlet Connection: 1/4" Compression Fitting (SS)	
	Suitable for use with: 100ppm 1,1- Difuloroethane (R152A), 50ppm 1-Chlorooctane, Balance Nitrogen	

Delivery time (approximate from receipt of order) 1 week

Item 2	Description	Price *(per Cyl)*
	100ppm 1,1- Difuloroethane (R152A), 50ppm 1-Chlorooctane, Balance Nitrogen	
	Price includes C (certificate value has an uncertainty of +/–5%) certificate Blend Tolerance Components >=10ppm < 1% = +/-10% filling tolerance	£497.51 per cyl
	Material number: TBC (new material number to be raised) Cylinder size: L (50L water capacity, 1.54m height x 0.23m diameter) Nominal pressure (bar): 17.2 @ 15°C Contents: 905litres Valve outlet: BS4 Shelf-life: 12 months Certification basis: Molar	
	Cylinder Rental: *(per Month)*	£4.26 per month
	Note: The actual pressure in the cylinder supplied may vary slightly from the nominal pressure quoted. Variations are due to: • Gas quantity used in certification / analysis as a proportion of total filled in cylinder • Changes in ambient temperature	

Figure E2: Quote and chromatograms (from BOC) for internal standard

Haltermann Carless

Haltermann Carless UK LTD. Grove House Guildford Rd, Leatherhead,
Surrey, KT22 9DF UK

Department of Mechanical Engineerin
Roberts Building
London
WC1E 7JE

Certificate 100000184897

Date:	16/03/2020
Customer PO:	F45-3041017
Delivery Note:	80162210 000010
Order No.:	66154236 000010
Customer No.:	1764862

GMID:	2014685		Revision No.: 2
Material:	Carcal RF-06-03 K02N		
	54L KEG		
Cust. Mat.:			
Batch:	0000029075		
Dlvy. Qty:	216.0 L15		
Container ID:	COATES		
Ship from:	Harwich	Harwich, ES, United Kingdom	Page: 1 / 2

Feature	Units	Results	Limits Minimum	Maximum	Method
Density 15° C	kg/m³	836.0	833.0	837.0	ASTM D4052
Density at 20° C	kg/m3	832.4			ASTM D4052
I.B.Pt.	° C	189.9			ASTM D86
10% v/v Recovered at	° C	216.4			ASTM D86
50% v/v Recovered at	° C	278.6	245.0	-	ASTM D86
90% v/v Recovered at	° C	332.0			ASTM D86
95% v/v Recovered at	° C	349.0	345.0	350.0	ASTM D86
F.B.Pt.	° C	355.5	-	370.0	ASTM D86
Cetane Number		52.2	52.0	54.0	ASTM D613
Aromatics by FIA	%(V/V)	22.5			ASTM D1319
Olefins by FIA	%(V/V)	5.6			ASTM D1319
Polycyclic Aromatic Hydrocarbons	%(m/m)	4.7	3.0	6.0	EN 12916
Water Content	mg/kg	110	-	200	IP 438
Strong Acid Number	mg KOH/g	0.00	-	0.02	ASTM D974
Oxidation Stability	mg /100ml	< 0.1	-	2.5	ASTM D2274
Copper Corrosion, 3hrs at 100° C	-	1B	-	-	ASTM D130
Viscosity at 40° C	mm2/s	2.941	2.300	3.300	ASTM D445
Sulphur content	mg/kg	1.0	-	10.0	ASTM D5453
Lubricity (WSD 1,4) at 60° C	μm	360	-	400	ISO 12156-1
Carbon Residue (on 10% Dist. Res)	%(m/m)	< 0.10	-	0.20	ASTM D4530
Ash	%(m/m)	< 0.001	-	0.010	ASTM D482
CFPP	° C	-18	-	-15	EN 116
Cloud Point	° C	-18			ASTM D2500
Gross Heat of Combustion	MJ/kg	45.80			IP 12
Net Heat of Combustion	MJ/kg	43.00			IP 12
Net Heat of Combustion	Btu/lb	18480			IP 12 / CALCULATION
Oxygen Content	%(m/m)	< 0.04			ELEMENTAL ANALYSIS

Haltermann Carless

Department of Mechanical Engineerin	Delivery item/date	Page
Roberts Building	80162210 000010 / 17/03/2020	2 / 2
London WC1E 7JE		

Feature	Units	Results	Limits Minimum	Maximum	Method
Carbon Content	% (m/m)	86.78			ASTM D5291
Hydrogen Content	% (m/m)	13.22			ASTM D5291
Atomic H/C Ratio		1.8153			CALCULATION
Atomic O/C Ratio		< 0.0003			CALCULATION
C/H Mass Ratio		6.56			CALCULATION
Total Aromatic Hydrocarbons	% (m/m)	24.0			EN 12916
Water & Sediment	% (V/V)	< 0.010			ASTM D2709
Carbon Weight Fraction		0.8678			CALCULATION
Fatty Acid Methyl Ester (FAME) Content	-	None detected	-	-	EN 14078

COA Additional Information

The certificate is electronically generated and valid without signature.

Haltermann Carless UK Ltd.

For enquiries please contact Customer Service or local Sales

Figure E3: Specification sheet of zero-FAME diesel used during combustion experiments

References

1. Yu, L. Jia, S. & Shi, Q. Research on transportation-related emissions: Current status and future directions. *Journal of the Air and Waste Management Association* (2009) doi:10.3155/1047-3289.59.2.183.

2. Ong, H. C. Mahlia, T. M. I. & Masjuki, H. H. A review on energy pattern and policy for transportation sector in Malaysia. *Renewable and Sustainable Energy Reviews* (2012) doi:10.1016/j.rser.2011.08.019.

3. Yan, F. … Zhang, Y. Global emission projections for the transportation sector using dynamic technology modeling. *Atmos. Chem. Phys.* (2014) doi:10.5194/acp-14-5709-2014.

4. Geng, P. Cao, E. Tan, Q. & Wei, L. Effects of alternative fuels on the combustion characteristics and emission products from diesel engines: A review. *Renewable and Sustainable Energy Reviews* (2017) doi:10.1016/j.rser.2016.12.080.

5. Duarte Souza Alvarenga Santos, N. Rückert Roso, V. Teixeira Malaquias, A. C. & Coelho Baêta, J. G. Internal combustion engines and biofuels: Examining why this robust combination should not be ignored for future sustainable transportation. *Renewable and Sustainable Energy Reviews* vol. 148 (2021).

6. Heywood, J. . *Internal Combustion Engine Fundamentals.* (McGraw-Hill Inc, 1988).

7. Stone, R. *Introduction to Internal Combustion Engines.* (Macmillan Press Ltd, 1999).

8. Myung, C. L. & Park, S. Exhaust nanoparticle emissions from internal combustion engines: A review. *International Journal of Automotive Technology* vol. 13 (2012).

9. GIECHASKIEL, B. … MARTINI, G. Particle number measurements in the European legislation and future JRC activities. *Combust. Engines* **174**, (2018).

10. Frank, B. Schlögl, R. & Su, D. S. Diesel soot toxification. *Environmental Science and Technology* vol. 47 (2013).

11.   Gangwar, J. N. Gupta, T. & Agarwal, A. K. Composition and comparative toxicity of particulate matter emitted from a diesel and biodiesel fuelled CRDI engine. *Atmos. Environ.* (2012) doi:10.1016/j.atmosenv.2011.09.007.

12.   Soriano, J. A. … Agudelo, J. R. Genotoxicity and mutagenicity of particulate matter emitted from diesel, gas to liquid, biodiesel, and farnesane fuels: A toxicological risk assessment. *Fuel* **282**, (2020).

13.   Lewtas, J. Air pollution combustion emissions: Characterization of causative agents and mechanisms associated with cancer, reproductive, and cardiovascular effects. *Mutation Research - Reviews in Mutation Research* vol. 636 (2007).

14.   Richter, H. & Howard, J. B. Formation of polycyclic aromatic hydrocarbons and their growth to soot-a review of chemical reaction pathways. *Progress in Energy and Combustion Science* (2000) doi:10.1016/S0360-1285(00)00009-5.

15.   Wang, Y. … Huang, X. A review of the effects of hydrogen, carbon dioxide, and water vapor addition on soot formation in hydrocarbon flames. *Int. J. Hydrogen Energy* (2021) doi:10.1016/j.ijhydene.2021.07.011.

16.   Michelsen, H. A. … Wang, H. A review of terminology used to describe soot formation and evolution under combustion and pyrolytic conditions. *ACS Nano* vol. 14 (2020).

17.   Wu, S. Bao, J. Wang, Z. Zhang, H. & Xiao, R. The regulated emissions and PAH emissions of bio-based long-chain ethers in a diesel engine. *Fuel Process. Technol.* **214**, (2021).

18.   Verma, P. … Ristovski, Z. The impact of chemical composition of oxygenated fuels on morphology and nanostructure of soot particles. *Fuel* **259**, (2020).

19.   Park, W. Park, S. Reitz, R. D. & Kurtz, E. The effect of oxygenated fuel properties on diesel spray combustion and soot formation. *Combust. Flame* **180**, (2017).

20.   Liu, X. Wang, H. & Yao, M. Experimental and Modeling Investigations on Soot Formation of Ethanol, n-Butanol, 2,5-Dimethylfuran, and Biodiesel in Diesel Engines.

Energy and Fuels **31**, (2017).

21. Chu, H. … E, J. Effects of ethanol and 2, 5-dimethylfuran addition on the morphology and nanostructure evolution of soot in gasoline primary reference fuel-air coflow diffusion flames. *Fuel* **281**, (2020).

22. Dong, X. Jia, M. Chang, Y. Wang, P. & Niu, B. Kinetic Modeling Study of Polycyclic Aromatic Hydrocarbon Formation and Oxidation for Oxygenated Fuels including Methanol, n-Butanol, Methyl Butanoate, and Dimethyl Ether. *Energy and Fuels* **34**, (2020).

23. Tartakovsky, L. & Sheintuch, M. Fuel reforming in internal combustion engines. *Progress in Energy and Combustion Science* (2018) doi:10.1016/j.pecs.2018.02.003.

24. Hoque, M. E. Singh, A. & Chuan, Y. L. Biodiesel from low cost feedstocks: The effects of process parameters on the biodiesel yield. *Biomass and Bioenergy* **35**, (2011).

25. Athar, M. & Zaidi, S. A review of the feedstocks, catalysts, and intensification techniques for sustainable biodiesel production. *J. Environ. Chem. Eng.* **8**, (2020).

26. Rezania, S. … Cho, J. Review on transesterification of non-edible sources for biodiesel production with a focus on economic aspects, fuel properties and by-product applications. *Energy Conversion and Management* vol. 201 (2019).

27. Maroa, S. & Inambao, F. Effects of Biodiesel Blends Varied by Cetane Numbers and Oxygen Contents on Stationary Diesel Engine Performance and Exhaust Emissions. in *Numerical and Experimental Studies on Combustion Engines and Vehicles* (2020). doi:10.5772/intechopen.92569.

28. Serrano-Ruiz, J. C. Luque, R. & Sepúlveda-Escribano, A. Transformations of biomass-derived platform molecules: From high added-value chemicals to fuels via aqueous-phase processing. *Chemical Society Reviews* (2011) doi:10.1039/c1cs15131b.

29. Rajesh Kumar, B. & Saravanan, S. Use of higher alcohol biofuels in diesel engines: A review. *Renewable and Sustainable Energy Reviews* (2016)

doi:10.1016/j.rser.2016.01.085.

30. Agarwal, A. K. Biofuels (alcohols and biodiesel) applications as fuels for internal combustion engines. *Progress in Energy and Combustion Science* (2007) doi:10.1016/j.pecs.2006.08.003.

31. Haghighi Mood, S. … Ardjmand, M. Lignocellulosic biomass to bioethanol, a comprehensive review with a focus on pretreatment. *Renew. Sustain. Energy Rev.* (2013) doi:10.1016/j.rser.2013.06.033.

32. Sandalcı, T. Karagöz, Y. Orak, E. & Yüksek, L. An Experimental Investigation of Ethanol-Diesel Blends on Performance and Exhaust Emissions of Diesel Engines. *Adv. Mech. Eng.* (2014) doi:10.1155/2014/409739.

33. Omidvarborna, H. Kumar, A. & Kim, D. S. Variation of diesel soot characteristics by different types and blends of biodiesel in a laboratory combustion chamber. *Sci. Total Environ.* (2016) doi:10.1016/j.scitotenv.2015.11.076.

34. Menon, V. & Rao, M. Trends in bioconversion of lignocellulose: Biofuels, platform chemicals & biorefinery concept. *Progress in Energy and Combustion Science* (2012) doi:10.1016/j.pecs.2012.02.002.

35. Makhubela, B. C. E. & Darkwa, J. The Role of Noble Metal Catalysts in Conversion of Biomass and Bio-derived Intermediates to Fuels and Chemicals. *Johnson Matthey Technol. Rev.* (2018) doi:10.1595/205651317X696261.

36. Climent, M. J. Corma, A. & Iborra, S. Conversion of biomass platform molecules into fuel additives and liquid hydrocarbon fuels. *Green Chemistry* (2014) doi:10.1039/c3gc41492b.

37. Xia, Z. … Zhang, J. Processing and valorization of cellulose, lignin and lignocellulose using ionic liquids. *Journal of Bioresources and Bioproducts* vol. 5 (2020).

38. Hasanov, I. Raud, M. & Kikas, T. The role of ionic liquids in the lignin separation from lignocellulosic biomass. *Energies* vol. 13 (2020).

39. Binder, J. B. & Raines, R. T. Fermentable sugars by chemical hydrolysis of biomass. *Proc. Natl. Acad. Sci.* (2010) doi:10.1073/pnas.0912073107.

40. Sun, Y. & Cheng, J. Hydrolysis of lignocellulosic materials for ethanol production : a review q. *Bioresour. Technol.* (2002) doi:10.1016/S0960-8524(01)00212-7.

41. Knežević, A. Đokić, I. Tosti, T. Popović, S. & Vukojević, J. Biological pretreatment of wheat straw: Effect of fungal culturing on enzymatic hydrolysis of carbohydrate polymers. (2021) doi:10.21203/rs.3.rs-227697/v1.

42. Sharma, D. & Rai, R. European Journal of Molecular & Clinical Medicine Biological Pretreatment Strategies For Enhanced Saccharification Of Lignocellulosic Biomass In 2G Ethanol Biorefineries. *Eur. J. Mol. Clin. Med.* **7**, (2020).

43. Zanellati, A. … Scarpeci, T. E. Screening and evaluation of phenols and furans degrading fungi for the biological pretreatment of lignocellulosic biomass. *Int. Biodeterior. Biodegrad.* **161**, (2021).

44. Lange, J. P. Van Der Heide, E. Van Buijtenen, J. & Price, R. Furfural-A promising platform for lignocellulosic biofuels. *ChemSusChem* (2012) doi:10.1002/cssc.201100648.

45. Mittal, A. … Johnson, D. K. Production of Furfural from Process-Relevant Biomass-Derived Pentoses in a Biphasic Reaction System. *ACS Sustain. Chem. Eng.* (2017) doi:10.1021/acssuschemeng.7b00215.

46. Zhao, Y. Lu, K. Xu, H. Zhu, L. & Wang, S. A critical review of recent advances in the production of furfural and 5-hydroxymethylfurfural from lignocellulosic biomass through homogeneous catalytic hydrothermal conversion. *Renewable and Sustainable Energy Reviews* vol. 139 (2021).

47. Xing, R. … Huber, G. W. Production of jet and diesel fuel range alkanes from waste hemicellulose-derived aqueous solutions. *Green Chem.* (2010) doi:10.1039/c0gc00263a.

48. Zhang, J. Lin, L. & Liu, S. Efficient production of furan derivatives from a sugar mixture by catalytic process. in *Energy and Fuels* (2012). doi:10.1021/ef300606v.

49. Li, X. … Lu, X. Kinetics of Furfural Production from Corn Cob in γ-Valerolactone Using Dilute Sulfuric Acid as Catalyst. *ACS Sustain. Chem. Eng.* **5**, (2017).

50. Binder, J. B. Blank, J. J. Cefali, A. V. & Raines, R. T. Synthesis of furfural from xylose and xylan. *ChemSusChem* (2010) doi:10.1002/cssc.201000181.

51. Li, H. Ren, J. Zhong, L. Sun, R. & Liang, L. Production of furfural from xylose, water-insoluble hemicelluloses and water-soluble fraction of corncob via a tin-loaded montmorillonite solid acid catalyst. *Bioresour. Technol.* **176**, (2015).

52. Takagaki, A. Ohara, M. Nishimura, S. & Ebitani, K. One-pot Formation of Furfural from Xylose via Isomerization and Successive Dehydration Reactions over Heterogeneous Acid and Base Catalysts. *Chem. Lett.* (2010) doi:10.1246/cl.2010.838.

53. Kläusli, T. AVA Biochem: commercialising renewable platform chemical 5-HMF. *Green Process. Synth.* (2014) doi:10.1515/gps-2014-0029.

54. Liu, J. Tang, Y. Wu, K. Bi, C. & Cui, Q. Conversion of fructose into 5-hydroxymethylfurfural (HMF) and its derivatives promoted by inorganic salt in alcohol. *Carbohydr. Res.* (2012) doi:10.1016/j.carres.2011.12.006.

55. Cai, X. … Li, S. Conversion of chitin biomass into 5-hydroxymethylfurfural: A review. *Renew. Sustain. Energy Rev.* **150**, (2021).

56. Motagamwala, A. H. Huang, K. Maravelias, C. T. & Dumesic, J. A. Solvent system for effective near-term production of hydroxymethylfurfural (HMF) with potential for long-term process improvement. *Energy Environ. Sci.* **12**, (2019).

57. Zhou, X. Broadbelt, L. J. & Vinu, R. Mechanistic Understanding of Thermochemical Conversion of Polymers and Lignocellulosic Biomass. in *Advances in Chemical Engineering* (2016). doi:10.1016/bs.ache.2016.09.002.

58. Mayer, S. F. … Fierro, J. L. G. Dehydration of fructose to HMF in presence of

(H3O)xSbxTe(2-x)O6 (x = 1, 1.1, 1.25) in H2O-MIBK. *Mol. Catal.* **481**, (2020).

59.   Zhang, T. Li, W. Xin, H. Jin, L. & Liu, Q. Production of HMF from glucose using an Al3+-promoted acidic phenol-formaldehyde resin catalyst. *Catal. Commun.* **124**, (2019).

60.   Candu, N. … Coman, S. M. Efficient glucose dehydration to HMF onto Nb-BEA catalysts. *Catal. Today* **325**, (2019).

61.   Choi, S. Song, C. W. Shin, J. H. & Lee, S. Y. Biorefineries for the production of top building block chemicals and their derivatives. *Metabolic Engineering* (2015) doi:10.1016/j.ymben.2014.12.007.

62.   Mascal, M. & Nikitin, E. B. Direct, high-yield conversion of cellulose into biofuel. *Angew. Chemie - Int. Ed.* (2008) doi:10.1002/anie.200801594.

63.   Chheda, J. N. Román-Leshkov, Y. & Dumesic, J. A. Production of 5-hydroxymethylfurfural and furfural by dehydration of biomass-derived mono- and poly-saccharides. *Green Chem.* (2007) doi:10.1039/b611568c.

64.   Chang, H. Bajaj, I. Huber, G. W. Maravelias, C. T. & Dumesic, J. A. Catalytic strategy for conversion of fructose to organic dyes, polymers, and liquid fuels. *Green Chem.* **22**, (2020).

65.   Mellmer, M. A. … Dumesic, J. A. Effects of chloride ions in acid-catalyzed biomass dehydration reactions in polar aprotic solvents. *Nat. Commun.* **10**, (2019).

66.   Chaffey, D. R. … Graham, A. E. Conversion of levulinic acid to levulinate ester biofuels by heterogeneous catalysts in the presence of acetals and ketals. *Appl. Catal. B Environ.* **293**, (2021).

67.   Adeleye, A. T. … Michael, D. P. A Review on the conversion of levulinic acid and its esters to various useful chemicals. *AIMS Energy* vol. 7 (2019).

68.   Texaco/NYSERDA/Biofine Inc. *Ethyl Levulinate D-975 Diesel Additive Test Program.* (2000).

69. Alonso, D. M. Wettstein, S. G. & Dumesic, J. A. Bimetallic catalysts for upgrading of biomass to fuels and chemicals. *Chemical Society Reviews* (2012) doi:10.1039/c2cs35188a.

70. Liang, X. Duan, Y. Fan, Y. Huang, Z. & Han, D. Influences of C5 esters addition on anti-knock and auto-ignition tendency of a gasoline surrogate fuel. *Int. J. Engine Res.* (2021) doi:10.1177/14680874211030898.

71. Chen, Z. Wang, Z. Lei, T. & Gupta, A. K. Physical-Chemical Properties and Engine Performance of Blends of Biofuels with Gasoline. *J. Biobased Mater. Bioenergy* **15**, (2021).

72. Carlos Serrano-Ruiz, J. & Dumesic, J. A. Catalytic upgrading of lactic acid to fuels and chemicals by dehydration/hydrogenation and C-C coupling reactions. *Green Chem.* (2009) doi:10.1039/b906869d.

73. Rakopoulos, D. C. Rakopoulos, C. D. Giakoumis, E. G. Dimaratos, A. M. & Kyritsis, D. C. Effects of butanol-diesel fuel blends on the performance and emissions of a high-speed di diesel engine. *Energy Convers. Manag.* (2010) doi:10.1016/j.enconman.2010.02.032.

74. Henao, C. A. Simonetti, D. Dumesic, J. A. & Maravelias, C. T. Conversion of glycerol to liquid fuels. in *Computer Aided Chemical Engineering* (2009). doi:10.1016/S1570-7946(09)70677-7.

75. Bu, Q. … Ruan, R. A review of catalytic hydrodeoxygenation of lignin-derived phenols from biomass pyrolysis. *Bioresource Technology* (2012) doi:10.1016/j.biortech.2012.08.089.

76. Zhou, L. Boot, M. D. Johansson, B. H. & Reijnders, J. J. E. Performance of lignin derived aromatic oxygenates in a heavy-duty diesel engine. *Fuel* (2014) doi:10.1016/j.fuel.2013.07.047.

77. Zhou, S. Xue, Y. Sharma, A. & Bai, X. Lignin Valorization through Thermochemical

Conversion: Comparison of Hardwood, Softwood and Herbaceous Lignin. *ACS Sustain. Chem. Eng.* (2016) doi:10.1021/acssuschemeng.6b01488.

78. Zhou, L. Heuser, B. Boot, M. Kremer, F. & Pischinger, S. Performance and Emissions of Lignin and Cellulose Based Oxygenated Fuels in a Compression-Ignition Engine. in (2015). doi:10.4271/2015-01-0910.

79. Lange, H. Decina, S. & Crestini, C. Oxidative upgrade of lignin - Recent routes reviewed. in *European Polymer Journal* (2013). doi:10.1016/j.eurpolymj.2013.03.002.

80. Arevalo-Gallegos, A. Ahmad, Z. Asgher, M. Parra-Saldivar, R. & Iqbal, H. M. N. Lignocellulose: A sustainable material to produce value-added products with a zero waste approach—A review. *International Journal of Biological Macromolecules* (2017) doi:10.1016/j.ijbiomac.2017.02.097.

81. Herreros, J. M. Jones, A. Sukjit, E. & Tsolakis, A. Blending lignin-derived oxygenate in enhanced multi-component diesel fuel for improved emissions. *Appl. Energy* (2014) doi:10.1016/j.apenergy.2013.11.022.

82. Corma, A. De La Torre, O. & Renz, M. Production of high quality diesel from cellulose and hemicellulose by the Sylvan process: Catalysts and process variables. *Energy Environ. Sci.* (2012) doi:10.1039/c2ee02778j.

83. Hellier, P. Talibi, M. Eveleigh, A. & Ladommatos, N. An overview of the effects of fuel molecular structure on the combustion and emissions characteristics of compression ignition engines. *Proc. Inst. Mech. Eng. Part D J. Automob. Eng.* (2017) doi:10.1177/0954407016687453.

84. Wang, H. & Yao, J. Use of Poly(furfuryl alcohol) in the fabrication of nanostructured carbons and nanocomposites. *Industrial and Engineering Chemistry Research* (2006) doi:10.1021/ie0602660.

85. Vetere, V. Merlo, A. B. Ruggera, J. F. & Casella, M. L. Transition metal-based bimetallic catalysts for the chemoselective hydrogenation of furfuraldehyde. *J. Braz.*

Chem. Soc. (2010) doi:10.1590/S0103-50532010000500021.

86.   Gong, W. … Zhao, H. Efficient Synthesis of Furfuryl Alcohol from H2-
Hydrogenation/Transfer Hydrogenation of Furfural Using Sulfonate Group Modified Cu
Catalyst. *ACS Sustain. Chem. Eng.* (2017) doi:10.1021/acssuschemeng.6b02343.

87.   Wang, G. H. … Schüth, F. Platinum-cobalt bimetallic nanoparticles in hollow carbon
nanospheres for hydrogenolysis of 5-hydroxymethylfurfural. *Nat. Mater.* (2014)
doi:10.1038/nmat3872.

88.   Sudholt, A. … Dryer, F. L. Ignition characteristics of a bio-derived class of saturated
and unsaturated furans for engine applications. *Proc. Combust. Inst.* (2015)
doi:10.1016/j.proci.2014.06.147.

89.   Xiao, H. Zeng, P. Li, Z. Zhao, L. & Fu, X. Combustion performance and emissions of
2-methylfuran diesel blends in a diesel engine. *Fuel* (2016)
doi:10.1016/j.fuel.2016.02.006.

90.   Gogoi, B. … Bojanampati, S. Effects of 2,5-dimethylfuran addition to diesel on soot
nanostructures and reactivity. *Fuel* (2015) doi:10.1016/j.fuel.2015.07.038.

91.   Bui, T. T. … Tran, V. N. Characteristics of PM and soot emissions of internal
combustion engines running on biomass-derived DMF biofuel: a review. *Energy
Sources, Part A: Recovery, Utilization and Environmental Effects* (2021)
doi:10.1080/15567036.2020.1869868.

92.   Hoang, A. T. Ölçer, A. I. & Nižetić, S. Prospective review on the application of biofuel
2,5-dimethylfuran to diesel engine. *Journal of the Energy Institute* vol. 94 (2021).

93.   Alexandrino, K. Comprehensive Review of the Impact of 2,5-Dimethylfuran and 2-
Methylfuran on Soot Emissions: Experiments in Diesel Engines and at Laboratory-
Scale. *Energy and Fuels* **34**, (2020).

94.   Xiao, H. … Ruan, J. Effects of pilot injection on combustion and emissions
characteristics using 2-methylfuran/diesel blends in a diesel engine. *Therm. Sci.* **2018**,

(2018).

95. Alipour, S. Omidvarborna, H. & Kim, D. S. A review on synthesis of alkoxymethyl furfural, a biofuel candidate. *Renewable and Sustainable Energy Reviews* (2017) doi:10.1016/j.rser.2016.12.118.

96. Addepally, U. & Thulluri, C. Recent progress in production of fuel range liquid hydrocarbons from biomass-derived furanics via strategic catalytic routes. *Fuel* (2015) doi:10.1016/j.fuel.2015.07.036.

97. Yang, F. … Zhou, J. A biodiesel additive: Etherification of 5-hydroxymethylfurfural with isobutene to tert-butoxymethylfurfural. *Catal. Sci. Technol.* (2015) doi:10.1039/c5cy00750j.

98. Balakrishnan, M. Sacia, E. R. & Bell, A. T. Etherification and reductive etherification of 5-(hydroxymethyl)furfural: 5-(alkoxymethyl)furfurals and 2,5-bis(alkoxymethyl)furans as potential bio-diesel candidates. *Green Chem.* (2012) doi:10.1039/c2gc35102a.

99. Natsir, T. A. & Shimazu, S. Fuels and fuel additives from furfural derivatives via etherification and formation of methylfurans. *Fuel Processing Technology* vol. 200 (2020).

100. Elsayed, I. Jackson, M. A. & Hassan, E. B. Catalytic hydrogenation and etherification of 5-Hydroxymethylfurfural into 2-(alkoxymethyl)-5-methylfuran and 2,5-bis(alkoxymethyl)furan as potential biofuel additives. *Fuel Process. Technol.* **213**, (2021).

101. Sacia, E. R. Balakrishnan, M. & Bell, A. T. Biomass conversion to diesel via the etherification of furanyl alcohols catalyzed by Amberlyst-15. *J. Catal.* (2014) doi:10.1016/j.jcat.2014.02.012.

102. Lanzafame, P. Papanikolaou, G. Barbera, K. Centi, G. & Perathoner, S. Etherification of HMF to biodiesel additives: The role of NH4+ confinement in Beta zeolites. *J. Energy Chem.* **36**, (2019).

103. Wu, L. Moteki, T. Gokhale, A. A. Flaherty, D. W. & Toste, F. D. Production of Fuels and Chemicals from Biomass: Condensation Reactions and Beyond. *Chem* (2016) doi:10.1016/j.chempr.2016.05.002.

104. Mulik, N. L. Niphadkar, P. S. & Bokade, V. V. Synthesis of ethyl furfuryl ether (potential biofuel) by etherification of furfuryl alcohol with ethanol over heterogenized reusable H1Cs2PW12O40 catalyst. *Res. Chem. Intermed.* **46**, (2020).

105. Bhansali, K. J. & Bhagat, P. R. Perylene supported metal free brønsted acid-functionalized porphyrin intertwined with benzimidazolium moiety for enhanced photocatalytic etherification of furfuryl alcohol. *Fuel* **278**, (2020).

106. Allen, M. C. … Schwartz, T. J. Highly Selective Cross-Etherification of 5-Hydroxymethylfurfural with Ethanol. *ACS Catal.* **10**, (2020).

107. Gruter, G. J. M. HYDROXYMETHYLFURFURAL ETHERS FROM SUGARS OR HMF AND BRANCHED ALCOHOLS CROSS-REFERENCE TO RELATED APPLICATIONS. (2010).

108. Gerardus Johannes Maria (30) Foreign Application Priority Data & Gruter, H. (NL). Hydroxymethylfurfural ethers from sugars or HMF and branched alcohols. (2010).

109. de Jong, E. & Gruter, G.-J. Furanics: A Novel Diesel Fuel with Superior Characteristics. in (2009). doi:10.4271/2009-01-2767.

110. Bui, T. V, Crossley, S. & Resasco, D. E. 7 C–C Coupling for Biomass-Derived Furanics Upgrading to Chemicals and Fuels.

111. Barrett, C. J. Chheda, J. N. Huber, G. W. & Dumesic, J. A. Single-reactor process for sequential aldol-condensation and hydrogenation of biomass-derived compounds in water. *Appl. Catal. B Environ.* (2006) doi:10.1016/j.apcatb.2006.03.001.

112. He, J. … Li, C. Upgrading of biomass-derived furanic compounds into high-quality fuels involving aldol condensation strategy. *Fuel* **306**, 121765 (2021).

113. Brown, W. H. & H.Sawatzky. The Condensation of Furan and Sylvan with some

Carbonyl Compounds. *Can. J. Chem.* **34**, (1956).

114. Pennanen, S. & Nyman, G. Studies on the Furan Series. Part 1: The Acidic Condensation of Aldehydes with Methyl-2-Furoate. *Acta Chem. Scandanavia* 1018– 1022 (1972).

115. Corma, A. De La Torre, O. Renz, M. & Villandier, N. Production of high-quality diesel from biomass waste products. *Angew. Chemie - Int. Ed.* (2011) doi:10.1002/anie.201007508.

116. Corma, A. Delatorre, O. & Renz, M. High-quality diesel from hexose- and pentose- derived biomass platform molecules. *ChemSusChem* (2011) doi:10.1002/cssc.201100296.

117. Ramírez, E. Soto, R. Bringué, R. Iborra, M. & Tejero, J. Catalytic Hydroxyalkylation/Alkylation of 2-Methylfuran with Butanal to Form a Biodiesel Precursor Using Acidic Ion-Exchange Resins. *Ind. Eng. Chem. Res.* **59**, (2020).

118. Wen, C. Barrow, E. Hattrick-Simpers, J. & Lauterbach, J. One-step production of long- chain hydrocarbons from waste-biomass-derived chemicals using bi-functional heterogeneous catalysts. *Phys. Chem. Chem. Phys.* (2014) doi:10.1039/c3cp54495h.

119. Strohmann, M. Bordet, A. Vorholt, A. J. & Leitner, W. Tailor-made biofuel 2- butyltetrahydrofuran from the continuous flow hydrogenation and deoxygenation of furfuralacetone. *Green Chem.* **21**, (2019).

120. Eldeeb, M. & Akih-Kumgeh, B. Recent Trends in the Production, Combustion and Modeling of Furan-Based Fuels. *Energies* (2018) doi:10.3390/en11030512.

121. Srinivasamurthy, V. S. T. Böttcher, D. Engel, J. Kara, S. & Bornscheuer, U. T. A whole-cell process for the production of ε-caprolactone in aqueous media. *Process Biochem.* (2020) doi:10.1016/j.procbio.2019.10.009.

122. Buntara, T. … Heeres, H. J. Caprolactam from renewable resources: Catalytic conversion of 5-hydroxymethylfurfural into caprolactone. *Angew. Chemie - Int. Ed.*

(2011) doi:10.1002/anie.201102156.

123. Schmidt, S. … Bornscheuer, U. T. An enzyme cascade synthesis of ε-caprolactone and its oligomers. *Angew. Chemie - Int. Ed.* (2015) doi:10.1002/anie.201410633.

124. Haan, R. J. & Lange, J.-P. Process for Preparing an Ester. (2010).

125. Lange, J.-P. Process for Hydrogenation. (2010).

126. Van Den Brink, P. J. PROCESS FOR THE HYDROGENATION OFA LACTONE OR OF A CARBOXYLIC ACID OR ANESTER HAVING A GAMMA-CARBONYL GROUP. (2005).

127. Page, G. V, Eilerman, R. G. & Merrick, N. Y. PROCESS FOR THE PREPARATION OF GAMMA AND DELTA LACTONES. (1988).

128. Chia, M. … Dumesic, J. A. Mechanistic insights into ring-opening and decarboxylation of 2-pyrones in liquid water and tetrahydrofuran. *J. Am. Chem. Soc.* (2013) doi:10.1021/ja312075r.

129. Gupta, S. Arora, R. Sinha, N. Alam, M. I. & Haider, M. A. Mechanistic insights into the ring-opening of biomass derived lactones. *RSC Adv.* (2016) doi:10.1039/c5ra22832h.

130. Cross, J. H. … Burkholder, W. E. Sex pheromone components and calling behavior of the female dermestid beetle, Trogoderma variabile Ballion (Coleoptera: Dermestidae). *J. Chem. Ecol.* (1977) doi:10.1007/BF00994138.

131. Naoshima, Y. Ozawa, H. Kondo, H. & Hayashi, S. Synthesis of Racemates and (+)-Enantiomers of γ-Caprolactone, γ -Dodecanolactone and δ-Hexadecanolactone, Lactonic Sex Pheromones of the Dermestid Beetle, Rove Beetle and Oriental Hornet. *Agric. Biol. Chem.* (1983) doi:10.1271/bbb1961.47.1431.

132. Page, G. V. Process for the Preparation of gamma and delta Lactones. (1989).

133. Neto, R. S. Pastore, G. M. & Macedo, G. A. Biocatalysis and Biotransformation Producing γ-Decalactone. *J. Food Sci.* (2006) doi:10.1111/j.1365-2621.2004.tb09914.x.

134. Schrader, J. Etschmann, M. M. W. Sell, D. Hilmer, J. M. & Rabenhorst, J. Applied biocatalysis for the synthesis of natural flavour compounds - Current industrial processes and future prospects. *Biotechnology Letters* (2004) doi:10.1023/B:BILE.0000019576.80594.0e.

135. Tahara, S. Fujiwara, K. & Mizutani, J. Neutral constituents of volatiles in cultured broth of sporobolomyces odorus. *Agric. Biol. Chem.* (1973) doi:10.1271/bbb1961.37.2855.

136. Lin, S. J. Lee, S. L. & Chou, C. C. Effects of various fatty acid components of castor oil on the growth and production of γ-decalactone by Sporobolomyces odorus. *J. Ferment. Bioeng.* (1996) doi:10.1016/0922-338X(96)89452-9.

137. Pagot, Y. Endrizzi, A. Nicaud, J. M. & Belin, J. M. Utilization of an auxotrophic strain of the yeast Yarrowia lipolytica to improve γ-decalactone production yields. *Lett. Appl. Microbiol.* (1997) doi:10.1046/j.1472-765X.1997.00182.x.

138. Moradi, H. Asadollahi, M. A. & Nahvi, I. Improved γ-decalactone production from castor oil by fed-batch cultivation of Yarrowia lipolytica. *Biocatal. Agric. Biotechnol.* (2013) doi:10.1016/j.bcab.2012.11.001.

139. Aguedo, M. … Belo, I. Decalactone production by Yarrowia lipolytica under increased O2 transfer rates. *Biotechnol. Lett.* (2005) doi:10.1007/s10529-005-2517-z.

140. An, J. U. Joo, Y. C. & Oh, D. K. New biotransformation process for production of the fragrant compound γ-dodecalactone from 10-hydroxystearate by permeabilized waltomyces lipofer cells. *Appl. Environ. Microbiol.* (2013) doi:10.1128/AEM.02602-12.

141. Jo, Y. S. An, J. U. & Oh, D. K. γ-Dodecelactone production from safflower oil via 10-hydroxy-12(z)-octadecenoic acid intermediate by whole cells of candida boidinii and stenotrophomonas nitritireducens. *J. Agric. Food Chem.* (2014) doi:10.1021/jf501081z.

142. Serra, S. & De Simeis, D. Use of Lactobacillus rhamnosus (ATCC 53103) as whole-cell biocatalyst for the regio- and stereoselective hydration of oleic, linoleic, and linolenic acid. *Catalysts* (2018) doi:10.3390/catal8030109.

143. Corma, A. Iborra, S. Mifsud, M. Renz, M. & Susarte, M. A new environmentally benign catalytic process for the asymmetric synthesis of lactones: Synthesis of the flavouring δ-decalactone molecule. *Adv. Synth. Catal.* (2004) doi:10.1002/adsc.200303234.

144. Alam, M. I. Khan, T. S. & Haider, M. A. Alternate Biobased Route to Produce Î-Decalactone: Elucidating the Role of Solvent and Hydrogen Evolution in Catalytic Transfer Hydrogenation. *ACS Sustain. Chem. Eng.* (2019) doi:10.1021/acssuschemeng.8b05014.

145. Brown, H. C. Brewster, J. H. & Shechter, H. An Interpretation of the Chemical Behavior of Five- and Six-membered Ring Compounds. *J. Am. Chem. Soc.* (1954) doi:10.1021/ja01631a041.

146. Ha, L. Mao, J. Zhou, J. Zhang, Z. C. & Zhang, S. Skeletal isomerization of unsaturated fatty acids on Beta zeolites: Effects of calcination temperature and additives. *Appl. Catal. A Gen.* (2009) doi:10.1016/j.apcata.2008.12.018.

147. Gupta, C. A Biotechnological Approach to Microbial Based Perfumes and Flavours. *J. Microbiol. Exp.* (2015) doi:10.15406/jmen.2015.02.00034.

148. van der Schaft, P. H. ter Burg, N. van den Bosch, S. & Cohen, A. M. Microbial production of natural δ-decalactone and δ-dodecalactone from the corresponding α,β-unsaturated lactones in Massoi bark oil. *Appl. Microbiol. Biotechnol.* (1992) doi:10.1007/BF00172180.

149. Yang, E. J. Kim, Y. S. & Chang, H. C. Purification and characterization of antifungal δ-dodecalactone from lactobacillus plantarum AF1 isolated from kimchi. *J. Food Prot.* (2011) doi:10.4315/0362-028X.JFP-10-512.

150. Saitoh. *(12) United States Patent) Date of Patent: (54) PROCESS FOR PRODUCING HYDROXYLATED FATTY ACID AND DELTA-LACTONE.* (2004).

151. Weeks, M. H. D. B. J. *Topical Hazard Evaluation Program of Candidate Insect Repellent A13-36030 d-dodecalactone.* (1976).

152. Bretler, Gil. Dean, C. PROCESS FOR THE BiOTECHNOLOGICAL PRODUCTION OF D-DECALACTONE AND D-DODECALACTONE. (2000).

153. Zamfirescu, C. & Dincer, I. Ammonia as a green fuel and hydrogen source for vehicular applications. *Fuel Process. Technol.* (2009) doi:10.1016/j.fuproc.2009.02.004.

154. Kroch, E. Ammonia - A Fuel for Motor Buses. *J. Inst. Pet.* **31**, 213–223 (1945).

155. Gray, J. T. Dimitroff, E. Meckel, N. T. & Quillian, R. D. Ammonia fuel - Engine compatibility and combustion. in *SAE Technical Papers* (1966). doi:10.4271/660156.

156. Dec, J. E. A Conceptual Model of DI Diesel Combustion Based on Laser-Sheet Imaging*. in (1997). doi:10.4271/970873.

157. Arrègle, J. López, J. J. García, J. M. & Fenollosa, C. Development of a zero-dimensional Diesel combustion model: Part 2: Analysis of the transient initial and final diffusion combustion phases. *Appl. Therm. Eng.* **23**, 1319–1331 (2003).

158. TAO, F. SRINIVAS, S. REITZ, R. D. & FOSTER, D. E. Comparison of Three Soot Models Applied to Multi-Dimensional Diesel Combustion Simulations. *JSME Int. J. Ser. B* (2005) doi:10.1299/jsmeb.48.671.

159. Arrègle, J. López, J. J. García, J. M. & Fenollosa, C. Development of a zero-dimensional Diesel combustion model. Part 1: Analysis of the quasi-steady diffusion combustion phase. *Appl. Therm. Eng.* **23**, 1301–1317 (2003).

160. Westbrook, C. K. *CHEMICAL KINETICS OF HYDROCARBON IGNITION IN PRACTICAL COMBUSTION SYSTEMS. Proceedings of the Combustion Institute* vol. 28 (2000).

161. Zádor, J. Taatjes, C. A. & Fernandes, R. X. Kinetics of elementary reactions in low-temperature autoignition chemistry. *Progress in Energy and Combustion Science* (2011) doi:10.1016/j.pecs.2010.06.006.

162. Huynh, L. K. Panasewicz, S. Ratkiewicz, A. & Truong, T. N. Ab initio study on the

kinetics of hydrogen abstraction for the H + alkene → H2 + alkenyl reaction class. *J. Phys. Chem. A* (2007) doi:10.1021/jp066659u.

163. Hu, W. P. Rossi, I. Corchado, J. C. & Truhlar, D. G. Molecular modeling of combustion kinetics. The abstraction of primary and secondary hydrogens by hydroxyl radical. *J. Phys. Chem. A* (1997) doi:10.1021/jp970188h.

164. Whitehouse, N. D. & Way, R. *RATE OF HEAT RELEASE IN DIESEL ENGINES AND ITS CORRELATION WITH FUEL INJECTION DATA*.

165. Neshat, E. Honnery, D. & Saray, R. K. Multi-zone model for diesel engine simulation based on chemical kinetics mechanism. *Appl. Therm. Eng.* (2017) doi:10.1016/j.applthermaleng.2017.04.090.

166. Asad, U. & Zheng, M. Fast heat release characterization of a diesel engine. *Int. J. Therm. Sci.* **47**, 1688–1700 (2008).

167. LAVOIE, G. A. & BLUMBERG, P. N. A Fundamental Model for Predicting Fuel Consumption, NOx and HC Emissions of the Conventional Spark-Ignited Engine. *Combust. Sci. Technol.* **21**, 225–258 (1980).

168. Bär, F. Hopf, H. Knorr, M. Schröder, O. & Krahl, J. Effect of hydrazides as fuel additives for biodiesel and biodiesel blends on NOx formation. *Fuel* (2016) doi:10.1016/j.fuel.2016.04.028.

169. Reşitołlu, I. A. Altinişik, K. & Keskin, A. The pollutant emissions from diesel-engine vehicles and exhaust aftertreatment systems. *Clean Technologies and Environmental Policy* (2015) doi:10.1007/s10098-014-0793-9.

170. Zheng, M. Reader, G. T. & Hawley, J. G. Diesel engine exhaust gas recirculation—a review on advanced and novel concepts. *Energy Convers. Manag.* **45**, 883–900 (2004).

171. Dhal, G. C. Mohan, D. & Prasad, R. Preparation and application of effective different catalysts for simultaneous control of diesel soot and NO$_X$ emissions: An overview.

Catal. Sci. Technol. (2017) doi:10.1039/C6CY02612E.

172. Makwana, N. R. & Dabhi, S. K. *Automotive Exhaust Technology after Treatment for the Reduction of Emission-A Review Study.* www.ijert.org.

173. Koebel, M. Elsener, M. & Kleemann, M. Urea-SCR: a promising technique to reduce NOx emissions from automotive diesel engines. *Catal. Today* (2000) doi:10.1016/S0920-5861(00)00299-6.

174. Mitianiec, W. PREDICTION OF NOx REDUCTION IN THE SELECTIVE CATALYTIC REACTOR. in (2014).

175. Lee, K. Ogita, Y. Sato, S. & Kosaka, H. NOx Reduction with the HC-SCR System over Cu/Zeolite Based Catalysts. in *SAE Technical Paper Series* vol. 1 (SAE International, 2015).

176. Frobert, A. … Blanchard, G. HC-SCR on Silver-Based Catalyst: From Synthetic Gas Bench to Real Use. *SAE Int. J. Fuels Lubr.* **5**, 389–398 (2011).

177. Colsa, A. *DIRECTORATE GENERAL FOR INTERNAL POLICIES Comparative study on the differences between the EU and US legislation on emissions in the automotive sector.* (2016).

178. Mahmudul, H. M. … Alenezi, R. Production, characterization and performance of biodiesel as an alternative fuel in diesel engines – A review. *Renewable and Sustainable Energy Reviews* (2017) doi:10.1016/j.rser.2017.01.001.

179. Knothe, G. *History of Vegetable Oil-Based Diesel Fuels. The Biodiesel Handbook* (AOCS Press, 2010). doi:10.1016/B978-1-893997-62-2.50007-3.

180. Can, ï¿½zer, ï¿½ztï¿½rk, E. & Yï¿½cesu, H. S. Combustion and exhaust emissions of canola biodiesel blends in a single cylinder DI diesel engine. *Renew. Energy* (2017) doi:10.1016/j.renene.2017.03.017.

181. Hellier, P. Ladommatos, N. & Yusaf, T. The influence of straight vegetable oil fatty acid composition on compression ignition combustion and emissions. *Fuel* (2015)

doi:10.1016/j.fuel.2014.11.021.

182. Kumar, M. … Tsang, D. C. W. Algae as potential feedstock for the production of biofuels and value-added products: Opportunities and challenges. *Science of the Total Environment* vol. 716 (2020).

183. Sathish, T. & Singaravelu, D. K. Combustion analysis using third generation biofuels in diesel engine. *J. Sci. Ind. Res. (India).* **79**, (2020).

184. Karthikeyan, S. Periyasamy, M. Prathima, A. & Sabariswaran, K. Combustion analysis of single-cylinder CI engine fueled with S. Marginatum Macro algae biofuel - Diesel blends. in *Materials Today: Proceedings* vol. 33 (2020).

185. Yilmaz, N. & Atmanli, A. Experimental assessment of a diesel engine fueled with diesel-biodiesel-1-pentanol blends. *Fuel* (2017) doi:10.1016/j.fuel.2016.11.065.

186. Singh, D. … Jhalani, A. A comprehensive review of biodiesel production from waste cooking oil and its use as fuel in compression ignition engines: 3rd generation cleaner feedstock. *Journal of Cleaner Production* vol. 307 (2021).

187. Li, G. … Zhang, T. Synthesis of high-quality diesel with furfural and 2-methylfuran from hemicellulose. *ChemSusChem* (2012) doi:10.1002/cssc.201200228.

188. Zheng, Z. Wang, X. Yue, L. Liu, H. & Yao, M. Effects of six-carbon alcohols, ethers and ketones with chain or ring molecular structures on diesel low temperature combustion. *Energy Convers. Manag.* (2016) doi:10.1016/j.enconman.2016.07.057.

189. Westbrook, C. K. Pitz, W. J. & Curran, H. J. Chemical kinetic modeling study of the effects of oxygenated hydrocarbons on soot emissions from diesel engines. *J. Phys. Chem. A* (2006) doi:10.1021/jp056362g.

190. Buchholz, B. A. … Westbrook, C. K. Using Carbon-14 Isotope Tracing to Investigate Molecular Structure Effects of the Oxygenate Dibutyl Maleate on Soot Emissions from a DI Diesel Engine. (2004).

191. Fang, J. … Wang, J. Sooting tendency analysis of oxygenate-diesel blended fuels by

the affecting indicators of carbon number, oxygen content and H/C ratio. *Fuel* **290**, (2021).

192. Jenkins, R. W. … Sutton, A. D. The Effect of Functional Groups in Bio-Derived Fuel Candidates. *ChemSusChem* (2016) doi:10.1002/cssc.201600159.

193. Dahmen, M. & Marquardt, W. A Novel Group Contribution Method for the Prediction of the Derived Cetane Number of Oxygenated Hydrocarbons. *Energy and Fuels* (2015) doi:10.1021/acs.energyfuels.5b01032.

194. Boot, M. D. Tian, M. Hensen, E. J. M. & Mani Sarathy, S. Impact of fuel molecular structure on auto-ignition behavior – Design rules for future high performance gasolines. *Progress in Energy and Combustion Science* (2017) doi:10.1016/j.pecs.2016.12.001.

195. Zhang, Z. H. & Balasubramanian, R. Investigation of particulate emission characteristics of a diesel engine fueled with higher alcohols/biodiesel blends. *Appl. Energy* (2016) doi:10.1016/j.apenergy.2015.10.173.

196. Xiao, H. … Ruan, J. Combustion performance and emission characteristics of diesel engine fueled with iso-butanol/biodiesel blends. *Fuel* **268**, (2020).

197. Fayad, M. A. Investigating the influence of oxygenated fuel on particulate size distribution and NOX control in a common-rail diesel engine at rated EGR levels. *Therm. Sci. Eng. Prog.* **19**, (2020).

198. Zeng, A. P. & Sabra, W. Microbial production of diols as platform chemicals: Recent progresses. *Current Opinion in Biotechnology* (2011) doi:10.1016/j.copbio.2011.05.005.

199. Yim, H. … Van Dien, S. Metabolic engineering of Escherichia coli for direct production of 1,4-butanediol. *Nat. Chem. Biol.* **7**, (2011).

200. Huang, W.-C. Ramey, D. E. & Yang, S.-T. Continuous production of butanol by clostridium acetobutylicum immobilized in a fibrous bed bioreactor. *Appl. Biochem.*

Biotechnol. **115**, 887–898 (2004).

201. Vinod Babu, V. B. M. Madhu Murthy, M. M. K. & Amba Prasad Rao, G. Butanol and pentanol: The promising biofuels for CI engines – A review. *Renewable and Sustainable Energy Reviews* (2017) doi:10.1016/j.rser.2017.05.038.

202. Koivisto, E. Ladommatos, N. & Gold, M. Systematic study of the effect of the hydroxyl functional group in alcohol molecules on compression ignition and exhaust gas emissions. *Fuel* (2015) doi:10.1016/j.fuel.2015.03.042.

203. Rakopoulos, D. C. … Papagiannakis, R. G. Investigation of the performance and emissions of bus engine operating on butanol/diesel fuel blends. *Fuel* (2010) doi:10.1016/j.fuel.2010.03.047.

204. Yilmaz, N. Vigil, F. M. Benalil, K. Davis, S. M. & Calva, A. Effect of biodiesel-butanol fuel blends on emissions and performance characteristics of a diesel engine. *Fuel* (2014) doi:10.1016/j.fuel.2014.06.022.

205. Yilmaz, N. Atmanli, A. & Vigil, F. M. Quaternary blends of diesel, biodiesel, higher alcohols and vegetable oil in a compression ignition engine. *Fuel* (2018) doi:10.1016/j.fuel.2017.10.050.

206. Rajesh Kumar, B. Saravanan, S. Rana, D. & Nagendran, A. Use of some advanced biofuels for overcoming smoke/NO x trade-off in a light-duty DI diesel engine. (2016) doi:10.1016/j.renene.2016.05.029.

207. Fayad, M. A. … Lapuerta, M. Manipulating modern diesel engine particulate emission characteristics through butanol fuel blending and fuel injection strategies for efficient diesel oxidation catalysts. *Appl. Energy* (2017) doi:10.1016/j.apenergy.2016.12.102.

208. Yesilyurt, M. K. Yilbasi, Z. & Aydin, M. The performance, emissions, and combustion characteristics of an unmodified diesel engine running on the ternary blends of pentanol/safflower oil biodiesel/diesel fuel. *J. Therm. Anal. Calorim.* **140**, 2903–2942 (2020).

209. Lapuerta, M. Rodrïguez-Fernandez, J. Fernandez-Rodriguez, D. & Patino-Camino, R. Modeling viscosity of butanol and ethanol blends with diesel and biodiesel fuels. *Fuel* (2017) doi:10.1016/j.fuel.2017.02.101.

210. Ibrahim, A. Performance and combustion characteristics of a diesel engine fuelled by butanol-biodiesel-diesel blends. *Appl. Therm. Eng.* (2016) doi:10.1016/j.applthermaleng.2016.04.144.

211. Wang, C. … Ma, X. Combustion characteristics and emissions of 2-methylfuran compared to 2,5-dimethylfuran, gasoline and ethanol in a DISI engine. in *Fuel* (2013). doi:10.1016/j.fuel.2012.05.043.

212. Daniel, R. … Huang, Z. Effect of spark timing and load on a DISI engine fuelled with 2,5-dimethylfuran. *Fuel* (2011) doi:10.1016/j.fuel.2010.10.008.

213. Hoang, A. T. Nizetic, S. Olcer, A. . & Ong, H. C. Synthesis pathway and combustion mechanism of a sustainable biofuel 2,5-Dimethylfuran: Progress and prospective. *Fuel* **286**, (2021).

214. Tuan Hoang, A. & Viet Pham, V. 2-Methylfuran (MF) as a potential biofuel: A thorough review on the production pathway from biomass, combustion progress, and application in engines. *Renewable and Sustainable Energy Reviews* vol. 148 (2021).

215. Liu, H. Olalere, R. Wang, C. Ma, X. & Xu, H. Combustion characteristics and engine performance of 2-methylfuran compared to gasoline and ethanol in a direct injection spark ignition engine. *Fuel* **299**, (2021).

216. Xiao, H. … Ju, H. Combustion performance and pollutant emissions analysis of a diesel engine fueled with biodiesel and its blend with 2-methylfuran. *Fuel* **237**, (2019).

217. Wu, S. Tay, K. L. Li, J. Yang, W. & Yang, S. Development of a compact and robust kinetic mechanism for furan group biofuels combustion in internal combustion engines. *Fuel* **298**, (2021).

218. Jiang, C. Wang, C. Xu, H. Liu, H. & Ma, X. Engine performance and emissions of

furan-series biofuels under stratified lean-burn combustion mode. *Fuel* **285**, (2021).

219. Xu, N. … Huang, Z. Ignition delay times of low alkylfurans at high pressures using a rapid compression machine. *Proc. Combust. Inst.* (2017) doi:10.1016/j.proci.2016.07.075.

220. Xu, C. … Wei, L. Experimental and numerical study on laminar premixed flame characteristics of 2-ethylfuran. *Combust. Flame* **234**, (2021).

221. Song, S. … Wei, L. Experimental and kinetic modeling studies of 2-ethylfuran pyrolysis at low and atmospheric pressures. *Combust. Flame* **226**, 430–444 (2021).

222. Cai, L. … Pitsch, H. Experimental and numerical study of a novel biofuel: 2-Butyltetrahydrofuran. *Combust. Flame* **178**, 257–267 (2016).

223. Eldeeb, M. A. & Akih-Kumgeh, B. Reactivity trends in furan and alkyl furan combustion. *Energy and Fuels* (2014) doi:10.1021/ef501181z.

224. Eldeeb, M. A. & Akih-Kumgeh, B. Investigation of 2,5-dimethyl furan and iso-octane ignition. *Combust. Flame* (2015) doi:10.1016/j.combustflame.2015.02.013.

225. Jouzdani, S. Eldeeb, M. A. Zhang, L. & Akih-Kumgeh, B. High-Temperature Study of 2-Methyl Furan and 2-Methyl Tetrahydrofuran Combustion. *Int. J. Chem. Kinet.* (2016) doi:10.1002/kin.21008.

226. Wang, J. Wang, X. Fan, X. Yang, K. & Zhang, Y. An ignition delay time and kinetic study of 2-methyltetrahydrofuran at high temperatures. *Fuel* (2016) doi:10.1016/j.fuel.2016.08.104.

227. Fan, X. Wang, X. Wang, J. & Yang, K. Comparative Shock Tube and Kinetic Study on High-Temperature Ignition of 2,3-Dihydrofuran and 2,5-Dihydrofuran. doi:10.1021/acs.energyfuels.6b01332.

228. de Jong, E. Vijlbrief, T. Hijkoop, R. Gruter, G. J. M. & van der Waal, J. C. Promising results with YXY Diesel components in an ESC test cycle using a PACCAR Diesel engine. *Biomass and Bioenergy* (2012) doi:10.1016/j.biombioe.2011.10.034.

229. Tuan Hoang, A. … Vang Le, V. Combustion and emission characteristics of spark and compression ignition engine fueled with 2,5-dimethylfuran (DMF): A comprehensive review. *Fuel* vol. 288 (2021).

230. Sirignano, M. Conturso, M. & D'Anna, A. Effect of furans on particle formation in diffusion flames: An experimental and modeling study. *Proc. Combust. Inst.* (2015) doi:10.1016/j.proci.2014.05.062.

231. Chen, G. … Liu, H. Experimental study on combustion and emission characteristics of a diesel engine fueled with 2,5-dimethylfuran-diesel, n-butanol-diesel and gasoline-diesel blends. *Energy* (2013) doi:10.1016/j.energy.2013.02.069.

232. Chen, G. Di, L. Zhang, Q. Zheng, Z. & Zhang, W. Effects of 2,5-dimethylfuran fuel properties coupling with EGR (exhaust gas recirculation) on combustion and emission characteristics in common-rail diesel engines. *Energy* (2015) doi:10.1016/j.energy.2015.09.066.

233. Lima, C. G. S. Monteiro, J. L. de Melo Lima, T. Weber Paixão, M. & Corrêa, A. G. Angelica Lactones: From Biomass-Derived Platform Chemicals to Value-Added Products. *ChemSusChem* (2018) doi:10.1002/cssc.201701469.

234. Raspolli Galletti, A. M. … Bonari, E. From giant reed to levulinic acid and gamma-valerolactone: A high yield catalytic route to valeric biofuels. *Appl. Energy* (2013) doi:10.1016/j.apenergy.2012.05.061.

235. Bereczky, Á. Lukács, K. Farkas, M. & Dóbé, S. Effect of <i>γ</i>-Valerolactone Blending on Engine Performance, Combustion Characteristics and Exhaust Emissions in a Diesel Engine. *Nat. Resour.* (2014) doi:10.4236/nr.2014.55017.

236. Horváth, I. T. Mehdi, H. Fábos, V. Boda, L. & Mika, L. T. γ-Valerolactone—a sustainable liquid for energy and carbon-based chemicals. *Green Chem.* (2008) doi:10.1039/b712863k.

237.   Gschwend, D. Soltic, P. Wokaun, A. & Vogel, F. Review and Performance Evaluation of Fifty Alternative Liquid Fuels for Spark-Ignition Engines. *Energy and Fuels* (2019) doi:10.1021/acs.energyfuels.8b02910.

238.   Bohre, A. Dutta, S. Saha, B. & Abu-Omar, M. M. Upgrading Furfurals to Drop-in Biofuels: An Overview. *ACS Sustainable Chemistry and Engineering* (2015) doi:10.1021/acssuschemeng.5b00271.

239.   Kobayashi, S. Takeya, K. Suda, S. & Uyama, H. Lipase-catalyzed ring-opening polymerization of medium-size lactones to polyesters. *Macromol. Chem. Phys.* (1998) doi:10.1002/(SICI)1521-3935(19980801)199:8<1729::AID-MACP1729>3.0.CO;2-V.

240.   Saravanan, N. Nagarajan, G. Sanjay, G. Dhanasekaran, C. & Kalaiselvan, K. M. Combustion analysis on a DI diesel engine with hydrogen in dual fuel mode. *Fuel* (2008) doi:10.1016/j.fuel.2008.07.011.

241.   Lee, L. C. W. An investigation of a cause of backfire and its control due to crevice volumes in hydrogen fueled engine. *J. Eng. Gas Turbines Power* (2001) doi:10.1115/1.1339985.

242.   Christodoulou, F. & Megaritis, A. Experimental investigation of the effects of separate hydrogen and nitrogen addition on the emissions and combustion of a diesel engine. *Int. J. Hydrogen Energy* (2013) doi:10.1016/j.ijhydene.2013.05.173.

243.   Talibi, M. Hellier, P. Balachandran, R. & Ladommatos, N. Effect of hydrogen-diesel fuel co-combustion on exhaust emissions with verification using an in-cylinder gas sampling technique. *Int. J. Hydrogen Energy* (2014) doi:10.1016/j.ijhydene.2014.07.039.

244.   Casanovas, A. Divins, N. J. Rejas, A. Bosch, R. & Llorca, J. Finding a suitable catalyst for on-board ethanol reforming using exhaust heat from an internal combustion engine. *Int. J. Hydrogen Energy* (2017) doi:10.1016/j.ijhydene.2016.11.197.

245.   Li, H. … Zhu, L. On-board methanol catalytic reforming for hydrogen Production-A

review. *International Journal of Hydrogen Energy* (2021)
doi:10.1016/j.ijhydene.2021.04.062.

246. Woo, S. Baek, S. & Lee, K. On-board LPG reforming system for an LPG · hydrogen
mixed combustion engine. *Int. J. Hydrogen Energy* (2020)
doi:10.1016/j.ijhydene.2020.02.139.

247. Umar, M. … Tsolakis, A. Hydrogen production from bioethanol fuel mixtures via
exhaust heat recovery in diesel engines: A promising route towards more energy
efficient road vehicles. *Int. J. Hydrogen Energy* (2021)
doi:10.1016/j.ijhydene.2021.04.146.

248. Lhuillier, C. Brequigny, P. Contino, F. & Mounaïm-Rousselle, C. Experimental study on
ammonia/hydrogen/air combustion in spark ignition engine conditions. *Fuel* (2020)
doi:10.1016/j.fuel.2020.117448.

249. Reiter, A. J. & Kong, S. C. Demonstration of compression-ignition engine combustion
using ammonia in reducing greenhouse gas emissions. *Energy and Fuels* (2008)
doi:10.1021/ef800140f.

250. Duynslaegher, C. & Jeanmart Pr O Gicquel Pr J Martin Pr D Peeters Pr D Puechberty,
P. H. *Université catholique de Louvain Experimental and numerical study of ammonia
combustion.* (2011).

251. Fenimore, C. P. & Jones, G. W. Oxidation of ammonia in flames. *J. Phys. Chem.*
(1961) doi:10.1021/j100820a027.

252. Bian, J. Vandooren, J. & Van Tiggelen, P. J. Experimental study of the structure of an
ammonia-oxygen flame. *Symp. Combust.* (1988) doi:10.1016/S0082-0784(88)80327-
8.

253. Frigo, S. & Gentili, R. Analysis of the behaviour of a 4-stroke Si engine fuelled with
ammonia and hydrogen. *Int. J. Hydrogen Energy* (2013)
doi:10.1016/j.ijhydene.2012.10.114.

254. Grannell, S. M. Assanis, D. N. Bohac, S. V. & Gillespie, D. E. The fuel mix limits and efficiency of a stoichiometric, ammonia, and gasoline dual fueled spark ignition engine. *J. Eng. Gas Turbines Power* (2008) doi:10.1115/1.2898837.

255. Grannell, S. M. Assanis, D. N. Bohac, S. V. & Gillespie, D. E. The operating features of a stoichiometric, ammonia and gasoline dual fueled spark ignition engine. in *2006 ASME International Mechanical Engineering Congress and Exposition, IMECE2006 - Energy* (2006). doi:10.1115/IMECE2006-13048.

256. Grannell, S. M. Assanis, D. N. Gillespie, D. E. & Bohac, S. V. Exhaust emissions from a stoichiometric, ammonia and gasoline dual fueled spark ignition engine. in *Proceedings of the Spring Technical Conference of the ASME Internal Combustion Engine Division* (2009). doi:10.1115/ICES2009-76131.

257. Starkman, E. S. Newhall, H. K. Sutton, R. Maguire, T. & Farbar, L. Ammonia as a spark ignition engine fuel: Theory and application. in *SAE Technical Papers* (1966). doi:10.4271/660155.

258. Wang, W. Herreros, J. M. Tsolakis, A. & York, A. P. E. Ammonia as hydrogen carrier for transportation; Investigation of the ammonia exhaust gas fuel reforming. *Int. J. Hydrogen Energy* (2013) doi:10.1016/j.ijhydene.2013.05.144.

259. Sawyer, R. F. Starkman, E. S. Muzio, L. & Schmidt, W. L. Oxides of nitrogen in the combustion products of an ammonia fueled reciprocating engine. in *SAE Technical Papers* (1968). doi:10.4271/680401.

260. Tanaka, S. Ayala, F. Keck, J. C. & Heywood, J. B. Two-stage ignition in HCCI combustion and HCCI control by fuels and additives. *Combust. Flame* (2003) doi:10.1016/S0010-2180(02)00457-1.

261. Westlye, F. R. Ivarsson, A. & Schramm, J. Experimental investigation of nitrogen based emissions from an ammonia fueled SI-engine. *Fuel* (2013) doi:10.1016/j.fuel.2013.03.055.

262. Ryu, K. Zacharakis-Jutz, G. E. & Kong, S. C. Effects of gaseous ammonia direct injection on performance characteristics of a spark-ignition engine. *Appl. Energy* (2014) doi:10.1016/j.apenergy.2013.11.067.

263. Pochet, M. Dias, V. Jeanmart, H. Verhelst, S. & Contino, F. Multifuel CHP HCCI Engine towards Flexible Power-to-fuel: Numerical Study of Operating Range. in *Energy Procedia* (2017). doi:10.1016/j.egypro.2017.03.468.

264. Christensen, M. Johansson, B. Amnéus, P. & Mauss, F. Supercharged homogeneous charge compression ignition. in *SAE Technical Papers* (1998). doi:10.4271/980787.

265. Kittelson, D. & Kraft, M. Particle Formation and Models in Internal Combustion Engines. (2014).

266. Palmer, H. B. & Cullis, C. F. The formation of carbon from gases. *Chem. Phys. carbon* **1**, 265–325 (1965).

267. Frenklach, M. & Wang, H. Detailed modeling of soot particle nucleation and growth. *Symp. Combust.* (1991) doi:10.1016/S0082-0784(06)80426-1.

268. Tree, D. R. & Svensson, K. I. Soot processes in compression ignition engines. *Progress in Energy and Combustion Science* (2007) doi:10.1016/j.pecs.2006.03.002.

269. Zhong, B.-J. Dang, S. Song, Y.-N. & Gong, J.-S. 3-D simulation of soot formation in a direct-injection diesel engine based on a comprehensive chemical mechanism and method of moments. *Combust. Theory Model.* **16**, 143–171 (2012).

270. Frenklach, M. Reaction mechanism of soot formation in flames. *Phys. Chem. Chem. Phys.* **4**, 2028–2037 (2002).

271. Wang, Y. Raj, A. & Chung, S. H. A PAH growth mechanism and synergistic effect on PAH formation in counterflow diffusion flames. *Combust. Flame* (2013) doi:10.1016/j.combustflame.2013.03.013.

272. Wang, Y. Raj, A. & Chung, S. H. Soot modeling of counterflow diffusion flames of ethylene-based binary mixture fuels. *Combust. Flame* (2015)

doi:10.1016/j.combustflame.2014.08.016.

273. Abdel-Shafy, H. I. & Mansour, M. S. M. A review on polycyclic aromatic hydrocarbons: Source, environmental impact, effect on human health and remediation. *Egyptian Journal of Petroleum* (2016) doi:10.1016/j.ejpe.2015.03.011.

274. Bruzzoniti, M. C. Fungi, M. & Sarzanini, C. Determination of EPA's priority pollutant polycyclic aromatic hydrocarbons in drinking waters by solid phase extraction-HPLC. *Anal. Methods* (2010) doi:10.1039/b9ay00203k.

275. Dandajeh, H. A. Ladommatos, N. Hellier, P. & Eveleigh, A. Effects of unsaturation of C2and C3hydrocarbons on the formation of PAHs and on the toxicity of soot particles. *Fuel* (2017) doi:10.1016/j.fuel.2017.01.015.

276. Kislov, V. V. Sadovnikov, A. I. & Mebel, A. M. Formation mechanism of polycyclic aromatic hydrocarbons beyond the second aromatic ring. *J. Phys. Chem. A* (2013) doi:10.1021/jp402481y.

277. Chernov, V. Thomson, M. J. Dworkin, S. B. Slavinskaya, N. A. & Riedel, U. Soot formation with C 1 and C 2 fuels using an improved chemical mechanism for PAH growth. *Combust. Flame* **161**, 592–601 (2014).

278. Shukla, B. & Koshi, M. Importance of Fundamental sp, sp 2 , and sp 3 Hydrocarbon Radicals in the Growth of Polycyclic Aromatic Hydrocarbons. (2012) doi:10.1021/ac3006236.

279. Llamas, A. … Canoira, L. Polycyclic Aromatic Hydrocarbons (PAHs) produced in the combustion of fatty acid alkyl esters from different feedstocks: Quantification, statistical analysis and mechanisms of formation. *Sci. Total Environ.* (2017) doi:10.1016/j.scitotenv.2017.01.180.

280. Gómez, A. Soriano, J. A. & Armas, O. Evaluation of sooting tendency of different oxygenated and paraffinic fuels blended with diesel fuel. *Fuel* (2016) doi:10.1016/j.fuel.2016.07.049.

281. Liu, H. Bi, X. Huo, M. Lee, C. F. F. & Yao, M. Soot Emissions of Various Oxygenated Biofuels in Conventional Diesel Combustion and Low-Temperature Combustion Conditions. *Energy and Fuels* (2012) doi:10.1021/ef201720d.

282. Tran, L. S. Sirjean, B. Glaude, P. A. Kohse-Höinghaus, K. & Battin-Leclerc, F. Influence of substituted furans on the formation of Polycyclic Aromatic Hydrocarbons in flames. *Proc. Combust. Inst.* (2015) doi:10.1016/j.proci.2014.06.137.

283. Liu, H. … Yao, M. Laser diagnostics and chemical kinetic analysis of PAHs and soot in co-flow partially premixed flames using diesel surrogate and oxygenated additives of n-butanol and DMF. *Combust. Flame* **188**, (2018).

284. Cheng, Z. … Chen, G. Experimental and kinetic modeling study of 2-methylfuran pyrolysis at low and atmospheric pressures. *Energy and Fuels* **31**, (2017).

285. Zhang, Z. H. & Balasubramanian, R. Effects of oxygenated fuel blends on the composition of size-segregated engine-out diesel particulate emissions and on the toxicity of quasi-ultrafine particles. *Fuel* (2018) doi:10.1016/j.fuel.2017.10.097.

286. Smith, O. I. Fundamentals of soot formation in flames with application to diesel engine particulate emissions. *Prog. Energy Combust. Sci.* (1981) doi:10.1016/0360-1285(81)90002-2.

287. Berthelot, M. & Hebd, C. . No Title. *C. R. Hebd. Seances Acad. Sci* **62**, (1866).

288. Glassman, I. *Phenomenological Models of Soot Processes in Combustion Systems.* (1979).

289. Bittner, J. . & Howard, J. . No Title. in *Eighteenth Symposium (Int.) on Combustion (August 1980) to be presented.*

290. Hurd, C. D. & Spence, L. U. The pyrolysis of hydrocarbons: Isobutylene. *J. Am. Chem. Soc.* (1929) doi:10.1021/ja01387a008.

291. Hague, E. N. & Wheeler, R. V. The mechanism of thermal decomposition of the normal paraffins. *J. Chem. Soc.* (1929) doi:10.1039/jr9290000378.

292. Davidson, J. G. The formation of aromatic hydrocarbons from natural gas condensate. *Ind. Eng. Chem.* (1918) doi:10.1021/ie50107a013.

293. Cole, J. A. Bittner, J. D. Longwell, J. P. & Howard, J. B. Formation mechanisms of aromatic compounds in aliphatic flames. *Combust. Flame* (1984) doi:10.1016/0010-2180(84)90005-1.

294. Frenklach, M. Clary, D. W. Yuan, T. Gardiner, W. C. & Stein, S. E. Mechanism of Soot Formation in Acetylene-Oxygen Mixtures. *Combust. Sci. Technol.* (1986) doi:10.1080/00102208608923927.

295. Frenklach, M. & Warnatz, J. Detailed Modeling of PAH Profiles in a Sooting Low-Pressure Acetylene Flame. *Combust. Sci. Technol.* (1987) doi:10.1080/00102208708960325.

296. Colket, M. B. The pyrolysis of acetylene and vinylacetylene in a single-pulse shock tube. *Symp. Combust.* (1988) doi:10.1016/S0082-0784(88)80317-5.

297. Warnatz, J. Chemistry of high temperature combustion of alkanes up to octane. *Symp. Combust.* (1985) doi:10.1016/S0082-0784(85)80574-9.

298. Jin, H. … Farooq, A. Experimental and numerical study of polycyclic aromatic hydrocarbon formation in ethylene laminar co-flow diffusion flames. *Fuel* (2021) doi:10.1016/j.fuel.2020.119931.

299. SHUKLA, B. MIYOSHI, A. & KOSHI, M. Chemical Kinetic Mechanism of Polycyclic Aromatic Hydrocarbon Growth and Soot Formation. *J. Combust. Soc. Japan* (2008) doi:10.20619/jcombsj.50.151_8.

300. Skjøth-Rasmussen, M. S. … Christensen, T. S. A study of benzene formation in a laminar flow reactor. *Proc. Combust. Inst.* (2002) doi:10.1016/s1540-7489(02)80163-8.

301. Miller, J. A. & Klippenstein, S. J. The recombination of propargyl radicals and other reactions on a C6H6 potential. *J. Phys. Chem. A* (2003) doi:10.1021/jp030375h.

302. McEnally, C. S. & Pfefferle, L. D. Improved sooting tendency measurements for

aromatic hydrocarbons and their implications for naphthalene formation pathways. *Combust. Flame* (2007) doi:10.1016/j.combustflame.2006.11.003.

303. D'Anna, A. & Kent, J. H. Aromatic formation pathways in non-premixed methane flames. *Combust. Flame* (2003) doi:10.1016/S0010-2180(02)00522-9.

304. Wang, Y. & Chung, S. H. Soot formation in laminar counterflow flames. *Progress in Energy and Combustion Science* (2019) doi:10.1016/j.pecs.2019.05.003.

305. Westmoreland, P. R. Howard, J. B. & Longwell, J. P. Tests of published mechanisms by comparison with measured laminar flame structure in fuel-rich acetylene combustion. *Symp. Combust.* (1988) doi:10.1016/S0082-0784(88)80309-6.

306. Miller, J. A. & Melius, C. F. Kinetic and thermodynamic issues in the formation of aromatic compounds in flames of aliphatic fuels. *Combust. Flame* (1992) doi:10.1016/0010-2180(92)90124-8.

307. Georgievskii, Y. Miller, J. A. & Klippenstein, S. J. Association rate constants for reactions between resonance-stabilized radicals: C3H3 + C3H3, C 3H3 + C3H5, and C3H 5 + C3H5. *Phys. Chem. Chem. Phys.* (2007) doi:10.1039/b703261g.

308. Kislov, V. V. Islamova, N. I. Kolker, A. M. Lin, S. H. & Mebel, A. M. Hydrogen abstraction acetylene addition and Diels-Alder mechanisms of PAH formation: A detailed study using first principles calculations. *J. Chem. Theory Comput.* (2005) doi:10.1021/ct0500491.

309. Melius, C. F. Colvin, M. E. Marinov, N. M. Pit, W. J. & Senkan, S. M. Reaction mechanisms in aromatic hydrocarbon formation involving the C5H5 cyclopentadienyl moiety. *Symp. Combust.* (1996) doi:10.1016/S0082-0784(96)80276-1.

310. Moskaleva, L. V. Mebel, A. M. & Lin, M. C. The CH3+C5H5 reaction: A potential source of benene at high temperatures. *Symp. Combust.* (1996) doi:10.1016/S0082-0784(96)80255-4.

311. Blanquart, G. Pepiot-Desjardins, P. & Pitsch, H. Chemical mechanism for high

temperature combustion of engine relevant fuels with emphasis on soot precursors. *Combust. Flame* (2009) doi:10.1016/j.combustflame.2008.12.007.

312. Mueller, C. J. … Westbrook, C. K. Effects of oxygenates on soot processes in di diesel engines: Experiments and numerical simulations. in *SAE Technical Papers* (2003). doi:10.4271/2003-01-1791.

313. Eveleigh, A. Ladommatos, N. Balachandran, R. & Marca, A. Conversion of oxygenated and hydrocarbon molecules to particulate matter using stable isotopes as tracers. *Combust. Flame* (2014) doi:10.1016/j.combustflame.2014.05.008.

314. Eveleigh, A. Ladommatos, N. Hellier, P. & Jourdan, A. L. Quantification of the Fraction of Particulate Matter Derived from a Range of 13C-Labeled Fuels Blended into Heptane, Studied in a Diesel Engine and Tube Reactor. *Energy and Fuels* (2016) doi:10.1021/acs.energyfuels.6b00322.

315. Argachoy, C. Temperature analysis in the combustion of the fuel spray in diesel engines. in *SAE Technical Papers* (2007). doi:10.4271/2007-01-2524.

316. Flynn, P. F. … Westbrook, C. K. Diesel combustion: An integrated view combining laser diagnostics, chemical kinetics, and empirical validation. in *SAE Technical Papers* (1999). doi:10.4271/1999-01-0509.

317. Hielscher, K. Brauer, M. & Baar, R. Reduction of soot emissions in diesel engines due to increased air utilization by new spray hole configurations. *Automot. Engine Technol.* (2016) doi:10.1007/s41104-016-0010-4.

318. Eveleigh, A. The influence of fuel molecular structure on particulate emission investigated with isotope tracing. *Undefined* (2015).

319. Hellier, P. Ladommatos, N. Allan, R. & Rogerson, J. Influence of carbonate ester molecular structure on compression ignition combustion and emissions. *Energy and Fuels* (2013) doi:10.1021/ef401415j.

320. Liu, Y. … Wu, H. Experimental investigation on soot formation characteristics of n-

heptane/butanol isomers blends in laminar diffusion flames. *Energy* (2020) doi:10.1016/j.energy.2020.118714.

321. Saffaripour, M. Veshkini, A. Kholghy, M. & Thomson, M. J. Experimental investigation and detailed modeling of soot aggregate formation and size distribution in laminar coflow diffusion flames of Jet A-1, a synthetic kerosene, and n-decane. *Combust. Flame* (2014) doi:10.1016/j.combustflame.2013.10.016.

322. Botero, M. L. Mosbach, S. & Kraft, M. Sooting tendency of paraffin components of diesel and gasoline in diffusion flames. *Fuel* (2014) doi:10.1016/j.fuel.2014.02.005.

323. Blacha, T. Di Domenico, M. Gerlinger, P. & Aigner, M. Soot predictions in premixed and non-premixed laminar flames using a sectional approach for PAHs and soot. *Combust. Flame* (2012) doi:10.1016/j.combustflame.2011.07.006.

324. KC, U. Beshir, M. & Farooq, A. Simultaneous measurements of acetylene and soot during the pyrolysis of ethylene and benzene in a shock tube. *Proc. Combust. Inst.* (2017) doi:10.1016/j.proci.2016.08.087.

325. Manzello, S. L. … Tsang, W. Soot particle size distributions in a well-stirred reactor/plug flow reactor. *Proc. Combust. Inst.* (2007) doi:10.1016/j.proci.2006.07.013.

326. Sánchez, N. E. Millera, Á. Bilbao, R. & Alzueta, M. U. Polycyclic aromatic hydrocarbons (PAH), soot and light gases formed in the pyrolysis of acetylene at different temperatures: Effect of fuel concentration. in *Journal of Analytical and Applied Pyrolysis* (2013). doi:10.1016/j.jaap.2012.10.027.

327. Sánchez, N. E. Callejas, A. Millera, Á. Bilbao, R. & Alzueta, M. U. Influence of the oxygen presence on polycyclic aromatic hydrocarbon (PAH) formation from acetylene pyrolysis under sooting conditions. *Energy and Fuels* (2013) doi:10.1021/ef401484s.

328. Esarte, C. Millera, Á. Bilbao, R. & Alzueta, M. U. Gas and soot products formed in the pyrolysis of acetylene-ethanol blends under flow reactor conditions. *Fuel Process. Technol.* (2009) doi:10.1016/j.fuproc.2009.01.011.

329. Bensabath, T. Le, M. D. Monnier, H. & Glaude, P. A. Polycyclic aromatic hydrocarbon (PAH) formation during acetylene pyrolysis in tubular reactor under low pressure carburizing conditions. *Chem. Eng. Sci.* (2019) doi:10.1016/j.ces.2019.03.030.

330. Jiang, B. Jia, P. & Liu, D. Comparative study on soot characteristics of non-swirling and swirling inverse diffusion iso-octane flames with biofuel 2,5-dimethylfuran addition. *J. Energy Inst.* (2020) doi:10.1016/j.joei.2020.05.006.

331. Wang, W. Zhang, Z. Shi, D. Huang, Y. & Zhou, L. Study of soot formations in co-flow laminar diffusion flames of n-heptane and oxygenated aromatic biofuels from atmospheric condition to 2.3 bar. *Fuel* (2021) doi:10.1016/j.fuel.2021.120753.

332. Liu, Y. … Xu, Y. Effects of ammonia addition on soot formation in ethylene laminar diffusion flames. *Fuel* (2021) doi:10.1016/j.fuel.2021.120416.

333. Viteri, F. López, A. Millera, Bilbao, R. & Alzueta, M. U. Influence of temperature and gas residence time on the formation of polycyclic aromatic hydrocarbons (PAH) during the pyrolysis of ethanol. *Fuel* (2019) doi:10.1016/j.fuel.2018.09.061.

334. Zhao, Q. … Ran, S. An experimental study on the gas and soot formation in ethanol pyrolysis. *Int. J. Oil, Gas Coal Technol.* (2019) doi:10.1504/ijogct.2019.10018665.

335. Alexandrino, K. Salinas, J. Millera, Á. Bilbao, R. & Alzueta, M. U. Sooting propensity of dimethyl carbonate, soot reactivity and characterization. *Fuel* (2016) doi:10.1016/j.fuel.2016.06.058.

336. Alexandrino, K. Salvo, P. Millera, Á. Bilbao, R. & Alzueta, M. U. Influence of the Temperature and 2,5-Dimethylfuran Concentration on Its Sooting Tendency. *Combust. Sci. Technol.* (2016) doi:10.1080/00102202.2016.1138828.

337. De Bruycker, R. … Van Geem, K. M. An experimental and kinetic modeling study of γ-valerolactone pyrolysis. *Combust. Flame* (2016) doi:10.1016/j.combustflame.2015.11.016.

338. Bennethum, J. E. Mattavi, J. N. & Toepel, R. R. Diesel combustion chamber sampling

- Hardware, procedures, and data interpretation. in *SAE Technical Papers* (1975). doi:10.4271/750849.

339. Duggal, V. K. Priede, T. & Khan, I. M. A study of pollutant formation within the combustion space of a diesel engine. in *SAE Technical Papers* (1978). doi:10.4271/780227.

340. Miwa, K. Ikegami, M. & Nakano, R. Combustion and pollutant formation in an indirect injection diesel engine. in *SAE Technical Papers* (1980). doi:10.4271/800026.

341. Alcock, J. F. & Scott, W. M. Some More Light on Diesel Combustion. *Proc. Inst. Mech. Eng. Automob. Div.* (1962) doi:10.1243/pime_auto_1962_000_022_02.

342. Nagao, F. Ikegami, M. Mitsuda, T. Kawatei, K. & Fujikawa, T. STUDY ON COMBUSTION IN DIRECT-INJECTION DIESEL ENGINES - 2. IN THE CASE OF DEEP-BOWL CHAMBER. *Bull JSME* (1973) doi:10.1299/jsme1958.16.599.

343. Aoyagi, Y. Kamimoto, T. Matsui, Y. & Matsuoka, S. A gas sampling study on the formation processes of soot and NO in a DI diesel engine. in *SAE Technical Papers* (1980). doi:10.4271/800254.

344. Hedding, G. H. Kittelson, D. B. Scherrer, H. Liu, X. & Dolan, D. F. Total cylinder sampling from a diesel engine. in *SAE Technical Papers* (1981). doi:10.4271/810257.

345. Kittelson, D. B. Pipho, M. J. Ambs, J. L. & Siegla, D. C. Particle concentrations in a diesel cylinder: Comparison of theory and experiment. in *SAE Technical Papers* (1986). doi:10.4271/861569.

346. Kittelson, D. B. Pipho, M. J. Ambs, J. L. & Luo, L. In-cylinder measurements of soot production in a direct-injection diesel engine. in *SAE Technical Papers* (1988). doi:10.4271/880344.

347. Liu, X. & Kittelson, D. B. Total cylinder sampling from a diesel engine (Part II). in *SAE Technical Papers* (1982). doi:10.4271/820360.

348. Pipho, M. J. Ambs, J. L. & Kittelson, D. B. In-cylinder measurements of particulate

formation in an indirect injection diesel engine. in *SAE Technical Papers* (1986). doi:10.4271/860024.

349. Du, C. J. & Kittelson, D. B. Total cylinder sampling from a diesel engine: Part III - Particle measurements. in *SAE Technical Papers* (1983). doi:10.4271/830243.

350. Pipho, M. J. Kittelson, D. B. & Zarling, D. D. NO2 formation in a diesel engine. in *SAE Technical Papers* (1991). doi:10.4271/910231.

351. Kittelson, D. B. Ambs, J. L. & Hadjkacem, H. Particulate emissions from diesel engines:influence of in-cylinder surface. in *SAE Technical Papers* (1990). doi:10.4271/900645.

352. Bertoli, C. Del Giacomo, N. & Beatrice, C. Diesel combustion improvements by the use of oxygenated synthetic fuels. in *SAE Technical Papers* (1997). doi:10.4271/972972.

353. Pungs, A. Pischinger, S. Bäcker, H. & Lepperhoff, G. Analysis of the particle size distribution in the cylinder of a common rail di diesel engine during combustion and expansion. in *SAE Technical Papers* (2000). doi:10.4271/2000-01-1999.

354. Barbella, R. Bertoli, C. Ciajolo, A. D'Anna, A. & Masi, S. In-cylinder sampling of high molecular weight hydrocarbons from a D.I. light duty diesel engine. in *SAE Technical Papers* (1989). doi:10.4271/890437.

355. Barbella, R. Bertoli, C. Ciajolo, A. & D'anna, A. Behavior of a fuel oil during the combustion cycle of a direct injection diesel engine. *Combust. Flame* (1990) doi:10.1016/0010-2180(90)90097-B.

356. Ciajolo, A. D'anna, A. Barbella, R. & Bertoli, C. Combustion of tetradecane and tetradecane/ α-Methylnaphthalene in a diesel engine with regard to soot and PAH formation. *Combust. Sci. Technol.* (1993) doi:10.1080/00102209208947211.

357. Wang, X. … Li, B. Evolution of in-cylinder polycyclic aromatic hydrocarbons in a diesel engine fueled with n-heptane and n-heptane/toluene. *Fuel* (2015)

doi:10.1016/j.fuel.2015.05.053.

358.   Ledesma, E. B. Wornat, M. J. Felton, P. G. & Sivo, J. A. The effects of pressure on the yields of polycyclic aromatic hydrocarbons produced during the supercritical pyrolysis of toluene. *Proc. Combust. Inst.* (2005) doi:10.1016/j.proci.2004.08.086.

359.   Liu, Y. … Yang, X. Surface functional groups and sp3/sp2 hybridization ratios of in-cylinder soot from a diesel engine fueled with n-heptane and n-heptane/toluene. *Fuel* (2016) doi:10.1016/j.fuel.2016.03.082.

360.   Alfè, M. … Ciajolo, A. Structure-property relationship in nanostructures of young and mature soot in premixed flames. *Proc. Combust. Inst.* (2009) doi:10.1016/j.proci.2008.06.193.

361.   Vander Wal, R. L. Bryg, V. M. & Hays, M. D. XPS analysis of combustion aerosols for chemical composition, surface chemistry, and carbon chemical state. *Anal. Chem.* (2011) doi:10.1021/ac102365s.

362.   Malmborg, V. B. … Pagels, J. Evolution of In-Cylinder Diesel Engine Soot and Emission Characteristics Investigated with Online Aerosol Mass Spectrometry. *Environ. Sci. Technol.* (2017) doi:10.1021/acs.est.6b03391.

363.   Savic, N. … Ristovski, Z. D. Influence of biodiesel fuel composition on the morphology and microstructure of particles emitted from diesel engines. *Carbon N. Y.* (2016) doi:10.1016/j.carbon.2016.03.061.

364.   Talibi, M. *Co-combustion of diesel and gaseous fuels with exhaust emissions analysis and in-cylinder gas sampling*. (2015).

365.   IR Spectrum. http://www.wag.caltech.edu/home/jang/genchem/infrared.htm.

366.   Horiba Instruments. *MEXA 9100HEGR instructions manual,*. (1984).

367.   Cambustion. *DMS500 Fast Particulate Spectrometer.Cambustion User Manual*. (2011).

368.   Talibi, M. Balachandran, R. & Ladommatos, N. Influence of combusting methane-

hydrogen mixtures on compression–ignition engine exhaust emissions and in-cylinder gas composition. *Int. J. Hydrogen Energy* (2017) doi:10.1016/j.ijhydene.2016.10.049.

369. Talibi, M. Hellier, P. Balachandran, R. & Ladommatos, N. Development of a Fast-Acting, Time-Resolved Gas Sampling System for Combustion and Fuels Analysis. *SAE Int. J. Engines* (2016) doi:10.4271/2016-01-0791.

370. Seilly, A. H. Colenoid actuators - Further developments in extremely fast acting solenoids. in *SAE Technical Papers* (1981). doi:10.4271/810462.

371. Norinaga, K. … Hayashi, J. ichiro. A mechanistic study on the reaction pathways leading to benzene and naphthalene in cellulose vapor phase cracking. *Biomass and Bioenergy* (2014) doi:10.1016/j.biombioe.2014.07.008.

372. Eveleigh, A. Ladommatos, N. Hellier, P. & Jourdan, A. L. An investigation into the conversion of specific carbon atoms in oleic acid and methyl oleate to particulate matter in a diesel engine and tube reactor. *Fuel* (2015) doi:10.1016/j.fuel.2015.03.037.

373. Khan, Z. (University C. L. Decomposition of some hydrocarbon and oxygenated fuel molecules and subsequent formation of PAHs under pyrolysis conditions in a flow reactor. (University College London, 2021).

374. Ogbunuzor, C. C. Hellier, P. R. Talibi, M. & Ladommatos, N. In-Cylinder Polycyclic Aromatic Hydrocarbons Sampled during Diesel Engine Combustion. *Environ. Sci. Technol.* (2021) doi:10.1021/acs.est.0c05561.

375. Leaney, P. W. The Isothermal Pyrolysis of n-Butane in a Laminar Flow Reactor. *Thesis* (1982).

376. Keller, B. P. … Loyalka, S. K. Total hemispherical emissivity of Inconel 718. *Nucl. Eng. Des.* (2015) doi:10.1016/j.nucengdes.2015.02.018.

377. Hilscher, W. No Title. (1996).

378. Agilent. Troubleshooting tips and tricks for your GC analyzer & CFT application. (2014).

379. Chaulya, S. K. & Prasad, G. M. Gas Sensors for Underground Mines and Hazardous Areas. in *Sensing and Monitoring Technologies for Mines and Hazardous Areas* (2016). doi:10.1016/b978-0-12-803194-0.00003-9.

380. BGB. HP-1. https://www.bgb-info.com/home.php?cat=4971.

381. Marques, A. V. & Pereira, H. A methodological approach for the simultaneous quantification of glycerol and fatty acids from cork suberin in a single GC run. *Phytochem. Anal.* (2019) doi:10.1002/pca.2846.

382. El-Naggar, A. Y. Factors affecting linearity and response of flame ionization detector. *Pet. Sci. Technol.* (2006) doi:10.1081/LFT-200044407.

383. Sidebotham, G. W. & Glassman, I. Flame temperature, fuel structure, and fuel concentration effects on soot formation in inverse diffusion flames. *Combust. Flame* (1992) doi:10.1016/0010-2180(92)90088-7.

384. Lapuerta, M. Hernández, J. J. Fernández-Rodríguez, D. & Cova-Bonillo, A. Autoignition of blends of n-butanol and ethanol with diesel or biodiesel fuels in a constant-volume combustion chamber. *Energy* (2017) doi:10.1016/j.energy.2016.10.090.

385. Sigma Aldrich (Product Properties). www.sigmaaldrich.com/.

386. Buckingham, G. T. & Carleton, B. A. *PYROLYSIS AND SPECTROSCOPY OF CYCLIC AROMATIC COMBUSTION INTERMEDIATES*. (2010).

387. Grela, M. A. Amorebieta, V. T. & Colussi, A. J. Very low pressure pyrolysis of furan, 2-methylfuran, and 2,5-dimethylfuran. The stability of the furan ring. *J. Phys. Chem.* (1985) doi:10.1021/j100247a011.

388. Liu, D. … Kohse-Höinghaus, K. Combustion chemistry and flame structure of furan group biofuels using molecular-beam mass spectrometry and gas chromatography - Part I: Furan. *Combust. Flame* (2014) doi:10.1016/j.combustflame.2013.05.028.

389. Tran, L. S. … Kohse-Höinghaus, K. Combustion chemistry and flame structure of

furan group biofuels using molecular-beam mass spectrometry and gas chromatography - Part II: 2-Methylfuran. *Combust. Flame* (2014) doi:10.1016/j.combustflame.2013.05.027.

390. Togbé, C. … Kohse-Höinghaus, K. Combustion chemistry and flame structure of furan group biofuels using molecular-beam mass spectrometry and gas chromatography - Part III: 2,5-Dimethylfuran. *Combust. Flame* (2014) doi:10.1016/j.combustflame.2013.05.026.

391. Koivisto, E. Ladommatos, N. & Gold, M. Compression Ignition and Exhaust Gas Emissions of Fuel Molecules Which Can Be Produced from Lignocellulosic Biomass: Levulinates, Valeric Esters, and Ketones. *Energy and Fuels* (2015) doi:10.1021/acs.energyfuels.5b01314.

392. Hellier, P. Al-Haj, L. Talibi, M. Purton, S. & Ladommatos, N. Combustion and emissions characterization of terpenes with a view to their biological production in cyanobacteria. *Fuel* (2013) doi:10.1016/j.fuel.2013.04.042.

393. Liu, J. … Yao, M. Effects of diesel/PODE (polyoxymethylene dimethyl ethers) blends on combustion and emission characteristics in a heavy duty diesel engine. *Fuel* (2016) doi:10.1016/j.fuel.2016.03.019.

394. Koivisto, E. *Ignition and combustion of future oxygenated fuels in compression-ignition engines.* (2015).

395. Zhang, P. … Geng, L. Spray, atomization and combustion characteristics of oxygenated fuels in a constant volume bomb: A review. *Journal of Traffic and Transportation Engineering (English Edition)* (2020) doi:10.1016/j.jtte.2020.05.001.

396. Karavalakis, G. … Durbin, T. D. Evaluating the effects of aromatics content in gasoline on gaseous and particulate matter emissions from SI-PFI and SIDI vehicles. *Environ. Sci. Technol.* (2015) doi:10.1021/es5061726.

397. Alexandrino, K. Millera, Á. Bilbao, R. & Alzueta, M. U. Novel aspects in the pyrolysis

and oxidation of 2,5-dimethylfuran. *Proc. Combust. Inst.* (2015) doi:10.1016/j.proci.2014.06.002.

398.   Xiao, H. Hou, B. Zeng, P. & Jiang, A. Combustion and emissions characteristics of a diesel engine fueled with blends of diesel and DMF. *Kexue Tongbao/Chinese Sci. Bull.* (2017) doi:10.1360/N972017-00020.

399.   Liu, Y. Li, J. Gao, Y. & Yuan, X. Analysis of micro-explosion phenomenon in a constant volume chamber by butanol-biodiesel-diesel blend fuel. in *Advanced Materials Research* (2012). doi:10.4028/www.scientific.net/AMR.443-444.996.

400.   Cheng, A. S. Dibble, R. W. & Buchholz, B. A. The Effect of Oxygenates on Diesel Engine Particulate Matter. in (2002). doi:10.4271/2002-01-1705.

401.   Eveleigh, A. & Ladommatos, N. Isotopic Tracers for Combustion Research. *Combustion Science and Technology* (2017) doi:10.1080/00102202.2016.1246440.

402.   Yang, Miao; Wang, Zhiwei; Lei, Tingzhou; Lin, Lu; He, Xiaofeng; Qi, Tian; Xin, Xiaofei; Li, Zijie; Shi, J. Influence of Gamma-Valerolactone-n-Butanol-Diesel Blends on Physicochemical Characteristics and Emissions of a Diesel Engine. *J. Biobased Mater. Bioenergy,* **11**, 66–72 (2017).

403.   Kumbár, V. & Skřivánek, A. Temperature dependence viscosity and density of different biodiesel blends. *Acta Univ. Agric. Silvic. Mendelianae Brun.* **63**, (2015).

404.   Jacobson, R. S. Korte, A. R. Vertes, A. & Miller, J. H. The Molecular Composition of Soot. *Angew. Chemie* (2020) doi:10.1002/ange.201914115.

405.   Salamanca, M. … Kraft, M. The impact of cyclic fuels on the formation and structure of soot. *Combust. Flame* (2020) doi:10.1016/j.combustflame.2020.04.026.

406.   Commodo, M. … Gross, L. On the early stages of soot formation: Molecular structure elucidation by high-resolution atomic force microscopy. *Combust. Flame* (2019) doi:10.1016/j.combustflame.2019.03.042.

407.   Svensson, K. I. Richards, M. J. MacKrory, A. J. & Tree, D. R. Fuel composition and

molecular structure effects on soot formation in direct-injection flames under diesel engine conditions. in *SAE Technical Papers* (2005). doi:10.4271/2005-01-0381.

408. Xin, L. … Cheng, Q. Thermal decomposition mechanism of some hydrocarbons by ReaxFF-based molecular dynamics and density functional theory study. *Fuel* (2020) doi:10.1016/j.fuel.2020.117885.

409. Bergthorson, J. M. & Thomson, M. J. A review of the combustion and emissions properties of advanced transportation biofuels and their impact on existing and future engines. *Renewable and Sustainable Energy Reviews* (2015) doi:10.1016/j.rser.2014.10.034.

410. Talibi, M. Hellier, P. & Ladommatos, N. Combustion and exhaust emission characteristics, and in-cylinder gas composition, of hydrogen enriched biogas mixtures in a diesel engine. *Energy* (2017) doi:10.1016/j.energy.2017.02.070.

411. Valencia, S. Ruiz, S. Manrique, J. Celis, C. & Figueira da Silva, L. F. Soot modeling in turbulent diffusion flames: review and prospects. *Journal of the Brazilian Society of Mechanical Sciences and Engineering* (2021) doi:10.1007/s40430-021-02876-y.

412. Leigh, C. H. & Szwaec, M. The pyrolysis of n-propyl-benzene and the heat of formation of ethyl radical. *J. Chem. Phys.* (1952) doi:10.1063/1.1700433.

413. Pant, K. K. & Kunzru, D. Pyrolysis of n-heptane: Kinetics and modeling. *J. Anal. Appl. Pyrolysis* (1996) doi:10.1016/0165-2370(95)00925-6.

414. Ciawi, E. Ashokkumar, M. & Grieser, F. Limitations of the methyl radical recombination method for acoustic cavitation bubble temperature measurements in aqueous solutions. *J. Phys. Chem. B* (2006) doi:10.1021/jp0618734.

415. Davidson, D. F. Oehlschlaeger, M. A. & Hanson, R. K. Methyl concentration time-histories during iso-octane and n-heptane oxidation and pyrolysis. *Proc. Combust. Inst.* (2007) doi:10.1016/j.proci.2006.07.087.

416. Aribike, D. S. & Susu, A. A. Kinetics and mechanism of the thermal cracking of n-

heptane. *Thermochim. Acta* (1988) doi:10.1016/0040-6031(88)87501-4.

417. Chakraborty, J. P. & Kunzru, D. High pressure pyrolysis of n-heptane. *J. Anal. Appl. Pyrolysis* (2009) doi:10.1016/j.jaap.2009.04.001.

418. Ranzi, E. Frassoldati, A. Granata, S. & Faravelli, T. Wide-range kinetic modeling study of the pyrolysis, partial oxidation, and combustion of heavy n-alkanes. *Ind. Eng. Chem. Res.* **44**, (2005).

419. Kim, D. H. Mulholland, J. A. Wang, D. & Violi, A. Pyrolytic hydrocarbon growth from cyclopentadiene. *J. Phys. Chem. A* (2010) doi:10.1021/jp106749k.

420. Blanksby, S. J. & Ellison, G. B. Bond dissociation energies of organic molecules. *Acc. Chem. Res.* (2003) doi:10.1021/ar020230d.

421. McEnally, C. S. & Pfefferle, L. D. Fuel decomposition and hydrocarbon growth processes for oxygenated hydrocarbons: Butyl alcohols. *Proc. Combust. Inst.* (2005) doi:10.1016/j.proci.2004.07.033.

422. Farooq, A. … Westbrook, C. K. Shock tube studies of methyl butanoate pyrolysis with relevance to biodiesel. *Combust. Flame* (2012) doi:10.1016/j.combustflame.2012.05.013.

423. Zhang, Y. Yang, Y. & Boehman, A. L. Premixed ignition behavior of C9 fatty acid esters: A motored engine study. *Combust. Flame* (2009) doi:10.1016/j.combustflame.2009.01.024.

424. Zhang, L. Yang, K. Zhao, R. Ying, Y. & Liu, D. Formation and nanoscale-characteristics of soot from pyrolysis of ethylene blended with ethanol/dimethyl ether. *J. Energy Inst.* (2020) doi:10.1016/j.joei.2019.11.012.

425. Oyeyemi, V. B. … Carter, E. A. Size-extensivity-corrected multireference configuration interaction schemes to accurately predict bond dissociation energies of oxygenated hydrocarbons. *J. Chem. Phys.* (2014) doi:10.1063/1.4862159.

426. Golea, D. Rezgui, Y. Guemini, M. & Hamdane, S. Reduction of PAH and soot

precursors in benzene flames by addition of ethanol. *J. Phys. Chem. A* (2012) doi:10.1021/jp211350f.

427. Faravelli, T. Goldaniga, A. & Ranzi, E. The kinetic modeling of soot precursors in ethylene flames. in *Symposium (International) on Combustion* (1998). doi:10.1016/S0082-0784(98)80556-0.

428. Johansson, K. O. … Michelsen, H. A. Soot precursor formation and limitations of the stabilomer grid. *Proc. Combust. Inst.* (2015) doi:10.1016/j.proci.2014.05.033.

429. Blanquart, G. G. Chemical and Statistical Soot Modeling. 199 (2008).

430. Sun, W. Hamadi, A. Abid, S. Chaumeix, N. & Comandini, A. Probing PAH formation chemical kinetics from benzene and toluene pyrolysis in a single-pulse shock tube. in *Proceedings of the Combustion Institute* (2021). doi:10.1016/j.proci.2020.06.077.

431. Morris, J. C. The Thermal Decomposition of Acetaldehyde. *J. Am. Chem. Soc.* (1944) doi:10.1021/ja01232a023.

432. Bicer, Y. & Dincer, I. Clean fuel options with hydrogen for sea transportation: A life cycle approach. *Int. J. Hydrogen Energy* (2018) doi:10.1016/j.ijhydene.2017.10.157.

433. Pochet, M. Truedsson, I. Foucher, F. Jeanmart, H. & Contino, F. Ammonia-Hydrogen Blends in Homogeneous-Charge Compression-Ignition Engine. in *SAE Technical Papers* (2017). doi:10.4271/2017-24-0087.

434. Duraisamy, G. Rangasamy, M. & Nagarajan, G. Effect of EGR and Premixed Mass Percentage on Cycle to Cycle Variation of Methanol/Diesel Dual Fuel RCCI Combustion. in *SAE Technical Papers* (2019). doi:10.4271/2019-26-0090.

435. Saravanan, S. Nagarajan, G. Anand, S. & Sampath, S. Correlation for thermal NOx formation in compression ignition (CI) engine fuelled with diesel and biodiesel. *Energy* (2012) doi:10.1016/j.energy.2012.03.028.

436. Reiter, A. J. & Kong, S. C. Combustion and emissions characteristics of compression-ignition engine using dual ammonia-diesel fuel. *Fuel* (2011)

doi:10.1016/j.fuel.2010.07.055.

437. Zhu, S. … Dabdub, D. Modeling reactive ammonia uptake by secondary organic aerosol in CMAQ: Application to the continental US. *Atmos. Chem. Phys.* (2018) doi:10.5194/acp-18-3641-2018.

438. Goss, K. U. & Eisenreich, S. J. Sorption of volatile organic compounds to particles from a combustion source at different temperatures and relative humidities. *Atmos. Environ.* (1997) doi:10.1016/S1352-2310(97)00048-4.